The effect of Granulocyte-Macrophage colony-stimulating factor (GM-CSF) on the immune response against *Candida albicans* using human inflammatory monocytes.

School of Life Sciences

Supervisors

Prof. Luisa Martinez-Pomares

Prof. Miguel Camara

Submitted by

Khawalah Abid Munshi

14305319

Thesis submitted to the University of Nottingham for the degree of Doctor of Philosophy.

August 2025

Acknowledgement

First and foremost, I would like to express my deepest gratitude to Almighty Allah for granting me the strength, capability, and opportunity to undertake and complete this project.

I would like to extend my appreciation to my sponsors, the Government of Saudi Arabia, the Saudi Arabian Cultural Bureau in the United Kingdom, and King Abdullah Medical City, for their support in helping me achieve a long-term dream and pursue a high-demand field in the Kingdom of Saudi Arabia.

My deepest and profound gratitude goes to my supervisor, Prof. Luisa Martinez-Pomares, for her unwavering support, guidance, and encouragement throughout this journey. Her expertise and patience, combined with valuable feedback, have helped me navigate challenges and deepen my understanding of the field of Immunology. During this journey, I faced a brutal family tragedy that made it challenging to complete my studies at times; meanwhile, Prof. Luisa was highly supportive and fully understanding of the situation, all of which gave me the courage and potential to reach this point finally. I am deeply thankful for her inspiration every step of the way, and in my heart, I believe that reaching this stage wouldn't have been accomplished without her support.

I would like to thank Prof. Miguel Camara, my second supervisor. Prof. Miguel warmly acknowledged my achievements and kindly offered feedback when I asked.

I would like to thank my lovely group members: Mr. Darryl Jackson, my manager, and my lovely office mate. Dr. Kelly Lee, the motivated scientist who welcomed me on my first day and taught me a great deal, may God rest her soul in peace. Dr. Sonali Singh always has a wealth of wisdom to share; my infection assays wouldn't be nearly as effective if she hadn't taken the time to count all those cells with me. I also want to sincerely thank my ally team, Nusrat, Khaleel and Ahmed; they made the journey fun with their support, great ideas, and all the laughs along the way.

I would like to extend my heartfelt thanks to all the collaborators and everyone who has supported me throughout this journey, especially those who warmly supported me, including Dr. Danielle Scott and Dr. Hatoon Al Amri, who happens to be one of my best friends.

I would like to take a special moment to mainly express my heartfelt appreciation to my family for their uncountable love and support. My father, Abid, my life mentor, who has been an exceptional and supportive father throughout my life, and my mother, Amirah, my role model, who was a smooth, warm, and strong mom, she was always by my side, and even now, her spirit continues to be, may Allah rest her soul in peace. I would like to thank my kind and soft-hearted sister Khireyah, whom I call a sister with a mommy flavour, and my dearest brothers Abdullatif, Alaa, Asim and Luay. I would also like to thank my sister-in-law, Aysha, for being friendly and always caring.

Finally, I would like to thank my support system, their presence has been a source of strength and comfort throughout this journey. They stood by me, celebrating my achievements, lifting me in moments of doubt, and reminding me that this path was never walked alone, I am deeply grateful. Their encouragement, laughter, and companionship have made even the most challenging times bearable and the joyful moments even brighter. I owe special thanks to Ms. Alaa Bannani. I am also thankful to all my UK friends who made this journey both tolerable and memorable, especially Dr. Nahlah Ghouth.

A special thanks to:

Dr. Waleed Abdurrab Hafiz, my best friend and my jar of positivity, I appreciate the kindness, generosity, and support during this journey.

Dedication

This thesis is dedicated to the memory of my late, beautiful mother and to my devoted father.

Declaration

I declare that the work presented in this thesis is my own, carried out as part of my PhD research at the University of Nottingham under the supervision of Prof. Luisa Martinez-Pomares. This thesis has not been submitted, in whole or in part, for any other degree at this or any other institution.
The experimental design, the majority of the laboratory work, data analysis, and the writing of this thesis were carried out by me. However, I acknowledge the contributions of several colleagues and collaborators whose support enriched various aspects of this research:

- Darryl Jackson, who assisted with PCR-related, used in Chapters 3.
- Dr. Danielle Scott, who kindly provided the in vitro-derived macrophages (iMacs) used in several experiments for Chapter 6.
- Dr. David Onion, who ran the first repeat of the ImageStreamX analysis of the infected and non-infected monocytes treated with GM-CSF, used in Chapter 4.
- Adrianna Kozlowska, a master's student who contributed to the run of 3 replicates of (CCL-22-TNF-α), a hyphae quantification experiment (first repeat), we refined the protocol after and subsequently employed the enhanced method in Chapter 4.
- Dr. Joelle Goulding, who fixed the plates used for live-cell microscopy experiments, used in Chapter 3.
- Dr. Hatoon Al Amri, who performed the proteomics data analysis, used in Chapter 3.
- Georgina Hopkins from Dr. Lucy Fairclough Lab, who processed my samples of Macrophages for the EVs project, used in Chapter 3.
- Evren Akyuz from Dr. Anna Malecka Lab, who ran ELISA for the cytokine VEGF, used in Chapter 4.

I am deeply grateful for their collaboration, and their contributions are fully acknowledged in the relevant chapters. All other work presented in this thesis is my own.
All sources of information have been appropriately cited and acknowledged.

Publications and Conference Proceedings

Manuscript in preparation

Granulocyte-macrophage colony-stimulating factor (GM-CSF) increases the contribution of CD206 to human monocyte responses to C. albicans.

Khawalah Abid Munshi1, Darryl Jackson1, Sirina Muntaka1,2, Joshua Petch1,3, David Onion1, Gokhan Yilmaz3,4, Sonali Singh1, Daniel Scott1, Hatoon Al Amri, Miguel Camara1, Giuseppe Mantovani3 and Luisa Martinez-Pomares1*.

Conferences/Meetings attended:

- **IIIM division meeting**, University of Nottingham – February 13, 2025 **Oral Presentation:** *CD206-specific glycopolymers modulate the response of human monocytes to Candida albicans in the presence of Granulocyte-macrophage colony-stimulating factor (GM-CSF).*
- **PGR Symposium**, University of Nottingham – June 16-17, 2024 **Oral Presentation:** *The effect of Granulocyte-Macrophage-colony stimulatory factor (GM-CSF) on the immune response against Candida albicans using human inflammatory monocytes.*
- **PGR Symposium**, University of Nottingham – July 13–14, 2023 **Poster Presentation:** *Effect of GM-CSF on the Immune Response of Human Monocytes Against Candida albicans*
- **BSI Midlands Immunology Group Symposium**, Leicester, UK – June 8, 2023, **Poster Presentation:** *Effect of GM-CSF on the Immune Response of Human Monocytes Against Candida albicans*
- **Midland Innovation Flow Cytometry Meeting**, Nottingham, UK – April 25, 2023, **Attendance**
- **BSI Congress**, Liverpool, UK – December 5–8, 2022 **Poster Presentation:** *Effect of GM-CSF on the Recognition of Candida albicans by Lectin Receptors Using a Human Inflammatory Monocyte Model.*

Award

- **BSI Midlands Immunology Group Symposium**, Loughborough, UK – June 2024 **Poster Presentation (Selected poster as one of the top three posters):** The effect of GM-CSF on the immune response against Candida albicans using human inflammatory monocytes

Abstract

Granulocyte-macrophage colony-stimulating factor (GM-CSF) plays a pivotal role in antimicrobial immunity by enhancing survival, adhesion, and migration of innate immune cells, including neutrophils, macrophages, and monocytes. Monocytes and macrophages are central for host defence against fungal pathogens such as *Candida albicans (C. albicans)*, acting independently or synergistically with neutrophils. *C. albicans* is an opportunistic fungal pathogen that lives typically as a commensal. Infection with *C. albicans* occurs when it shifts from innocuous to pathogenic, often leading to mucosal or systemic diseases. This study investigates how GM-CSF modulates the activity of human inflammatory monocytes during *C. albicans* infection, aiming to uncover protective mechanisms and determine the therapeutic potential of GM-CSF in the context of fungal infection. The work is presented in three results chapters.

Chapter 3 centres on the characterisation of monocytes treated with GM-CSF in comparison to M-CSF-treated monocytes, used as negative controls. GM-CSF and M-CSF monocytes display similar viability (~95%), but GM-CSF monocytes had enhanced expression of CD11b, and HLA-DR compared to M-CSF monocytes. This indicates a significant effect of GM-CSF on monocyte activation. In addition, we observed a substantial increased expression of the mannose receptor MR (CD206), Dectin-1 and CLEC5A, all of which are C-type lectin receptors that specialise in carbohydrate recognition and play a crucial role in detecting infections. Levels of Dectin-2 and the production of extracellular vesicles (EVs), were not affected by GM-CSF.

Chapter 4 centres on responses of monocytes to infection with *C. albicans* and how are affected by GM-CSF. We exposed M-CSF and GM-CSF-monocytes to *C. albicans* at MOI 1 (cytokine secretion, CFU) or MOI 10 (phagocytosis), at 37 °C, 5% CO_2, in the presence of human serum for 1 and 3 h. In response to infection with *C. albicans,* GM-CSF-treated monocytes, compared to M-CSF-treated monocytes, increased TNF-α, IL-6, IL-1β and CCL22 secretion despite similar phagocytic activity and fungal viability (CFU). Interestingly, GM-CSF-monocytes more effectively control hypha growth, indicating enhanced anti-fungal activity and differential phagosome maturation. These results were linked to a drastic reduction of surface MR after *C. albicans* uptake in GM-CSF monocytes, which would be consistent with enhanced MR shedding.

Chapter 5 considers the role of MR in the response of GM-CSF- monocytes to *C. albicans*. MR surface expression was inhibited using specific sulfated glycopolymers (sGP). sGP treatment reduced MR expression, which resulted in the reduction of TNF-α production during infection, indicating that MR plays an essential role in modulating inflammation during *C. albicans* infection.

Chapter 6 extended the investigation to induced pluripotent stem cell–derived macrophages (iMacs). The expression of CD45 and CD14 confirmed their macrophage identity. Although the study was limited in both replicates and experimental diversity, we were able to show that iMacs treated with GM-CSF expressed MR and Dectin-1, as determined by qPCR analysis (N=3). In contrast, cytokine secretion was not detected in these cells under the conditions tested. We also performed a CFU assay following the same experimental design used with primary monocytes; although conducted only once, the outcome was consistent with the results obtained from primary cells.

Overall, ongoing work aims to clarify the mechanisms underlying hyphal growth restriction and MR-mediated responses, thereby improving our understanding of how GM-CSF confers antifungal protection. Further research will be required to elucidate the effector functions of iMacs and to explore their potential as a model system for studying fungal infections.

Table of Contents

List of figures

LIST OF TABLES

Aabbreviations

5-FC	5-Flucytosine
5-FU	5-Fluorouracil
A. fumigatus	*Aspergillus Fumigatus*
AMPs	Antimicrobial Peptides
ASC	Apoptosis-Associated Speck-Like Protein
BBB	Blood-Brain Barrier
BCL10	B Cell Lymphoma 10
C. albicans	*Candida albicans*
CARD9	Caspase Recruitment Domain-Containing Protein 9
CBM	CARD9/BCL10/MALT1
CD	Crohn's disease
CD9	Cluster of Differentiation 9
CD11b	Cluster of Differentiation 11b
CD14	Cluster of Differentiation 14
CD15	Cluster of Differentiation 15
CD16	Cluster of Differentiation 16
CD28	Cluster of Differentiation 28
CD37	Cluster of Differentiation 37
CD53	Cluster of Differentiation 53
CD63	Cluster of Differentiation 63
CD80	Cluster of Differentiation 80
CD81	Cluster of Differentiation 81
CD82	Cluster of Differentiation 82
CD86	Cluster of Differentiation 86
CF	Cystic Fibrosis
CLRs	C-Type Lectin Receptors
CNS	Central Nervous System
COVID-19	Coronavirus Disease 2019
Cph1	*Candida* Pheromone Response 1
CR	Cysteine-Rich Domain
CR3	Complement Receptor 3
CRD	Carbohydrate Recognition Domain
CTLDs	C-Type Lectin-Like Signalling Motifs Domains
CXCL1	C-X-C Motif Chemokine Ligand 1

CXCL10	C-X-C Motif Chemokine Ligand 10
CXCL2	C-X-C Motif Chemokine Ligand 2
CXCL9	C-X-C Motif Chemokine Ligand 9
DAMPs	Damage-Associated Molecular Patterns
DAP12	DNAX-Activating Protein of 12 kDa
DCIR	Dendritic Cell Immunoreceptor
DCs	Dendritic Cells
DC-SIGN	Dendritic Cell-Specific Intercellular Adhesion Molecule-3-Grabbing Non-Integrin
DNA	Deoxyribonucleic Acid
dsRNA	Double-Stranded RNA
DV	Dengue Virus
EAE	Experimental Autoimmune Encephalomyelitis
eDNA	Extracellular DNA
Efg1	Enhanced Filamentous Growth Protein 1
EPS	Extracellular Polysaccharide Material
ER	Endoplasmic Reticulum
ERG11	Sterol 14α-Demethylase
ERK	Extracellular Signal-Regulated Kinase
EVs	Extracellular Vesicles
FcγR	FC Gamma Receptor
FN-II	Fibronectin II
GM-CSF	Granulocyte-Macrophage Colony-Stimulating Factor
GIT	Gastrointestinal Tract
HAI	Healthcare-Associated Illnesses
H1N1	Hemagglutinin Type 1, Neuraminidase Type 1
H5N1	Hemagglutinin Type 5, Neuraminidase Type 1
H7N9	Hemagglutinin Type 7, Neuraminidase Type 9
HIV	Human Immunodeficiency Virus
HLA-DR	Human Leukocyte Antigen- DR isotype
H-RAS	Harvey Rat Sarcoma Viral Oncogene Homolog
IBD	Inflammatory Bowel Disease
IC	Invasive Candidiasis
IFD	Invasive Fungal Disease
IFN-γ	Interferon-γ
IPA	Invasive Pulmonary Aspergillosis

IL-1β	Interleukin-1 β
IL-10	Interleukin-10
IL-12	Interleukin-12
IL-17	Interleukin-17
IL-18	Interleukin-18
IL-23	Interleukin-23
IL-6	Interleukin-6
IRAK1	Interleukin-1 Receptor-Associated Kinase 1
IRAK4	Interleukin-1 Receptor-Associated Kinase 4
ITAM	Tyrosine Activation Motif
ITIM	Tyrosine Inhibitory Motif
JAK2	Janus Kinase 2
JEV	Japanese Encephalitis Virus
KARAP	Killer Cell Activating Receptor-Associated Protein
LPS	Lipopolysaccharide
mAb	Monoclonal Antibody
MALT1	Mucosa-Associated Lymphoid Tissue Lymphoma Translocation Protein 1
$Man_8GlcNAc_2$	Mannos e_8 N-Acetylglucosamine$_2$
$Man_9GlcNAc_2$	Mannose$_9$ N-Acetylglucosamine$_2$
MAP kinase	Mitogen-Activated Protein Kinase
MCA1	Metacaspase 1
MCC	Mucocutaneous Candidiasis Syndromes
MDL-1	Myeloid DAP12-Associating Lectin-1
MHC II	Major Histocompatibility Complex Class II
Mincle	Macrophage-Inducible C-Type Lectin
miRNAs	MicroRNAs
mRNA	Messenger RNA
MyD88	Myeloid Differentiation Primary Response 88
NADPH	Nicotinamide Adenine Dinucleotide Phosphate
NETs	Neutrophil Extracellular Traps
NF-κB	Nuclear Factor Kappa-Light-Chain-Enhancer of Activated B Cells
NK	Natural Killer

NLRP	NOD-Like Receptor Pyrin Domain-Containing
NLRs	NOD-Like Receptors
Nrg1	Negative Regulator Gene 1
OPC	Oropharyngeal Candidiasis
PAMPs	Pathogen-Associated Molecule Patterns
PBMCs	Peripheral Blood Mononuclear Cells
PI3K	Phosphoinositide 3-Kinase
PKC	Protein Kinase C
PKCδ	Protein Kinase Cδ
pDCs	Plasmacytoid Dendritic Cells
PRRs	Pattern Recognition Receptors
RAF1	Rapidly Accelerated Fibrosarcoma 1
RASGRF-1	Ras Protein-Specific Guanine Nucleotide-Releasing Factor 1
Rfg1	Repressor Of Filamentous Growth 1
RIG-I	RIG-I-Like Receptors
RLRs	RIG-I-Like Receptors
ROS	Reactive Oxygen Species
SAP	SLAM-Associated Protein Family
SFKs	Src Family Kinases
SIGNR1	Specific Intercellular Adhesion Molecule-Grabbing Non-Integrin Receptor 1
SSI	Surgical Site Infections
ssDNA	Single-Stranded DNA
ssRNA	Single-Stranded RNA
STAT5	Signal Transducer and activator of Transcription 5
Syk	Spleen Tyrosine Kinase
TAK1	TGF-β-Activated Kinase 1
TEMs	Tetraspanin-Enriched Microdomains
TCR	T Cell Receptor
TGF-β	Transforming Growth Factor β
Th1	T Helper Type 1
Th17	T Helper Type 17
Th2	T Helper Type 2
Thr231	Threonine 23
TLRs	Toll-Like Receptors

TNF-α	Tumour Necrosis Factor α
TRAF6	TNF Receptor-Associated Factor 6
Treg	T Regulatory T-Cell
Tup1	Transcriptional Repressor Protein 1

Chapter 1
General Introduction

1. Introduction

1.1. *C. albicans* Biology and Significance

1.1.1. Overview of Fungal Infections

Fungal infections are a major public health risk linked to potentially fatal mycoses in susceptible patients, such as those with HIV or COVID-19 [1]. Depending on their severity, fungal infections can be superficial, cutaneous, subcutaneous, mucosal, or systemic. The human microbiota includes organisms like *Candida* spp. that can cause serious damage and potentially fatal infections in immunocompromised patients, like HIV patients, cancer patients undergoing chemotherapy, and patients taking immunosuppressive medications, as well as opportunistic infections in healthy individuals [2]. In addition to systemic and opportunistic illnesses, *Moulds, Aspergillus, Fusarium, Mucorales* and *Candida* are examples of fungal pathogens that can result in healthcare-associated illnesses (HAI) in individuals with underlying medical conditions [3].

1.1.2. Nosocomial infections related to fungal infections

HAI occur at healthcare institutions and are particularly prevalent in immunocompromised patients, patients hospitalised for prolonged periods of time suffering from chronic diseases and post-surgery wounded patients. The central issue of these infections is their high rate of morbidity and mortality, in addition to the elevated treatment and hospitalisation costs. Fungi such as *Candida* cause mild to severe HAI infections involving surgical sites (SSI) or wounds, as well as central line-associated bloodstream infections, catheter-associated urinary tract infections, and ventilator-associated pneumonia [4]. Despite advances in preventive treatments, biofilm formation on wounds promotes chronic wound infections, and it is one of the most prevalent adverse outcomes in hospitalised patients undergoing surgery or outpatient surgical procedures. Chronic wound infection is the most frequent postoperative surgical complication, is associated with high morbidity and mortality rates, and causes extensive strain on national budgets and individual patients. Fungal biofilms are highly resistant to antifungal drugs [5]. *Candida* species are the most prevalent infectious agent among all other fungi and cause about 8% of nosocomial infections. As an opportunistic organism, *Candida* can transition from being part of the commensal flora to a pathogenic state due to various factors such as pH variation, which can cause local infections in the skin and mucosa or systemic

infections, including those in the liver and kidneys [6]. The physiological pH is maintained by the human body to stabilise internal balance, which is essential for preserving homeostasis [7]. Under some clinical conditions, the body's pH may become more acidic, causing health problems and disruptions in one or more body parts. This could involve metabolic disorders like diabetes mellitus, which is a severe, complex metabolic condition of the human body that causes the blood to become more acidic due to free radicals and glucose [8]. Vaginal or oral pH shift that might occur in order of antibiotics administration [9]. In addition to the activity of effector immune cells that are responsible for acidifying infected tissues during inflammation [10].

Among ~200 recognised species of the genus Candida, *Candida albicans (C. albicans)* is the most predominant source of nosocomial systemic infections worldwide, accounting for ~80%, with a mortality rate of around 40% [11]. The genus *Candida* also *includes* other species that can cause infections in humans, such as *C. glabrata, C. tropicalis, C. parapsilosis,* and *C. krusei*; however, *C. albicans* is the most virulent one [6]. Concerns about the impact of antifungal resistance in invasive candidiasis (IC) patients are increasing. IC is one of the leading causes of death for patients with impaired immune systems. Although cases of antifungal resistance in HIV patients receiving fluconazole treatment for oral candidiasis and echinocandin resistance in cases of *C. albicans* oesophagitis are documented, resistance to antifungals in *C. albicans* is currently thought to be uncommon but, increasing [12]. Nevertheless, to better understand resistance mechanisms, prevalence, and clinical repercussions in *C. albicans* infections, ongoing surveillance and additional studies are clearly necessary, given the possibility of increasing resistance and its impact on treatment efficacy.

1.1.3. *C. albicans* pathogenicity across different body sites

As a benign commensal, *C. albicans* commonly lives on healthy people's oral, vaginal, and gastrointestinal mucosa [13]. However, if the immune system is impaired, the local microbiota is disturbed, or normal tissue barriers are compromised, this fungus can lead to infection. Different host body sites might be infected with *C. albicans,* causing superficial or deep tissue infections (Figure 1.1) [14].

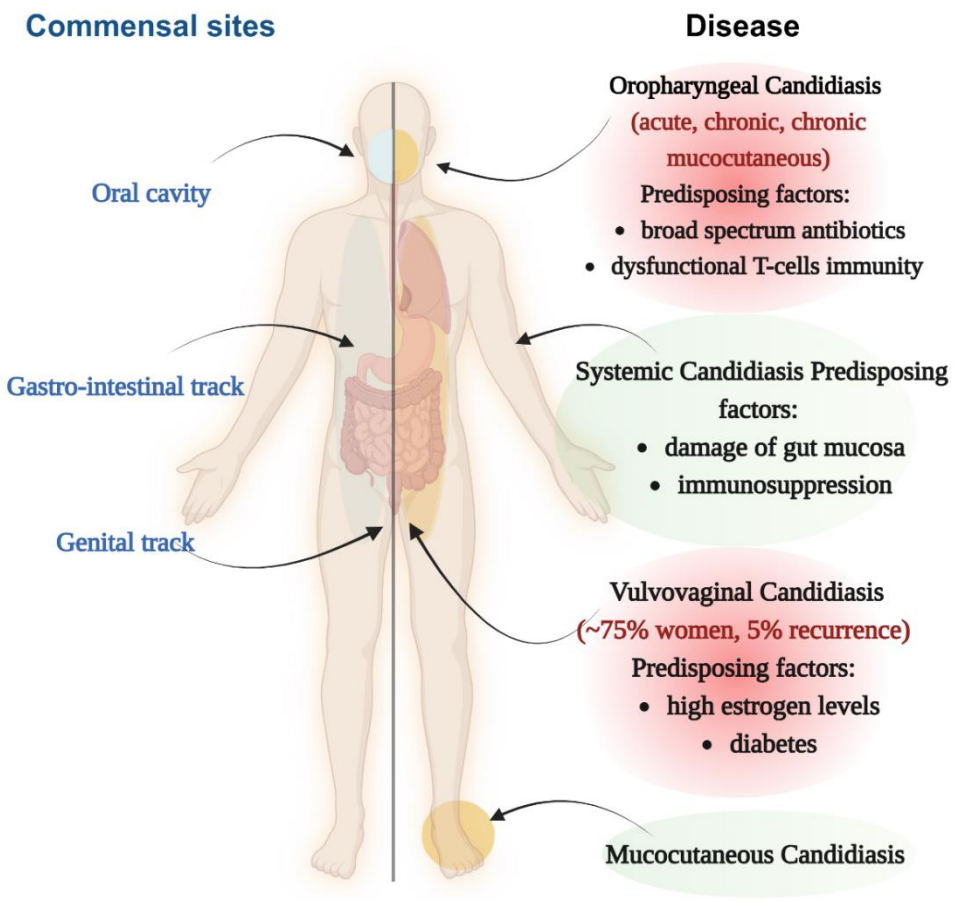

Figure 1.1. The human body's commensal and disease-causing sites for *C. albicans*. The vaginal system, gastrointestinal tract, and oral cavity are locations of *C. albicans* commensalism (left side). *C. albicans* can cause vulvovaginal or oropharyngeal candidiasis by infecting these locations (right side). As a result of *C. albicans* moving from the gastrointestinal track into the bloodstream, it can also result in systemic infections of the blood and internal organs. Additionally, *C. albicans* causes skin and nail mucocutaneous infections [14]. Created using BioRender.

Oral infections

Oral cavity infection by *C. albicans* is the most common local infection, primarily caused by poor oral hygiene, smoking, or the use of orthodontic appliances. Other factors such as age, pregnancy and diseases like cancer and chronic diseases like diabetes can also predispose to oral infections [15]. According to Vila *et al*, oropharyngeal candidiasis (OPC) can be broadly divided into three conditions: acute, chronic, and chronic mucocutaneous candidiasis syndromes (MCC). Predisposing variables include smoking, wearing dentures, local dysbiosis, salivary hypofunction, dietary inadequacies, and malfunctioning T-cell immunity resulting from infections or genetic mutations. In fact, OPC is the most common oral opportunistic infection in people with HIV. Broad-spectrum antibiotics are often the cause of acute cases [16].

Skin infections

C. albicans commonly causes skin infections, especially in folded areas such as pannus folds and inguinal folds in overweight individuals, patients under antibiotic treatment or post-surgery patients. *C. albicans* typically causes superficial skin infections; "deep" mycoses, where *C. albicans* affects the dermis and subcutis, are uncommon. An invasive fungal infection, on the other hand, can happen in people with impaired immune systems, leading to deep penetration and systemic candidiasis, which frequently has deadly consequences [17].

Genital tract infections

About 15–30% of women who do not have any symptoms are vaginal carriers of *Candida* species; during pregnancy, this number increases to 40% [18]. Nearly all women are thought to experience vulvovaginal candidiasis at least once in their lifetime. Balanitis and balanoposthitis are observed in men. The perianal region may also get involved in both sexes. Localised pruritus of the vaginal and perianal areas by itself may indicate candidiasis even in the absence of skin symptoms [19].

Invasive disease

Invasive candidiasis is a bloodstream infection caused by *Candida* species that typically occurs after translocation through the intestinal barrier. For instance, *C. albicans* might spread to the abdominal cavity following surgery and get into the circulation [19].

1.1.4. The biology of *C. albicans*

C. albicans is a diploid, polymorphic fungus that typically lives innocuously as part of the normal human microbiota. It is most commonly found in the yeast form on human mucosal surfaces [20]. As mentioned above, *C. albicans* constitutes a major cause of systemic infections in tertiary healthcare institutions worldwide; a major issue caused by *C. albicans* is invasive candidiasis (IC) [21]. When the environmental balance is impaired, such as during tissue stress, nutrient limitation, high temperatures, or pH changes, *C. albicans* can become pathogenic and cause severe diseases [22]. *C. albicans* growth takes different forms during its transition from commensal to pathogenic states, starting originally as a unicellular yeast and forming pseudo-hyphae, which then develop into hyphae —the highly infectious, penetrating-damaging form (Figure 1.2) [23].

a.

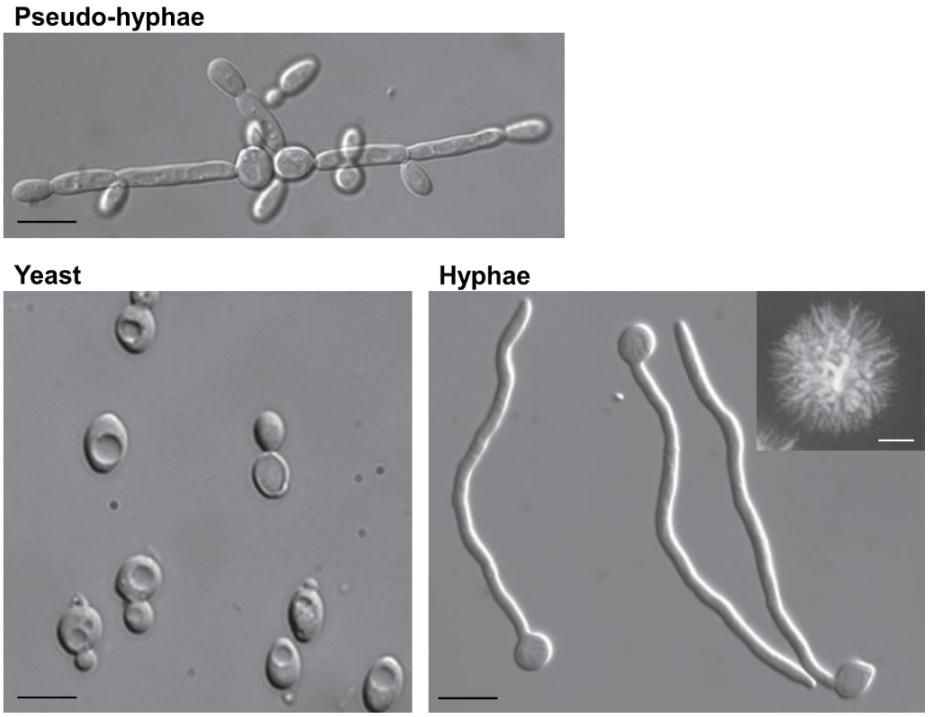
Pseudo-hyphae
Yeast
Hyphae

b.

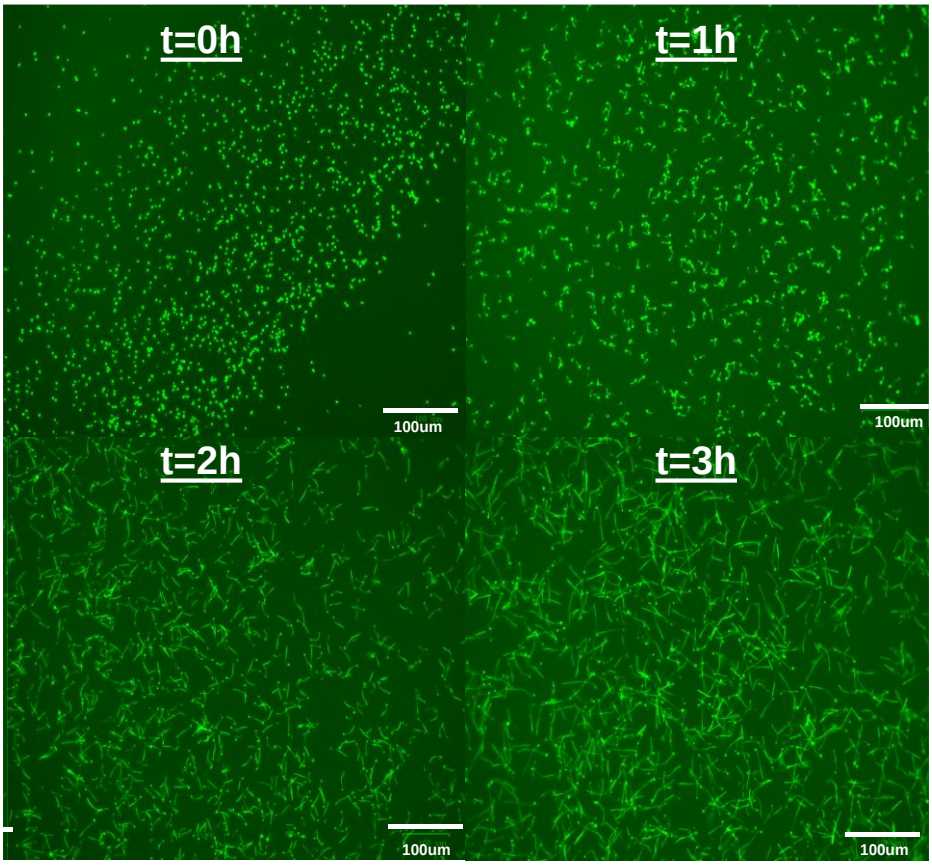
t=0h
t=1h
t=2h
t=3h
100um
100um
100um
100um

Figure 1.2. *C. albicans* morphology from yeast to hyphae. **a**. The figure illustrates yeast form (down, left) growing into pseudo-hyphae (upper image), then a complete growth of hyphae (down, right), figures from [24]. **b. GFP** *C. albicans* cultured in RPMI supplemented with human serum in 3 h demonstrated yeast cells at time of culture, then hyphae starts to grow the first hour, elongated through the second to the third hour. Images taken by Zoe microscope at the green channel.

The outcomes of *C. albicans* infections are influenced by the host immune response, anatomical site of infections, and *C. albicans* virulence, including hyphal morphology and hyphal-specific gene expression [21]. *C. albicans* hyphae can penetrate mucosal surfaces, causing infections that damages the underlying tissue. If it progresses to the point where the fungus gains access to the host's vasculature, it can spread throughout the body. In addition, many fungal infections are caused by the use of indwelling medical devices, such as intravenous lines, catheters, and drains, which circumvent the physical barrier of the mucosal surface, allowing access to the bloodstream [25, 26].

Three distinct and dynamic stages can be distinguished during *C. albicans* infections: adhesion, invasion, and tissue damage, all of which trigger the onset of inflammation [27]. Central to these processes is the yeast cell wall, which is composed of approximately 90% carbohydrate and 10% protein, and plays a critical role in host-pathogen interactions and immune activation [28]. The cell wall has two layers: the outer layer is composed of a substantial amount of glycoprotein, specifically a mannose-rich layer (mannan), and the inner layer is made of chitin, which increases wall integrity [29]. This results in the formation of a solid structure that helps preserve the organism's shape [30]. The most stimulatory part of *C. albicans* cell wall is the β-glucan, which sits below the outer structure of the cell wall as a mechanism to avoid immune recognition by the immune system (Figure 2) [31]. β-glucan is the most important molecular pattern associated with fungal pathogens and a key structural element of the fungal cell wall [32]. It is also an important proinflammatory mediator, and circumstances that increase its exposure at the cell surface increase the quantity of proinflammatory cytokines produced [33]. When β-glucan is absent or hidden within the fungal cell wall, the immune system struggles to detect this pathogen, allowing the fungus to escape immune responses and potentially cause more persistent infections [34].

The innate immune system recognises *C. albicans* yeast and hyphae in different ways because the composition of their cell wall varies between the two forms [35]. The primary distinction between the hyphal and yeast forms is that the hyphal wall contains slightly more chitin than the yeast form [36]. In addition, the

structure of cell wall mannans varies between the yeast and hyphal forms, with the hyphal form showing a noticeable reduction in β-1,2 manno-oligosaccharides with hidden β-glucan to avoid recognition (Figure 1.3) [37].

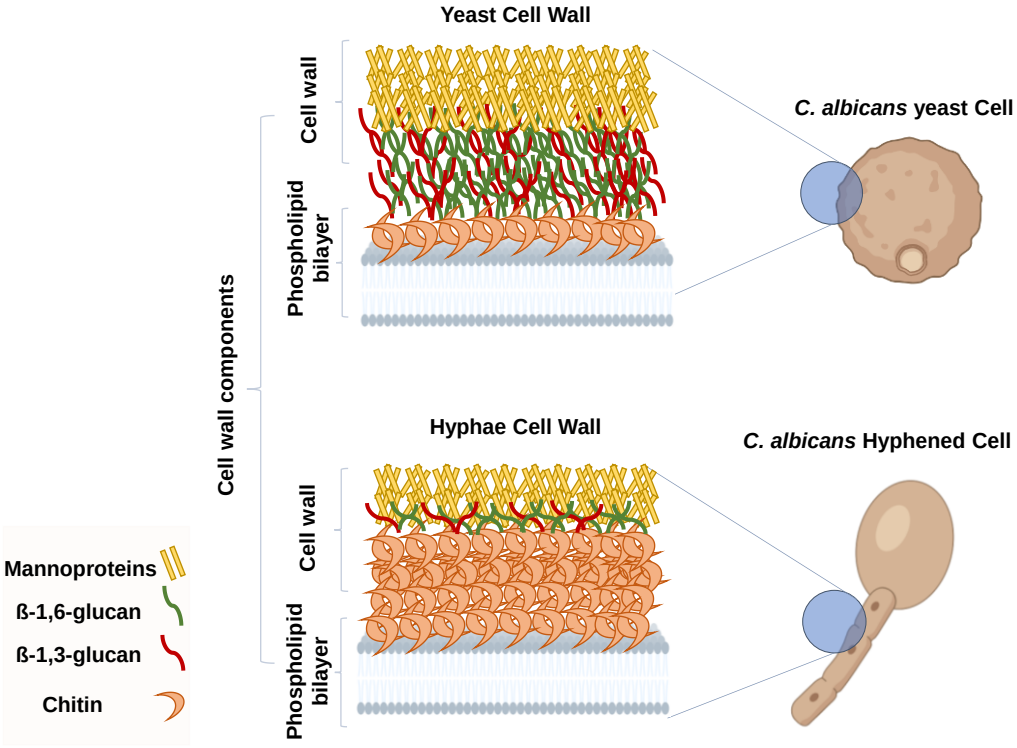

Figure 1.3. *C. albicans* cell wall composition. The cell wall plays a crucial role in providing structural integrity. The main constituents of the cell wall include Chitin, β-Glucans, and Mannoproteins. Adopted from [38]. Created by BioRender.

1.1.5. Hypha initiation, elongation and directionality maintenance

The transition from yeast to hyphae determines whether *C. albicans* remains a harmless commensal or becomes a pathogen capable of infecting tissues, attaching to host cells, escaping immune cells like macrophages, and forming biofilms that are often seen in clinical infections [39]. Hyphae also produce surface proteins that allow them to bind to and enter host cells, form protective biofilms, sense and respond to their surroundings (a behaviour called thigmotropism), they release enzymes that break down host tissue. These processes are controlled by genes that are switched on during either hyphal growth or the transition phase. Several key signalling pathways regulate hyphae initiation, including the MAP kinase pathway (via Cph1) and the cAMP-PKA pathway (via Efg1). At the same time, transcriptional repressors like Tup1and Nrg1 shut down yeast-specific genes, helping to preserve the hyphal state [20].

Once hyphal development is triggered, the elongation process starts (Figure 1.2.b). Here, other pathways remain active to sustain the process. These maintain cytoskeletal changes, direct the cell to grow in a polarised way, and activate more genes involved in tissue invasion. During this elongation phase, specific hyphal proteins, such as Hwp1 and Als3, are highly expressed. These proteins play key roles in helping the fungus adhere to and invade host cells (Figure 1.4) [40].

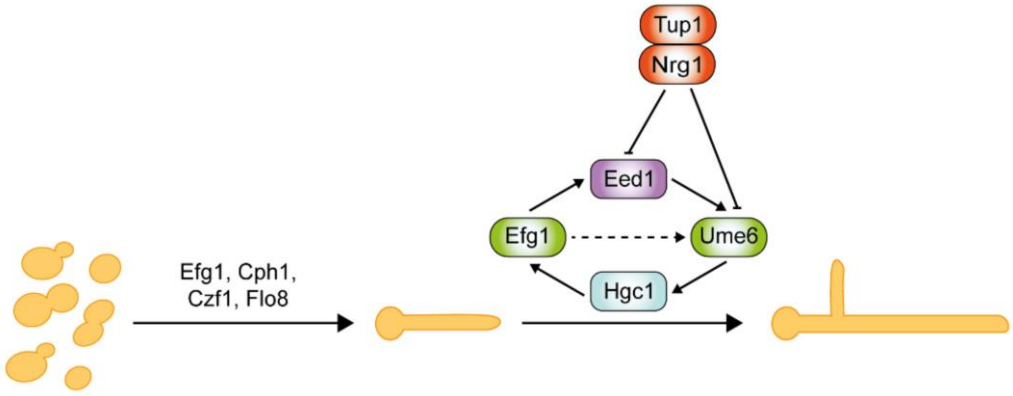

Figure 1.4. Initiation and elongation maintenance mechanisms are essential for regulating hyphal formation and elongation in *C. albicans*. Transcription factors, including Efg1, Cph1, Czf1, and Flo8, are necessary for the initiation of hypha growth. Hgc1, Eed1, and Ume6 are essential for subsequent elongation and maintenance processes. Tup1 and Nrg1 adversely regulate both Eed1 and Ume6 [40].

In mucosal infections, the hyphal forms of the fungus penetrate and destroy endothelial and epithelial cells by releasing hydrolytic enzymes. For *C. albicans* to cause bloodstream infections (candidaemia), it first needs to cross the mucosal barriers to reach the blood and then break through the endothelial lining to spread and infect internal organs. *In vitro* research using both reconstituted epithelia and endothelia demonstrates that the hyphal form is particularly invasive [41]. Furthermore, biopsy samples from mucosal infection patients reveal that epithelial cells only contain hyphal forms [24]. Moreover, yeast cells escape phagocytosis by macrophages by transforming into the hyphal form [42]. Antifungal medications can reduce *C. albicans* infections; however, resistance to these medications becomes frequent. Interestingly, growing hyphae can protect *C. albicans* against antifungal drugs like amphotericin B by inhibiting some effector proteins, such as Metacaspase 1 (MCA1), which mediates fungal cell death [43].

1.1.6. *C. albicans* biofilm formation

Biofilms are intricate three-dimensional formations made up of a community of core microbial cells (either a single species or a mixed species) attached to abiotic surfaces or host tissue and embedded in an extracellular polysaccharide material (EPS) that protects the microorganism (fungi, bacteria or both) from immune attack and/or antimicrobials [44]. The phenotype of biofilm cells differs from that of planktonic cells and underpins high resistance to drugs and the ability to cause chronic infections [45]. For example, the pathogenicity of *C. albicans* depends on the SLAM-associated protein family (SAP) (SAP1–SAP10), which binds to the epithelium of host tissue and degrades host tissue proteins. Secreted proteases such as aspartyl proteases (SAP5-SAP6), which are only elevated in the yeast form growing in biofilms, are not upregulated in planktonic cells (yeast or hyphae). Resulting in distinct proteolytic cleavage patterns for each growth state [46].

Another important feature of biofilms is that they tend to create an ecosystem comprising two or more species of microorganisms, including multiple bacterial and/or fungal species [47]. For example, *C. albicans* is typically observed in mixed infections with *Pseudomonas aeruginosa*, particularly in the lungs of patients with cystic fibrosis (CF) [48]. Multispecies biofilms facilitate the cohabitation of microbial species, promoting a viable and successful interaction. However, due to the high competition between organisms within the biofilm matrix for nutrients, organisms develop mechanisms to eliminate competitive interactions and establish a stable interaction through co-metabolism and synergistic social behaviours [45]. Biofilm generation is one of the primary virulence factors that contribute to the pathophysiology of candidiasis because it complicates therapy and raises rates of morbidity and mortality [49]. *In vitro* experiments revealed that biofilm formation occurs in a sequence of successive phases over a 24-48-hour period. The four primary phases of the *C. albicans* biofilm growth process are adhesion, proliferation, maturation, and dispersion (Figure 1.5) [50].

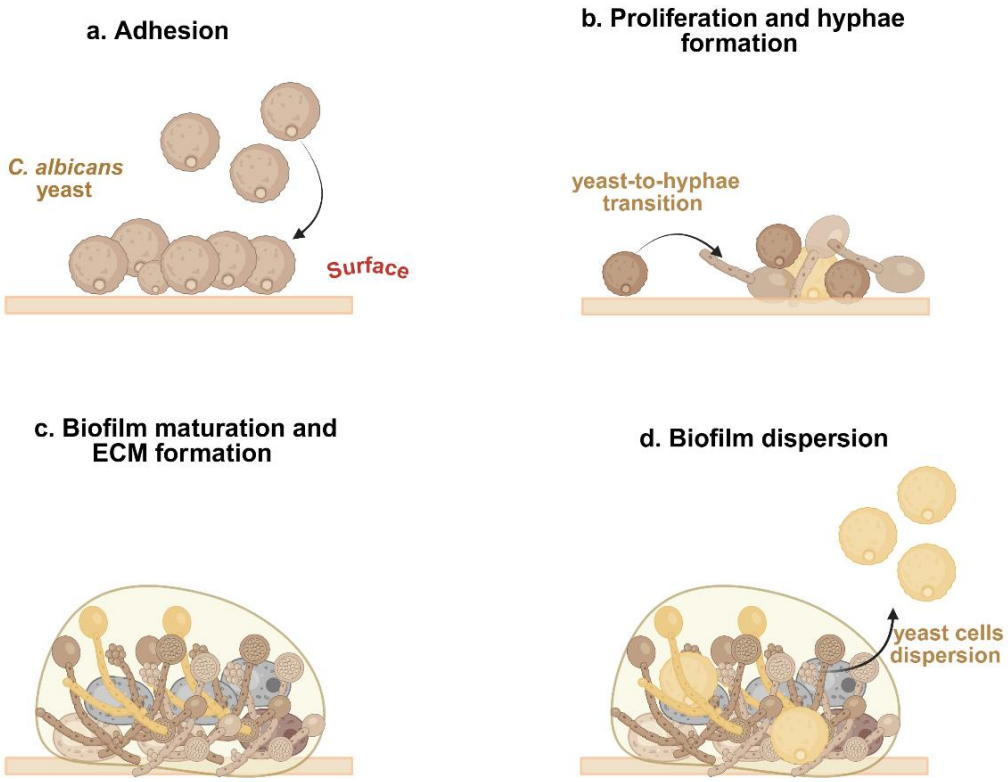

Figure 1.5. Biofilm formation stages in *C. albicans*. yeasts **a.** Initiated by cellular adhesion of *C. albica*ns yeasts **b.** followed by microcolony cellular proliferation and maturation (mix of yeast and hyphal form cells) **c.** then formation of complex cell aggregates when extracellular matrix material rich in polysaccharides, proteins, lipids, and eDNA. **d.** that starts to disperse. Adopted from [51]. Created using BioRender.

During the adhesion phase, yeast cells adhere to a substrate, forming a basal layer that is crucial for biofilm initiation. The presence of naturally existing extracellular DNA (eDNA) and the deposition of material by non-adhering or detached bacteria have also been shown to boost the rate of fungal cell adhesion [52]. Adhesion is followed by the proliferation stage, when attached cells start to form filamentous hyphae and release hydrolytic enzymes such as phospholipases and proteases, which aid in tissue penetration and subsequent growth. During the dispersion stage, yeast cells are liberated from the mature biofilm. This enables them to enter the bloodstream, colonise other locations, or form new biofilms, helping the spread of the infection and making therapy more difficult. Cells of the dispersed population exhibit upregulated characteristics to adapt to a new, nutrient-rich environment distinct from that of the planktonic phenotype (Figure 1.5) [51].

1.1.7. Therapeutic strategies targeting *C. albicans* infections

Current antifungals are incredibly limited in comparison to the vast diversity of antibiotics, which have many recognised classes and multiple mechanisms of action against bacterial targets [53]. The majority of fungal infections are treated with just four major kinds of antifungal medications: azole derivatives, polyenes, echinocandins, and nucleoside analogues [54].

Azole derivatives like fluconazole, clotrimazole, miconazole and ketoconazole inhibit the synthesis of ergosterol (a key component of fungal cell walls) by binding to the haem group of the cytochrome P450 enzyme lanosterol 14α-demethylase via the nitrogen atom in their azole ring. When this enzyme is blocked, toxic methylation intermediates accumulate, and the amount of ergosterol in the membrane decreases. This disrupts the function of the fungal cell membrane, inhibits growth, and occasionally causes cell death (Figure 1.6.a) [55].

The fungicides polyenes (nystatin and amphotericin B) are naturally occurring substances that have a heterocyclic amphipathic structure, meaning that one side is hydrophilic and the other is hydrophobic. They target ergosterol in the fungal membrane, where they penetrate the lipid bilayer and form holes that compromise the membrane's integrity, killing the cell (Figure 1.6.b) [56].

The third type of treatment for IC infections is echinocandins [57]. These substances work against yeasts *in vitro* as fungicides. Three agents, caspofungin, micafungin, and anidulafungin, are now approved for clinical use. They prevent the activity of β-(1,3) glucan, the most stimulatory part of the *C. albicans'* cell wall. They exhibit fungistatic action and block the β-(1,3) glucan synthase enzyme, which is encoded by genes in the fungal kexin-like subunit (FKS) family and is necessary for the synthesis of β-(1,3) glucan in the cell walls (Figure 1.6.c) [56].

The last group of antifungal agents is the nucleoside analogues (pyrimidine analogues). The most widely used for treating candidiasis is 5-flucytosine (5-FC, a fluoropyrimidine). 5-FC is the only member of this class that enters fungal cells via cytosine transporters. Inside the cell, 5-FC is then converted by the pyrimidine rescue pathway into 5-fluorouracil (5-FU), which is considered to be the active form of 5-FC. 5-FU inhibits the action of thymidylate synthase, an enzyme necessary for DNA synthesis, resulting in premature chain termination (Figure 1.6.c) [58].

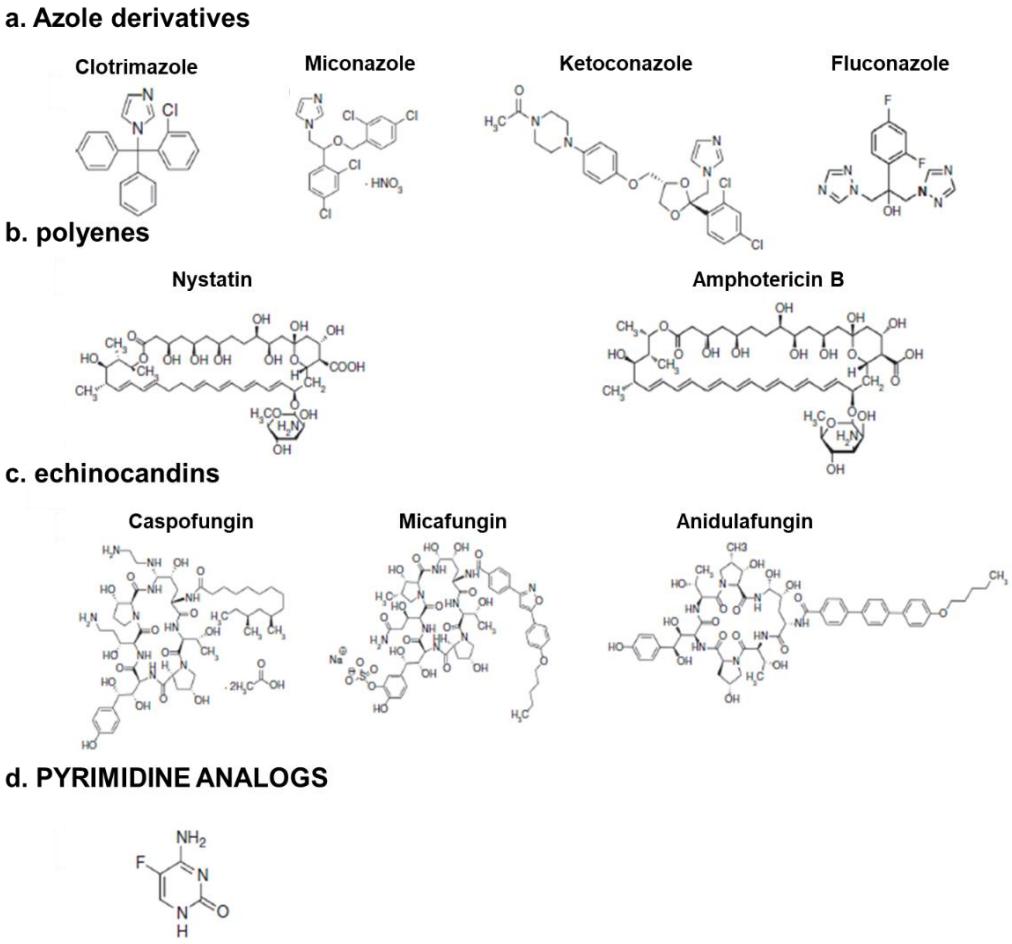

Figure 1.6. Chemical structure of the antifungals currently on the market. a. azole derivatives, b. polyenes, c. echinocandins, and d. PYRIMIDINE ANALOGS [51].

1.1.8. Resistance to antifungals: an obstacle to treating fungal infections

Fungal pathogens are becoming increasingly resistant to current antifungal medications, which poses a new clinical challenge [59]. The increase in resistance is influenced by host, fungal, and environmental factors and is fuelled by chromosomal aneuploidy, sexual reproduction, horizontal gene transfer, phenotypic plasticity, and alterations in target genes, all of which undergo natural selection [60]. For example, resistance to azoles is mediated by overexpression of ABC (ATP-binding cassette) transporters, the MFS (major facilitator superfamily) class of efflux pumps, mutations in the Cyp51 or ERG11 genes that result in modified target enzymes with a low or no affinity for azole medications, and overexpression of the ERG11 enzyme [59]. The main resistance mechanisms that fungi exhibit are compiled in Figure 1.7. Higher resistance to antifungals is also conferred by biofilm formation by *Candida* spp. on medical devices and tissues [61]. Treating fungal infections with antifungal medications in the case of biofilms is challenging because of the resistance to

the conventional therapy, interrelated mechanisms such as limited drug penetration, shifting metabolic activity, and cell population persistence, which make it difficult to eradicate [62]. Therefore, using natural compounds to modulate immune response in cases of fungal infection has the potential to enhance host-directed therapies and improve the physiological compatibility.

In conclusion, *C. albicans* is a fungus with a complex pathogenesis process, ultimately leading to infections. The yeast, pseudo-hyphae and hyphal forms of *C. albicans* require different recognition mechanisms and are responsible for different immune responses by the innate and adaptive immune systems [63].

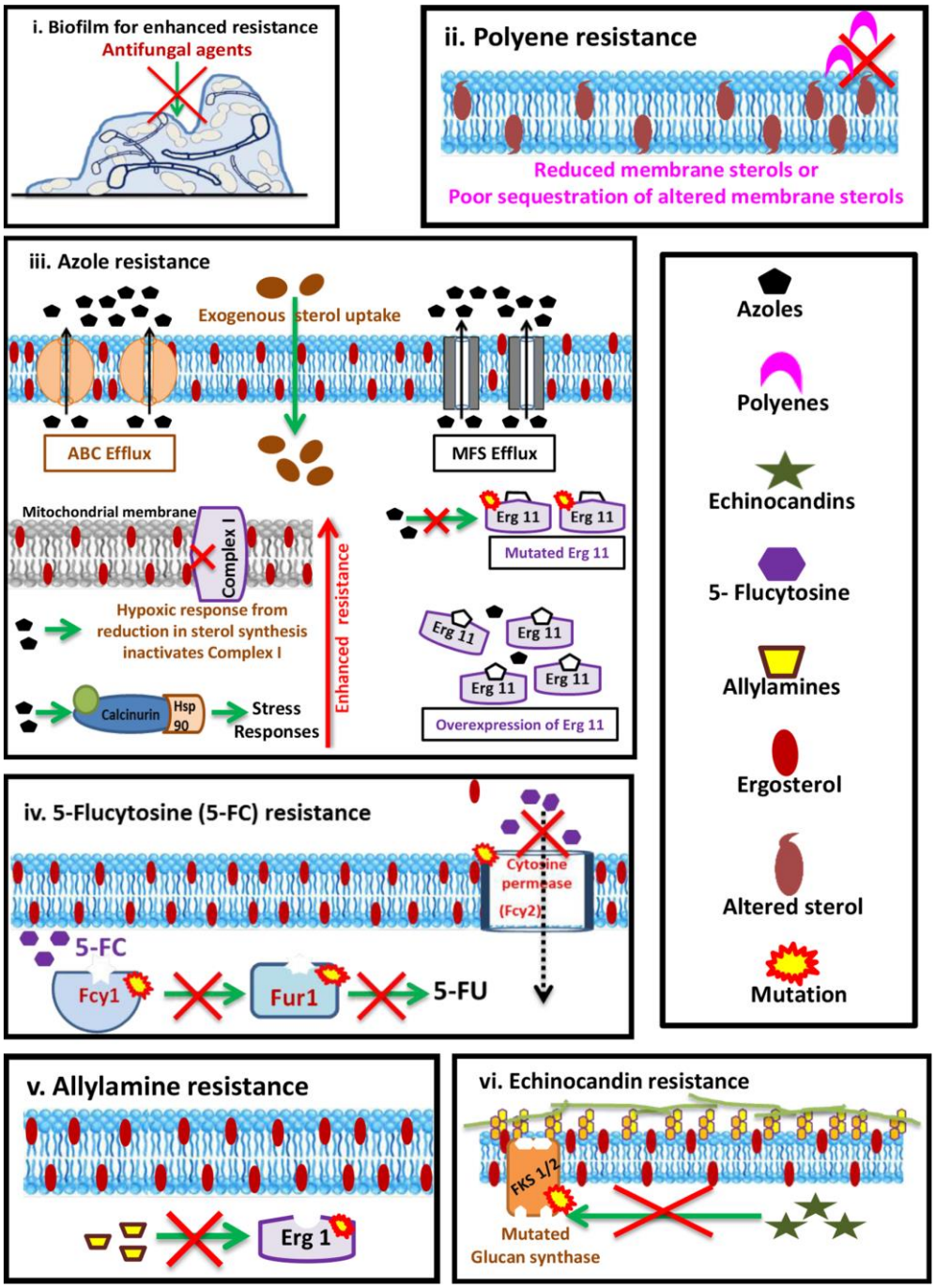

Figure 1.7. Key mechanisms of resistance to popular antifungal medications. i. biofilm resistance, ii. Polyene resistance, iii. Azole resistance, iv. 5-FC resistance, v. allylamine resistance. vi. Echinocandin resistance. From [61].

1.2. Immune responses to *C. albicans* infections

The immune system provides an integral defence against pathogens such as viruses, bacteria, and fungi like *C. albicans*. It recognises pathogens through multiple different recognition molecules, such as pattern recognition receptors (PRRs) and has discrimination mechanisms to differentiate between foreign and self-antigens, thereby preventing autoimmune or allergic diseases [64]. When *C. albicans* starts to spread within tissues, causing infections, the host organism activates its immunity to first recognise and then eradicate the infections [65].

Skin is the first line of defence as a physical barrier. It contains layers, such as the epidermis, that contain keratinocytes, making microbial penetration difficult [66]. Tight junctions, which help to protect the body against infections and provide a controlled barrier around endothelial and epithelial cells to prevent pathogens' entry between the cells [67]. Secreted fluids from various body parts, such as mucus membranes along the respiratory and reproductive tracts, saliva, and tears, all release enzymes (such as lysozyme) to destroy pathogens. The lipids secreted from the oil glands of the skin inhibit microbial growth [68]. Cilia that line the airways help in transporting pathogens out of the body [69]. In addition, secreted chemicals at barrier sites such as acids in the stomach, vagina and skin inhibit the growth of microorganisms [68].

If *C. albicans* breaches one of these barriers, innate immune components in tissues will collaborate to recognise and destroy this pathogen. There are two main components of the immune system: the innate system, which activates rapidly to recognise the pathogen and restrict its growth [70]. The other component is the adaptive system, which is characterised by a slow response, variable and selectively specified, that takes days to weeks to be fully activated and provide long-term immunity (Figure 1.8) [71].

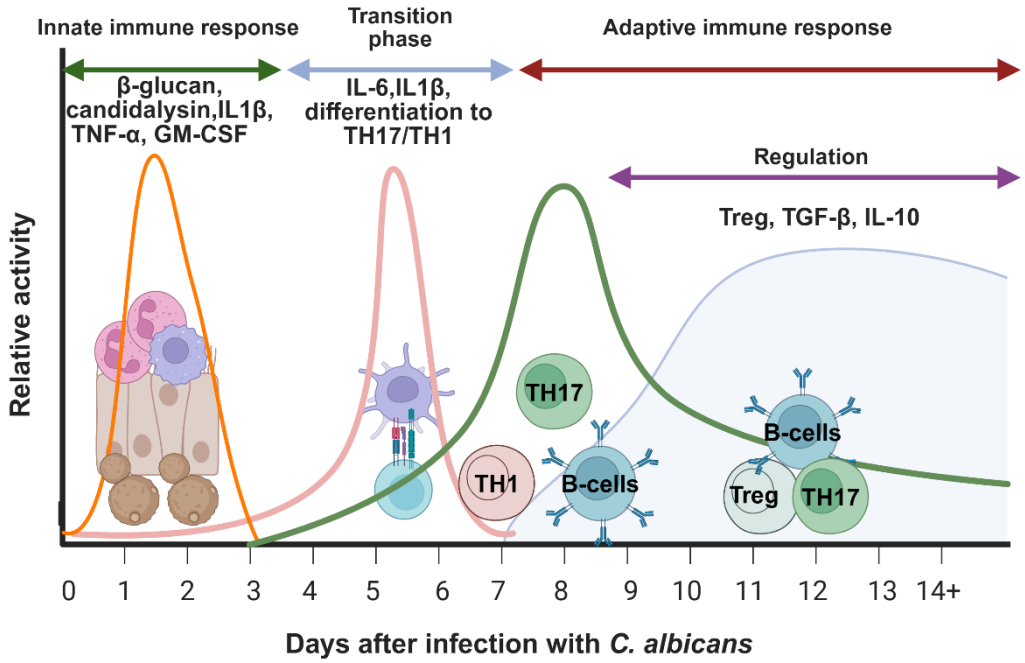

Figure 1.8. Innate and adaptive immune responses during acute fungal infections. Day (0-~3) rapid recognition of fungal PAMPs like β-glucan and proteolytic enzymes by innate immune cells (epithelium, neutrophils, macrophages and NK cells). Day (3-7) initiation of the adaptive phase activated DCs present antigens in lymph nodes to T cells, differentiation of CD4 T cells into Th17 and Th1, and secretion of cytokines (IL-23, IL-6 and IL-1β). Day (7-14+) Th17 cells (producers of IL-17A/F, IL-22, GM-CSF) enhance neutrophil responses; Th1 cells (producers of IFN-γ) enhance macrophage function; B cells produce IgG/IgA; memory T-cell responses become established within 1–2 weeks. Later stage (around 10 days onward), regulation occurs through Treg cells and immunosuppressive cytokines like TGF-β and IL-10 [72-74]. Created using BioRender.

1.2.1. Innate immunity to *C. albicans*

Cellular and soluble components of the innate immune system collaborate to sense and control *C. albicans* infections. Epithelial cells, in addition to acting as barriers, sense *C. albicans* infections through PRRs. They function synergistically with resident immune cells or in isolation to trigger an inflammatory response through recognition of pathogen-associated molecule patterns (PAMPs) and damage-associated molecular patterns (DAMPs) [75]. PAMPs are molecules of microbial origin, like β-glucan and lipopolysaccharide (LPS) [76]. DAMPs are endogenous molecules commonly found inside host cells, such as DNA or mitochondrial peptides, released during tissue stress and injury [77]. Detection of PAMPs and DAMPs by PRRs will induce inflammation by promoting proinflammatory cytokines production and recruitment of immune cells to the site of infections [78].

1.2.1.1. The concept of Pattern Recognition Receptors in the innate immune system

PRRs are germline-encoded receptors that recognise different components of microorganisms, including proteins, nucleic acids, carbohydrates, and lipids. They are located either extracellularly, at the cell surface, in endosomes or in the cytosol. The main PRRs that contribute to the recognition of *C. albicans* are C-type lectin receptors (CLRs), Toll-like receptors (TLRs), and NLR family pyrin domain containing 3 (NLRP3) (Figure 1.9) [79], in addition to extracellular soluble pattern recognition molecules (PRMs).

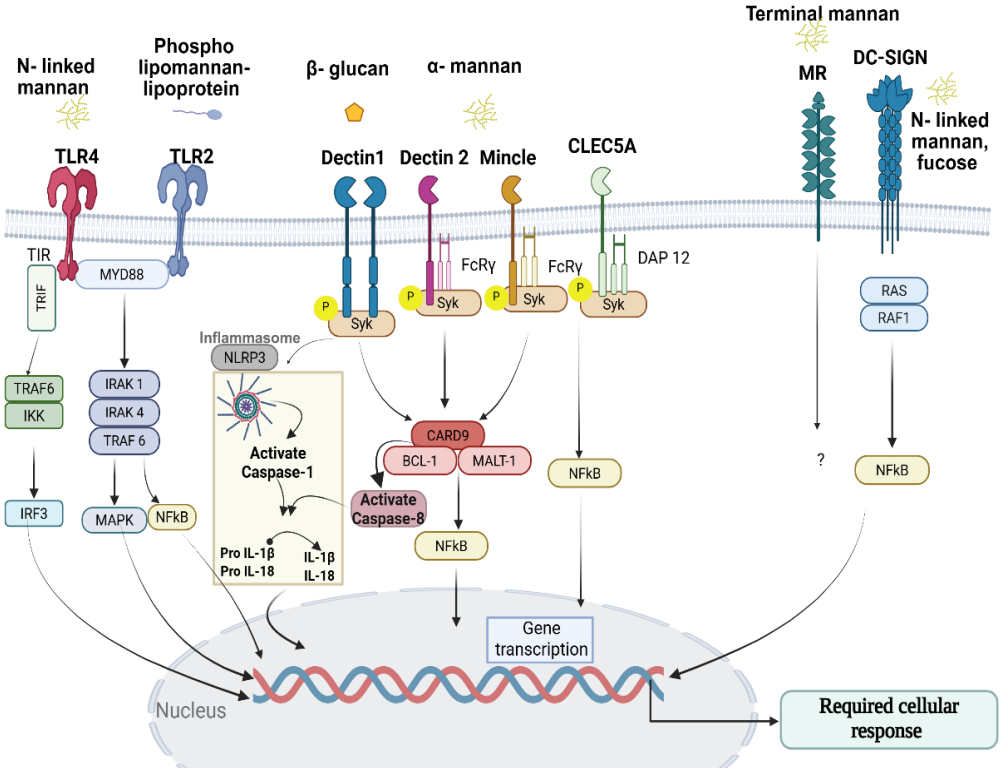

Figure 1.9. **PPRs are involved in the recognition of *C. albicans*.** TLR4 and 2 activate MyD88 to activate IRF3 to release type I IFNs, and IRAK1 pathway to activate NF-kB, which is also activated by endosomal TLR9 that recognises fungal DNA. NF-kB is also activated by RAF1, stimulated by the CLR, DC-SIGN, as well as other CLRs that activate CARD9 through the Syk kinase. NLRP3 forms inflammasome complexes via apoptosis-associated speck-like protein containing a CARD (ASC) with caspase-1 to convert pro-IL1β to the active form IL1β and pro-IL18 to the active form IL18. Additionally, non-canonical inflammasome activation and IL1β generation via caspase-8 are caused by downstream Dectin-1/β-glucan signalling via CARD9 [23, 80]. Created by BioRender.

1.2.1.1.1. Extracellular soluble pattern recognition molecules (PRM)

Extracellular soluble PRMs contribute to the activation of the innate immune response. These molecules are members of a class of soluble receptors that have anti-microbial properties in the blood. Through opsonisation, neutralisation, phagocytosis enhancement, and activation of the complement system, PRMs in the fluid phase are believed to be evolutionary forerunners of antibodies, providing immunological protection and regulation. They also interact with cell-associated PRRs, controlling their activity to synchronise an all-encompassing innate immune response [81].

The complement system is a network of soluble plasma factors, proteases, cleavage products, cell surface receptors, and regulatory protein complexes [82]. *C. albicans* can be recognised by the complement system through different pathways, but mainly via the lectin pathway through the mannose-binding lectins (MBL), which bind to the carbohydrates (mannan) on the surface of *C. albicans*. Additionally, it might activate other pathways like the classical or sometimes the alternative system, for the opsonisation and inflammation [83, 84].

The lectin pathway is activated by foreign carbohydrate structures on surfaces; the alternative pathway is activated by the deposition of spontaneously formed C3b on foreign surfaces, and the classical pathway is primarily induced by the binding of immunoglobulins on target surfaces like IgM and IgG. The covalent deposition of C3-convertase that cleaves C3 into the large C3b fragment and smaller C3a anaphylatoxin is the outcome of all three routes. Depending on the activation pathway, the C3-convertase composition changes (C3bBb for the alternative pathway, C4b2b for the classical and lectin pathways). The newly generated C3b can either form a complex with the existing C3-convertases to produce a C5-convertase, or it can enhance the alternative pathway by producing more C3-convertase molecules. The final pathway's sequence is started by the enzymatic activity of the C5-convertases, which cleaves the complement protein C5 into the C5b fragment and C5a anaphylatoxin. The C5b-9 complex is ultimately produced as a result of protein interaction events. C5b-9, also known as the membrane attack complex (MAC), is inserted into the target membrane and causes the pathogen or modified cell to lyse [84]. Figure 1.10 summarises all three pathways in the initiation of the immune response by opsonisation or activation of the membrane attack complex.

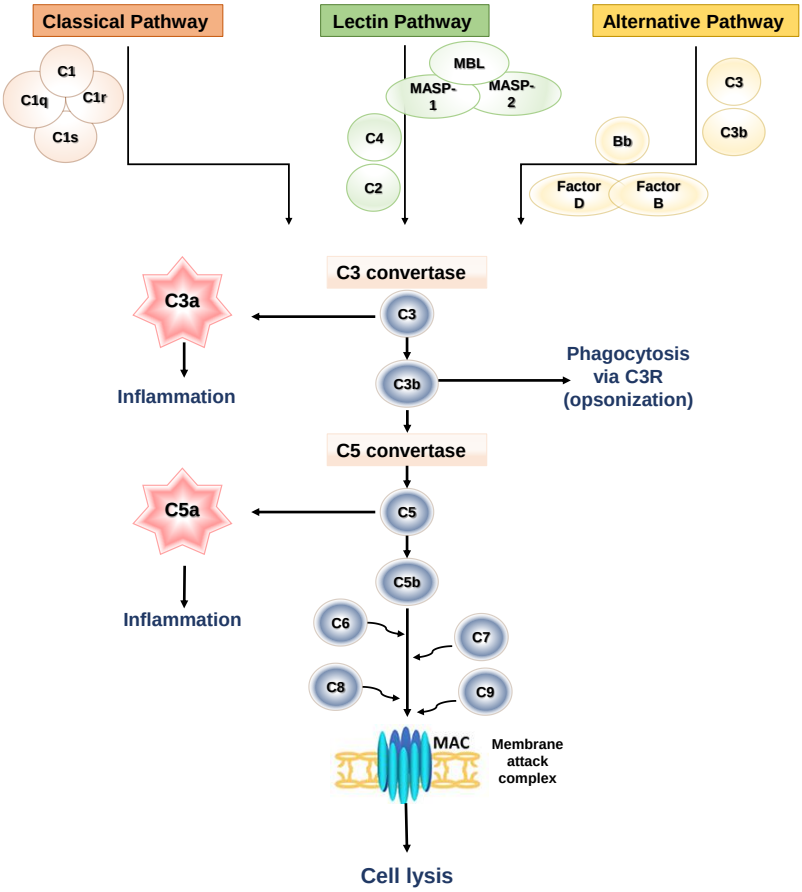

Figure 1.10. Complement system activation. An outline of the pathways that activate the complement system. Adopted from [85]. Created using Microsoft PowerPoint.

Complement receptor 3 (CR3)

CR3 is an integrin composed of the chains CD11b and CD18. Through processes that may or may not be reliant on other complement system elements, CR3 is implicated in leukocyte adherence, phagocytosis, and chemotaxis. CR3 is the most prominent receptor for C3b and iC3b deposition on *C. albicans* surface; it is extensively expressed on professional phagocytes [84]. It has been demonstrated that CR3 binds particles containing β-glucan; hence, it could serve as the main receptor for β-glucan phagocytosis in human neutrophils, unlike murine neutrophils, as they did not require Dectin-1 for β-glucan phagocytosis [86]. CR3 may also serve as a crucial mediator between the innate and adaptive immune systems by performing tasks unrelated to β-glucan detection. It has been demonstrated that during *A. fumigatus* infections, CR3 aids in triggering Th1 and Th17 responses and has also been shown to facilitate complement-dependent phagocytosis by binding to iC3b [87].

1.2.1.2.2. Detection of *C. albicans* by C-type lectin receptors (CLRs)

CLRs, a family of PRRs that recognise carbohydrates, recognise polysaccharide structures from endogenous ligands and microbes by through one or more carbohydrate recognition domains (CRD). The detection of fungi and the activation of the innate antifungal immune response depend heavily on these receptors [75, 88]. In some instances, the sugars and CLRs bind in a way that is reliant on Ca^{2+}. These Ca^{2+}-dependent proteins, based on their molecular makeup, can be classified as either soluble, like MBL, or transmembrane CLRs, such as mannose receptor (MR), Dectin-2, DC-SIGN and Mincle, but not Dectin-1, which is transmembrane and Ca^{2+}-independent [89]. Based on the number of CRD sections and the placement of the N-terminus, the transmembrane CLRs are further separated into two groups, namely type I and type II transmembrane proteins. The soluble CLRs, such as MBL, have an oligomeric protein structure with multiple CRDs that binds to the repeated carbohydrate molecular arrangement found on the pathogen's surface. (Figure 1.11) [90].

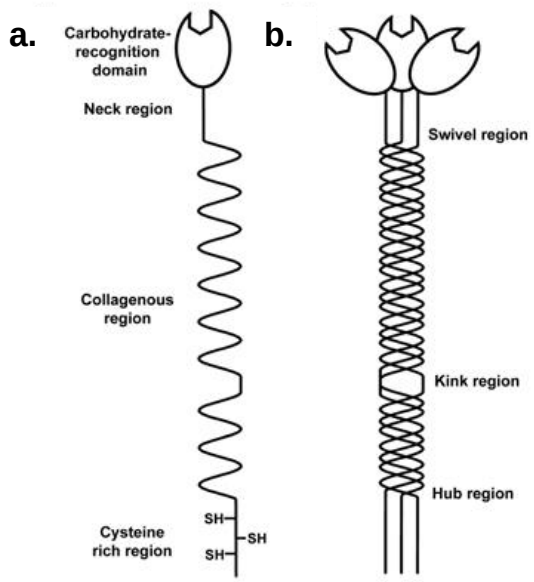

Figure 1.11. MBL structure. a, MBL monomer. MBL polypeptide has a C-terminal carbohydrate recognition domain, a collagenous region, a helical neck region, and an N-terminal cysteine-rich region**. b.** The three polypeptide chains that make up the MBL monomer are identical. The hub region between the N-terminal cysteine-rich region and the collagenous region, the kink region where the triple repeat of the collagenous region is interrupted, and the swivel region, which lies between the neck and collagenous regions, are all possible locations for flexibility in the monomer [91]**.**

On the other hand, membrane receptors CLRs are a big family of receptors composed of type I transmembrane proteins, such as MR (CD206), and type II transmembrane proteins, like Dectin-1 [92]. This family is classified into 17 categories based on functional and structural properties [93]. They all contain one or multiple CRDs; however, they differ in their structural arrangements, cytosolic tails and dependency on adaptor proteins such as FcγR [94, 95].

1. Mannose receptor (MR or CD206)

MR (CD206) is a type I membrane receptor with three different extracellular functional regions [96]. It contains a cysteine-rich (CR) domain at the N terminus that has lectin activity, followed by the fibronectin II (FN-II) domain, and eight tandemly organised C-type lectin-like signalling motifs domains (CTLDs) [97]. The receptor is anchored to the plasma membrane by a transmembrane domain followed by a short cytoplasmic C-terminal tail with no known signalling motifs, but with an endocytic motif that includes a specific sequence (F13ENTLY18) to promote clathrin-mediated internalisation (Figure 1.12) [98].

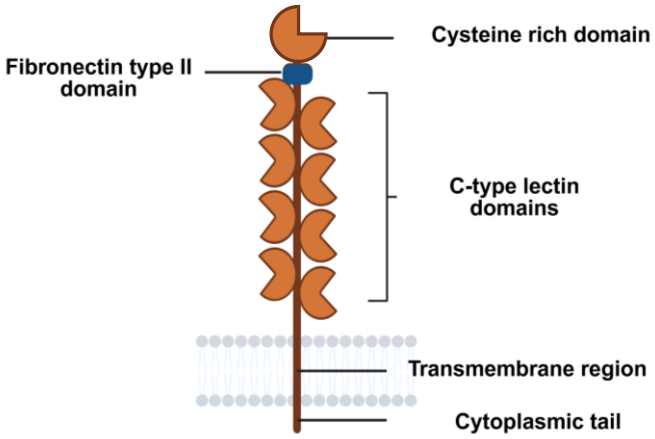

Figure 1.12. MR structure. The MR domain structure comprises a cysteine-rich domain (CR), a fibronectin-like domain (FNII), 8 CTLDs, a transmembrane domain and a short intracellular domain. Adopted from [97]. Created by BioRender.

MR is the only receptor of the MR superfamily that contains a functional CR domain that binds sulfated sugar ligands, particularly sulfated galactose or sulfated N-acetyl-galactosamine (GalNAc), in a calcium-independent manner, the FNII domain binds to collagen [97]. MR is thought to play a non-redundant role in the absorption of collagen by macrophages and in the uptake of collagen by liver endothelial sinusoidal cells [99]. The 8 CTLDs share 30% homology, the degree of homology between human and murine CD206 CTLDs ranges from 76% to 92%, with CRD4 exhibiting the highest similarity [100]. The binding and

endocytosis of sugar ligands needs CTLD4-8, but only CTLD4 has been demonstrated to bind ligands containing mannose, glucose, or N-acetyl-glucosamine on its own, in a Ca^{2+}-dependent manner, with CTLD5 potentially playing a role [97]. However, the rest of the CTLDs are thought to lack sugar-binding activity [101]. It has been proposed that the MR binds to the mannan component of yeast cell walls, contributing to recognition *of C. albicans* [102, 103]. Although the exact cellular pathway mediated by MR has not yet been elucidated, MR supports antifungal mechanisms. For example, when MR recognises fungal mannan, it helps in the secretion of inflammatory cytokines, such as IL-23, IL-1β, and IL-6, which promote IL-17 secretion [104]. However, the $MR^{-/-}$ mouse did not show increased susceptibility to systemic *C. albicans* infection [105]. Additionally, MR is not an essential receptor for activating phagocytosis on its own; it was suggested that it functions in conjunction with other receptors, such as TLR2 or Dectin-1, to activate phagosome formation [106]. Heinsbroek et al. also showed that MR and Dectin-1 cooperate to recognise *C. albicans,* but that Dectin-1 is the only receptor that triggers phagocytosis. MR participates in the subsequent sampling of phagosomes and the release of cytokines [107]. As mentioned above, the cytoplasmic tail of MR lacks signalling motifs, yet it contains a sequence that promotes clathrin-mediated cell internalisation. According to early research by Schweizer et al., an aromatic motif composed of tryptophan and phenylalanine, Y18-F19, mediates endocytosis. Notably, internalisation and endosomal sorting depend on the cytosolic tail Y18, a tyrosine residue, which exhibits overlapping signals in these two successive processes [97]. Further information on this receptor is discussed in (Chapter 5, Mannose Receptor Inhibition as a Strategy to Modulate Monocyte Immune Function During Fungal Infections).

2. DC-SIGN

Dendritic Cell-Specific Intercellular adhesion molecule-3-Grabbing Non-integrin (DC-SIGN) is a type II transmembrane human CLR receptor expressed mainly on the surface of DCs. It has a high affinity for glycans containing fucose/mannose [108]. DC-SIGN is a Ca^{2+}-dependent lectin that functions as a receptor for pathogen identification and cell adhesion. The CRD, which binds high-mannose-type carbohydrates, is followed by a long neck region comprised of tandem repetitions of a highly conserved 23-amino-acid sequence. The pathogen-binding capabilities of this receptor are influenced by this neck region, which is essential for the oligomerisation and maintenance of the CRD multimers that enable high avidity interaction (Figure 1.13) [109].

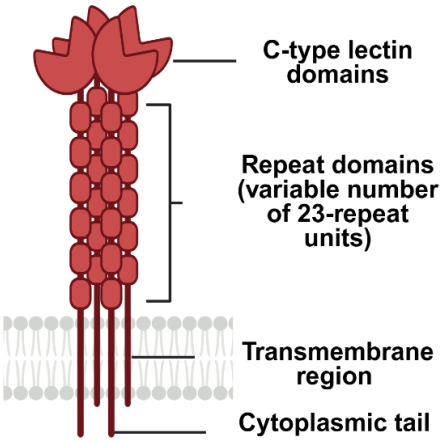

Figure 1.13. DC-SIGN structure. The structure of DC-SIGN comprises a transmembrane domain, an extracellular domain that is further subdivided into two regions, the CRD and the neck repeat region, and an intracytoplasmic tail domain responsible for internalisation and signal transduction [109]. Created by BioRender.

Unlike other CLRs, DE-SIGN lacks intrinsic ITAM or ITIM motifs in its cytoplasmic tail; therefore, it doesn't directly initiate a proinflammatory signalling. Rather, it contains dileucines and tyrosine-based motifs that recruit adaptor complexes like Connector Enhancer of Kinase Suppressor of Ras-1 (CNK-1), Kinase Suppressor of Ras-1 (KSR-1) and Rapidly Accelerated Fibrosarcoma-1 (RAF-1), leading to the activation of the RAF1 kinase pathway. RAF1 phosphorylates and acetylates the NF-κB p65 subunit, modifying the transcriptional program of the cell. This signalling pathway doesn't independently induce cytokine secretion but modulates responses triggered by other PRRs like TLR4 [110].

The animal model of DC-SIGN, a specific intercellular adhesion molecule-grabbing Non-integrin Receptor 1 (SIGNR1), was studied to explore the receptor's role in antifungal processes. It has been seen that SIGNR1 works alongside Dectin-1, leading to the production of cytokines and Reactive Oxygen Species (ROS) [76]. A limited patient cohort demonstrated that DC-SIGN polymorphisms are linked to the development of invasive pulmonary aspergillosis (IPA), while the exact mechanism is yet unknown [111].

3. Dectin-1

Dectin-1 comprises a CRD, a transmembrane region, and a hemITAM cytoplasmic domain with a single tyrosine in the tail domain (Figure 1.15). Upon ligand binding, Dectin-1 recruits Syk to its phosphorylated immunoreceptor ITAM-like motif (hem-ITAM) at its cytoplasmic tail, a process is regulated by Src kinases [112]. Src family kinases (SFKs) are non-receptor tyrosine kinases,

which are involved in the control of critical cellular processes such as migration, metabolism, apoptosis, differentiation, and cell proliferation [113]. Syk is a key mediator linking immune cells to stimulated immunoreceptors. Syk is phosphorylated upon recruitment, which then triggers the activation of protein kinase Cδ (PKCδ). This kinase, in turn, recruits CARD9 and phosphorylates it at threonine 23 (Thr23), a specific amino acid residue located at position 23 in the linear sequence of the IKK-α protein (Inhibitor of NF-κB kinase α) [114]. Vav proteins are very important proteins to activate CARD9 and bind Syk and CARD9 similarly to PKCδ [15]. In contrast to Dectin-1, Dectin-2, Dectin-3, and Mincle associate with the ITAM-containing adaptor FcR common γ chain to signal through Syk indirectly [115]. Activated CARD9 forms a CARD9/BCL10/MALT1 (CBM) complex domain by binding to both B cell lymphoma 10 (BCL10) and mucosa-associated lymphoid tissue lymphoma translocation protein 1 (MALT1). As a result, nuclear factor kappa-light-chain-enhancer of activated B cells (NF-κB) and MAPK are activated, triggering gene transcription, leading to the secretion of proinflammatory cytokines including TNF-α, CXCL-2, GM-CSF, IL-6, IL-1β and IL-23 (Figure 1.14) [116].

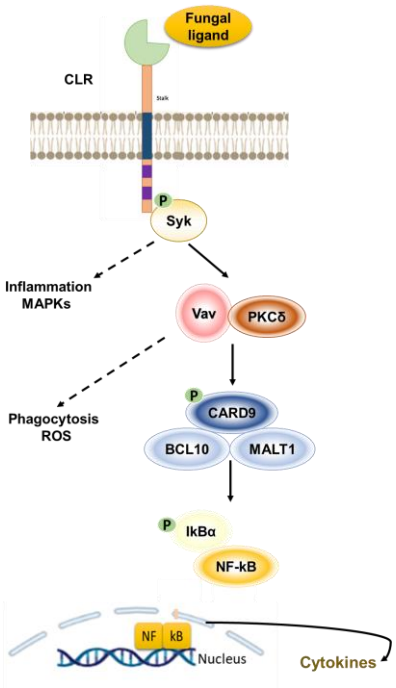

Figure 1.14. CARD9 pathway. CARD9 is activated upon fungal recognition and forms the CBM complex, then phosphorylates IkB-α, which gets degraded, and NF-kB dimer translocates into the nucleus for gene transcription to initiate cytokine secretion. Adopted from [15]. Created by Microsoft PowerPoint.

Dectin-1 dimerisation activates downstream activating pathways [117]. Dectin-1 utilises its single carbohydrate domain to bind β-1,3-glucan, culminating in enhanced phagocytosis, inflammasome formation, and the secretion of proinflammatory cytokines through Syk and CARD9 activation, and mediating the non-canonical rapidly accelerated fibrosarcoma 1 (Raf1) pathway to activate the NF-κB gene [118]. Recent studies have also demonstrated that Dectin-1 contributes to the autophagy pathway, thereby enhancing the presentation of fungal antigens through MHC II, which leads to the secretion of type I interferons during systemic candidiasis in mice [119]. Additionally, patients with Dectin-1 mutations have increased susceptibility to mucocutaneous *C. albicans* infections [120]. Although some of the killing mechanisms are not essentially stimulated by Dectin-1, patients with the mutated form hardly secrete key anti-candidal cytokines, such as IL-17, IL-6, or TNF-α, after exposure to β-glucan or *C. albicans* [121]. Finally, human Dectin-1 polymorphism (Y238X) has been connected to a higher risk of invasive aspergillosis after transplant surgery and a higher vulnerability to mucosal candidiasis [122].

4. Dectin-2 and Mincle

Initially, Dectin-2 was described as a Langerhans cell-specific CTLR, but it has been demonstrated to be expressed on a range of myeloid cells, including tissue macrophages, neutrophils, and many DC subsets [94]. Peripheral blood monocytes also express Dectin-2 at modest levels, but inflammatory stimuli increase its expression significantly [123]. Human Dectin-2 has been found on monocytes and DCs, and messenger RNA (mRNA) findings indicate that lymphocytes may also express it [124]. Dectin-2 and Mincle share a structure similar to Dectin-1, yet their cytoplasmic domain is shorter. This deprives Dectin-2 and Mincle from initiating signal transduction on their own. They both couple with the FcγR common γ chain to activate the Syk-CARD9 pathway (Figure 1.15) [125]. Dectin-2 triggers the production of multiple cytokines and chemokines, such as TNF, IL-2, IL-10, IL-23, IL-1β, IL-6, and IL-12, through the Syk, PKCδ, and CARD9–Bcl10–Malt1 pathway [126].

It is noteworthy that the responses of Dectin-2 appear to vary between the hyphal and yeast forms of *C. albicans*, presumably due to exposure to distinct ligands. This suggests that this PRR can differentiate between the various morphological forms of this pathogen [115]. Hence, it produces proinflammatory cytokines in response to fungal hyphae. Recently, it was demonstrated that Dectin-2 exhibits important Th-17-inducing activity during *C. albicans* infection [59]. Dectin-2 has a “classical” CTLD with a EPN motif which contains Glutamic

acid (E), Proline (P), and Asparagine (N) and binds to mannosylated structures; EPN motifs also exists in MR and DC-SIGN [127]. Dectin-2 detects high mannose-containing structures, such as $Man_9GlcNAc_2$ and $Man_8GlcNAc_2$, that are exposed on the surface of *C. albicans* hyphae [128]. Additionally, Dectin-2 collaborates with TLR2 to stimulate CARD9. The lack of this synergistic function or deficiency of the receptors leads to invasive *C. albicans* [76]. According to Robinson et al. 2009, Dectin-2 $^{-/-}$ mice showed higher fungal loads and decreased survival [126].

Macrophage-inducible C-type lectin (Mincle), also known as CLEC4E, can identify ligands from a variety of fungal species; Mincle knockout mice are more vulnerable to infection by *C. albicans* and Malassezia species [129]. Vijayan D et al. studied Mincle's distinct roles in regulating the production of inflammatory cytokines and fungal clearance. According to their results, Mincle deficiency may hinder efficient fungal identification and removal while upsetting the equilibrium of inflammatory reactions, which may result in a higher risk of fungal infections [130]. Mincle is primarily expressed in macrophages, and it has been demonstrated to play a role in macrophage responses to *C. albicans*. *In vitro*, Mincle localised to the phagocytic cup after exposure to yeast, but it is not required for phagocytosis [129].

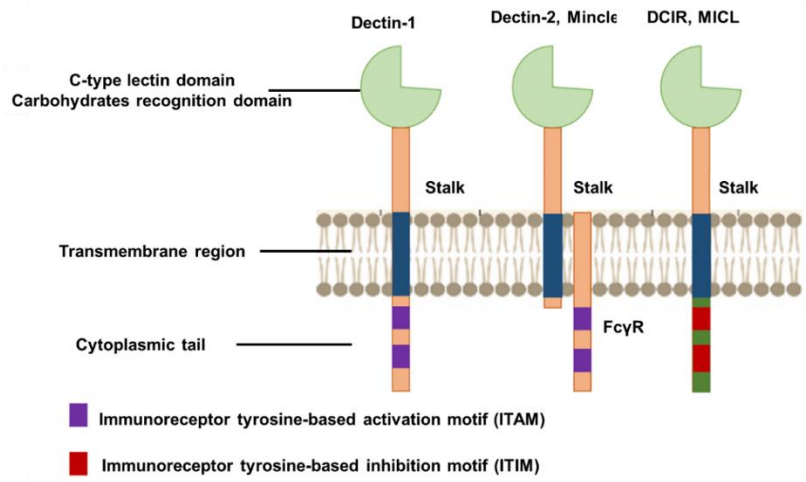

Figure 1.15. The unique structures of C-type lectin receptor family members, Dectin-1, Dectin-2, and MICL/DCIR, are highlighted. Each receptor contains an extracellular CRD domain, a transmembrane domain, and a cytoplasmic domain. The key distinction lies in their cytoplasm domains. Dectin-1 feature a cytoplasmic domain with an ITAM-like, while Dectin-2 family members have a short cytoplasmic domain that associates with the FcγR common γ chain, which also has an ITAM. In contrast, DCIR family members have an ITIM-containing cytoplasmic domain. These unique features define the distinct roles of these receptors in the immune response. ITAM, immunoreceptor tyrosine-based activation motif; CRD, carbohydrate recognition domain. Adapted from [95]. Created by Microsoft PowerPoint.

Conversely, the CLR, known as the dendritic cell immunoreceptor (DCIR), is expressed on most myeloid cells and has an inhibitory motif in its intracellular domain (ITIM) (Figure 1.15), which makes it a negative regulator of the immune response [131]. The immunomodulatory function of human DCIR and/or mouse DCIR1 in various autoimmune disorders, infectious diseases, and inflammatory-related pathologies has been emphasised by several *in vitro* and *in vivo* investigations. For instance, Yoshikawa et al studied the DCIR effector mechanism in *A. fumigatus* hyphae by modulating neutrophil degranulation. Due to increased PLCγ2 phosphorylation and intracellular Ca2+ mobilisation, neutrophils in DCIR-deficient mice demonstrated greater deregulatory activity and more effective fungal killing, resulting in accelerated fungal clearance without increased inflammation. Therefore, by altering neutrophil effector functions, DCIR functions as a negative regulator of antifungal immunity [132]. The function of DCIR1 on immunological homeostasis is more complicated than first believed, though, as it has been demonstrated to either enhance or suppress the innate and/or adaptive immune response, depending on the pathogenic setting [133].

5. CLEC5A

CLEC5A or Myeloid DAP12-associating lectin-1 (MDL-1) is widely expressed in myeloid lineages, such as microglia, osteoclasts, neutrophils, monocytes, macrophages, and dendritic cells. CLEC5A lacks a cytoplasmic domain and mediates cellular activation through the adaptor protein DAP12 that is phosphorylated after Mincle engagement, initiating Syk-mediated downstream signalling to secrete inflammatory cytokines. The transmembrane adapter DAP12, also known as killer cell activating receptor-associated protein (KARAP), is well-known for its role in transducing activation signals for a wide variety of receptors in DCs, NK cells, granulocytes, and monocytes/macrophages. The first analysis of DAP12-deficient animals showed that they were unable to activate NK cell receptors, that DCs accumulated in peripheral tissues, and that Th1 responses were impaired. This could be because DCs were less able to migrate to lymph nodes and prime T-cell responses [134]. According to structural studies, human CLEC5A is a homodimer glycoprotein expressed on the cell surface (Figure 1.16) [135].

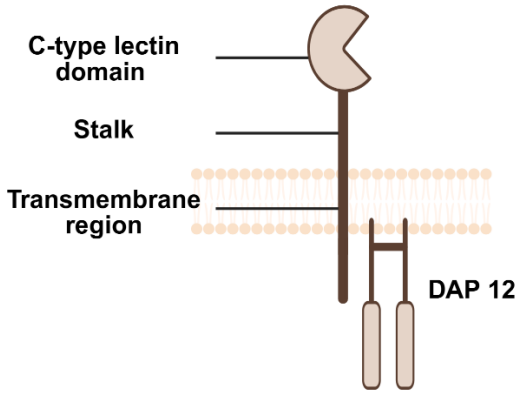

Figure 1.16. CLEC5A structure. The structure contains a C-type lectin domain, a transmembrane domain, and an intracellular cytoplasmic tail connected to DAP12. Adopted from [135]. Created by BioRender.

The identification that Dengue Virus (DV) is a direct ligand of CLEC5A clarifies the process by which the receptor induces inflammation and emphasises its importance as a PPR receptor in the pathogenesis of DV infection. To verify the specificity of the CLEC5A-DV interaction, complexes were immunoprecipitated using Protein A-Sepharose beads and subsequently probed with an anti-DV envelope (anti-E) monoclonal antibody (mAb). DC-SIGN/Fc and CLEC5A/Fc immunoprecipitants contained E protein, indicating that CLEC5A interacts with the dengue virion [136]. DV infection leads to inflammatory macrophages producing substantial quantities of IL-1β and IL-18, which in turn causes pyroptosis in these cells by upregulating pro-IL-1β, pro-IL-18, and NLRP3 and permitting caspase-1 activation; blockade of CLEC5A prevents DV-induced NLRP3 inflammasome activation and cell death [137].

Additionally, CLEC5A directly binds to the Japanese encephalitis virus (JEV) to recruit DAP12, becoming phosphorylated and inducing macrophages to release proinflammatory cytokines and chemokines. Although JEV infection of neurones and astrocytes cannot be prevented by blocking CLEC5A, anti-CLEC5A mAb significantly reduced JEV-induced cell death and proinflammatory cytokines in a microglia-neurons-astrocyte mixed culture. By inhibiting JEV-CLEC5A interactions in microglia, proinflammatory cytokines and other toxic compounds released by microglia are attenuated, restoring the integrity of the blood-brain barrier (BBB) following JEV infection [138]. Additionally, CLEC5A interacts with the hemagglutinin protein of influenza viruses (H1N1, H5N1, and H7N9). Anti-CLEC5A antibodies that inhibit these interactions lower the production of proinflammatory cytokines without reducing the replication of the influenza virus

in human macrophages. Additionally, clec5a−/−BMDMs (bone marrow-derived macrophages) had lower levels of TNF-α than wild-type cells from influenza-infected mice [139].

Currently, no studies directly connect *C. albicans* and CLEC5A; rather, CLEC5A is more well-known for its function in the immune system's reaction to certain bacteria and viruses, as described above. Nevertheless, CLEC5A belongs to a larger family of CLRs, which are crucially known for identifying sugars in fungal cell walls, hence infections.

1.2.1.2.3. Toll-like receptors

All TLRs share an N-terminal ectodomain composed of leucine-rich repeats, a single transmembrane domain, and a cytosolic Toll/interleukin-1 receptor TIR domain [140]. There are 10 TLRs (1-10) in humans and 12 (1-9, 11-13) in mice. They are present in the cell membrane (TLRs 1, 2, 4, 5, 6) or endosomes (TLRs 3, 7, 8, 9) [95, 141]. Mammalian TLRs that reside in the plasma membrane include those that identify elements of the microbial cell surface, such as TLR1, TLR2, and TLR6 (bacterial lipoproteins), TLR5 (flagellin), and TLR4, which recognises LPS. Endosome-resident TLRs detect nucleic acids, including bacterial ribosomal RNA (TLR13), unmethylated CpG-containing single-stranded DNA (ssDNA) (TLR9), double-stranded RNA (dsRNA) (TLR3), and single-stranded RNA (ssRNA) (TLR7 and TLR8). The ligand for human TLR10 remains unclear at present (Figure 1.17) [140].

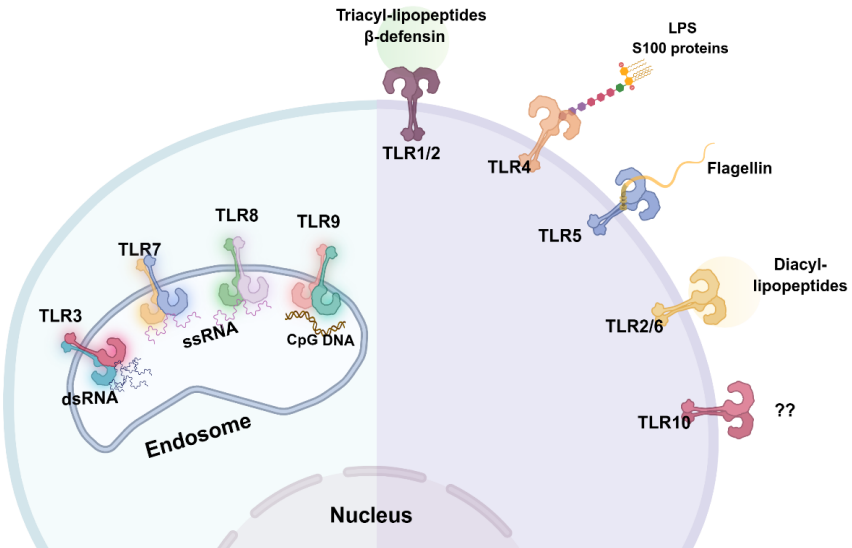

Figure 1.17. TLR localisations and forms. The illustration displays several types of endosomal and cell surface toll-like receptors (TLRs). Adopted from [140]. Created by BioRender.

C. albicans is recognised by TLR2/TLR6 and TLR2/TLR1 heterodimers that recognise phospholipomannas expressed on the *C. albicans* wall; in addition, TLR2, in cooperation with galectin-3, senses mannosidase [142]. Both *C. albicans* and host cells have mannosidases, which are glycosidic enzymes that aid in the processing and modification of mannose-rich glycoconjugates like N-linked glycans and fungal cell wall mannans [143]. The TLR signalling pathway of all TLRs except TLR-3 is initiated when microbial ligands bind to TLRs, causing the receptors to dimerise and recruit the adaptor protein MyD88. Once in place, MyD88 stimulates interleukin-1 receptor-associated kinase 4 (IRAK4) and interleukin-1 receptor-associated kinase 4 (IRAK1) to form what's known as the myddosome complex. Within this complex, IRAK4 phosphorylates IRAK1, enabling the signal to proceed. The activated IRAK1 is then coupled with TNF receptor-associated factor 6 (TRAF6), an E3 ubiquitin ligase, which adds K63-linked polyubiquitin chains. TRAF6 triggers the activation of the TGF-β-activated kinase 1 (TAK1), resulting in the activation of the IKKγ-scaffolded IKKα and IKKβ kinases within the IκB kinase complex, also known as NEMO. Once switched on, the IKK complex targets the inhibitor IκB, tagging it for breakdown. With IκB degraded, NF-κB is free to enter the nucleus, where it turns on genes that drive the production of inflammatory cytokines and other key immune proteins (Figure 1.18) [140].

MyD88 deficiency was studied in mice, and it was correlated with susceptibility to various fungal infections, including those caused by *C. albicans, A. fumigatus,* and *C. neoformans*. However, this was not the case in humans, where MyD88 deficiency led to a high susceptibility to selected bacterial infections but not fungal infections. As mentioned above, TLRs also collaborate with CLRs to induce cytokine production and tailor immune responses, resulting from cross-regulation of signal pathways [144].

TLR3- or TLR4-induced IFN production in macrophages and normal dendritic cells (DCs) is dependent on the TRIF pathway and its associated proteins, including TRAM, TRAF6, and TRAF3. The TRIF pathway plays a crucial role in TLR3 and TLR4 signalling from the phagosome/endosome [145]. TRAM is believed to interact with TRIF and facilitate TRAF3-dependent activation of the kinase TBK1 upon the recognition of dimerised TLR4 in endosomes. After that, TBK1 promotes the expression of IFN and may possibly induce comparable glycolytic reactions to those triggered by TBK1 activation in the MyD88 pathway [145]. The discovery that TRIF contains a 39-amino-acid pLxIS motif provided an explanation for why TRIF (but not MyD88) can stimulate TBK1-mediated IFN

responses [146]. This motif interacts with IRF3, an IFN-inducing transcription factor and TBK1 substrate, when it is phosphorylated by TBK1. Therefore, the TBK1-IRF3 enzyme-substrate pair can be recruited by TRIF rather than MyD88, which results in IRF3 activation and IFN expression. TRAM's ability to trigger TRIF (triffosome)-dependent reactions is limited to TLR4. TRAM is unable to interact with TLR3, and it is not a protein that controls TLR3 signalling. It's unclear if a sorting adapter that functions similarly to TRAM or TIRAP/MAL links TLR3 to TRIF (Figure 1.18) [147].

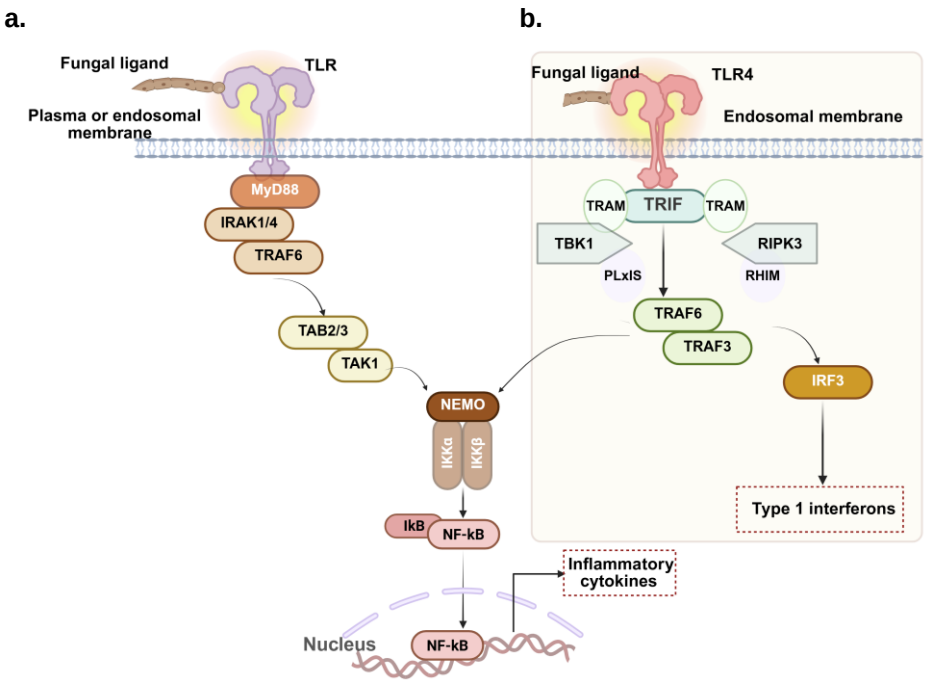

Figure 1.18. An outline of the Toll-like receptor (TLR) signalling pathway. a. Surface TLRs dimerise and attract downstream adaptor molecules, such as MyD88, working with other molecules, when triggered by their respective ligands. This activation of downstream molecules triggers signalling cascades that converge at the NF-kB, IRFs, and MAP kinases. Numerous proinflammatory cytokines, including TNF-α, IL-6, IL-8, and IL-12, are secreted. Adopted from [148]. **b.** In endosomes, TLR4 and TLR3 can interact with TRIF. Although this protein complex is not well described, it is thought to be structured and function as shown above. TRIF has a RHIM domain to boost RIPK3 and a pLxIS motif to increase TBK1-dependent gene expression. Only in the presence of caspase inhibition does this later activity take place [140]. Created by BioRender.

1.2.3.1.4. CARD9: A Key Molecule in anti-Fungal Immunity in humans

The CARD protein family includes the intracellular adaptor CARD9, which is distinguished by its specific binding to the CARD domain of BCL10. The majority of CARD9 expression occurs in myeloid cells. Its structure consists of an N-terminal CARD domain and a coiled-coil region at the C-terminus (Figure 1.19) [149].

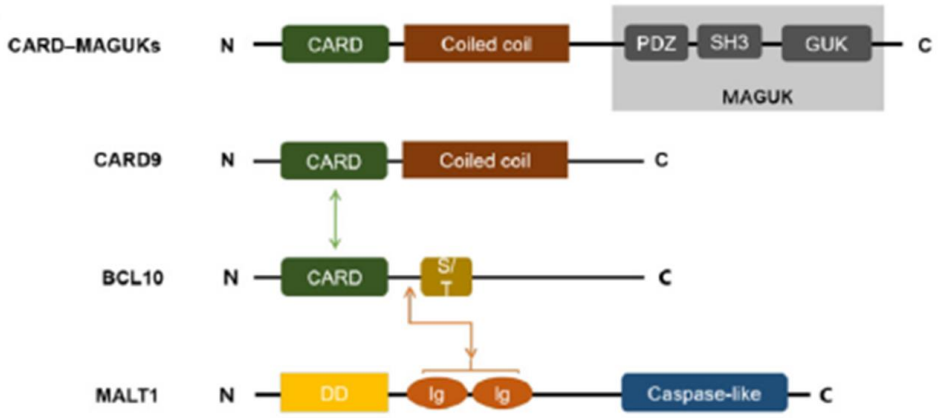

Figure 1.19. The main features of CARD9. MALT1 has two Ig-like domains at the N terminus and a caspase-like domain at the C terminus; BCL10 has an N-terminal CARD domain and a C-terminal Ser/Thr-rich effector region; and CARD9 has an N-terminal CARD domain and a C-terminal coiled-coil region. The Ser/Thr-rich effector region of BCL10 connects to MALT1 via its Ig-like domains, CARD9 interacts with BCL10 through its homologous CARD domain. Thus, a complex is formed by these three molecules [150].

CARD9 is a signalling adapter protein involved in the signalling pathways of various innate PRRs, including CLRs, intracellular NOD receptors, and nucleic acid sensors. As a result, CARD9 has been identified as a major regulator of immunity to bacteria, fungi, and viruses in animal models. However, studies on humans with autosomal recessive CARD9 impairment have shown that this molecule has a very specialised function in the activation of antifungal immune responses [151]. Together with the CLRs, they have a role in shaping the required adaptive system by modulating the secretion of adaptive cytokines like IL-17 [128].

In innate immunity, neutrophils are among the first immune cells to respond to invasive infections, and they exhibit the highest expression of CARD9, as indicated by the ImmGen database [152]. *In vivo*, Card9-/- neutrophils exhibited decreased accumulation in inflammatory sites due to an impaired inflammatory environment, characterised by a noticeably lower amount of the cytokine IL-1β and the chemokines CXCL1, CCL3, and CXCL2. However, the inherent ability of Card9-/- neutrophils to migrate was unaffected [153]. Furthermore, research on the *in vitro* function of Card9-/-neutrophils using lineage-specific deletion studies revealed a significant decrease in gene expression upon immune complex stimulation. This reduction is connected to the impaired signalling within the NF-κB pathway, specifically in the decreased phosphorylation and degradation of IκB-α. Notably, despite these signalling defects and reduced inflammatory gene response, the basic short-term effector functions of neutrophils, such as ROS production, degranulation, and migration, were not

affected by the deletion of CARD9 [152]. Expression of CARD9 by macrophages is necessary for immunological responses to microbial infections. Lack of CARD9 leads to a complete failure of macrophages to eliminate *Listeria monocytogenes* and a partial failure to inhibit *C. albicans* due to compromised respiratory burst [154]. At the organ scale, CARD9 is one of the key regulators of intestinal homeostasis, with recent studies showing a strong correlation between CARD9 genetic variation and the risk of inflammatory bowel disease (IBD), which encompasses Crohn's disease (CD) and ulcerative colitis [155].

1.2.3.1.5. GM-CSF as a therapy for human CARD9 deficiency

Pathogenic fungi are predominantly recognised by the CLRs and TLR families, of which many members are coupled to the signalling adaptor proteins CARD9 and MyD88, respectively [156]. Despite this, only CARD9 deficiency leads to fungal diseases in humans compared to MyD88 [149]. CARD9-deficient patients are uniquely highly susceptible to invasive fungal infections but not bacterial, viral, or parasitic infections [152, 157]. Mucocutaneous candidiasis is an outcome of CARD9 deficiency. However, the salient feature is the involvement of the central nervous system (CNS), resulting in spontaneous CNS candidiasis—a severe side effect of invasive *C. albicans*—due to a failure in neutrophil recruitment. Recombinant GM-CSF has been used as an adjunct immune-based treatment for human CARD9 deficiency, as these patients have a defect in GM-CSF production [158]. Recombinant GM-CSF was administered to a group of French-Canadian patients with CARD9 deficiency who carry the 'signature' p.Y91H CARD9 missense mutation; the treatment corrected defective signalling in CARD9-deficient myeloid cells and showed clinical benefits [159]. On the other hand, Rebecca Drummond et al. used the same strategy to treat a different group of CARD9-deficient patients with a different homozygous CARD9 missense mutation (p.R57H). After 15 months of treatment with recombinant human GM-CSF (no specific brand was mentioned in this study), GM-CSF did not alter the fungal load or increase peripheral neutrophil counts [160]. From these two contradictory findings, it appeared that successful treatment with GM-CSF depends on the mutated gene variant. The French-Canadian patients who have the CARD mutation (p.Y91H), the interaction between H-RAS and RASGFR-1 (key components involved in the cellular signalling pathways) was defective. Having defects in these two components leads to impaired ERK activation and consequently a reduction in the GM-CSF secretion. In contrast, in the other group of patients with (p.R57H)

CARD mutation, H-RAS and RASGFR-1 are functionally normal. Hence, there was no defect in the ERK pathway, resulting in normal secretion of GM-CSF. Thus, administering additional GM-CSF had no therapeutic impact, as the p.R57H mutation route lacked the deficiency that GM-CSF would ideally fix [161]. To determine the processes by which CARD9 regulates human immunity to fungi, further research is needed.

CARD9 contributes to shaping the adaptive system, and deletion of CARD9 alters the activation of the adaptive system, particularly Th17 polarisation. The underlying processes leading to susceptibility to fungal infections in individuals with CARD9 deficiency are not yet understood. However, they may be connected to the lack of inflammatory cytokines and chemokines in response to fungal agonists [162].

1.2.1.2.6. NLRP3 and Inflammasomes formation

A NOD-like receptor pyrin domain-containing NLRP3, the inflammatory protease caspase-1, and the apoptosis-associated speck-like protein (ASC) have traditionally been identified as the components of an active inflammasome [163]. The recruitment of ASC and caspase-1 by NLRP3 upon activation is necessary for the cleavage and maturation of the inflammatory cytokines IL-1β and IL-18. However, IL-1β appears to have a greater impact on fungal immunity than IL-18 [164]. Since basal expression of NLRP3 in resting cells is insufficient for successful inflammasome activation, the priming stage involves TLR-NF-κB-driven induction of inflammasome components and production of pro-IL-1β and pro-IL-18 (Figure 1.20) [165, 166]. Additionally, *C. albicans* uses the NLRP3 inflammasome to induce macrophage pyroptosis. Different from ordinary cell necrosis, pyroptosis is mediated by the inflammasome and caspase-1, and it differs from apoptosis in that the macrophages lose cell integrity, and the process is proinflammatory [167].

C. albicans activates the NLRP3 inflammasome via the Syk pathway through CLRs, such as Dectin-1, and in combination with TLR2 (Figure 1.9) [168]. The role of the NLRP3 inflammasome during *C. albicans* infections was studied *in vivo*, and they found that NLRP3 deficiency results in suppression of IL-1β production that leads to lower antifungal activity and increased susceptibility to mucosal candidiasis [169].

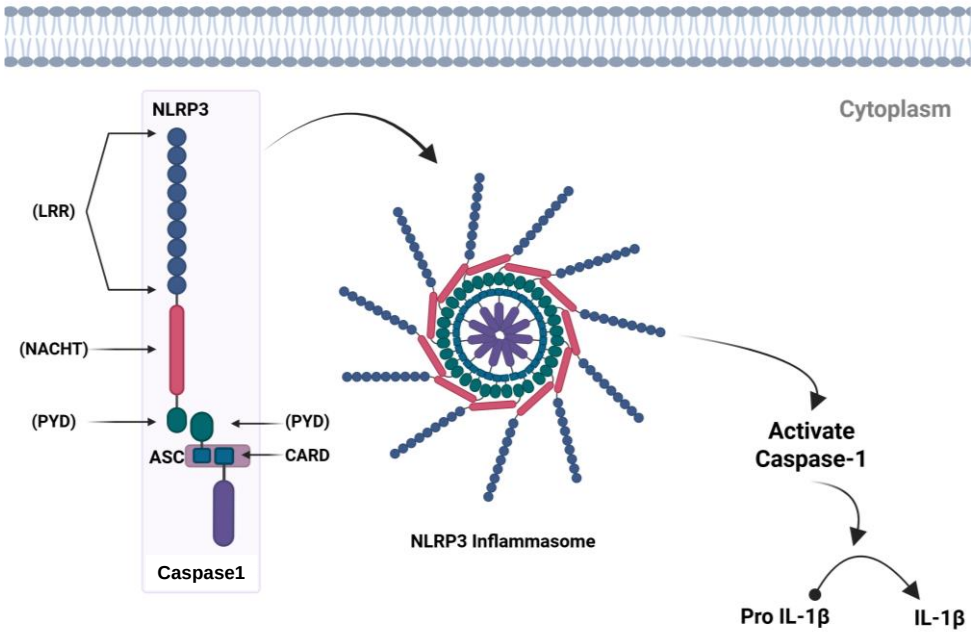

Figure 1.20. NLRP3 structure. Three domains make up the NLRP3 protein: the pyrin domain (PYD), the central nucleotide domain (NACHT), and the C-terminal leucine-rich repeats (LRR). The pyrin domain (PYD) and caspase recruitment domain (CARD) are the two interaction domains found in ASC. Caspase-1 has a catalytic domain and a CARD. The NLRP3 inflammasome comprises three key elements: caspase-1, ASC, and NLRP3. Adopted from [170]. Recreated by BioRender.

Extracellular Vesicles role in immune response during *C. albicans* infection.

There are two suggested ways that genetic or functional information might be passed down: horizontal gene transfer, which is caused by viruses or bacteriophages, and vertical gene transfer, which is the interchange of genes from one generation to the next. Exosomes and microvesicles, which are naturally occurring cell-derived vesicles, have recently been identified as an additional route of horizontal gene transfer and are collectively referred to as extracellular vesicles (EVs). The majority of cell types, though not all, create these EVs constitutively. EVs include proteins that can be functionally transferred between cell types and species, as well as mRNAs and non-coding RNAs, such as tiny regulatory microRNAs (miRNAs), proteins, lipids and surface receptors for the presentation and adhesion. Additionally, Tetraspanins, a protein superfamily that organises membrane microdomains known as tetraspanin-enriched microdomains (TEMs), are particularly abundant in EVs. While some tetraspanins, such as Tssc6, CD37, and CD53, are specific to certain tissues in haematopoietic cells, CD9, CD63, CD81, CD82, and CD151 are widely distributed throughout various tissues (Figure 3.1) [171]. EVs thus

significantly affect normal physiological functions [172]. A significant area of study is the reciprocated influence of EVs from host cells and *C. albicans* infections, which suggests mutual EVs synthesis and explains their important function in interkingdom communication and cell signalling [173]. The generation of extracellular vesicles (EVs) is one mechanism that contributes to *C. albicans* pathogenicity. These vesicles mediate various aspects of host-pathogen interactions and are essential for the pathogenicity of yeasts; yet, because they contain a large number of proteins with antigenic properties, they may also be protective against *C. albicans* infection [174].

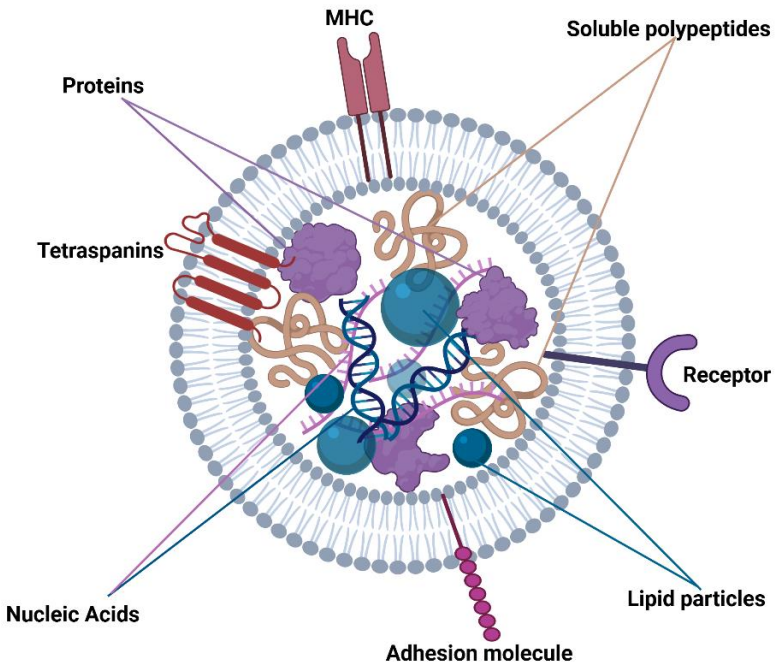

Figure 1.21. EVs structure. It contains membrane proteins such as tetraspanins (CD9, CD63 and CD81), adhesion molecules (EpCAM, integrins), MHC and nucleic acids (mRNA, miRNA and DNA), proteins (HSP70, HSP90, and EGFR), and lipids are all encased in this membrane. Adopted from [59]. Created by BioRender.

Although several possible uptake mechanisms, such as endocytosis, phagocytosis, and direct fusion with the cell membrane, have been proposed, none of these have been confirmed for *C. albicans* EVs affecting human cells. Instead, it is believed that communication between host cells and pathogens, mediated by EVs, is based on the contact and subsequent internalisation of vesicles by acceptor cells [175].

1.2.1.3. Role of innate immune cells during fungal infection

The immune system provides a quick and comprehensive defence against *C. albicans,* and trafficking immune cells such as neutrophils and macrophages [176]. Innate cells employ receptors, PRRs, to identify conserved PAMPs. In addition to triggering cellular reactions and killing mechanisms, signalling downstream from PRRs aids in the initiation and development of adaptive immune responses [76].

Neutrophils are highly phagocytic granulocytic polymorphonuclear cells [177]. They are among the immune cells that are the first to arrive at the site of infection, and they play a pivotal role in controlling *C. albicans.* Neutrophils generate Neutrophil Extracellular Traps (NETs), a mesh of antimicrobial proteins, chromatin, DNA and histones that are released by neutrophils into the extracellular matrix to target distant microorganisms, trapping and destroying yeast cells [178, 179]. The critical importance of neutrophils is evident from the high susceptibility to severe candidiasis in mice and individuals with neutropenia. In mice, neutrophil depletion lowers survival when challenged with *C. albicans* [151]. Patients with chemotherapy-induced neutropenia or neutrophil functional abnormalities, such as hereditary defects of the NADPH oxidase, as found in chronic granulomatous disease (CGD) patients, have a higher frequency of invasive fungal infections and high susceptibility to systemic and chronic infections [180]. Neutrophils recognise components of the cell wall of *C. albicans* through CLRs and TLRs. Mincle and Dectin-1 appear to be utilised by neutrophils in the recognition of β-glucan, while TLR2 recognises the phospholipomannas, all leading to the activation of antimicrobial response [130].

Monocytes are recruited from the blood circulation to the infected tissues and differentiate into macrophages and DCs while releasing proinflammatory cytokines that amplify the antifungal immune response [181]. Jorge Domínguez-Andrés et al. demonstrated in their study that type-I IFN-dependent IL-15 secreted from murine inflammatory monocytes plays a critical role in activating NK cells, which in turn produce GM-CSF, enabling splenic neutrophils to control fungal growth [182]. While murine monocytes exhibit the CSF1 receptor (CSF1R, CD115), cluster of differentiation 11 (CD11b), FcγR (CD64), and human leukocyte antigen (HLA-DR) complex, a specific group of human monocytes uniformly express the major histocompatibility class II (MHC II) receptors, integrin αM (CD11b), and CD86. Classical monocytes (CD14+CD16– in humans, $Ly6C^{hi}CD43^{lo}CX3CR1^{lo}$ in mice), nonclassical monocytes

(CD14^{lo}CD16+ in humans, Ly6C^{lo}CD43^{hi}CX3CR1^{hi} in mice), and intermediate monocytes (CD14+CD16+ in humans, Ly6CintCD43^{hi}CX3CR1^{hi} in mice) are the three monocyte subsets that are currently recognised [183]. This recognised nomenclature dates back to the late 1980s and was first used to identify CD14 and CD16 on human peripheral blood mononuclear cells (PBMCs) using two-colour flow cytometric detection [184]. In healthy individuals, the classical subset is the most predominant until exposure to GM-CSF, at which point the inflammatory phenotype begins to rise [185]. Mice with lower levels of monocytes were prone to *C. albicans* infections in comparison to wild types [186]. The role of monocytes during *C. albicans* infections have been studied *in vivo* mostly using murine cells; however, their contribution to fungal killing remains unclear [187]. However, monocytes play a protective role in antifungal immunity, with the notable exception of cryptococcosis, where, depending on host and fungal variables, monocytes may play either a protective or detrimental role [188].

Macrophages engulf *C. albicans* and destroy it within phagolysosomes using oxidative and enzymatic killing mechanisms. Additionally, they orchestrate inflammation by releasing cytokines, indicating the crucial role of macrophages in eliminating *C. albicans* at local mucosal sites and in the bloodstream, helping to rein in the infections and regulating the immune response [189]. Activated macrophages also release proinflammatory cytokines, such as IL-1β, IL-6, and TNF-α, leading to increased vascular permeability and the expression of adhesion molecules like P- and E-selectins, which facilitate the migration of immune cells from the blood into tissues. Macrophages can adopt a proinflammatory phenotype in response to PAMPs and interferon-γ (IFN-γ), termed M1-like. On the other hand, they can adopt an anti-inflammatory/pro-resolution phenotype (M2-like) in response to IL-4 and IL-13. Macrophages use phagocytosis to eliminate *C. albicans*, which is facilitated by CR3 [190].

Natural killer cells (NK), traditionally known for their role against virally infected cells and tumour cells, contribute to the antifungal responses. It has been reported that NK cells in humans and animals exhibit antifungal activity against a variety of fungi, including *C. albicans* and *A. fumigatus*, among others. NK cells might attack *C. albicans* directly by cytotoxic degradation or indirectly by the secretion of proinflammatory cytokines like IFN-γ and GM-CSF, which enhance the anti-fungicidal activity of phagocytes. However, the function of NK cells is unclear and complex; numerous studies have proposed that NK cells

have an impact on different cell types, and the finding that particular fungal species actively block NK-mediated killing adds to the complexity [87]. Finally, with the immune cells mentioned, it is crucial to note, nevertheless, that several additional cellular populations may also play a role in antifungal responses. Including mast cells, basophils, and eosinophils, for example, mast cells' advantageous position in the lung allows them to easily engage with invasive fungi, causing them to degranulate, secrete granular proteins and cytokines, and ultimately kill the fungus [191]. Additionally, eosinophils are the main cells in fungal-sensitisation-associated asthma, allergic bronchopulmonary mycosis (ABPMs), and asthma. Still, little is known about how these cells contribute to the immunopathology of these conditions [192].

Finally, to trigger the adaptive immune system, although Dendritic cells (DCs) are less potent at directly killing *C. albicans*. They are key in antigen presentation by expressing MHC II, internalising fragments of fungal components and migrating to secondary lymphoid organs to initiate the adaptive immune system. Mature DCs interact with naïve T cell CD4 through MHC II-peptide binding to specific T cell receptor (TCR) alongside interaction of co-stimulatory signals (such as CD80 and CD86) in DCs with counter receptors on T cells. This interaction leads to activated CD4 T cells that secrete different cytokines like IFN-γ (Figure 1.21) [193].

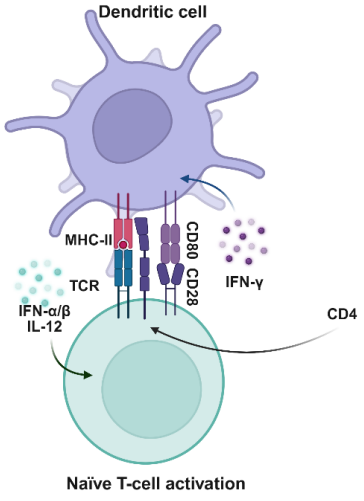

Figure 1.22. Mature DCs interact with Naïve T cells through three signals. 1. MHC-II TCR ligand 2. CD80 or CD86 and CD28.And 3. Cytokine production. Adopted from [194]. Created using BioRender.

1.2.2. Adaptive immune response to *C. albicans*

The primary adaptive immunological priming strategy employed by DCs involves presenting fungal antigen to naïve CD4+ T cells, resulting in a T-helper (Th) response that includes Th1, Th2, Th17, and Treg cells. At mucosal surfaces, the CD4+ Th cell response is the most common cell-mediated adaptive immunological response to *C. albicans* infection. In candidiasis, the yeast form activates Th1 cells, whereas the hyphal form primes Th2 immune responses [195]. During the interaction of DCs and naïve CD4 T cells, the cytokine environment dictates which modality of activated Th cells will be produced. For instance, DCs can release IL-12 that polarises CD4 T cells into Th1, which is very important in the response against *C. albicans* [94]. Presence of IL-4, which is probably produced by basophils and mast cells, will lead to Th2 polarisation, while IL-6, IL-23, IL-1β and TGF-β from mainly macrophages and promote Th17 polarisation (Figure 1.22) [196, 197].

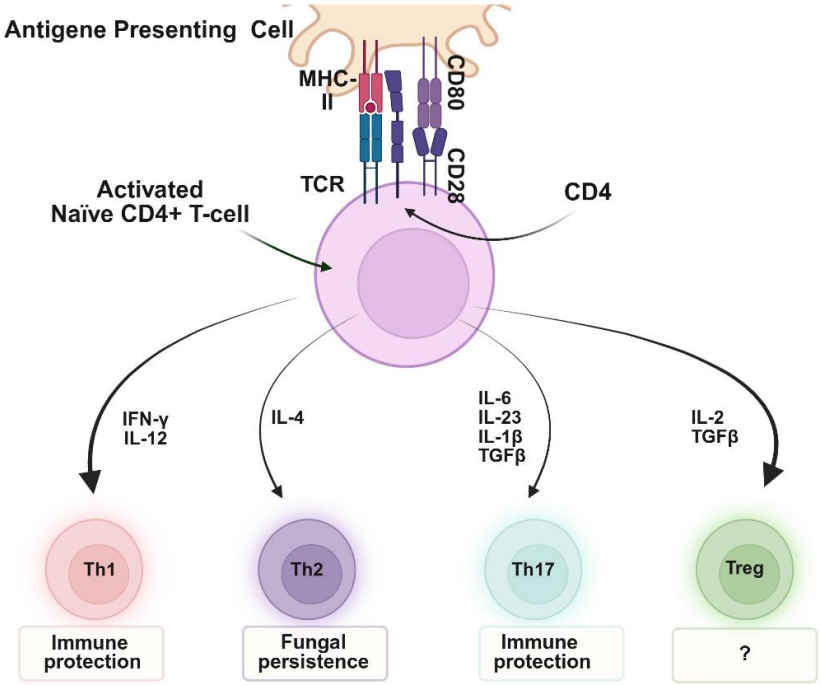

Figure 1.23. An overview of adaptive T-cell reactions to *C. albicans* infection. The presentation of peptides on MHC II molecules helps naive CD4+ T-cells become activated. When a T-cell receptor (TCR) recognises an antigen in the context of costimulation from CD28 and CD80/86, cytokine-directed polarisation to one of the four recognised Th subsets occurs. Immune protection is provided by Th1 and Th17 cellular responses, but Th2 responses are considered less effective in eliminating fungi. Adopted from [196]. Created using BioRender.

CD4+ T cells, unlike cytotoxic T cells, lack direct cytolytic activity but play a crucial role in the cellular adaptive response to fungal infections [196]. Data from both mutant mice and human patients demonstrate the relevance of Th17 cytokines in anti-Candida responses. Th17 cells secrete IL-17, which plays a significant protective role against mucosal damage caused by *C. albicans.* Additionally, Th17 cells responses play a significant role in the recruitment and activation of neutrophils. The importance of Th17 cells in combating *C. albicans* was highlighted by studies in knockout mice and humans. Mice lacking Th17 cells were more susceptible to oropharyngeal candidiasis and systemic infections due to their inability to produce cytokines such as IL-23 [198]. IL-23 is a key cytokine in anti-*C. albicans* immunity, it plays a central role in amplifying and sustaining Th17 responses, which are essential for effective mucosal and systemic antifungal immunity [199]. Patients who lack Th17 cells suffer from mucocutaneous candidiasis that causes relentless infections of the nails, skin, and gastrointestinal tract (GIT), as well as predominantly oropharyngeal candidiasis. Adaptive immune responses are crucial for the eradication of the pathogenic fungi and for promoting immune tolerance to commensal fungal species, thereby restoring long-term homeostasis [196].

Finally, immunological activity has been shown to persist at the subclinical level even after the inciting stimulus has been eliminated, proinflammatory signals have been suppressed, and resolution mechanisms have eliminated typical innate-type leukocytes. Feehan K and Gilroy D utilised a model for treating murine peritonitis brought on by bacterial infection with *S. pneumoniae*, low-dose yeast cell extract, or zymosan, revealed a previously unnoticed second wave of leukocyte infiltration into the tissue that lasted for months. Numerous investigations back up these findings of immunological activation following resolution. Polychromatic flow cytometric investigations have shown these cells constitute several discrete populations of innate immune cells, including CD11b+/CD49+/CD115+/MHC-II+ myeloid-derived suppressor cells (MDSCs), F-480^{lo}/MHC-II+/CD11c+ DCs, and F4-80int/CD11b^{hi}/CD11c- macrophages. After resolution, lymphoid-lineage cells also show up in the tissue, with natural killer cells reaching their maximum in quantity between days 9 and 14 and then starting to decline. Both CD4+ and CD8+T cell populations showed a similar pattern. These varied populations were seen in conjunction with the lymph nodes' growth, which revealed the presence of memory T and B lymphocytes from blood peritoneal origins, as well as DCs generated from blood Ly6C^{hi} monocytes [179].

1.2.2.1. Dynamic B cell targeting across infection reveals ongoing humoral engagement.

There is a significant humoral component to adaptive immunity against *C. albicans* in addition to T-cell-mediated pathways [196]. Although early research could not clearly demonstrate the importance of B cell responses for antifungal defence, more recent studies in murine models demonstrated that B cells contribute to protective responses in disseminated candidiasis [200]. However, it was also proposed that B cells' interactions with T cells could provide antibody-independent protection [201]. Healthy people generate detectable anti-Candida antibody titres, with systemic IgG and mucosal IgA frequently detected, as *C. albicans* often colonises mucosal sites. These antibodies support opsonisation, phagocytosis, and complement fixation, all of which aid host defence. Since antibodies against *C. albicans* cell wall components rise after fungal infection and can be readily measured by ELISA, antibodies to *C. albicans* can serve as a diagnostic marker. During an infection, the *C. albicans* proteins might be found [202], and the target identification pattern shifts throughout the infection, suggesting a continuous B cell response [203]. A protective antibody response can act independently in the setting of immunosuppression, compensating for other potentially impaired immune cells, such as neutrophils or macrophages. To do so, these antibodies need to be functional in affecting the pathogen's virulence attributes, rather than functioning in opsonisation or complement activation, which would require phagocytic activity for final clearance of the pathogen. Although these results show that antibodies play a protective role, the mechanisms underlying this protection have not been thoroughly examined. Macrophage phagocytosis was facilitated by classical opsonisation by human cloned IgGs [204].

1.2.2.2. Role of CARD9 in adaptive immunity.

CARD9 connects innate and adaptive immunity for example, Th17 cells are essential for oral mucosal defence against *C. albicans*, and CARD9-dependent DC activation promotes Th17 polarisation via IL-6/IL-23 [205]. CARD9 plays a major role in influencing antifungal T cell responses over time in murine oral candidiasis, as evidenced by the fact that it is necessary for adaptive (Th17-mediated) protection but not for immediate innate containment. These findings contribute to the explanation of why, despite generally robust neutrophil numbers, people with CARD9 deficiency frequently experience chronic mucosal illness [158].

1.3. GM-CSF as a crucial factor in tissue inflammation and myeloid cell function

1.3.1. GM-CSF cell biology and signalling

Granulocyte-colony stimulating factor (GM-CSF) or CSF2 is a glycoprotein first identified as a haemopoietic growth factor because of its capacity to generate colonies of granulocytes and macrophages *in vivo* from bone marrow precursor cells [206]. However, since then, it has also been viewed as a cytokine. GM-CSF acts through a specific receptor that is predominantly expressed by myeloid cells, including neutrophils, eosinophils, basophils and monocytes/macrophages. Its effects range from improved cell survival to greater activation, differentiation, and proliferation enhancing their survival and activation (Figure 1.23) [207, 208].

It's interesting to note that GM-CSF has been demonstrated to have a dual nature, acting primarily to promote inflammation and occasionally as an anti-inflammatory agent [208]. It has been established that GM-CSF expression in the kidneys and spleen of mice infected with *C. albicans* correlates with fungal infections [209]. According to *in vitro* research, GM-CSF is a growth factor for macrophages, stimulating the expression of IL-12 and IL-23, which in turn induce the cells to adopt an activated and proinflammatory state. Additionally, an *ex vivo* study on microglia and other human CNS, including astrocytes, neurons and oligodendrocytes, showed that they proliferate in response to GM-CSF [210].

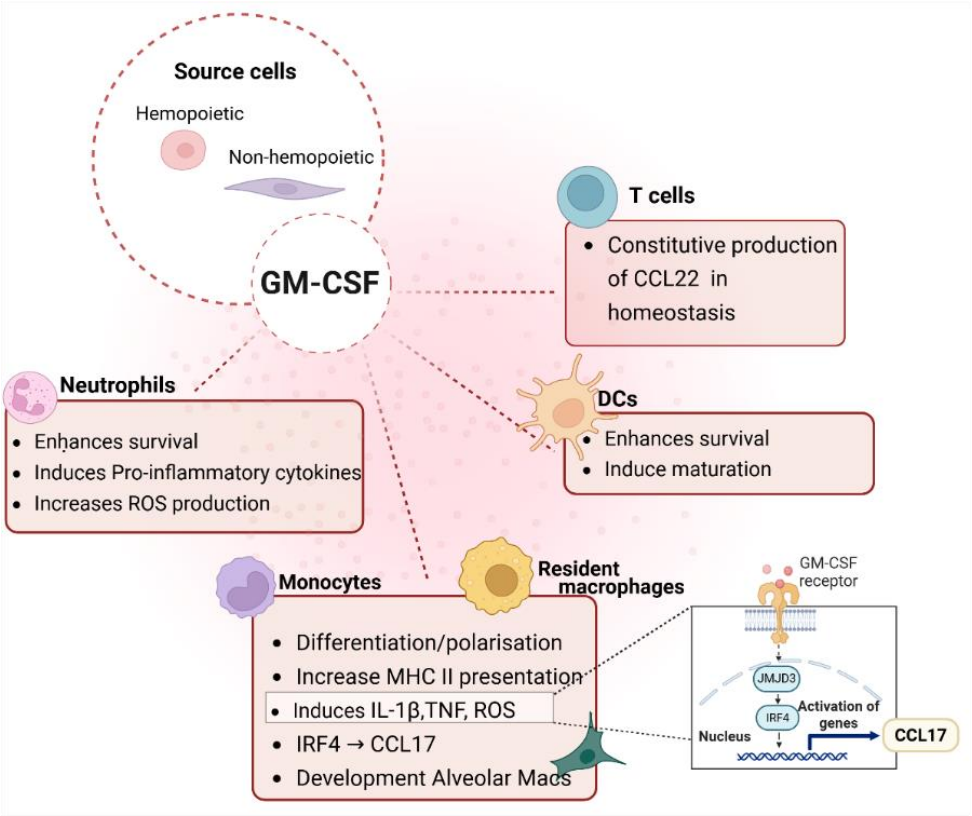

Figure 1.24. The diverse roles of GM-CSF across immune cell types. GM-CSF is produced by both hematopoietic and non-hematopoietic cells, and acts on multiple targets within the immune system. In neutrophils, it enhances survival, promotes the release of proinflammatory cytokines, and increases the production of ROS. Monocytes respond by differentiating and polarising into more specialised cells, upregulating MHC II expression, and producing TNF-α and ROS. And with the inflammasome formation IL-1β is produced, GM-CSF also drives CCL17 expression via the activation of IRF4 transcription and supports the development of alveolar macrophages. DCs benefit from enhanced survival and maturation, and resident macrophages respond similarly to monocytes. In steady-state conditions, T cells have been shown to constitutively generate CCL22 in the presence of GM-CSF. Adopted from [206]. Created using BioRender.

The GM-CSFR receptor is a type I cytokine receptor that forms a multimeric complex composed the ligand binding α chain that is specific for GM-CSF and a signalling β chain that is shared by IL-3 and IL-5 receptors [211]. Different pathways are initiated when GM-CSFR is activated. Janus kinase 2/ signal transducer and activator of transcription 5 (JAK2/STAT5) and ERK are frequently involved in GM-CSFR downstream signalling pathways, with ERK activity connected to the positive impact of GM-CSF on human monocyte survival *in vivo* [212]. Additionally, GM-CSF also promotes cell survival by engaging the PI3K pathway. Therefore, GM-CSF is essential for maintaining health and coordinating various innate and adaptive immune responses [213]. Intriguingly, GM-CSF appears to engage particular signalling pathways

downstream of the activated receptor in a dose-dependent and sequential manner, which might explain the distinct cellular responses (survival, proliferation, activation, and/or differentiation) (Figure 1.24). By primarily employing receptor mutants generated in cell lines, these pathways have been linked to key residues in the intracellular domains of GM-CSFR [211].

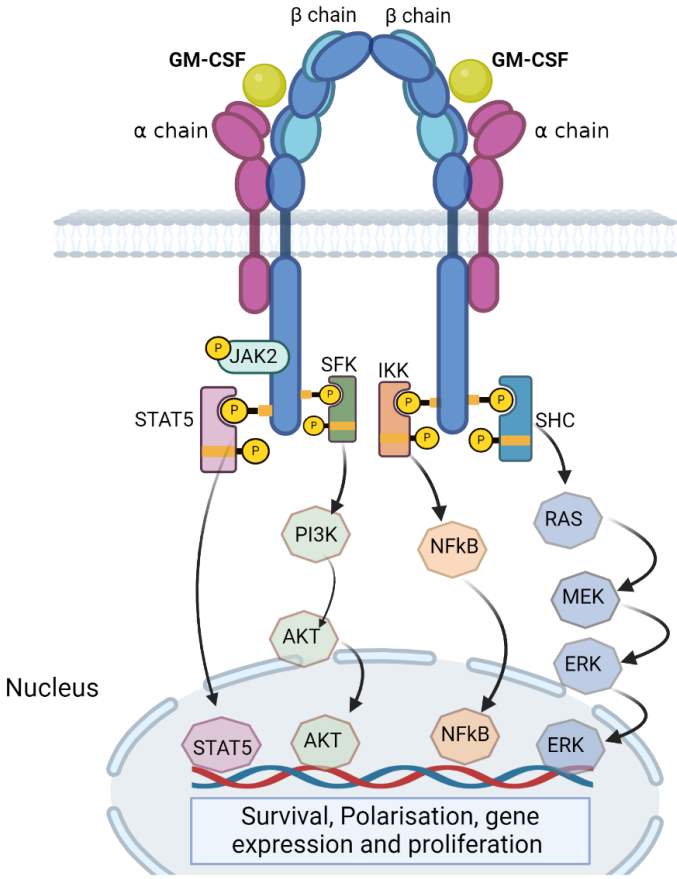

Figure 1.25. GM-CSF receptor structure and signalling pathways. The GM-CSF receptor comprises the GM-CSFRα chain, which is specific to GM-CSF, and the GM-CSFRβ chain, which is shared with other receptors (IL-5 and IL-3). Together, both chains activate multiple pathways for the required immune response. JAK2/STAT5 regulates transcription of genes for myeloid cell survival, differentiation and cytokine production. PI3K-Akt promotes cell survival, metabolism and cytoskeletal rearrangement. NF-kB induces the proinflammatory gene expression, increases antimicrobial function. MAPK/ERK pathway regulates proliferation, differentiation and activation of myeloid effector function. Adopted from [213]. Created by BioRender.

1.3.2. GM-CSF and enhanced monocyte/macrophage priming

GM-CSF alters the activation state of mature monocytes and macrophages, in addition to its well-studied effects on differentiation and proliferation. GM-CSF enhanced the production of ROS and surface MHC II in monocytes and

macrophages [214]. Additionally, without inducing these mediators on its own, GM-CSF enhances the release of several cytokines, including TNF-α, IL-1β, and IL-12, in response to LPS [215]. Since it possesses stimulatory qualities, GM-CSF may offer therapeutic benefits, compared to the current therapy available, for conditions such as infections or severe trauma, where the immune system malfunctions. However, it should be carefully considered since this activity may carry the risk of intensifying inflammatory reactions that lead to major unfavourable responses, especially when the host is experiencing infectious overload. Consequently, in-depth research on the molecular mechanisms underlying GM-CSF's ability to prime monocytes and other immune cells is required. Although GM-CSF priming is a well-documented occurrence, the signalling cascades that underlie it are not yet fully understood [216].

1.3.3. GM-CSF as a major regulator of immunity: contribution to wound healing

The transition of *C. albicans* from yeast to hyphal form is associated with several traits crucial for its interactions with the host, including adhesion to endothelial and epithelial cells. Invasion of host tissues via two mechanisms, induced endocytosis (when host cells actively engulf the fungus) and active penetration (when hyphae mechanically and enzymatically breach host cells barriers), as well as immune evasion and escape from phagocytes [40]. Fang et al. studied GM-CSF knockout mice to clarify the critical function of GM-CSF in wound healing. The results show that while collagen deposition increases in the later stages, the lack of GM-CSF causes delayed wound closure (Figure 1.25). This was associated with decreased recruitment of neutrophils and macrophages, decreased cytokine production, and impaired angiogenesis. These findings shed light on the crucial role of GM-CSF in guiding immune cells to the site of injury, regulating inflammation, and promoting the growth of new blood vessels, all essential steps for the body to heal effectively [217].

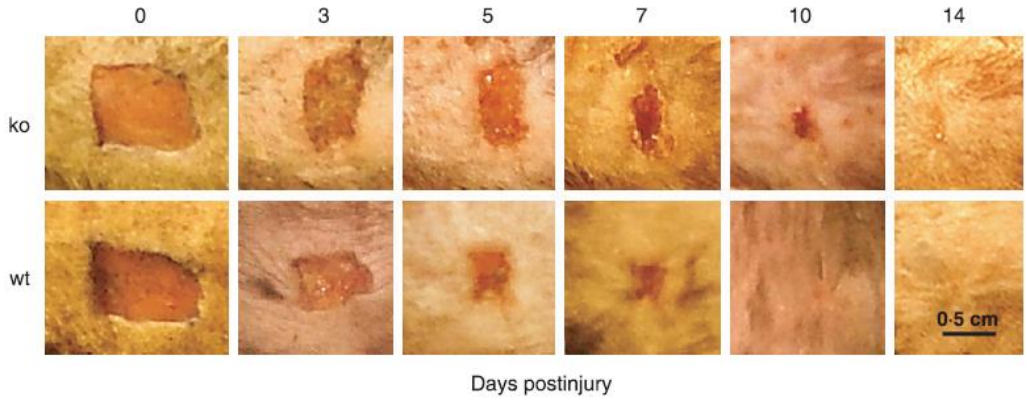

Figure 1.26. Effect of GM-CSF deficiency on skin wound closure. The closure was measured in both wild-type (wt) and granulocyte/macrophage colony-stimulating factor gene knockout (ko) mice following injury, photographs showing the macroscopic wound closure at 14 various days postinjury [217].

In order to promote keratinocyte proliferation and coordinate the intricate web of cytokines and immune cells necessary for efficient wound healing, GM-CSF functions as both an autocrine and paracrine factor. This emphasises how crucial GM-CSF is as a cytokine for controlling inflammation and encouraging tissue regeneration during wound repair [217]. Additionally, it is clear from GM-CSF gene-deficient animals or neutralising anti-GM-CSF mAbs that GM-CSF can play a significant role in tissue inflammation and the pain associated with it. Lung illness, cardiovascular disease, Experimental Autoimmune Encephalomyelitis (EAE), and arthritis are a few examples [218].

1.3.4. Role of GM-CSF in immunity against *C. albicans*

The most prevalent human fungal pathogen is *Candida* spp., and the main culprit behind invasive candidiasis is *C. albicans* [219]. Based on extensive studies, there is increasing scholarly agreement regarding the role of GM-CSF in preventing and treating fungal infections (Figure 1.26) [220].

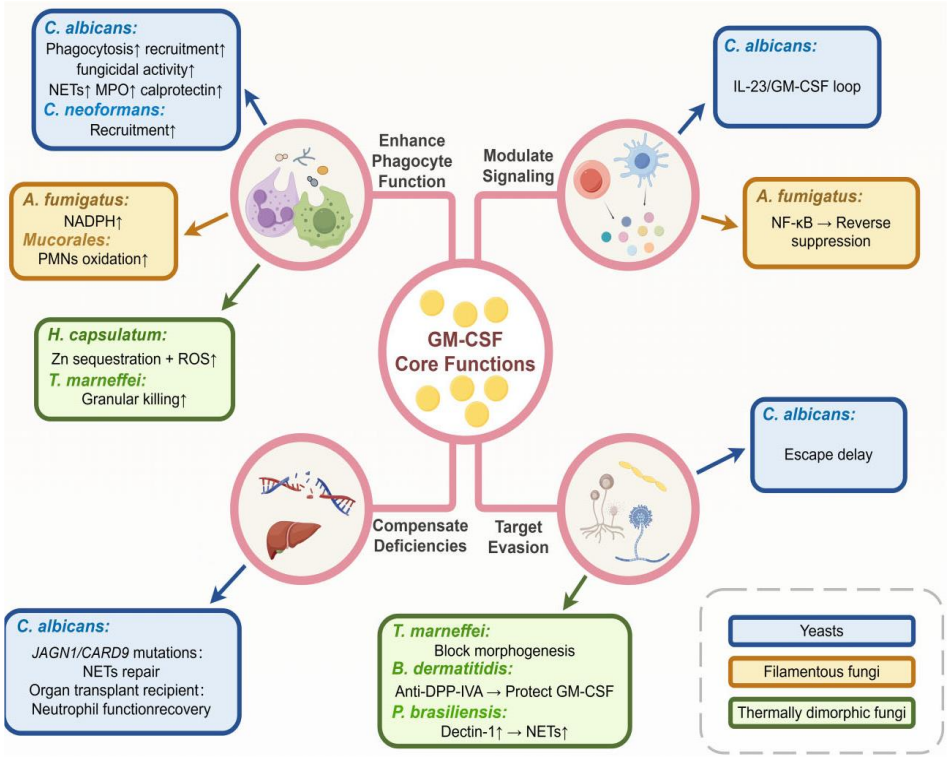

Figure 1.27. GM-CSF promotes multiple immunomodulatory defences against fungal infections. The primary roles of GM-CSF in antifungal immunity are summarised in this schematic, which illustrates filamentous fungi (yellow), thermally dimorphic fungi (green), and covering yeasts (blue). The symbols "↑" and "→" denote upregulation/enhancement and causal links, respectively. Enhancing phagocyte function and fungicidal mechanisms, regulating immune signalling, compensating for host immunological weaknesses, and targeting fungal evasion strategies are important methods. PMNs, Zn, zinc; ROS, reactive oxygen species; DPP-IV A, dipeptidyl-peptidase IV A; NETs, neutrophil extracellular traps; MPO, myeloperoxidase; and NADPH, nicotinamide adenine dinucleotide phosphate [220].

GM-CSF is essential for the neutrophil-mediated destruction of *C. albicans*. IL-17 induces NK cell precursors to produce GM-CSF during systemic *C. albicans* infection, which in turn increases neutrophil antifungal activity. High levels of GM-CSF are seen in inflammatory sites in various infections [209]. Furthermore, GM-CSF engages in a positive feedback loop with NK cells and DCs. NK cells are stimulated to produce more GM-CSF when *C. albicans* activates DCs to secrete IL-23. GM-CSF then stimulates DCs to secrete more IL-23, which intensifies the signalling cascade and increases GM-CSF release. Eventually, this process increases neutrophil phagocytic activity and strengthens the host's defences against fungus. In parallel, extensive *in vitro* research has shown that GM-CSF can partially ameliorate human neutrophil dysfunction in response to *C. albicans* infections [221]. For example, Knooihuizen et al. isolated human neutrophils from the peripheral blood of patients with liver cirrhosis and co-cultured them with *C. albicans*. They found that mycelial growth control and

neutrophil phagocytosis were significantly lower. Nevertheless, neutrophil phagocytosis against *C. albicans* and their capacity to regulate mycelial growth were recovered to almost healthy levels following pretreatment with GM-CSF [222].

1.3.5. Integration of GM-CSF in therapy as an antifungal agent

Medical advancements have made it possible for many patients who have received stem cell and solid organ transplants, rheumatological disorders, and cancer to live longer. However, many treatments alter or weaken the patient's immune system, making the immunocompromised patient more susceptible to infections from opportunistic microorganisms. Fungal infections are among the most troublesome opportunistic infections, and *C. albicans* is the major cause of invasive fungal disease (IFD) [223]. The shortage of antifungal treatment alternatives emphasises the necessity of creating innovative therapeutic approaches to improve patient outcomes. Although antifungals damage fungi, they are challenging to develop due to the eukaryotic nature of their target organisms, and they can be hazardous to patients. Increasing host immunity is an option; immunotherapy is particularly beneficial for patients with IFD who are immunocompromised. Recombinant human GM-CSF (rhGM-CSF) is a recombinant, laboratory-made form of human GM-CSF. It is a promising immunomodulatory treatment because it provides a targeted means of boosting immune responses by improving the activity of monocytes, macrophages, neutrophils, and DCs [224]. The currently available GM-CSF-based therapies include rhGM-CSF formulations, such as sargramostim, yeast-derived GM-CSF, and molgramostim, as well as *E. coli*-derived GM-CSF. They have a potent immunomodulatory property and have been investigated as adjunctive treatments during fungal infection, including *C. albicans*, to enhance host immunity [225].

1.3.6. GM-CSF-associated adverse events.

GM-CSF is frequently used to promote myeloid recovery and strengthen host defence. Still, rather than acting as a neutral supportive agent, its side-effect profile reflects its strong ability to activate and expand granulocytes and monocyte-macrophages. In addition to temporary laboratory changes like leucocytosis and mild elevations in liver enzymes or lactate dehydrogenase, which are typically dose-related and reversible after treatment interruption or dose reduction, clinical studies and post-marketing surveillance consistently

report flu-like symptoms (fever, fatigue, myalgia), headache, mild gastrointestinal disturbance, and bone or musculoskeletal pain as the most common adverse events. Although these events are best documented for G-CSF and pegylated G-CSF, they highlight the potential for severe cardiopulmonary and vascular toxicity in vulnerable patients and justify careful monitoring when GM-CSF is administered in the setting of severe systemic inflammation or pre-existing lung disease [226]. Rare but clinically significant complications have also been described in association with hematopoietic colony-stimulating factors, including splenic enlargement and rupture, acute respiratory distress syndrome (ARDS), and severe capillary leak phenomena. Peripheral oedema, capillary leak with serous effusions, hypotension, and tachyarrhythmias are less frequent but clinically significant GM-CSF-related toxicities, especially in patients with heart or lung conditions or when higher dosages are administered. As a key modulator of myeloid activation and cytokine production, GM-CSF may also worsen preexisting autoimmune or inflammatory conditions or cause inflammation in specific organs, especially the lung, where both beneficial and detrimental effects have been documented in both acute and chronic inflammatory contexts [227]. Having been considered, GM-CSF is a useful therapeutic tool; however, to balance the clinical benefit against the risk of undesired immune and vascular activation, including uncommon but potentially fatal complications such as splenic rupture and ARDS, its administration requires careful consideration of dosage, timing, and the patient's inflammatory and cardiopulmonary status.

In conclusion, due to its significant impact on immune responses, GM-CSF presents an exciting option to enhance the body's defences against fungal infections. In this project, I investigate how administering GM-CSF to primary human monocytes affects their response to *C. albicans*, specifically their recognition of the fungus, the signals they emit, and their ability to combat it.

1.4. Hypothesis

We hypothesise that by investigating GM-CSF-driven changes in monocytes during *C. albicans* infection, we will unveil novel biological processes implicated in protection against infection. These findings will inform us of the suitability of GM-CSF as a therapeutic agent against fungi.

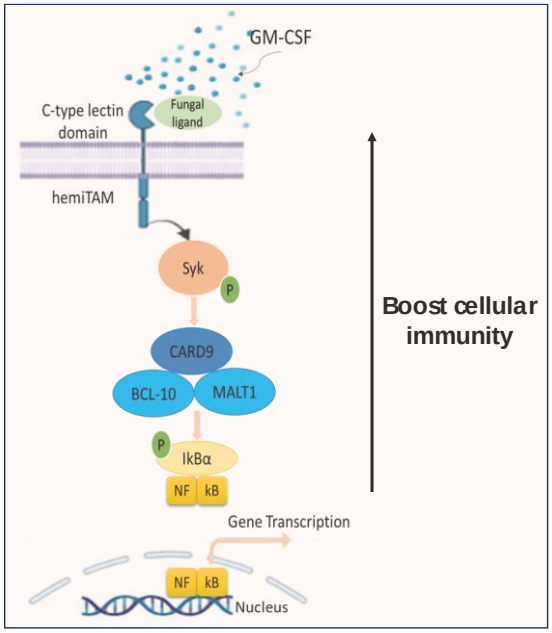

1.5. Aims

To address this hypothesis, the overarching aim of this study is to analyse the effect of GM-CSF on the interaction of human inflammatory monocytes with *C. albicans* using a novel infection assay.

Towards this aim this study has undertaken the following specific objectives:

1- Optimise the culture of inflammatory monocytes and analyse phenotypic changes in the presence of GM-CSF (Chapter 3).
2- Analyse the behaviour of *C. albicans* and monocytes when co-cultured in the presence and absence of GM-CSF (Chapter 4).
3- Investigation of the *In Vitro* Role of the Mannose Receptor in Monocyte responses to *C. albicans* (Chapter 5).
4- Establish the culture of iPSC-macrophages to dissect the pathways affected by GM-CSF that influence responses to *C. albicans* infection (Chapter 6).

Chapter 2

Materials and Methods

Introduction

This section outlines the methodologies and materials employed to investigate the effect of GM-CSF on the immune response against *C. albicans*. In general, human monocytes are isolated from healthy blood donors and cultured *in vitro*, providing a controlled environment to study the specific interactions between GM-CSF-treated monocytes and *C. albicans.*

2. Materials and methods

2.1. Isolation and culture of primary human monocytes (CD14+ cells).

Monocytes are isolated from a buffy coat of a healthy donor (NHS Blood Transfusion Services, Sheffield, Faculty of Medicine and Health Sciences Ethics Committee approval 428-1911, NCI No 1296, Customer Number D059). The buffy coat is diluted 1:2 with Hank's Balanced Salt Solution (HBSS) without Ca^{2+} and Mg^{2+} (cat number H8264-500ML, Sigma) and layered onto Histopaque 1077 (cat number 10771-100ML, Sigma) at a ratio of 35 mL cell suspension to 15 mL Histopaque in 50 mL tubes. Histopaque 1077 separated mononuclear cells from whole blood or other components [228]. Samples are centrifuged at 800 ×g for 30 minutes at 23°C with minimal acceleration and no brake. Mononuclear cells formed a distinct layer, with plasma above and red blood cells/granulocytes below, facilitating the isolation of peripheral blood mononuclear cells (PBMC) for subsequent processing (Figure 2.1).

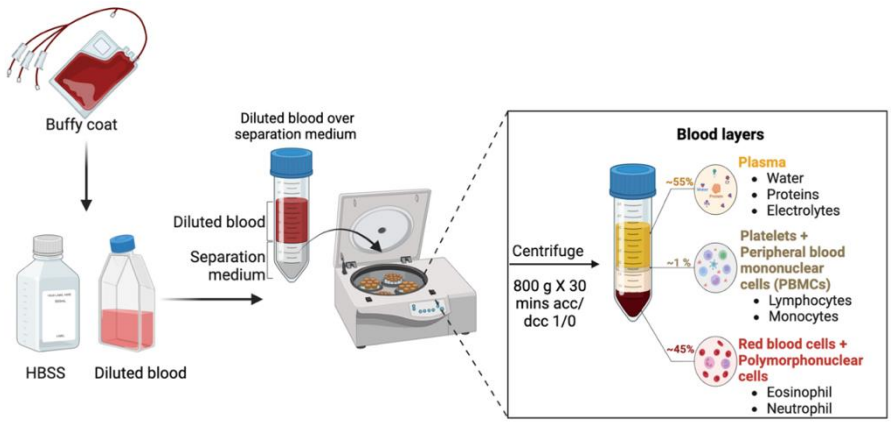

Figure 2.1. Procedure for PBMC isolation. A Buffy Coat from a healthy blood donor is emptied into a T75 flask, diluted, and then centrifuged over a density gradient. After separation, the PBMC layer is collected, washed and prepared for CD14+ selection. Figure created using BioRender.

The PBMC layer is collected, transferred to a new tube, and washed twice with HBSS. The pellet is resuspended in filter-sterilised MACS buffer containing 5% foetal bovine serum (FBS) (cat number F9665-500ml, Sigma-Aldrich) and 2 mM Ethylenediaminetetraacetic acid (EDTA, cat number E7889-100ML, Sigma) in phosphate-buffered saline (PBS, cat number D8537-500ML, Sigma). EDTA buffer is used to chelate Ca2+ and minimise cell-cell interaction or cell-plastic interactions [229]. CD14 Microbeads 400 µL (cat number 130050201, Miltenyi Biotec) are added, and the suspension is incubated for 15 minutes on ice, protected from light. After incubation, cells are washed in MACS buffer and centrifuged at 350 ×g for 5 minutes at 4°C, maintaining a cold temperature to remove the excess magnetic beads.

CD14+ cells (Monocytes) are selected following the manufacturer's recommendations. In brief, the cells are passed through a MACS column located in the magnet, and non-attached cells are removed by washing. After removing the column from the magnetic field, the CD14+ cells are eluted into the MACS buffer (Figure 2.2).

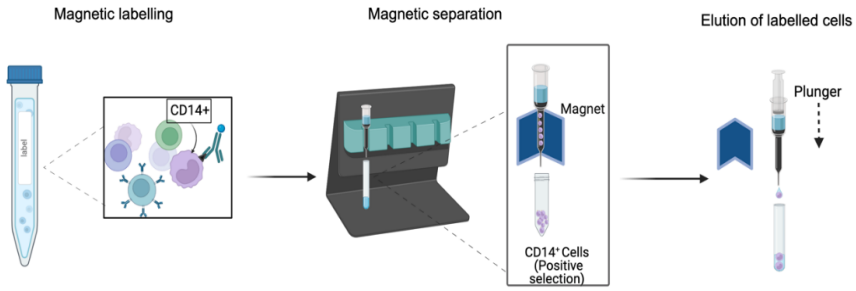

Figure 2.2. Magnetic cell sorting principle. CD14 beads are added to PBMCs, and a magnetic system is used to select CD14+ cells. Figure created using BioRender.

Monocyte viability is assessed using 4% (v/v) Trypan blue (cat number T8154, Sigma) and counted by the automated cell counter (TC20, BIO-RAD). Afterwards, monocytes are washed in phenol red-free RPMI-1640 (cat number R7509-500ML, Sigma), centrifuged at 350 ×g for 5 minutes at 23°C and resuspended in complete RPMI medium (RPMI-1640 media supplemented with 15% (v/v) AB serum (cat number H4522100ML, Sigma), 10 mM Hepes (cat number 15630056, Gibco), and 2mM L-glutamax-1 (cat number 35050038, Gibco). Cells are plated in 24-well UpCell plates (cat number 174899, Nunc) at 2 x 10^6 cells/mL, 0.5 mL per well. Half of the plate is treated with Macrophage Colony Stimulating Factor (M-CSF, 10 ng/mL cat number 130-093-963, Miltenyi Biotech) or left untreated as a negative control, and the other half is treated with

Granulocyte-Macrophage Colony Stimulating Factor (GM-CSF, 10 ng/ml, cat number 5210606282, Miltenyi Biotech). Cells were incubated at 37°C, 5% CO_2 for ~40-44 h. UpCell tissue cultures feature a temperature-responsive surface coating made of covalently immobilised poly (N-isopropyl acrylamide), which exhibits slight hydrophobicity at 37°C, allowing for cell adhesion and growth. The coating becomes highly hydrophilic when the temperature drops below 32°C, enabling easy retrieval [230]. UpCell plates enabled us to generate monocyte cultures with high viability, probably because of survival signals provided by adherent cells, and easy collection at 4°C. Incorporation of GM-CSF enabled us modelling monocytes recruited during inflammation.

2.1.1. Treatment of monocytes with Sulphated Glycopolymers (sGP)

In Chapter 5, the sGlycopolymer (S100-DP240, generously provided by Dr. Giuseppe Mantovani, School of Pharmacy, University of Nottingham) is employed to investigate MR activity. Purified monocytes (M-CSF or GM-CSF) are initially assessed for their response to sGP by incubating them with 80 µM or 160 µM concentrations for either 2 or 16 hours before monocyte collection. Based on these preliminary assessments, an incubation period of 2 hours with 80 µM sGP is selected for subsequent experiments. To calculate the sGP, the working solutions were prepared by first preparing a stock solution of the polymer (S100DP240) at a concentration of 2 mg/mL by dissolving 10 mg of the solid compound in 5 mL of PBS. The molarity of this stock solution was then calculated accordingly. For the experimental setup, 9.25 µL of this stock per well corresponds to a final concentration of 80 µM. To achieve this, we prepared a 50 µL polymer solution, which was then added to 500 µL of cell suspension in the UpCell plate. In untreated wells, the polymer treatment consisted of 40.75 µL of complete medium (GM-CSF-treated) combined with 9.25 µL of the polymer stock, while control wells received 40.75 µL of complete medium (GM-CSF-treated) with 9.25 µL of PBS. To streamline the process, a 250 µL master mix was prepared using 203.75 µL of complete medium and 46.25 µL of polymer stock, from which 50 µL was added per well.

Following treatment, monocytes are harvested and washed, the sGP is removed, and cells are adjusted to the required cell density. The cells are then either prepared for flow cytometry to evaluate surface receptor expression or infected with *C. albicans* to assess cytokine secretion and phagocytic activity.

2.1.2. Monocyte harvest and cell count

To harvest monocytes following ~40-44 h of incubation, UpCell plates are transferred from 37ºC to 4ºC for 30 minutes. M-CSF and GM-CSF monocytes are harvested from plates, washed in fresh complete-RPMI, centrifuged at 350 ×g for 5 minutes at 4°C, and resuspended in complete-RPMI medium. Finally, Monocyte viability is assessed using 4% (v/v) Trypan blue and counted by the automated cell counter from BioRad to adjust the cell number for the desired density of the following experiment, mainly 10^7 cells/mL. Which we obtain by the equation:

$$C_1V_1=C_2V_2$$

2.2. Isolation and culture of primary human macrophages (CD14+ cells).

In this project, we looked at the effect of GM-CSF on EV production by macrophages in collaboration with Dr. Lucy Fairclough's lab. The procedure for generating macrophages runs based on the monocyte purification method detailed in (Section 2.2. Isolation and culture of primary human monocytes (CD14+ cells)), which is followed up to the stage of cell treatment before incubation. After resuspending the cells in complete-RPMI, they are treated with 50 ng/mL M-CSF, plated in 24-well Ultra-Low Attachment plates, and incubated at 37°C with 5% CO_2 for six days, with feeding media on Day 3. On Day 6, cells are harvested, washed with X-Vivo-15, and seeded in 6-well tissue culture plates (cat number 0030720130, Eppendorf) at a density of 10^6 cells/mL (2 mL per well). The cells are then treated with 50 ng/mL of M-CSF and 10 ng/mL GM-CSF and incubated at 37°C with 5% CO_2 for 48 hours (Figure 2.3). After incubation, cells are harvested as described in (Section 2.2.2, Monocyte harvest and cell count).

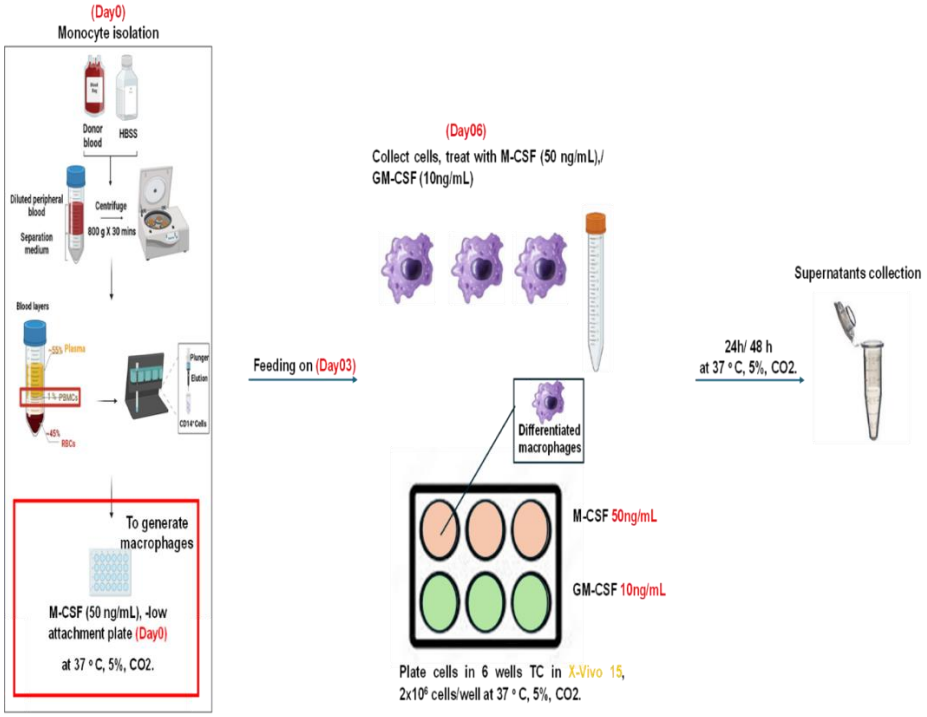

Figure 2.3. Generate macrophages from a buffy coat. CD14+ monocytes are first isolated using magnetic bead-based separation or density gradient centrifugation. The purified monocytes are resuspended in complete RPMI medium, treated with 50 ng/mL M-CSF, and seeded into 24-well Ultra-Low Attachment plates. Cells are incubated at 37°C with 5% CO_2 for six days, with media replenishment on Day 3. On Day 6, the differentiated macrophages are harvested, washed with X-Vivo-15 medium,

2.2.1. Extracellular vesicle (EV) production from macrophages

From generated macrophages, the supernatants are collected and transferred to Dr. Lucy Fairclough's laboratory, analysis of EV production following the procedure described in [231]. In brief, 20 µL of supernatants are stained with 10 µM of Calcein-AM dye for 1 h at 37°C to identify the EVs. CD9 APC, CD63 PE, and CD81 PEvio615 antibodies are used to determine tetraspanin expression. After 1 h incubation, the supernatants are diluted in 100 µL of PBS and run on the ImageStreamX MKII imaging flow cytometer (CYTEK®). Data was analysed in IDEAS software.

2.3. Culture of *C. albicans*

2.3.1. Strains used

The wild-type *C. albicans* (CS-5341) laboratory strain was kindly provided by Prof. Miguel Camara's Laboratory, Biodiscovery Institute, University of Nottingham. *C. albicans* strains labelled with GFP or dTomato were generously provided by Dr. Rebecca Drummond from the University of Birmingham (Table

2.1). All strains are prepared by harvesting cells from overnight cultures via centrifugation at 800 × g for 10 minutes at room temperature. The supernatant is carefully discarded, and the pellet is resuspended in 1 mL sterile YPD medium. Subsequently, 1 mL of sterile 80% (v/v) glycerol is added to the suspension, and the samples are stored at -80°C for long-term preservation.

Table 2.1. *C. albicans* strains employed in this thesis.

Strain	Description	Label	Relevant Details
C. albicans CS-5341	Wild-type strain	-	Standard laboratory strain used as a control
C. albicans GFP	Green Fluorescent Protein (GFP) expressing strain	GFP	Fluorescent marker for visualisation and tracking
C. albicans dTomato	dTomato Red Fluorescent Protein expressing strain	dTomato	Fluorescent marker for visualisation and tracking

2.3.2 *C. albicans* culture

C. albicans is streaked onto Sabouraud dextrose (SAB) agar (cat number KM0003, EO Laboratories LTD) and incubated at 30°C overnight. On day two, a single colony is transferred into Liquid yeast extract peptone dextrose (YPD) media (cat number 4001022, MB Biomedical) and incubated at 30°C, 200 RPM overnight.

The following day, cells are washed with PBS at room temperature. During cell counting to adjust the desired cell number, cells are maintained in PBS on ice to prevent accidental hyphal formation. Due to the high cell density in the suspension, which made counting challenging, a 1:50 dilution in PBS is prepared in 1 mL. Next, ~15 µL of the diluted cell suspension is carefully loaded onto a hemocytometer and examined under a light microscope. For counting yeast cells, the sample is observed at 10x magnification, focusing on the central grid. Cells are counted within five designated squares, and the average count is calculated. This value is then adjusted by applying the dilution factor and multiplying by 250,000 (a constant derived from the dimensions of the hemacytometer's central square). The resulting figure represents the cell concentration per millilitre (Figure 2.4).

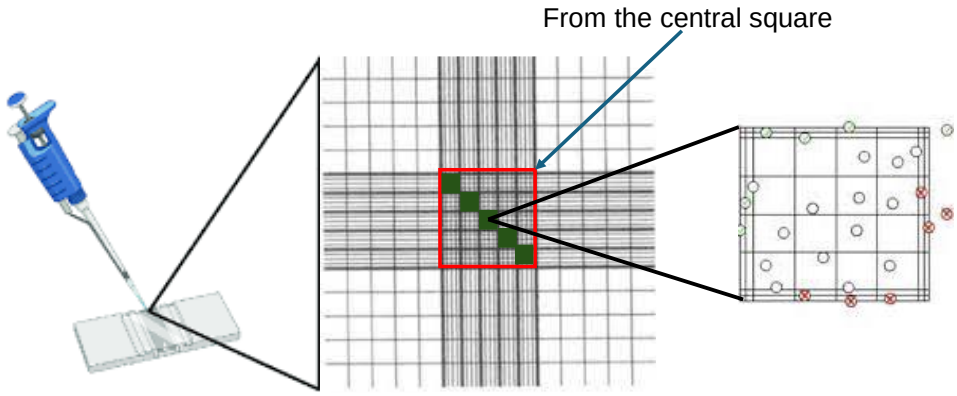

Figure 2.4. Counting of *C. albicans* **yeast cells using a haemocytometer.** The central square of the haemocytometer grid was selected for counting (outlined in red||). Cells within five smaller squares (highlighted in green) are counted based on cells located on the sub-squares, and the average number of cells per square is calculated and added to the dilution factor and the dimension measures. The resulting count is then used to calculate the required cell density for infection assays.

2.3.3. Infection of human monocytes with *C. albicans*

Infection assays are set up in 24 wells Ultra Low-attachment Plates (cat number CLS3473, Sigma-Aldrich). Five conditions are routinely used: uninfected M-CSF-monocytes (negative control), uninfected GM-CSF-monocytes, infected M-CSF-monocytes, infected GM-CSF-monocytes and *C. albicans* only (positive control). Isolated monocytes and grown *C. albicans* cocultured by both microorganisms are washed with complete-RPMI medium, counted and adjusted to 1 x 10^7 cells/mL and dispensed into wells (100 µl per well, final volume 200 µl, to achieve MOI 1). Monocytes (100µl) are added to the wells, then *C. albicans* (100µl) are added on top; for uninfected monocytes and *C. albicans* only, 100µl complete-RPMI medium is added. Cultures are then incubated at 37ºC, 5% CO_2, 3 h. In some instances, like phagocytosis assays, MOI 10 was used, and plates are incubated for 1 hour (Figure 2.5).

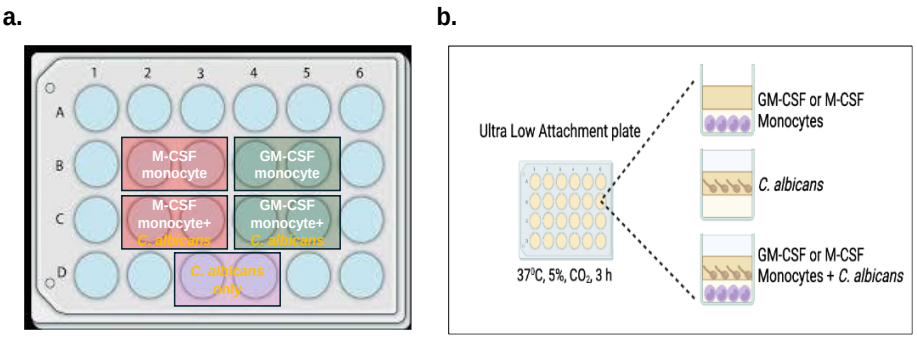

Figure 2.5. Infection assay set up. Infection assays were routinely set up at MOI1, i.e. 10^6 of monocytes and live *C. albicans* per well in a total volume of 200µL. **a.** Plate map of the infection assays showing the arrangement of five conditions, i.e. infected and non-infected M-CSF monocytes, infected and non-infected GM-CSF monocytes and *C. albicans* only. **b.** Schematic representation of how infections were set up with C. albicans added last to minimise hyphae formation prior encounter with monocytes. Clear squares represent complete RPMI media.

2.3.4. Quantification of *C. albicans* CFU and hyphae formation after incubation with human monocytes

A pivotal aim of this project is to demonstrate the GM-CSF-treated monocytes in enhancing the control of fungal viability. In order to achieve this aim, infection assays are tested for CFU and hypha growth. In addition to CFU, hyphal growth is measured by measuring the length of the produced hyphae.

The viability of *C. albicans* is assessed using CFU quantification. Serial 10-fold dilutions are made in PBS, and 20 µL from each dilution is dispensed on SAB agar and then incubated at 30°C overnight. The next day, colonies are collected and counted to calculate the CFU per mL based on the CFU formula:

CFU/mL = (number of colonies x dilution factor) / volume of culture plate.

To determine hypha growth infection assay, plates are fixed at the time of infection and at 1, 2 and 3 h post-infection using 4% paraformaldehyde (PFA, paraformaldehyde cat number 15710-5, Electron Microscopy Sciences) and bright-field images are collected using a ZOE™ microscope (Bio-Rad). Hyphae growth is measured using Fiji software. A line is manually drawn along each hypha to measure its length in micrometres. Using the ROI manager, each line is labelled, and the length is measured. To ensure consistency, five images are captured from each well: upper right, upper left, lower right, lower left, and the central field. Then, all measurements are averaged and plotted for statistics. The measurements are then compiled in an Excel sheet, which is repeated in three independent repeats. Finally, the hyphal lengths are statistically analysed using GraphPad Prism. Figure 2.6 below shows an example to illustrate how the analysis was done.

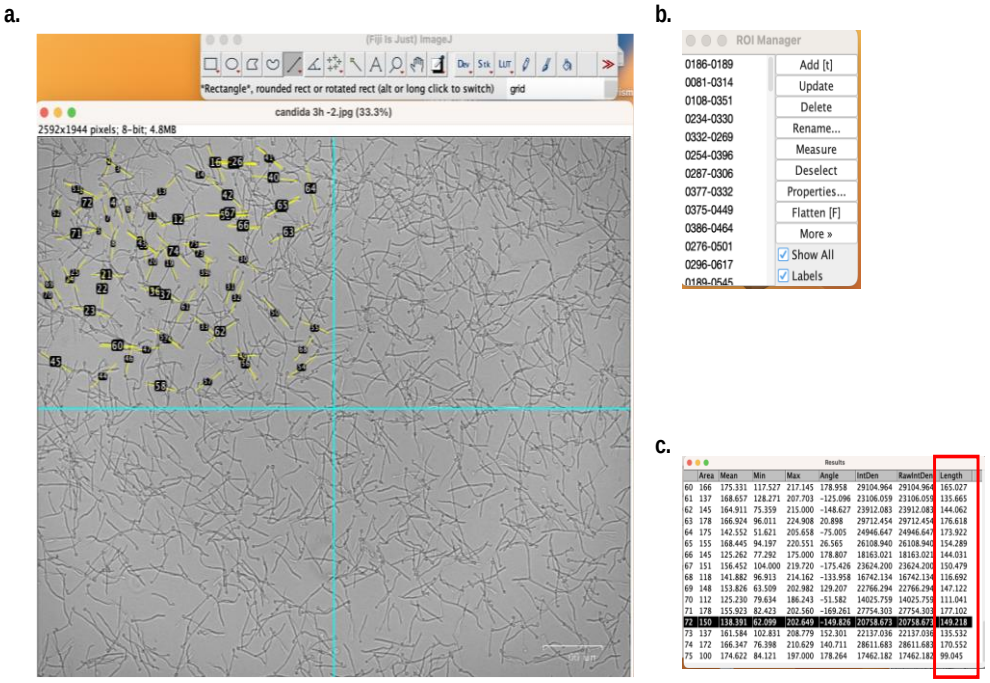

Figure 2.6. Hyphal length measurement. Images were captured from infected monocytes and *C. albicans* alone samples at various time points to assess hyphal length. **a.** Images were divided into four grids to minimise counting errors. A line was drawn over each hypha, from the beginning to the hypha tail end, and each line was labelled and numbered. Only straight hyphae were quantified, while overlapping, highly curved, or ambiguous hyphae were excluded. **b.** Each labelled line was collected and measured using the Region of Interest (ROI) tool. **c.** The measurement results are indicated by the Length parameter in micrometres (highlighted in red). Analysis was done using Fiji software.

2.5. Flow cytometry

Flow cytometry was used to analyse monocyte surface marker expression and study phagocytosis.

2.4.1. Expression of surface receptors

Monocytes are cultured as described in (Section 2.2. Isolation and culture of primary human monocytes (CD14+ cells)), then washed in PBS-FBS buffer containing (0.5% FBS and 0.1% sodium azide in PBS without Ca^{2+}/Mg^{2+}). Cells are then incubated in PBS-FBS buffer containing 5% (v/v) human serum for 1 h at 4°C to block the IgG. During flow cytometry experiments, PBS-FBS buffer is often used as a buffer to prevent cell clumping and non-specific binding [232]. After that, cells are labelled with specific antibodies and isotype control, as shown in table 2, then incubated for 1 h at 4°C. Finally, cells are washed with PBS-FBS buffer, resuspended in 4% PFA in PBS, and stored in the dark at 4°C

until analysis using an ID7000 in spectral Flow cytometry facility, University of Nottingham, run by Dr David Onion. Data was analysed in Kaluza.

Table 2.2. List of antibodies used for flow cytometry and concentrations used.

Antibody	Supplier	Concentration/ml	Catalogue number	Clone	Isotype	Volume per test (µl)
MR-Brilliant Violet 421	BioLegend	100µg/ml	321126	15-2	IgG1	5
IgG1-Brilliant Violet 421	BioLegend	100µg/ml	400158	MOPC-21	IgG1	5
CD11b-Brilliant Violet 711	BioLegend	100µg/ml	301344	ICRF44	IgG1	5
IgG1-Brilliant Violet 711	BioLegend	100µg/ml	400168	MOPC-21	IgG1	5
HLA-DR-Brilliant Violet 605	BioLegend	50µg/ml	307640	L243	IgG2a	5
IgG2a-Brilliant Violet 605	BioLegend	100µg/ml	400270	MOPC-173	IgG2a	2.5
Dectin-2 488-conjugated	R&D Systems	200µg/ml	FAB31141G-100UG	545925	IgG2b	5
Dectin-1 488-conjugated	R&D Systems	200µg/ml	FAB1859G-100UG	259931	IgG2b	5
IgG2 488-Conjugate	R&D Systems	200µg/ml	IC0041G	133303	IgG2b	5
PE/Cyanine7 anti-human CLEC5A Antibody	BioLegend	200µg/ml	371712	14H4-1-2	IgG2b, k	5
PE/Cyanine7 Mouse IgG2b, k Isotype Ctrl	BioLegend	100µg/ml	400326	MPC-11	IgG2b, k	5

.

2.4.2. Phagocytosis assay

For phagocytosis essays, infection assays are performed using MOI 10 and GFP-expressing *C. albicans* and incubated for 1h. post-infection, cells are collected and incubated in 5% human serum PBS-FBS buffer at 4^{o}C for 1 h and stained for either MR or CD11b as described above. Samples are analysed using an ID7000 flow cytometer and an ImageStreamX MKII imaging flow cytometer.

2.6. Enzyme-linked immunosorbent assay (ELISA)

Cytokines in supernatants from infection assays are quantified using Ready Set Go ELISA, DuoSet® assays shown in Table 2.3, following the manufacturer's guidelines.

Table 2.3. List of cytokine quantification kits used in this thesis from R&D DuoSet®.

Cytokine	Company	Cat number
TNF-α	DuoSet ELISA R&D	DY210-05
IL-6	DuoSet ELISA R&D	DY206-05
IL-1β	DuoSet ELISA R&D	DY201-05
CCL-22	DuoSet ELISA R&D	DY336
CCL-17	DuoSet ELISA R&D	DY364-05
CCL-5	DuoSet ELISA R&D	DY278-05
CXCL-9	DuoSet ELISA R&D	DY392-05

2.7. qPCR analysis

To quantify expression of CD206 (MRC1) and Dectin-1 (CLEC7A) in human monocytes by qPCR, cells treated with M-CSF or GM-CSF for ~40 hours as described in (Section 2.2. Isolation and culture of primary human monocytes (CD14+ cells)) are harvested and used for RNA extraction using the RNeasy kit (cat number 73104, Qiagen) following the manufacturer's specifications. The yield and purity of the RNA are measured photometrically using Thermo Scientific's NanoDrop™ Spectrophotometer. The RNA is reverse transcribed into cDNA using Fisher random hexamers (400 ng/µL) and Moloney Murine Leukaemia Virus (M-MLV) Reverse Transcriptase. Each sample had three replicates and a negative control (RT-). qPCR reactions are prepared with SYBR Green dye, gene-specific primers for MRC1 and Dectin-1 and used as housekeeping genes for HRPT or GAPDH. Primers are added to the master mix to reach a final concentration of 250nM in a 25µl reaction.

Primers are listed in Table 2.4:

Table 2.4. List of primers used in qPCR analysis

Target Gene	Primer Type	Sequence (5'-3')
MR	Forward	CACCATCGAGGAATTGGACT
	Reverse	ACAATTCGTCATTTGGCTCA
Dectin-1	Forward	TCCTAAAGATAGACAGCTCAAT
	Reverse	CCAGAGCCATGGTACCTCA
hGAPDH	Forward	AGCCACATCGCTCAGACAC
	Reverse	GCCCAATACGACCAAATCC
HRPT	Forward	AAATTCTTTGCTGACCTGCT
	Reverse	TTCCCTGTTGACTGGTCATT

The qPCR reaction is incubated under the following conditions: An initial denaturation phase at 95°C for 20 sec, followed by 40 cycles of denaturation at 95°C for 3 sec, annealing at 60°C for 30 sec, and extension at 72°C for 60 sec. A final extension step was performed for 15 seconds of extension at 95°C, followed by 60 seconds of annealing at 60°C and another 15 seconds of extension at 72°C. There were 42 cycles in all.

2.8. Proteomic analysis

Lysates are prepared from monocytes and sent by Dr. Daniel Scott to the biological mass spectrometry and clinical proteomics group at NTU. Led by David Boocock and Clare Coveney.

In brief monocytes are treated with 10 ng/mL of GM-CSF or M-CSF for ~44 hours. Then they are washed in RPMI-1640, centrifuged at 350 ×g for 5 minutes at 23°C and lysed in ice-cold Radio-Immunoprecipitation Assay buffer (RIPA buffer) to extract total protein (cat number 89901, Thermo Fisher). Protein concentrations were measured using a BCA assay (cat number 23227, Thermo Fisher Scientific). Additionally, lysates are analysed by SDS-PAGE to ensure that their quality is good (gels were run by Dr. Danielle Scott).

Protein identification and quantification are performed using Liquid Chromatography-Tandem Mass Spectrometry (LC-MS/MS). The proteomics facility at NTU provided the data on protein expression and further analysis.

2.9. Microscopy

2.9.1. ZOE Fluorescence microscopy

Infection assay plates using GFP-*C. albicans* are fixed with 4% PFA, and images are taken with a ZOE^{TM} Fluorescent Cell Imager (Bio-Rad). Full details of how images are taken are fully explained in (Section 2.3.4. Quantification of *C. albicans* CFU and hyphae formation after incubation with human monocytes).

2.9.2. Live microscopy

To determine whether GM-CSF affects the motility of monocytes. Monocytes are cultured as described in (Section 2.2. Isolation and culture of primary human monocytes (CD14+ cells)). Then, monocytes are washed in the complete-RPMI medium at 300 x g, 4°C, for 5 min and resuspended cells fresh complete-RPMI. Monocytes are plated on a 96-well plate (cat number 442404, Thermo Scientific). Monocytes are then adjusted for density at 2 x 10^5 cells/ml in duplicates (M-CSF and GM-CSF monocytes). The plate is taken immediately to real-time microscopy for imaging (transferred in ice). Images and videos are taken by LiveCyte® microscopy over 6 h, at SLIM facility, run by Dr. Joelle Goulding. The system captures both images and videos. While the machine can measure various parameters like phagocytosis, wound healing and cell signalling, we focus on motility, explicitly assessing the instantaneous velocity. Analysis is conducted across three independent repeats.

2.9.3. Confocal microscopy

Isolated monocytes are treated with 10 ng/mL GM-CSF or M-CSF and incubated for ~24 hours. Following incubation, cells are washed with complete RPMI and seeded into 8-well ibidi plates (cat number 80806, ibidi) at a density of 10^5 cells/well in complete RPMI containing either GM-CSF or M-CSF and allowed to adhere overnight. Three plates are prepared to assess different time points: at the time of infection (0 min), and after 5, 10, and 15 minutes.

The next day, cells are washed, and *C. albicans* is added at MOI 10. Infected cells are incubated for 5 minutes in complete RPMI to facilitate interaction. Subsequently, cells are washed with cold RPMI-1640 to remove unbound yeast. Warm complete RPMI is then added, and plates are incubated at 37°C, 5% CO_2 for the specified time points (5, 10, and 15 minutes). Post-incubation, cells are fixed, washed, and permeabilised with a blocking/permeabilisation buffer (5% normal donkey serum, 0.25% Triton X-100 in PEM buffer) for 1 hour. Primary antibodies—mouse anti-CD206 (cat number MA5-44033, Invitrogen) and/or

goat anti-CLEC5A (cat number PA5-47307, Invitrogen)—are added at a concentration of 10 µg/mL and incubated overnight at 4°C. Control wells are maintained in blocking buffer without primary antibodies.

The following day, cells are washed and incubated for 45 minutes with secondary antibodies: Alexa Fluor 488-conjugated donkey anti-mouse IgG (cat number 715-545-150, Jackson ImmunoResearch) and Alexa Fluor 594-conjugated donkey anti-goat IgG (cat number 705-585-147, Jackson ImmunoResearch). After washing, nuclei are stained with DAPI to label viable cells, and cells are subsequently fixed with 4% PFA in PBS (Figure 2.7).

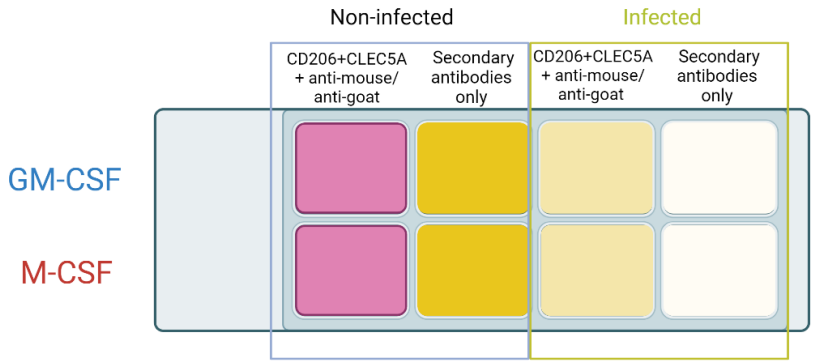

Figure 2.7. Set up for infection assay and antibody labelling in ibidi wells.

2.10. Macrophage generation from immortalised pluripotent stem cells (iMacs).

A stepwise differentiation protocol was used to generate macrophages from human induced pluripotent stem cells (iPSCs) [233]. The iPSC line KOLF2.1J, which is widely recognised for its robustness and broad applicability across experimental platforms [234], was maintained under feeder-free conditions in complete E8 medium (cat number 0599, STEMCELL). On day 1, iPSC colonies were gently dissociated into single cells using TrypLE™ (cat number 12605-010, Gibco by Life Technologies) to initiate embryoid body (EB) formation as the first step of iMacs generation. The single cells were then seeded into AggreWell™ plates (cat number 34825, STEMCELL Technologies) and centrifuged to promote the formation of uniform EBs within the microwells. EBs were cultured in E8 medium, supplemented with a combination of 50 ng/mL growth factors to support early haematopoiesis: ROCK inhibitor (cat number Y-27632, SelleckChem), BMP-4 (cat number 120-24B-50UG, PeproTech), SCF (cat number GMP300-07-100UG, PeproTech), and VEGF (cat number 100-20-10UG, PeproTech). In some experiments, iPSCs were also maintained on

inactivated feeder cells and used to generate EBs through enzymatic dissociation and culture on Ultra-Low attachment plates.

By day 4, EBs were transferred to standard tissue culture plates and cultured in X-VIVO^{TM} 15 medium supplemented with 50 ng/mL M-CSF and 25 ng/mL IL-3 (cat number 130-093-909, Miltenyi) to support differentiation into pre-macrophages. The medium was refreshed every six days to maintain cell health and encourage ongoing development. Pre-macrophages (a cellular estate maturation) were then matured into iPSC-derived macrophages (iMacs) by continuing culture in X-VIVOTM 15 medium with 50 ng/mL M-CSF for 5 to 7 days. During this time, cells acquired the characteristic morphology and surface markers of mature macrophages. On day 16, cells were treated with either 10 ng/mL M-CSF or GM-CSF for approximately 40 hours before being harvested for downstream analyses, including flow cytometry and qPCR. This experiment was carried out in collaboration with Dr. Daniel Scott's laboratory (Figure 2.8).

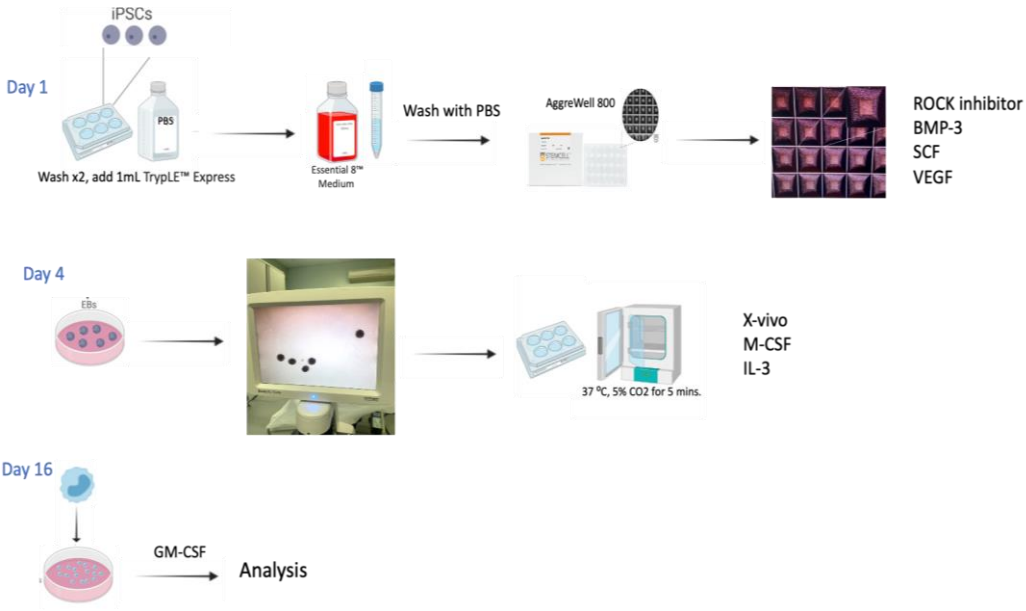

Figure 2.8. Generation of macrophages from iPSCs. Diagram outlining the defined protocols for the differentiation of macrophages from iPSC.

2.11. Statistical analysis

Data are analysed using GraphPad Prism. Results are presented as the mean and the standard error of the mean (SEM). Comparisons between groups were performed using appropriate tests, such as the student’s t-test, ANOVA, or the Mann-Whitney test, depending on the data's normality. P-values less than 0.05 were considered statistically significant. Data from at least three independent experiments were included to ensure the reliability of the results.

Chapter 3

Characterisation of the response of human monocytes to GM-CSF.

3.1. Introduction

Monocytes are crucial components of the immune response against infections, including fungi such as *C. albicans* [235]. These cells are some of the first immune cells to respond when *C. albicans* invades the host [186]. In addition to preventing fungal germination and mediating phagocytosis, these cells show rapid candidacidal activity [236]. Monocyte functionality during *C. albicans* infection has been investigated *in vivo* mainly using murine models [187]. To advance our understanding of the contribution of monocytes to the defence against *C. albicans* infection in humans and how it is affected by GM-CSF, it is imperative to establish the effects of GM-CSF on human monocytes within our laboratory settings to ensure accurate and reproducible results.

To investigate monocytes *in vitro*, obtaining a highly viable cell population is a fundamental prerequisite. Peripheral blood mononuclear cells (PBMCs) serve as a widely used starting material due to their accessibility and the presence of monocytes within this heterogeneous population. Various cell isolation procedures exist, each with distinct advantages and limitations. Old methods, such as microfluidic-based techniques, including hemodynamic and hydrodynamic separation, enable label-free isolation based on cell size and deformability, yielding high-purity monocyte populations with minimal cellular perturbation[237]. However, these methods are now less commonly used due to their high cost, limited throughput, and technical complexity compared to traditional methods [238].

Alternatively, monocyte isolation via adherence remains a well-established conventional method for generating monocyte-derived dendritic cells (MDDCs), leveraging the inherent ability of monocytes to adhere to glass or plastic surfaces [239]. Figueroa et al. compared two approaches to isolate monocytes and differentiate them into MDDCs: adherence-based selection and negative enrichment via magnetic separation. The isolated monocytes were cultured in the presence of IL-4 and GM-CSF to promote differentiation to DCs. After seven days, cells were harvested and stained with fluorochrome-conjugated antibodies targeting CD11c and CD14. Imaging flow cytometry analysis revealed that both isolation methods successfully generated MDDCs, with over 70% of cells expressing CD11c, confirming effective differentiation.

Among conventional techniques, density gradient centrifugation using positive selection, such as Ficoll-Paque separation, remains one of the most commonly employed methods, facilitating PBMC enrichment from whole blood. In our study, monocytes were positively selected using a combination of density

gradient centrifugation and magnetic-activated cell sorting (MACS). Density gradient centrifugation was performed to deplete granulocytes and erythrocytes, thereby enriching for PBMCs. This was followed by MACS-based selection using CD14+ microbeads for positive isolation of monocytes. For positive selection, specific beads are used to bind with the target cell-specific antigen (CD marker). For example, labs working with lymphocytes would use CD3 to identify T cells and CD19 to identify B cells [240]. For monocyte isolation, cells are positively selected by their expression of CD14, a monocyte surface marker that functions as a co-receptor for endotoxin, using CD14+ microbeads. The use of MACS enables the retrieval of a highly pure monocyte population (90% and above) while preserving cell viability and functionality, making it an optimal choice for downstream experimental applications. By employing this approach, a well-defined monocyte population was obtained and subsequently treated with GM-CSF to investigate its phenotypic and functional characteristics. The following results outline the effects of GM-CSF treatment on monocyte viability, surface marker expression, and immune function.

Monocytes are major targets for GM-CSF and, accordingly, express the GM-CSF receptor (GM-CSFR) [241]. Numerous *in vitro* models have been employed to investigate the effect of GM-CSF on monocytes. For instance, Lacey et al. examined various human and murine macrophage populations by isolating monocytes from human blood and bone marrow cells from mice, then treating them with M-CSF or GM-CSF. They subsequently compared the global gene expression profiles of macrophages derived from human monocytes treated with GM-CSF or M-CSF, and from murine bone marrow cells treated with either cytokine. Their findings revealed that GM-CSF promotes the differentiation of monocytes into macrophages with a different phenotype from those induced by M-CSF when GM-CSF was present. According to transcriptomic analyses, monocytes treated with GM-CSF exhibited characteristics more closely resembling those of macrophages than of DCs. Overall, their research shows that M-CSF and GM-CSF differentiate distinct macrophage morphologies, with GM-CSF adopting a profile more consistent with macrophages [242].

Current research has consistently shown that EV cargo can affect and change the condition of its acceptor cells. Determine the amount and composition of vesicles discharged into the environment, whether protein regulators are present, whether culture conditions such as hypoxia, oxidative or thermal stress, or pH fluctuations are present, and whether other substances, such as

medications, are present [243]. Finally, with a wide range of applications in the prevention, diagnosis, prognosis, and treatment of various medical conditions, EVs have been considered as potential disease biomarkers, vaccine components, or drug delivery vehicles due to the ongoing advancements in bio-nanotechnology and nanomedicine, as well as the increased focus on EV research [244].

In this chapter, we describe the development of a “monocyte to phagocyte transition” model to generate monocytes that mimic monocytes newly recruited to tissues. Due to monocytes having a strong adhesion to tissue culture surfaces, cell harvesting can be challenging, resulting in significant cellular loss. Therefore, we cultured monocytes in UpCell tissue culture plates. The UpCell™ surface is a temperature-responsive surface that supports non-enzymatic harvesting of adherent cells for the preservation of cell viability.

3.2. Hypothesis

We hypothesise that the use of the UpCells plate to culture freshly isolated CD14+ human monocytes in the presence and absence of GM-CSF will facilitate the generation of highly viable suspensions of monocytes suitable for future experimental work to study how GM-CSF influences the interaction of human monocytes with *C. albicans*.

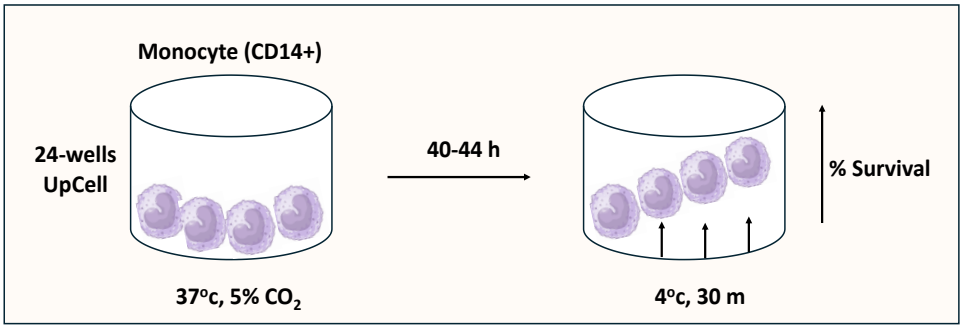

3.3 Specific objectives

To address the above hypothesis, cultures of purified CD14+ monocytes maintained in UpCells in the absence and presence of GM-CSF were tested for:

- Cell recovery and viability.
- Expression of selected surface markers.
- Changes in motility.
- Changes in protein expression.

In addition, we extended this study to analyse how GM-CSF influences the production of extracellular vesicles by human macrophages.

3.4. Results

3.4.1. Monocytes cultured in the absence of growth factor (untreated) display reduced viability compared to GM-CSF-treated monocytes.

At the beginning of this project, untreated monocytes were used as a negative control for GM-CSF-treated monocytes, as cell adherence using UpCell plates and the presence of human serum were considered suitable survival factors. Monocytes were purified by positive selection based on CD14 expression and cultured in UpCells in 15 % human serum and in the presence and absence of human GM-CSF (10 ng/ml) (see Chapter 2, 2.2. Isolation of human monocytes (CD14+ cells)). The dose of GM-CSF was selected based on previous experience in the laboratory with the generation of human macrophages treated with GM-CSF [245] and the optimised macrophage protocol developed in the laboratory. Quantification of cell numbers and viability after 40-44 h showed a reduced recovery of untreated monocytes ($7x10^5$ to $1.45x10^6$ cells/ml) in comparison to GM-CSF-treated monocytes ($1.18x10^6$ to $1.60x10^6$ cells/ml) (Figure 3.2. a) and lower percentages of viable cells (Figure 3.2.b) in untreated cultures (60-80%), compared to GM-CSF-treated cultures (~95%) (Figure 3.2.b).

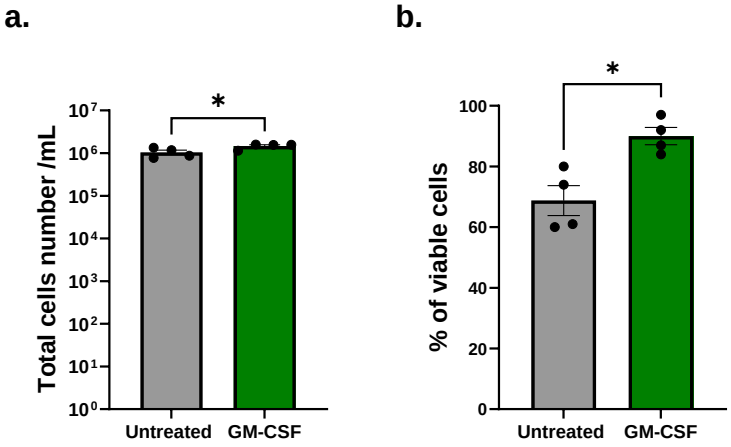

Figure 3.1. Effect of GM-CSF on human peripheral blood CD14 monocytes recovery and viability. Isolated monocytes were treated with 10 ng/mL GM-CSF or left untreated and incubated for 40-44 h, as described in Chapter 2. Cells were harvested and stained with Trypan blue for cell counting and calculation of percentage of viable cells. **a.** Total number of cells from untreated and GM-CSF-treated cultures per mL. **b.** Percentage of viable cells from untreated and GM-CSF-treated cultures (N=4). Graphs show mean +/- SEM and individual values. Data were analysed using paired t-test. (*) $p<0.05$.

3.4.2. GM-CSF alters expression of selected surface markers in human monocytes compared to untreated monocytes.

We used flow cytometry to determine potential phenotypical differences between GM-CSF-treated and untreated monocytes and analysed the expression of the surface markers HLA-DR and CD11b, as well as the C-type lectin receptors MR (CD206), Dectin-1, and Dectin-2 after 40-44 h culture. Figure 3.3. a and b show the gating strategy and selection of single cells, respectively, using Kaluza. In the plots, the x-axis displays FSC for size discrimination, and the y-axis displays SSC, a measurement of cellular granularity. Together, FSC and SSC provide valuable characteristics of the monocytes, including homogeneity of the populations. Monocytes are large cells with lower granularity than neutrophils [246], so the FSC and SSC of monocytes show intermediate values for monocytes treated with M-CSF (Figure 3.3. a.1) and GM-CSF (Figure 3.3. b.1). Followed by a singlet gate was created from the live cell gate to eliminate clumps of cells or any event that might confound the analysis. GM-CSF-treated monocytes appeared more homogeneous than untreated monocytes, with two distinct populations observed. The single gate was used to generate histograms displaying the expression of receptors detected using specific antibodies in comparison to their isotype controls and the unstained cells. For each repeat, we calculated the relative median fluorescence intensity (rMFI) by dividing specific antibody value on isotype control value. In some essays, we encountered an issue where the HLA-DR isotype control showed more binding than the specific antibody, which was resolved by titrating both the isotype and the specific antibodies. Representative histograms of singlet cell gates labelled with specific antibodies and the corresponding isotype and unstained controls are shown in Figure 3.3. a.2 and b.2 for both conditions.

Flow cytometry data analysis revealed that although untreated monocytes remained viable and expressed HLA-DR and CD11b, the levels were much lower than those of GM-CSF-treated monocytes. However, no MR was detected in the absence of GM-CSF treatment. Also, no clear trend was seen for Dectin-2, but Dectin-1 (tested only once) was slightly increased in GM-CSF-treated monocytes. In this repeat, MR was highly expressed in monocytes treated with GM-CSF, indicating that the GM-CSF treatment was effective (Figure 3.3. c).

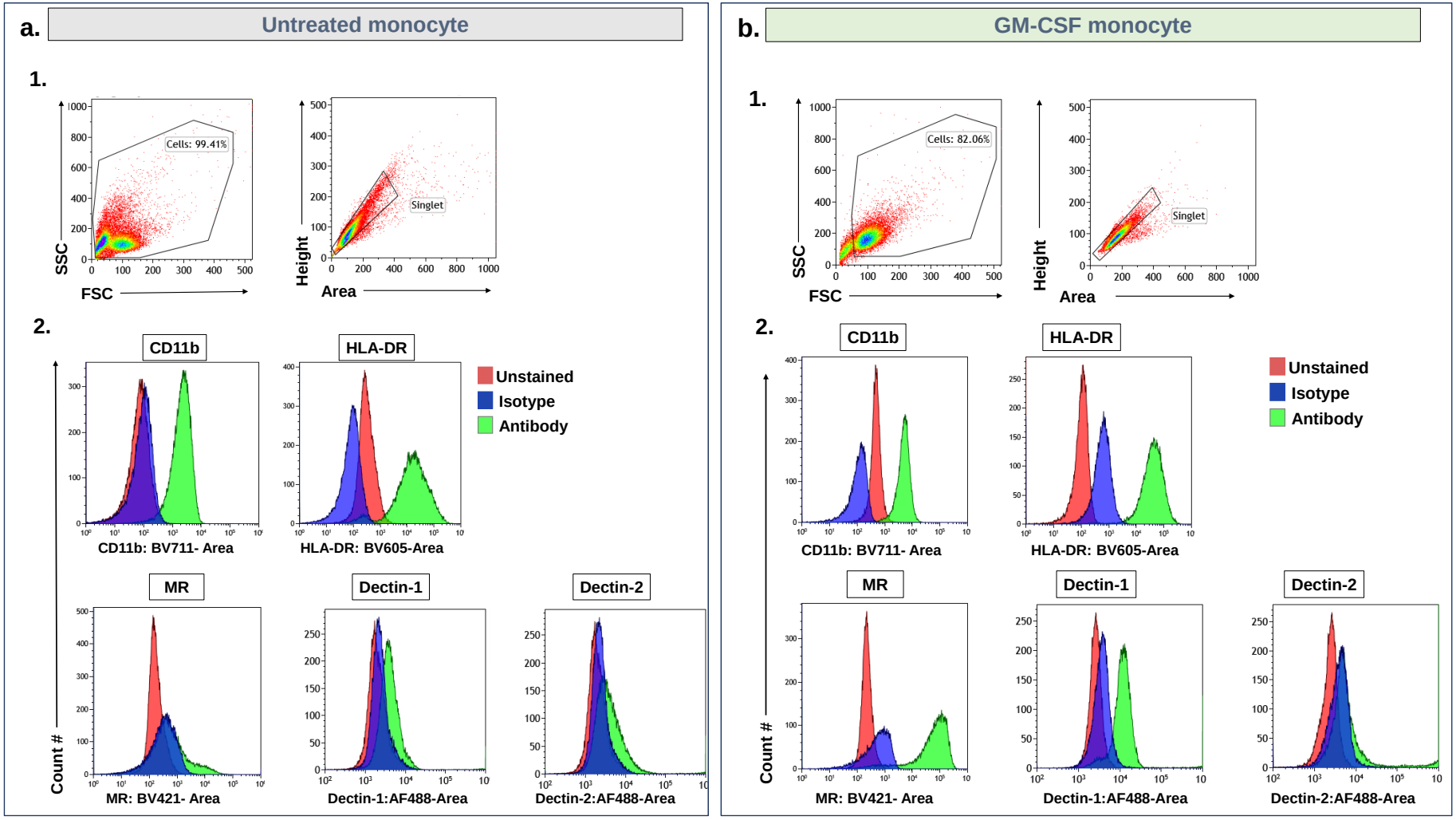
a.
Untreated monocyte
1.
Cells: 99.41%
SSC
FSC
Singlet
Height
Area
2.
CD11b
HLA-DR
Unstained
Isotype
Antibody
CD11b: BV711- Area
HLA-DR: BV605-Area
MR
Dectin-1
Dectin-2
Count #
MR: BV421- Area
Dectin-1:AF488-Area
Dectin-2:AF488-Area
b.
GM-CSF monocyte
1.
Cells: 82.06%
SSC
FSC
Singlet
Height
Area
2.
CD11b
HLA-DR
Unstained
Isotype
Antibody
CD11b: BV711- Area
HLA-DR: BV605-Area
MR
Dectin-1
Dectin-2
Count #
MR: BV421- Area
Dectin-1:AF488-Area
Dectin-2:AF488-Area

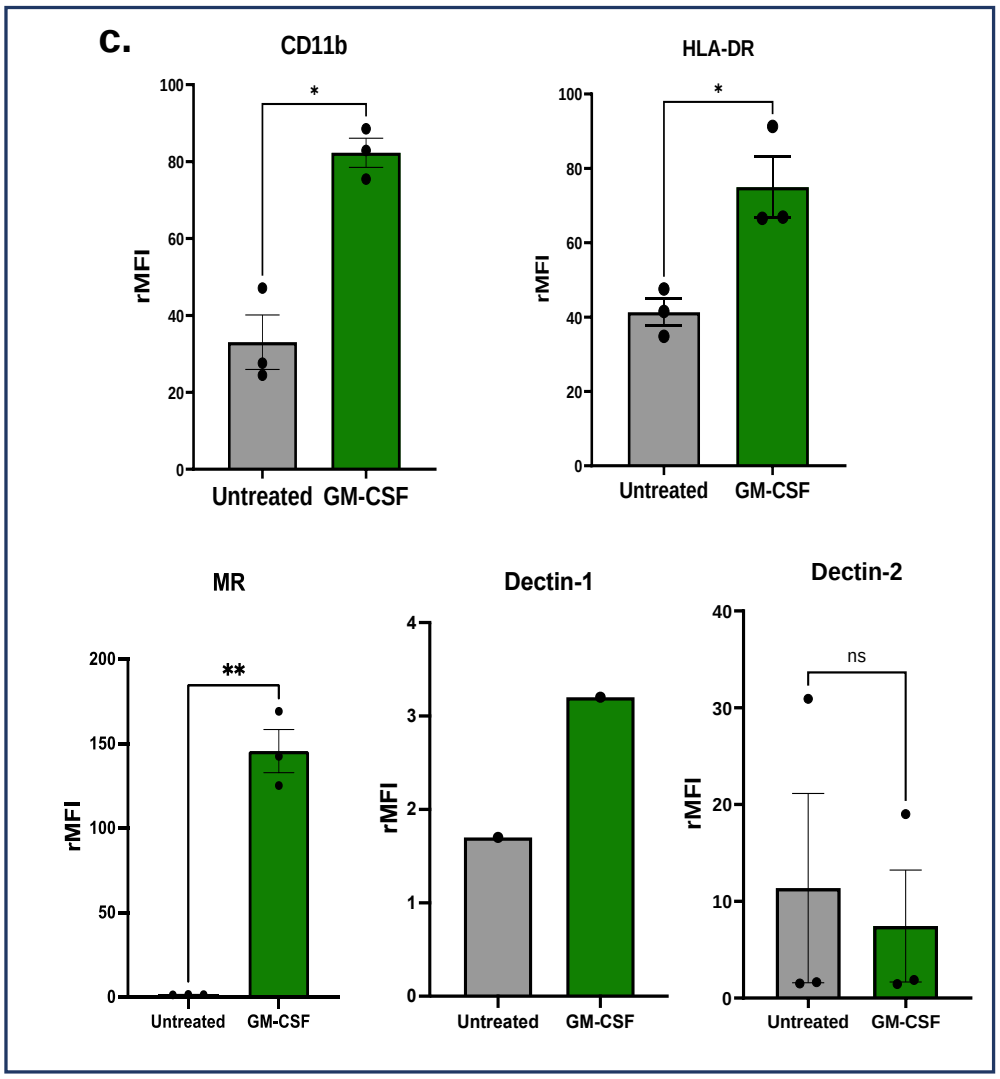

Figure 3.2. GM-CSF enhances receptor expression in human peripheral blood CD14 monocytes. Monocytes were purified, cultured in the presence or absence of GM-CSF 10 ng/mL for 40-44h, and labelled for selected surface markers. **a.** untreated monocytes**, 1.** Gating strategy based on the FSC and SSC axis, followed by the Singlet gate from the original population using the SSC Area and SSC Height. **2.** Representative histograms of CD11b, HLA-DR, MR, Dectin-1, and Dectin-2 **b.** GM-CSF-treated monocytes (**Note: The same organisation is followed for the remaining conditions). c.** Analysis of expression levels of CD11b, HLA-DR, MR Dectin-1 (N=1) and Dectin-2 expressed as rMFI, all are **(N=3)** except Dectin-2 **(N=1)**. Graphs show mean +/- SEM. Significance were analysed using paired t-test (*) $p<0.05$, (**) $p<0.01$ when appropriate.

3.4.3. M-CSF increases the survival of monocytes.

Despite the culture conditions described above generating two populations of monocytes (untreated and GM-CSF-treated) with distinct phenotypes, there were concerns regarding the lower viability of untreated cultures. For this reason, it was decided to explore the use of M-CSF-treated monocytes as controls for the GM-CSF-treated cells.

Hence, monocytes were purified by positive selection based on CD14 expression and cultured in UpCells in media supplemented by 15% human serum and in the presence of human GM-CSF (10 ng/ml) or M-CSF (10 ng/ml) (Chapter 2, section 2.2. Isolation of human monocytes (CD14+ cells)). The dose of M-CSF was low compared to doses normally used in the literature to develop macrophages (50 ng/ml) [247], but it was considered that this low M-CSF dose, alongside adherence and human serum, would be enough to increase and maintain cell viability. Although the viability of GM-CSF monocytes is significantly higher than that of M-CSF, cell viability in the presence of M-CSF nearly matched the viability of GM-CSF-treated cells based on the percentage and numbers of viable cells, which was consistently 80% and above in multiple preparations and almost $2x10^6$ cells/mL on average (Figure 3.4).

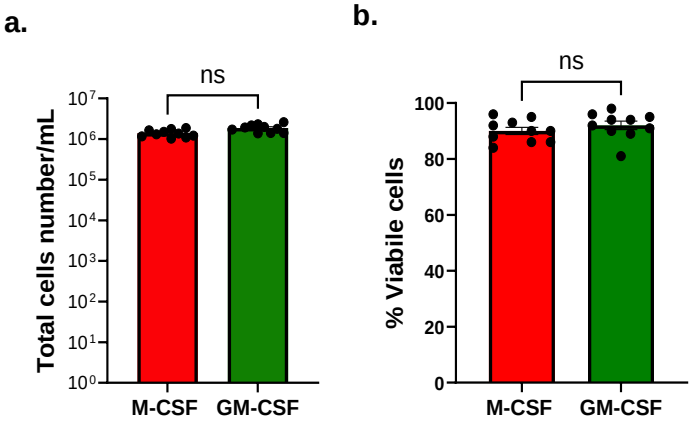

Figure 3.3. M-CSF enhances viability of human peripheral blood CD14 monocytes. Isolated monocytes were treated with GM-CSF (10ng/mL) or M-CSF (10 ng/mL) and incubated for 40-44 h as described in Chapter 2. Cells were harvested and stained with Trypan blue for cell counting and calculation of the percentage of viable cells. **a.** Number of viable cells/mL from M-CSF- and GM-CSF-treated cultures (N=10). **b.** Percentage of viable cells from M-CSF- and GM-CSF-treated cultures (N=10). Graphs show mean +/- SEM. Data was analysed using paired t-test. ns: not significant.

3.4.4. GM-CSF- and M-CSF-treated monocytes differ in expression of selected surface markers.

To test for phenotypical changes in monocytes in response to GM-CSF compared to M-CSF, surface expression of HLA-DR, CD11b, and C-type lectin receptors, MR (CD206), Dectin-1, and Dectin-2, as before, and CLEC5A were tested by flow cytometry as above.

Density plots show homogenous cell populations of M-CSF- (93.57% within the live cell gate) and GM-CSF-monocytes (94.77% within the live cell gate) (Figure 3.5. a and b). A single gate was created to identify individual cells while excluding cell aggregates or doublets by choosing SSC-Area- SSC-Height from the main gate. From this singlet gate, histograms of the antibody labelling were created and compared with their isotypes and the unstained controls (Figure 3.5. a.2) and (Figure 3.5. b.2). Subsequently, rMFI was calculated to compare all replicates and perform statistical analysis (Figure 3.5. c).

Graphs demonstrate that treating monocytes with 10 ng/mL of M-CSF upregulated the expression of MR, but GM-CSF monocytes substantially expressed more MR. In fact, GM-CSF significantly promoted expression of all surface markers tested, including CLEC5A. As previously observed, Dectin-1 was detected at low levels, but its expression was consistently higher in GM-CSF-monocytes than in M-CSF-monocytes, while Dectin-2 was detected at a very low level and expression was similar in M-CSF and GM-CSF monocytes (Figure 3.5.g and h).

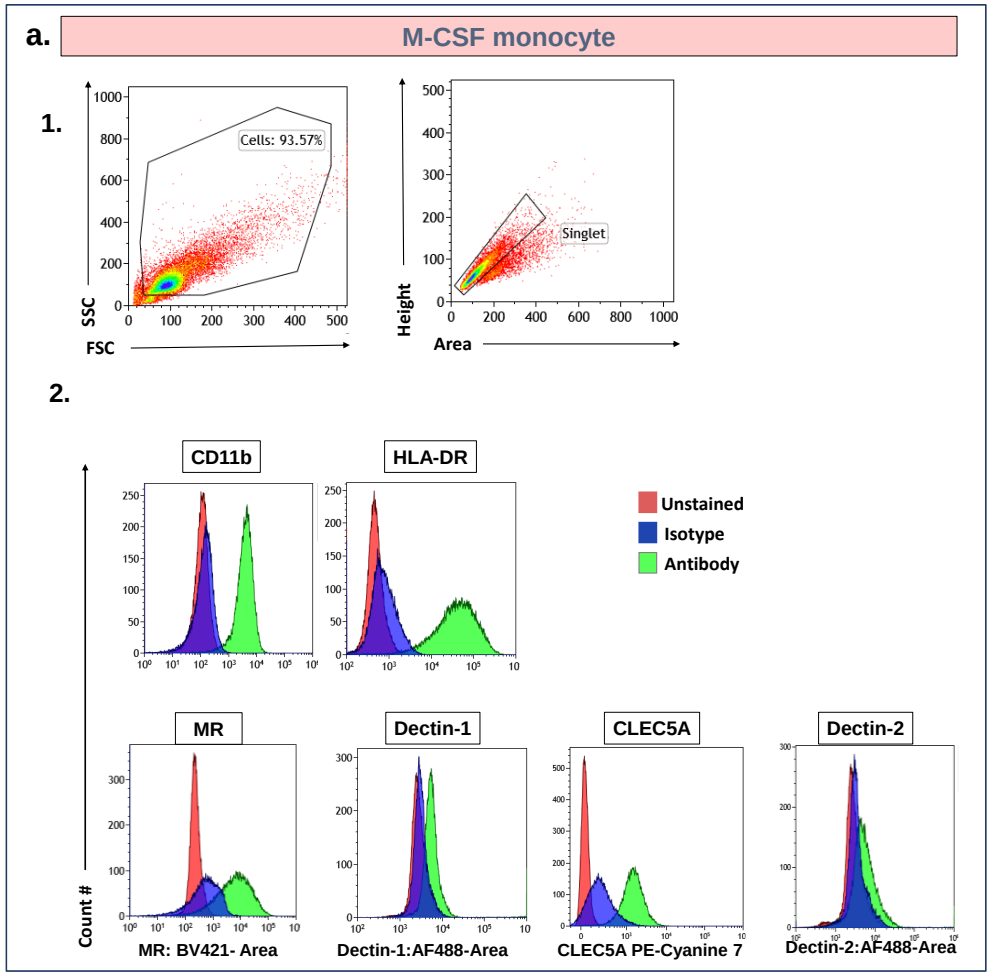
a.
M-CSF monocyte
1.
Cells: 93.57%
SSC
FSC
Singlet
Height
Area
2.
CD11b
HLA-DR
Unstained
Isotype
Antibody
MR
Dectin-1
CLEC5A
Dectin-2
Count #
MR: BV421- Area
Dectin-1:AF488-Area
CLEC5A PE-Cyanine 7
Dectin-2:AF488-Area

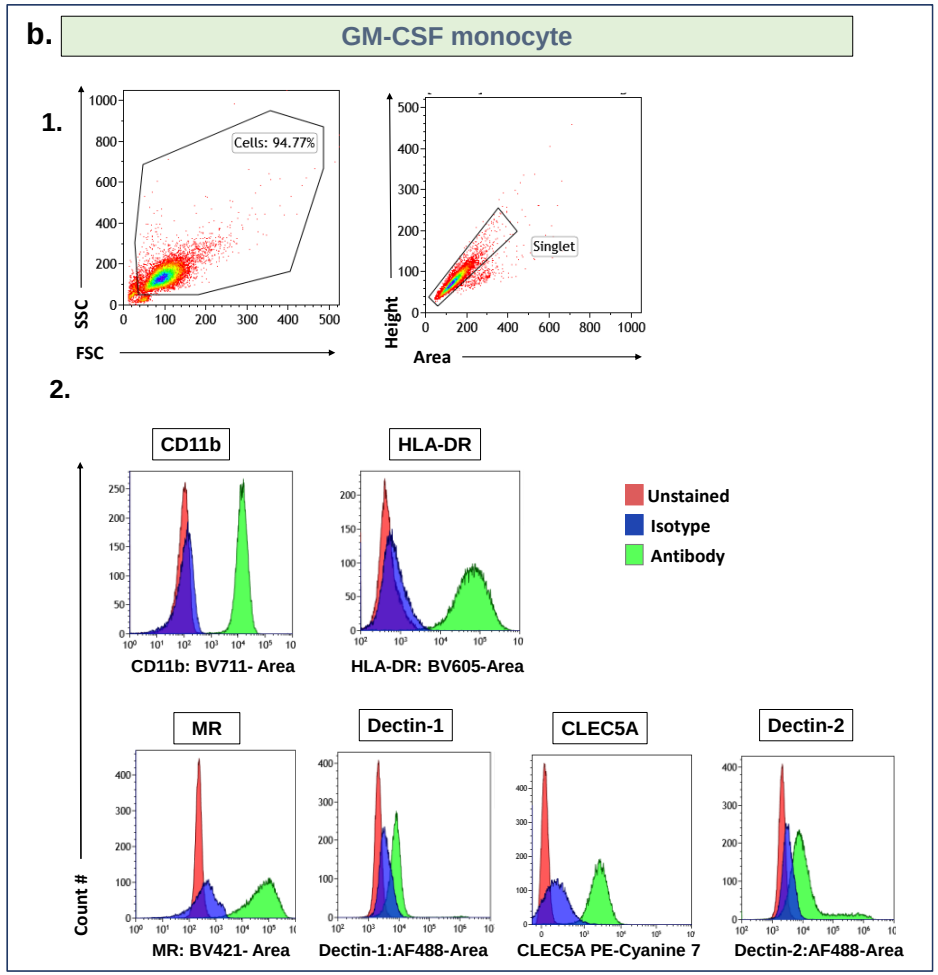
b.
GM-CSF monocyte
1.
Cells: 94.77%
SSC
FSC
Singlet
Height
Area
2.
CD11b
HLA-DR
Unstained
Isotype
Antibody
CD11b: BV711- Area
HLA-DR: BV605-Area
MR
Dectin-1
CLEC5A
Dectin-2
Count #
MR: BV421- Area
Dectin-1:AF488-Area
CLEC5A PE-Cyanine 7
Dectin-2:AF488-Area

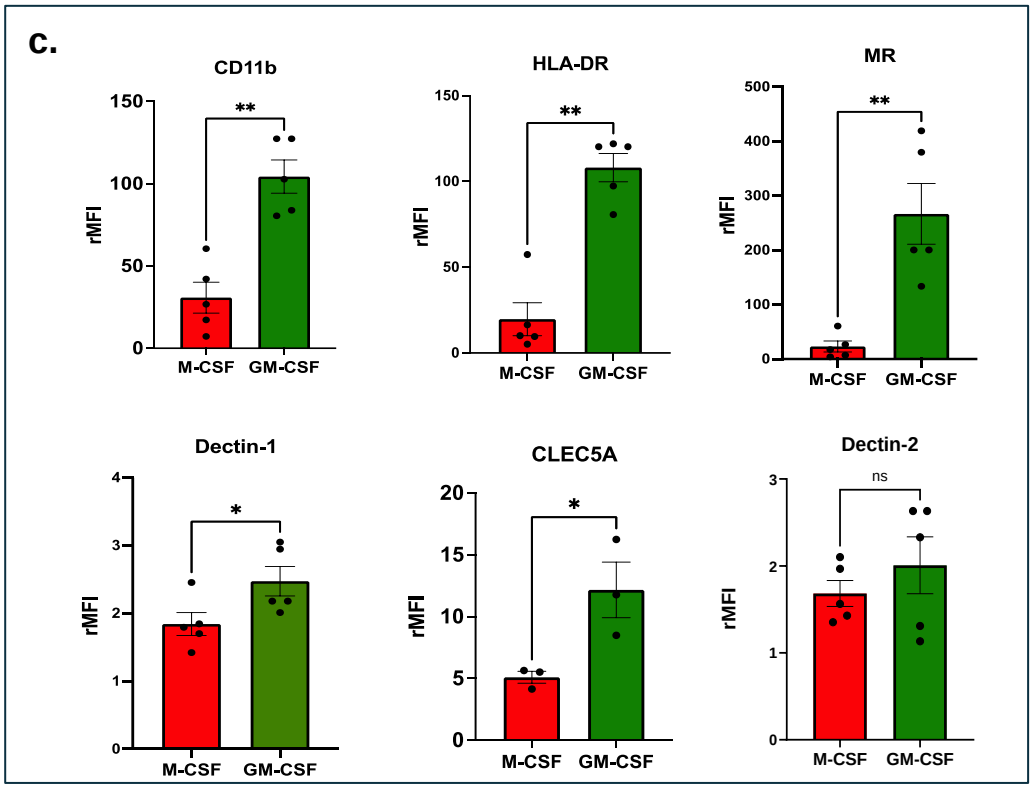

Figure 3.4. Effect of GM-CSF on cell surface markers expression in human peripheral blood CD14 monocytes. Monocytes are isolated and cultured with M-CSF or GM-CSF (both 10 ng/mL) for 40-44 hours and stained with the selected surface markers. **a.** M-CSF-treated monocytes**, 1.** Gating strategy based on the FSC and SSC axis, followed by the Singlet gate from the original population using the SSC Area and SSC Height. **2.** Representative histograms of CD11b, HLA-DR, MR, Dectin-1, CLEC5A and Dectin-2 **b.** GM-CSF-treated monocytes (**Note: The same organisation is followed for the remaining conditions). c.** Analysis of expression levels of CD11b, HLA-DR, MR, Dectin-1, CLEC5A and Dectin-2 expressed as rMFI, all are **(N=5)** except CLEC5A **(N=3)**. Graphs show mean +/- SEM. Significance were analysed using paired t-test (*) $p<0.05$, (**) $p<0.01$ when appropriate.

3.4.5. GM-CSF increases the motility of monocytes.

Monocyte migratory activity was tested to determine if GM-CSF modulates monocyte movement compared to M-CSF. In this assay, live microscopy captured cell movement in real time for 6 hours. Isolated monocytes were treated with 10 ng/mL M-CSF or GM-CSF, incubated for 40-44 h, resuspended in RPMI complete medium, and plated at 10^4 cells/well density in a tissue culture 96-well plate. Cell behaviour was analysed using a LiveCyte microscope for 6 hours at 37^{o}c, 5% CO_2.

Both populations of monocytes appeared morphologically healthy, round, and evenly distributed; they also seemed to remain well-adhered to the plate throughout the incubation period (Figure 3.6. a) and remained viable. There was no indication of cellular apoptosis, as evidenced by the velocity measurements in the linear diagram, which did not approach zero from the onset of incubation until the conclusion at six hours (Figure 3.6. b). Although cell velocity was reduced for both conditions in the last half hour. Treating monocytes with GM-CSF seems to enhance their mobility, as evident from the data presented in Figure 3.6. b, in which the velocity of GM-CSF-treated monocytes surpassed that of M-CSF-treated monocytes from the point of plating and then at various time points during the incubation.

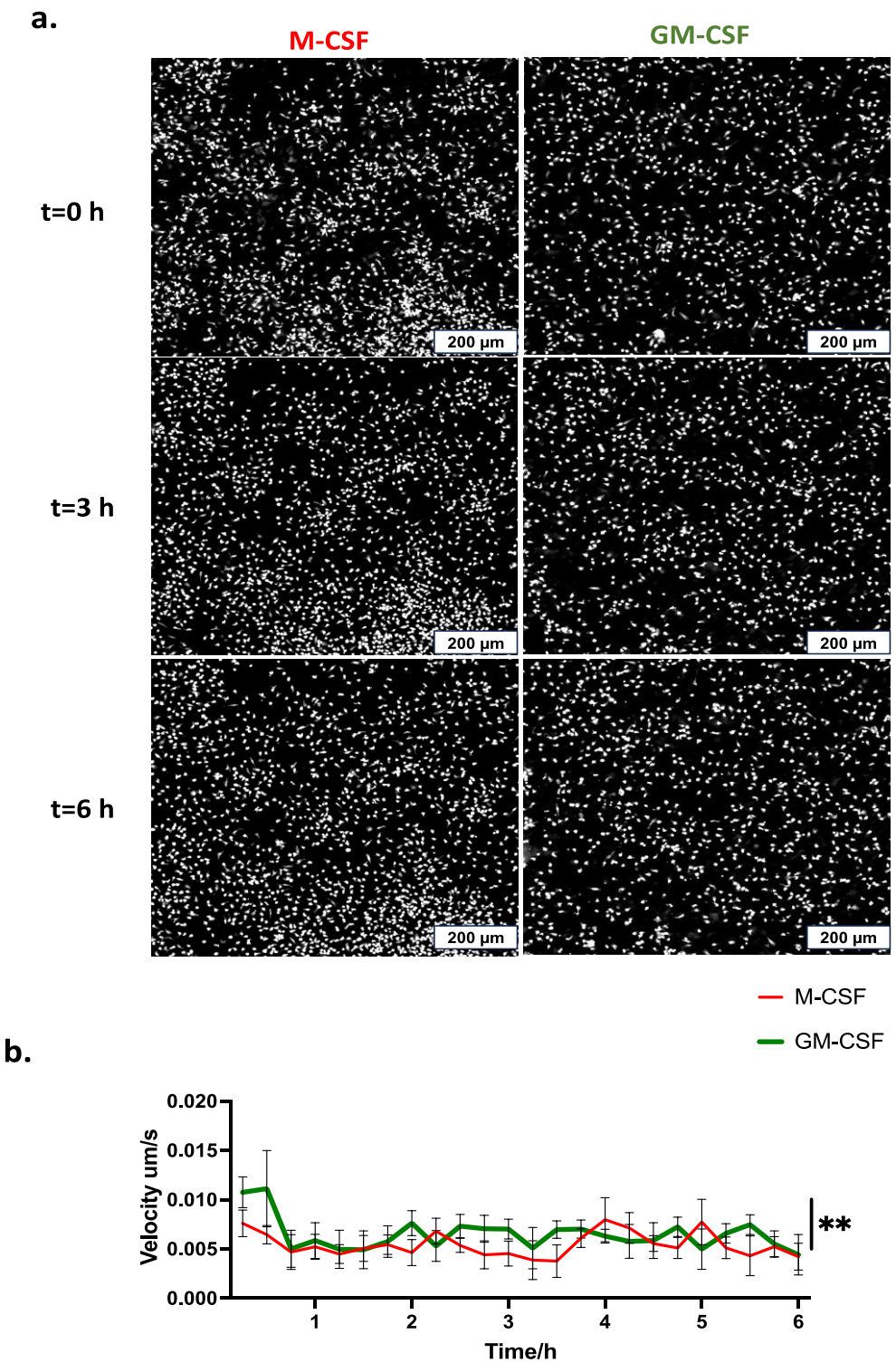

Figure 3.5. Effect of GM-CSF on human peripheral blood CD14 monocytes motility. M-CSF and GM-CSF monocytes were plated (10^4 cells/50µL/well in 96-well plate). Cells were then incubated for 6 hours and visualised using live imaging using a LiveCyte microscope. **a.** Representative images of M-CSF- and GM-CSF-monocytes at 0, 3 and 6 h incubation **b.** The graph displays monocyte velocity (N=3). Graphs show mean +/- SEM. Statistical significance was analysed using paired t-test (**) $p<0.01$. Scale bars 200 µm.

3.4.6. Analysis of potential changes in protein expression in human monocytes in response to GM-CSF using proteomics.

As an additional approach to characterising changes in monocytes induced by GM-CSF, we screened and quantified changes at the protein expression level using LC-MS/MS to generate a proteome profile of GM-CSF and M-CSF monocytes.

To achieve this aim, we performed proteomic analysis of monocytes incubated for 40-44 hours in the presence of cytokines, collected, adjusted to a concentration of 10^7 cells/mL, washed in PBS and lysed using RIPA buffer containing sodium deoxycholate for nuclear membrane disruption to extract total cellular proteins. These lysates were sent as three independent biological replicates for proteomic analysis to the Biological Mass Spectrometry and Clinical Proteomics group at NTU led by Drs David Boocock and Clare Coveney. This approach enabled the Identification of ~2,500 proteins that represent the monocyte proteome profile. Almost 140 of those proteins had their expression levels changed in response to GM-CSF. This analysis was performed and statistically analysed by the NTU group. Data were filtered to include only proteins identified by their expression in three replicates per group (M-CSF or GM-CSF). Later, t-test was performed with a permutation-based false discovery rate (FDR) set at 5%.

The volcano plot in Figure 3.7. represents the monocyte proteome profile distribution after treatment with GM-CSF or M-CSF. The upper right green side of the volcano plot represents proteins that are significantly upregulated in expression, potentially due to the GM-CSF treatment. The upper left red side represents the proteins expressed highly in M-CSF-treated monocytes, which are potentially downregulated by GM-CSF treatment.

Examining CLRs and inflammatory receptors, proteomics data demonstrated that GM-CSF monocytes did not increase MRC1 (MR) or CLEC5A, as well as Integrin alpha-M (ITGAM, CD11b) or HLA-DRA, as determined by flow cytometry. M-CSF and GM-CSF-treated monocytes had almost similar expression of these genes.

Examining other proteins, monocytes treated with GM-CSF significantly upregulated numerous key proteins that could be considered potential targets for further monocyte characterisation. These included proteins involved in cell survival, such as Cullin-1 (CUL1), NF-κB, and Serine/threonine-protein kinase

A-Raf (ARAF). Additionally, many GTPase family-related proteins were upregulated, including Rho GTPase-activating protein 17 (ARHGAP17), ARF GTPase-activating protein (GIT2), and Secretion Associated Ras Related GTPase 1A (SAR1A). Proteins that enhance immune response, like Interleukin-1 receptor accessory protein (IL1RAP) and Stimulator of interferon genes protein (STING1), also showed increased expression in response to GM-CSF. On the other hand, there was downregulation of some homeostatic proteins, including, but not limited to, Actin, cytoplasmic 1 (ACTB), PC4, and SFRS1 Interacting Protein 1 (PISP1), as well as Interferon-induced protein with tetratricopeptide repeats 1 (IFIT1).

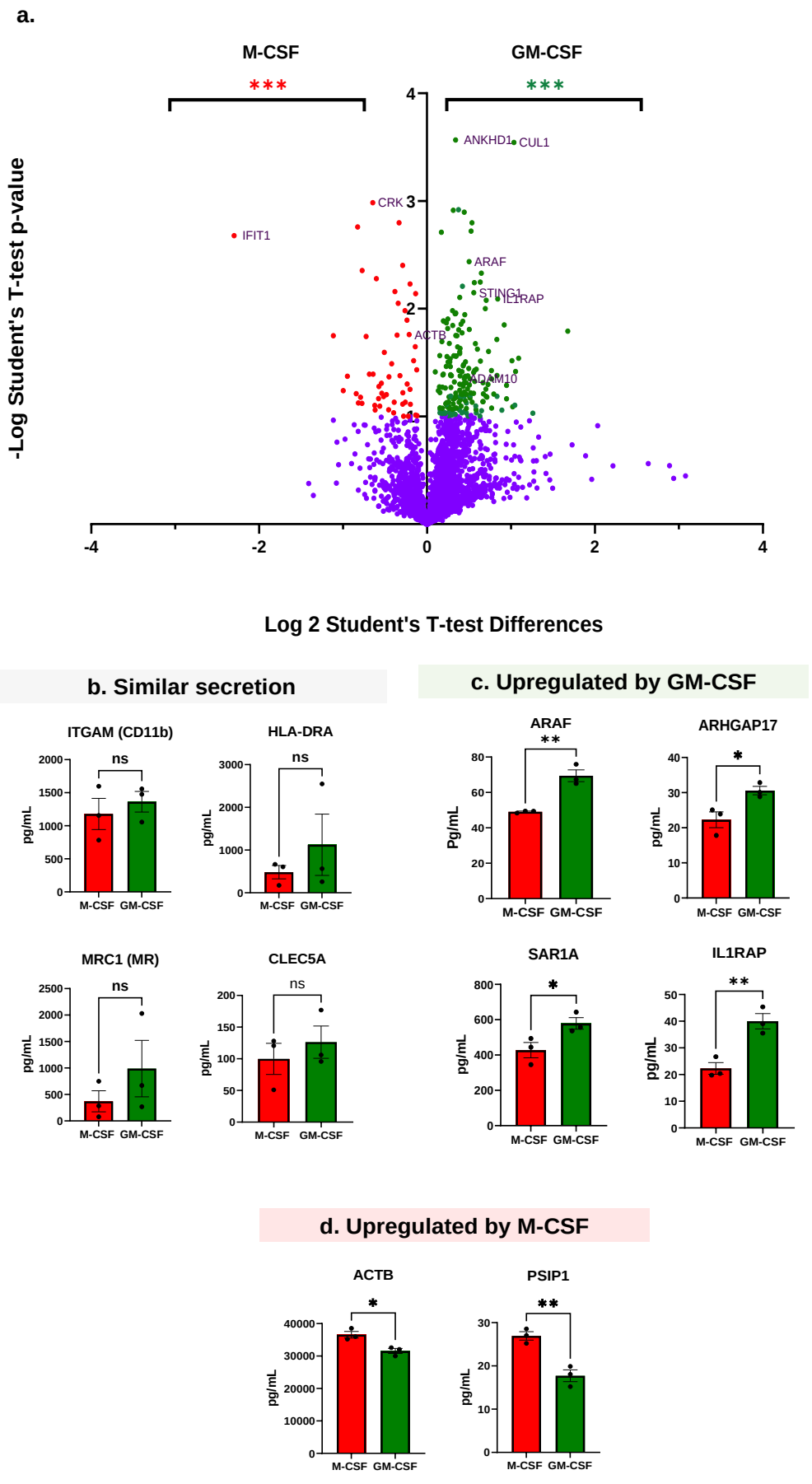
a.
M-CSF
GM-CSF
***
***
-Log Student's T-test p-value
Log 2 Student's T-test Differences
ANKHD1
CUL1
CRK
IFIT1
ARAF
STING1
IL1RAP
ACTB
ADAM10
b. Similar secretion
ITGAM (CD11b)
HLA-DRA
MRC1 (MR)
CLEC5A
c. Upregulated by GM-CSF
ARAF
ARHGAP17
SAR1A
IL1RAP
d. Upregulated by M-CSF
ACTB
PSIP1
pg/mL
Pg/mL
M-CSF
GM-CSF
ns

Figure 3.6. Volcano plot showing the effect of GM-CSF on the protein expression in human peripheral blood CD14 monocytes. a. Data was normalised by subtracting the median intensity value of each sample, and statistical analysis was performed using a t-test with a permutation-based FDR of 5%; Red and green dots represent significantly increased M-CSF (red stars) or GM-CSF (green stars) treated monocytes**.** Statistical significance was analysed using paired t-test (***) $p<0.05$. **b.** Examples of proteins that showed similar expressions between M-CSF and GM-CSF**. C.** Examples of proteins that are regulated by GM-CSF. **d.** Examples of proteins regulated by M-CSF (**N=3).** Graphs show mean +/- SEM. Significance was analysed using paired t-test (ns), non-significant, (*) $p<0.05$, (**) $p<0.01$ when appropriate.

3.4.7. Production of Extracellular Vesicles (EVs) by Macrophage isn't affected by GM-CSF treatment.

When macrophages are treated with GM-CSF, they undergo changes in phenotype that can affect EV production and content [248]. In this context, we aimed to investigate whether the administration of GM-CSF to macrophages would induce alterations in EV production and which could subsequently influence immune responses [231]. Therefore, monocytes were isolated from buffy coats as before, then treated with 50 ng/mL M-CSF for 6 days in low attachment plates to achieve macrophage differentiation. Macrophages were then collected and plated in 6-wells plates, $2x10^6$ cells/well, and incubated for ~44 hours in the presence of 10 ng/mL GM-CSF or M-CSF in serum-free media. Lastly, supernatants were collected and transferred to Dr. Lucy Fairclough's laboratory to test for EV production.

In general, EV production was similar in M-CSF- and GM-CSF-treated macrophages, which means that, under these conditions, GM-CSF does not affect EV production by macrophages (Figure 3.8. a). EVs are enriched in a wide range of tetraspanins [171], in this study, we tested for CD9, CD63, and CD81. Here, CD9 showed the highest expression among them, and it appeared that the % of CD9-expressing EVs was higher in M-CSF monocytes compared to GM-CSF monocytes. On the other hand, CD63 and CD81 were expressed in a similar % of EVs by M-CSF and GM-CSF macrophages (Figure 3.8. b).

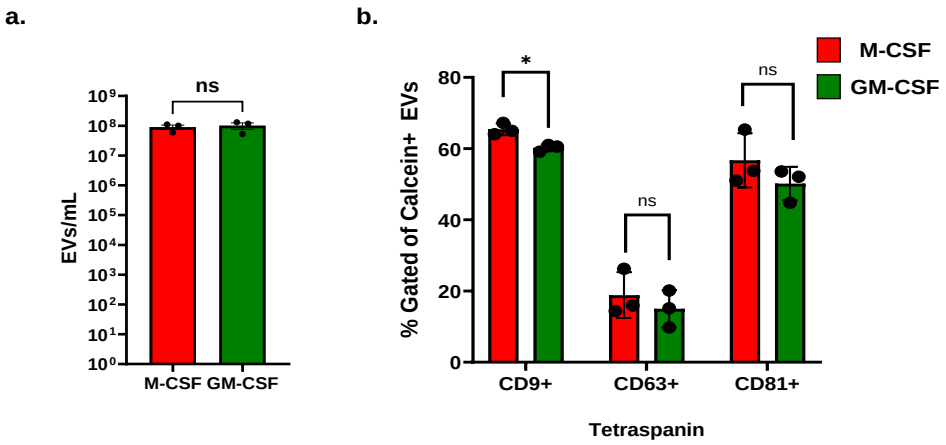

Figure 3.7. Effect of GM-CSF on EV production from human peripheral blood CD14 macrophages. Monocytes were isolated from a buffy coat, treated with 50 ng/mL M-CSF, and incubated for 6 days. The macrophages were then treated with 10 ng/mL GM-CSF or M-CSF after being plated at $2x10^6$ cells/well in 6-well plates in serum free media. After incubation for ~44 hours, supernatants were collected and transferred to Dr. Lucy Fairclough's laboratory for testing for EV production. **a.** Numbers of EVs expressed as EVs/mL in supernatants from M-CSF and GM-CSF-macrophages. **b.** Percentage of EVs expressing tetraspanins CD9, CD63 and CD81 **(N=3).** Graphs show mean +/- SEM. Data was analysed using paired t-test. (*) $p<0.05$, ns: not significant.

3.5. Summary

The main findings of this Chapter are:

- UpCell surfaces are a suitable choice for optimal non-enzymatic monocyte retrieval at low temperatures.
- M-CSF improved the viability of monocytes compared to untreated cells under our culture conditions.
- Monocytes treated with GM-CSF (10 ng/mL) showed upregulation of several C-type lectin receptors as well as HLA-DR and CD11b.
- GM-CSF increased monocyte migratory activity over a 6-hour period.
- Proteomic profile of GM-CSF-monocytes shows significant changes in protein expression.
- Treating macrophages with 10 ng/mL GM-CSF did not result in any significant alterations in the production of EVs compared to M-CSF treatment.

3.6. Discussion

Analysis of monocyte responses to GM-CSF is essential for studying monocyte biology and how they react to inflammatory stimuli; information that is essential for better understanding immune responses and the development of therapies to modulate immunity [249]. Several investigations have been conducted on the function of GM-CSF in regulating monocyte activity. It is well-recognised that GM-CSF primes monocytes for heightened inflammatory responses by affecting the expression of surface markers and cytokine production, and other mediators [250]. As mentioned in the introduction of this chapter, diverse monocyte models have been utilised to examine the impact of GM-CSF treatment. As this project focuses on the response of GM-CSF-treated monocytes against *C. albicans*, it was essential to characterise their properties when treated with this cytokine. This study included cell surface marker expression, protein expression, and microscopic examination.

Monocyte isolation and incubation on UpCell surfaces for several hours was one of our strategies for generating monocytes that are in the process of becoming macrophages, to model cells recently recruited to tissues (i.e., monocyte-phagocyte transition model). Obtaining monocytes from buffy coats allows us to work with cells from a diverse range of donors, all of whom have been tested negative for key pathogens and are considered healthy. Live cell counts after 40-44 hours in the presence of GM-CSF are generally higher compared to those left untreated, demonstrating the critical role of GM-CSF in promoting cellular viability, which is consistent with its role as a growth factor, in addition to supporting immune responses. This effect is probably due to its ability to activate various signalling pathways that prevent apoptosis and promote cell survival [213]. Cell survival and gentle cell recovery were crucial because cultures with high cell death or damaged by harsh cell harvesting methods could significantly bias findings, especially when using flow cytometry [251]. GM-CSF induces a more inflammatory and active state in monocytes and macrophages, whereas M-CSF tends to support a more stable, homeostatic state [160]. Therefore, it is possible to assess the precise inflammatory and immune-stimulating effects of GM-CSF on monocytes by employing M-CSF as a negative control [252]. In our model, we found that the expression of C-type lectin receptors such as MR (CD206), CLEC5A, and Dectin-1 was upregulated. C-type lectin receptors are the major family engaged in antifungal immunity;

they work independently or synergistically with TLRs [76]. Upon fungal recognition, an important subset of these receptors (such as Dectin-1) activates Syk (Chapter 1, 2.1.2.2.3. Dectin-1), phosphorylating CARD9. This leads to the formation of a complex that recruits and activates NF-κB, a key transcription factor that promotes inflammatory responses. Activating NF-κB induces proinflammatory cytokines, chemokines, and other mediators that coordinate the antifungal immune response [240]. Numerous studies have been conducted on CLRs and their responses on their own or together. For example, while MR directly captures fungal pathogens, it is unlikely to signal; in contrast, CLEC5A likely ensures that the inflammatory environment is conducive to an effective immune response [136]. This synergy improves pathogen clearance and helps orchestrate a coordinated defence involving innate and adaptive immunity as shown in the case of Dengue Virus [253]. MR and CLEC5A were investigated using confocal microscopy in the lab. Very preliminary data showed different locations of these two receptors, but both were expressed highly in the presence of GM-CSF (Chapter 2, 2.10. Microscopy, Confocal microscopy). Another example, Dectin-1 and MR together strengthen the immune system's defences against fungus-related infections. Although Dectin-1 plays a crucial role in identifying β-glucans and triggering inflammatory reactions on its own [254], MR is essential for internalising and breaking down pathogens containing mannose, and it is recruited later during phagosome maturation [97]. This coordinated effort guarantees a more effective and all-encompassing immune defence [240]. Mostly found on dendritic cells, neutrophils, and macrophages, Dectin-2 is a CLR that has been shown to recognise α-mannan, providing protection against systemic infection with *C. albicans* by triggering Th-17 immune responses [255]. In our lab, we couldn't detect an expression of Dectin-2 from GM-CSF monocytes even in the proteomics data.

Proteomics revealed that neither Syk nor CARD9 levels were influenced by GM-CSF, as well as similar levels of NF-κB in GM-CSF and M-CSF monocytes. However, the response to GM-CSF varied across the three independent experiments, indicating that donors might respond to GM-CSF in distinct ways. As noted by a proteomics specialist, conducting four repeats might yield more consistent results. For instance, the flow cytometry research confirmed that GM-CSF plays a role in promoting monocyte activation by upregulating the expression of CD11b and HLA-DR in addition to MR and CLEC5A. However,

based on the proteomics data, we found that these receptors exhibited comparable protein expression levels. Apart from the varying individual responses, the various cell treatments could also be important determinants. For example, we employed cells plated in TC plastic for proteomics, while monocytes were cultured in UpCells prior to harvesting for flow cytometry. Additionally, it was quite challenging to analyse readouts while the variations between repeats were quite variable.

The most prevalent adhesion and migration receptor, CD11b, increased considerably in response to GM-CSF (as determined by flow cytometry), which was not observed in the proteomics findings, indicating that GM-CSF may affect surface expression rather than total expression. CD206 proteomics data agreed with flow cytometry data in two of the samples. In this case, western blotting at our lab confirmed that GM-CSF increases total protein levels of CD206 and CLEC5A (data are in the appendix). CD11b mainly affects phagocyte adhesion, migration, and activation, which improves phagocytes' capacity to eradicate pathogens and clear inflammation [256]. This is in agreement with GM-CSF monocytes showing increased migration (Figure 3.6. b). Monocytes are MHC II+ cells and can differentiate into DCs, which would enhance their ability to rapidly activate the adaptive immune system in the event of fungal infections [257]. HLA-DR is a key player in antigen presentation to CD4+ T cells to initiate and regulate the adaptive immune system [258]. During inflammation, as occurs when there is an infection, the distribution and amount of monocyte subgroups can change dramatically. HLA-DR^{hi} inflammatory monocytes have been found to be more common in COVID-19 patients with mild symptoms than HLA-DR^{lo} monocytes, which are more common in patients with severe illness and some autoimmune diseases. These monocytes (HLA-DR^{hi}) also exhibit significant levels of proinflammatory cytokines and co-stimulatory molecules, [257]. Additionally, in sepsis, the low expression of HLA-DR in monocytes suggests impaired pathogen defence and is associated with poor clinical outcomes. HLA-DR may serve as a valuable marker for monitoring disease progression and predicting outcomes in sepsis [235].

Monocytes need to travel to sites of infection or tissue damage to eradicate the infection, whether in cooperation with other immune cells or on their own. At the site of inflammation, monocytes differentiate into macrophages or DCs to modulate inflammation, promote clearance and activate the adaptive immune system [259]. Monocyte velocity is important in understanding how quickly and

effectively they can respond to pathological conditions [260]. Observation of monocytes for several hours reveals that the velocity of GM-CSF-monocytes was substantially upregulated compared to M-CSF-monocytes. These observations could relate to the expression of different proteins from the GTPase family from the RAS superfamily, known for its numerous cellular functions [261]. Proteomics analysis also proved that different GTPase family members were upregulated under the effect of GM-CSF. Few examples are listed in table 3.1 below:

Table 3.1. Some genes from GTPase family.

Gene	First gene description	M-CSF (Ave of 3 repeats)	GM-CSF (Ave of 3 repeats)
ARHGAP17	Rho GTPase-activating protein 17	15.8814	32.5402
GIT2	ARF GTPase-activating protein GIT2	12.44361	25.06856667
IQGAP1	Ras GTPase-activating-like protein IQGAP1	49.0859	69.42196667
ARHGAP25	Rho GTPase-activating protein 25	26.15515	40.9338
ARHGAP1	Rho GTPase-activating protein 1	15.8814	32.5402
G3BP1	Ras GTPase-activating protein-binding protein 1	68.971	92.42446667
IRGQ	Immunity-related GTPase family Q protein	224.5876667	330.5586667
GAPVD1	GTPase-activating protein and VPS9 domain-containing protein 1	22.29316667	39.97356667
ARHGAP45	Rho GTPase-activating protein 45	56.5213	91.3642

Several proteins that were affected by GM-CSF are GIT2 and ARHGAP17. G-protein-coupled receptor kinase-interacting protein 2 (GIT2) could have a major impact in controlling the mobility of monocytes, as it has been shown to control migration and adhesion [262]. ARHGAP17, also known as RICH1, is a Rho GTPase-activating protein that plays a crucial role in regulating cell motility, including that of monocytes. Both proteins, GIT2 and ARHGAP17, modulate the activity of small GTPases such as Rac1 and Cdc42, which are essential for the cytoskeletal rearrangements required for cell movement. Despite the expression of RAC1 and Cdc42 in GM-CSF monocytes being slightly lower than in M-CSF monocytes, GIT2 and ARHGAP17 were significantly upregulated in GM-CSF-treated monocytes. In monocytes, ARHGAP17 facilitates directed migration by influencing the dynamics of actin filaments and focal adhesions, thereby aiding these immune cells in effectively reaching and responding to sites of infection or inflammation [263].

Proteomics data identified ~3000 proteins in monocytes; over 100 of them were significantly upregulated in GM-CSF monocytes, while 48 were substantially higher in M-CSF monocytes (data shown in the appendix). We believe this change in proteins might be caused in part by the use of M-CSF, which is a hematopoietic growth factor that controls monocyte differentiation, proliferation, and functional activation [264]. We observed important proteins implicated in

modulating the immune response and driving changes in monocyte fate, which is consistent with the functional enhancement of monocytes treated with GM-CSF. Serine/threonine-protein kinase A-Raf (ARAF) is a protein from a larger family, the RAF family, that is a part of the broader MAPK signalling pathway, known for its participation in key inflammatory signal transduction pathways like RAS, RAF, and ERK [265]. The expression of this protein increased in GM-CSF-treated monocytes. Another example is interleukin-1 receptor accessory protein (IL1RAP), which is one of the most promising marker antigens for the immunotherapy of numerous acute or chronic diseases and a very important protein in the IL-1 pathway [266]. In monocytes treated with GM-CSF, the expression of IL-1RAP was substantially high, indicating that in the case of infection, IL-1RAP would respond to IL-1β, as IL-1RAP is an adaptor protein for IL1βR [266]. One of the key proteins expressed on GM-CSF-treated monocytes is the stimulator of interferon genes (STING1), which mediates defensive mechanisms against bacterial, viral, and fungal infections. It detects exogenous cyclic dimeric guanosine and adenosine monophosphates (c-di-GMP and c-di-AMP) from bacteria, as well as endogenous cyclic dinucleotides such as 2, 3-cyclic GMP-AMP (2, 3-cGAMP) produced by cGAS in response to cytosolic DNA. By inducing the production of IFNs and other cytokines, as well as autophagy. However, mice lacking STING show improved antifungal immunity when infected with *C. albicans*, indicating that at the whole organism level, STING might have a negative effect during *C. albicans* infection [267].

On the other hand, some proteins were similarly expressed in monocytes treated with GM-CSF and M-CSF such as most Rho family proteins. Rho activation is critical for maintaining the balance of the monocyte-endothelial cell interaction [268]. SRGAP2 is a member of the RHO family that is involved in neuronal migration and differentiation [269]. RHOA is another example of a protein from the RHO family that controls several biological functions, such as cell migration, proliferation, and cytoskeletal organisation [270]. Lastly, some proteins were downregulated in monocytes treated with GM-CSF compared to those treated with M-CSF. Interferon-Induced Protein with Tetratricopeptide Repeats 1 (IFIT1**)** is one of the proteins that is downregulated in response to GM-CSF**.** In general, IFIT1 is a part of a family of proteins expressed in the cytoplasm of a wide variety of species, including fish and mammals, and it is expressed shortly after the type-I IFN response [271]. Another protein that is downregulated in monocytes treated with GM-CSF is CT10 Regulator of Kinase

(CRK). This adaptor protein plays a crucial role in cell biology, function, and immunological control. It is also highly significant in the expression of proteins in monocytes, NK cells, and lymphocytes [272]. That is clearly a correlation between the decrease of this protein in monocytes treated with GM-CSF.

EV production was another readout to study the effect of GM-CSF on myeloid cells. EVs differ between healthy and inflammatory conditions [273]. Macrophages were differentiated from monocytes, and EV production was assessed using specific markers, including tetraspanins CD9, CD81, and CD63. In this project, the focus was on monocytes as the precursors of tissue macrophages, which are the main cells that interact with *C. albicans* in tissues [186], so it made sense to look not only at what these cells do themselves but also at what they release into their environment. EVs constitute a significant component of that secreted material, carrying proteins and signals that reflect how GM-CSF has shaped macrophages and allow them to influence nearby immune cells without direct contact [173]. By analysing EVs from GM-CSF–treated macrophages, it was possible to ask whether the antifungal programme driven by GM-CSF is also packaged and released in a cell-free, vesicular form. In our case, it doesn't seem that GM-CSF affects EV production compared to M-CSF. EV production would increase under various factors related to cellular stress, including oxidative and thermal stress, hypoxia, pH, radiation, nutrient deprivation, protein and chemical exposure, and the culture environment [243]. Since GM-CSF is the only factor employed in this experiment to stimulate EVs, combining this factor with others could be necessary to increase EV output. Tetraspanins are essential proteins found in mammals, of which 33 have been identified in humans and mice so far [274]. Tetraspanins control a number of biological functions, including sperm-egg fusion, growth, differentiation, motility, adhesion, and signal transduction [275]. Among tetraspanins, CD9, CD63, CD81, CD82, and CD151 are widely expressed across various tissues, whereas others, like Tssc6, CD37, and CD53, are confined to specific tissues, particularly hematopoietic cells [171]. Studies using CD9 knockout mice suggest that CD9 plays an essential role in regulating inflammation and humoral immunity. It achieves this by influencing the production of myeloid cells and promoting the secretion of cytokines such as IL-10 [276]. CD9 also interacts with the metalloproteases ADAM10 and ADAM17 to regulate their sheddase activity [277]. Interestingly, ADAM10 seemed to be upregulated in GM-CSF-treated monocytes, as indicated by our proteomics data. In three repeats of monocytes

treated with GM-CSF (77.0843, 91.9354 and 85.7997) compared to the negative control (58.3081, 75.1693 and 53.8825). EV analysis revealed that the percentage of CD9 was higher in macrophages treated with M-CSF compared to those treated with GM-CSF. Several studies describe CD63 and CD81 as the most commonly identified proteins in exosomes, and they are regarded as classical markers of exosomes [278]. Neither marker showed any significant differences between M-CSF- and GM-CSF-treated macrophages. Although proteomics data were run on monocytes and EV investigation was on macrophages, it is worth showing protein expression on cells before and after monocyte differentiation into macrophages. Therefore, proteomics data showed no upregulation of each protein in monocytes treated with GM-CSF (Table 3.2).

Table 3.2. EVs production. Data represent the expression of EVs proteins identified by proteomics.

Gene	M-CSF monocytes (Ave of 3 repeats)	GM-CSF monocytes (Ave of 3 repeats)
CD9	123.0776667	122.0502333
CD63	497.253	493.6663333
CD81	26.9328	32.865
CD82	99.2354	95.924
CD151	39.00595	40.75405

In conclusion, GM-CSF treatment effectively primes monocytes to become more responsive and active, potentially mimicking inflammatory monocytes and thereby aiding in both innate and adaptive immunity. This characterisation underscores the functionality of GM-CSF in enhancing immune responses, especially in conditions requiring robust immune activation, like *C. albicans* infection.

Chapter 4

Improved Monocyte Effector Functions Against *C. albicans* Induced by GM-CSF

4.1. Introduction

This project builds on our experience in generating and characterising GM-CSF- and M-CSF-monocytes (Chapter 3) and focuses on the effect of GM-CSF on the ability of monocytes to respond to *C. albicans* infection as a means to assess the potential of GM-CSF as adjuvant therapy against fungal infection. We infected both GM-CSF- and M-CSF-treated monocytes with live *C. albicans*. To closely mimic physiological conditions, the culture medium was supplemented with 15% human serum, which acts as an opsonic source due to the presence of IgG (data not shown). Temperature (37 ˚C) is a key factor for *C. albicans* growth, particularly for pathogenic hypha formation [279]. *C. albicans* can exist in three distinct forms: yeast, pseudohyphae, and hyphae and the shift from yeast to hyphal form enables the fungus to evade macrophage phagocytosis, facilitating tissue invasion and damage [280]. Therefore, hyphal length in *C. albicans* incubated with GM-CSF-treated monocytes is also studied in this chapter.

Over the years, various *in vitro* models have been developed to investigate how myeloid cells, including monocytes and macrophages, respond to *C. albicans*. These models have been instrumental in advancing our understanding of innate immune recognition and response to fungal pathogens. Isolating human monocytes from peripheral blood and using them directly or treating them with GM-CSF or M-CSF to differentiate them into macrophages is a common method [210]. These two differentiation settings result in functionally divergent macrophage populations, where GM-CSF-treated cells exhibit higher proinflammatory and antifungal activity than M-CSF-treated cells, which display a more tissue-resident, regulatory phenotype [281]. These models enabled researchers to identify key receptors for *C. albicans*, including Dectin-1, TLR2, TLR6, and MR known for their recognition of cell wall components such as β-glucan [282]. In recent years, research has further enhanced these models by integrating transcriptome profiling, live-cell imaging, and multiplex cytokine analysis to better characterise the dynamic nature of host–pathogen interactions [283, 284]. Additionally, blocking antibodies or genetically engineered monocytes have been used to deconstruct the signalling cascades downstream of fungal recognition receptors [285]. These methods enabled researchers to understand how immunological polarisation, fungal morphology,

and strain diversity would influence the immune responses of monocytes and macrophages [286].

C. albicans (yeast or hyphae) has been added to monocyte or macrophage cultures to examine the immune cells' response in the recognition and initiation of the immune response. Investigations include phagocytosis, killing assays, cytokine secretion and expression of inflammatory surface markers [128]. Interestingly, Baltch et al. studied how various cytokines, including GM-CSF, affect the monocytes' response against *C. albicans* in the presence and absence of the antifungal drug fluconazole. They designed a model of isolated human monocyte-derived macrophages (MDM) and allowed them to adhere, then treated them with different cytokines (TNF-α, IL-1β, IFN-γ, IL-4, IL-10, and GM-CSF) individually or in a cocktail and incubated them for designated periods. Then, they infected MDMs with opsonised *C. albicans* in the presence and absence of fluconazole. Subsequently, they measured different cellular activities like phagocytosis and quantified the production of nitric oxide (NO) and superoxide (O_2^-), which are key oxidative mechanisms involved in microbial killing. They found that GM-CSF, in association with IFN-γ, enhance the phagocytic activity. Additionally, GM-CSF has a significant effect on monocytes' microbicidal activity, particularly in the presence of fluconazole, by enhancing NO production at 48 hours. Although other cytokines induced NO and O_2^- did not correlate with *C. albicans* direct killing, GM-CSF improved monocytes' ability to eliminate the fungus, highlighting its immunomodulatory effect during infection [287].

Similar models have been used, involving DCs or neutrophils, to demonstrate that fungal sensing triggers T cell activation and contributes to shaping the adaptive immune system [73, 288]. For instance, Gazendam et al. revealed that neutrophils kill *C. albicans* using two mechanisms, depending on whether the fungus is opsonised or not. In the absence of opsonisation, neutrophils rely on a pathway independent of NADPH oxidase, involving the surface receptor CR3 and the adaptor protein CARD9. In contrast, when *C. albicans* is opsonised with serum antibodies, neutrophils engage FcγR and protein kinase C (PKC) and generate reactive oxygen species (ROS) via the NADPH oxidase complex to mediate fungal killing. In their experiments, the researchers used *C. albicans* that expressed GFP at a 4:1 yeast-to-neutrophil ratio. To evaluate the efficacy of neutrophil-mediated fungal killing, they used a digital fluorescence microscope to track the development of *C. albicans* hyphae [180].

Animal studies investigating mucocutaneous fungal infection caused by *C. albicans* have shown that mice lacking IL-17, IL-17R, or the transcription factor RORγt expression are highly susceptible to fungal infection [289]. Nevertheless, it has been demonstrated that recurring fungal infections activate TH17 cells and trigger immunopathological reactions. Regarding other fungal infections, the use of *A. alternata* demonstrates that it can trigger a Th17 response in the lungs by binding to Dectin-1, thereby activating neutrophils, which can then stimulate Th17 cells. This increases the inflammatory response by encouraging the release of several cytokines [290]. Although these *in vitro* systems cannot fully capture the complexity of *in vivo* immune responses, they are essential for determining the ways in which different cell types contribute to fungal control [291].

In conclusion, this chapter builds on existing models by focusing on how GM-CSF pretreatment affects monocyte responses to *C. albicans*. Live fungal cells have been used in a co-culture setup to examine the effects on cytokine secretion, surface receptor expression, and overall antifungal activity, in order to better understand the role of this conditioning in fungal immunity.

4.2. Hypothesis

We hypothesise that treating monocytes with GM-CSF will enhance their responses against *C. albicans*, promoting immunity and infection control.

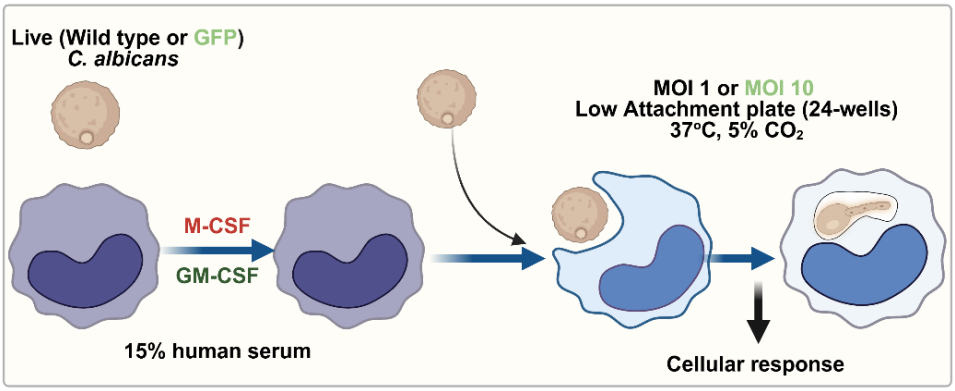

4.3. Specific objectives

To test this hypothesis, purified monocytes treated with either GM-CSF or M-CSF as described in Chapter 3 were infected with live *C. albicans*.

Cultures were analysed for:

- *C. albicans* colony-forming units (CFU).
- *C. albicans* hypha formation.
- *C. albicans* phagocytosis.
- Cytokines and chemokines secretion from infected and uninfected monocytes.
- Changes in surface marker expression, in particular MR, upon infection.
- Receptor localisation upon infection.

4.4. Results

4.4.1. Effect of GM-CSF monocytes on *C. albicans* CFU

Initially, to test the effect of GM-CSF on the response of peripheral human monocytes to infection with *C. albicans*, GM-CSF-treated and untreated monocytes (1 × 10^6 cells per well) were infected with live *C. albicans* at an MOI of 1 (1 × 10^6 yeasts) and cultured in 24-well ultra–low-attachment plates as described in (Chapter 2, Section 2.3.3. Infection of human monocytes with *C. albicans)* and incubated for 3 h at 37°C, 5% CO_2. Fungal survival was then quantified by CFU plating, expressed as CFU relative to the starting inoculum.

CFU analysis revealed a decrease in CFUs compared to the initial inoculum, both in the presence and absence of monocytes. Interestingly, the reduction was more obvious in the absence of monocytes (Figure 4.1). Despite providing reproducible results in two independent repeats, we changed the conditions to use M-CSF-treated monocytes as controls for the GM-CSF-treated cells because of the reduced viability observed in untreated monocytes compared to GM-CSF-treated cells.

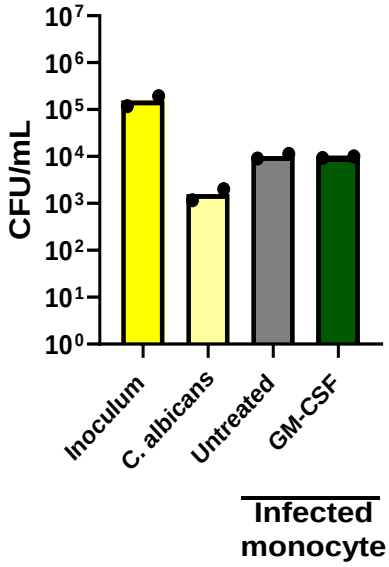

Figure 4.1. Analysis of *C. albicans* viability (CFU) in complete RPMI in the presence and absence of human peripheral blood CD14 monocytes, untreated or treated with GM-CSF. To test the influence of GM-CSF on the interaction of monocytes with *C. albicans,* untreated and GM-CSF-treated monocytes were exposed to *C. albicans* at MOI 1 at a cell density of 10^6 cells/well in a 24 well low attachment plate for 3 hours at 37°C with 5% CO_2 (N=2). No statistical analysis was performed because of the limited number of repeats.

Using the experimental conditions described above, GM-CSF- and M-CSF-monocytes were infected with *C. albicans* at MOI1. However, it was decided first to test the influence of cell density and analyse samples 1 hour post-infection instead of 3 hours.

Hence, monocytes and *C. albicans* were incubated for 1 hour at MOI1 but at two cell densities, 10^5 and 10^6. CFU quantification showed a similar reduction in *C. albicans* CFUs during incubation, in agreement with previous results. CFU counts significantly decreased after one hour in both M-CSF and GM-CSF monocyte cultures, with a more pronounced reduction in the *C. albicans* culture alone (Figure 4.2). Similar findings were seen at both cell densities.

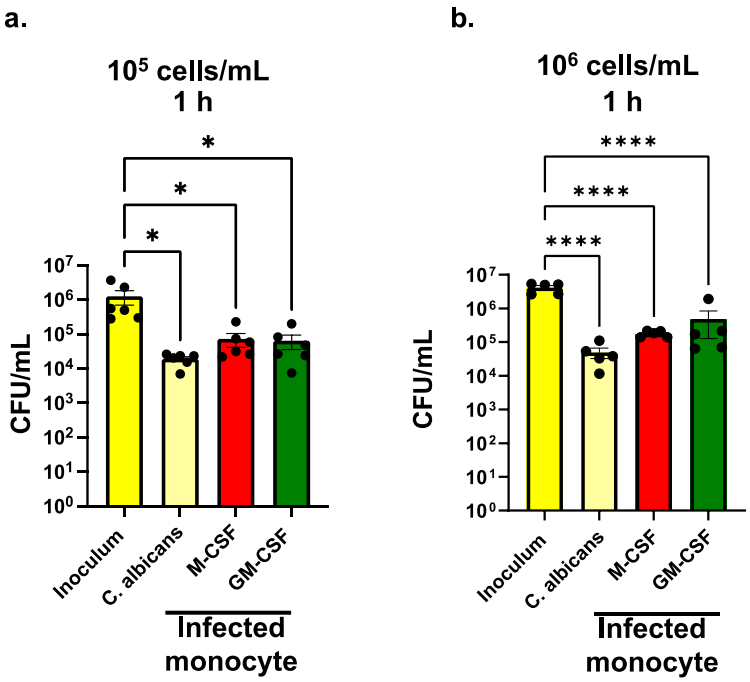

Figure 4.2. Effect of cell density on *C. albicans* CFUs, in the presence and absence of M-CSF and GM-CSF monocytes for 1 hour. To test the influence of GM-CSF on the interaction of monocytes with *C. albicans,* M-CSF/ GM-CSF treated monocytes were exposed to *C. albicans* at MOI 1 using two different cell densities: 10^5 and 10^6 cells/well in 200 µl final volume. CFUs were quantified 1 hour post-infection. **a**. 10^5 cells/well infections **(N=6) b**. 10^6 cells/well infections **(N=5)**. Graphs show mean +/- SEM and individual values. Data were analysed using One-Way ANOVA using GraphPad Prism, (*) $p<0.05$, (****) $p<0.0001$.

Next, the effect of GM-CSF- and M-CSF-monocytes on *C. albicans* CFU at 3 hours was analysed using MOI 1 and cell density 10^6 monocytes and yeasts per well. CFU analysis demonstrated a significant reduction in CFUs in these cultures in the presence and absence of monocytes. Only this time, *C. albicans* only cultures showed readings similar to those exposed to monocytes in both conditions (Figure 4.3).

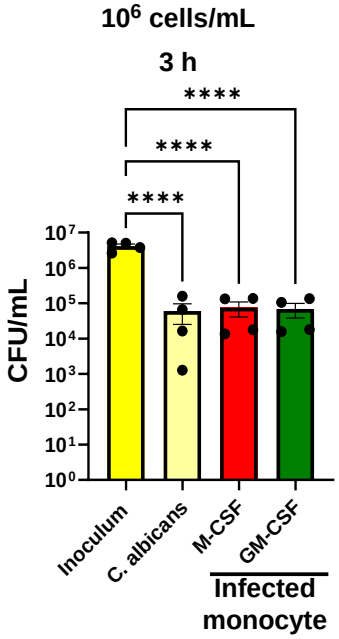

Figure 4.3. Analysis of *C. albicans* CFU after culture in the presence and absence of M-CSF/GM-CSF monocytes for 3 hours. To test the influence of GM-CSF on the interaction of monocytes with *C. albicans,* GM-CSF/M-CSF-treated monocytes were exposed to *C. albicans* at a density of 10^6 cells/well for 3 hours **(N=4).** Graphs show mean +/- SEM and individual values. Data were analysed using One-way ANOVA by GraphPad Prism (****) $p<0.0001$.

4.4.2. *Candida albicans*: from yeast to hyphae

The reduction in *C. albicans* CFUs in the absence of monocytes led to the study of *C. albicans'* behaviour under the experimental conditions used for the infection assay in the presence and absence of serum, i.e. RPMI containing 15% AB human serum (complete RPMI) or not containing serum and incubation at a density of 10^6 cells/well for 1, 2 and 3 hours at 37°C, 5% CO_2.

In brief, *C. albicans* cells cultured overnight were washed in PBS two times and then adjusted to 10^6 cells/well in complete RPMI and plated in 4 low-attachment plates. Plates were analysed at the time of infection, at 1 hour, 2 hours, and 3 hours of incubation. Cultures were imaged using bright microscopy and processed for CFU counts.

Images of the cultures revealed that hyphal formation within the cultures might interfere with CFU quantification. At the start of the culture (0 h), *C. albicans* generated the highest CFU count, which correlated with all plated *C. albicans* being in the yeast form. Upon exposure to serum and incubation at 37°C, the yeast cells began to bud, and by the first hour, hyphae started to form. By the second and third hours, it became evident that the hyphae continued to elongate, resulting in a complex network (Figure 4.4. a).

From three independent repeats, at time 0 (inoculum), CFU counts were at their highest, reflecting the initial number of viable yeast cells. However, after incubation, there was a consistent decline in CFU up to the third hour, and the analysis revealed a significant downregulation in CFU counts compared to time 0 (Figure 4.4. b).

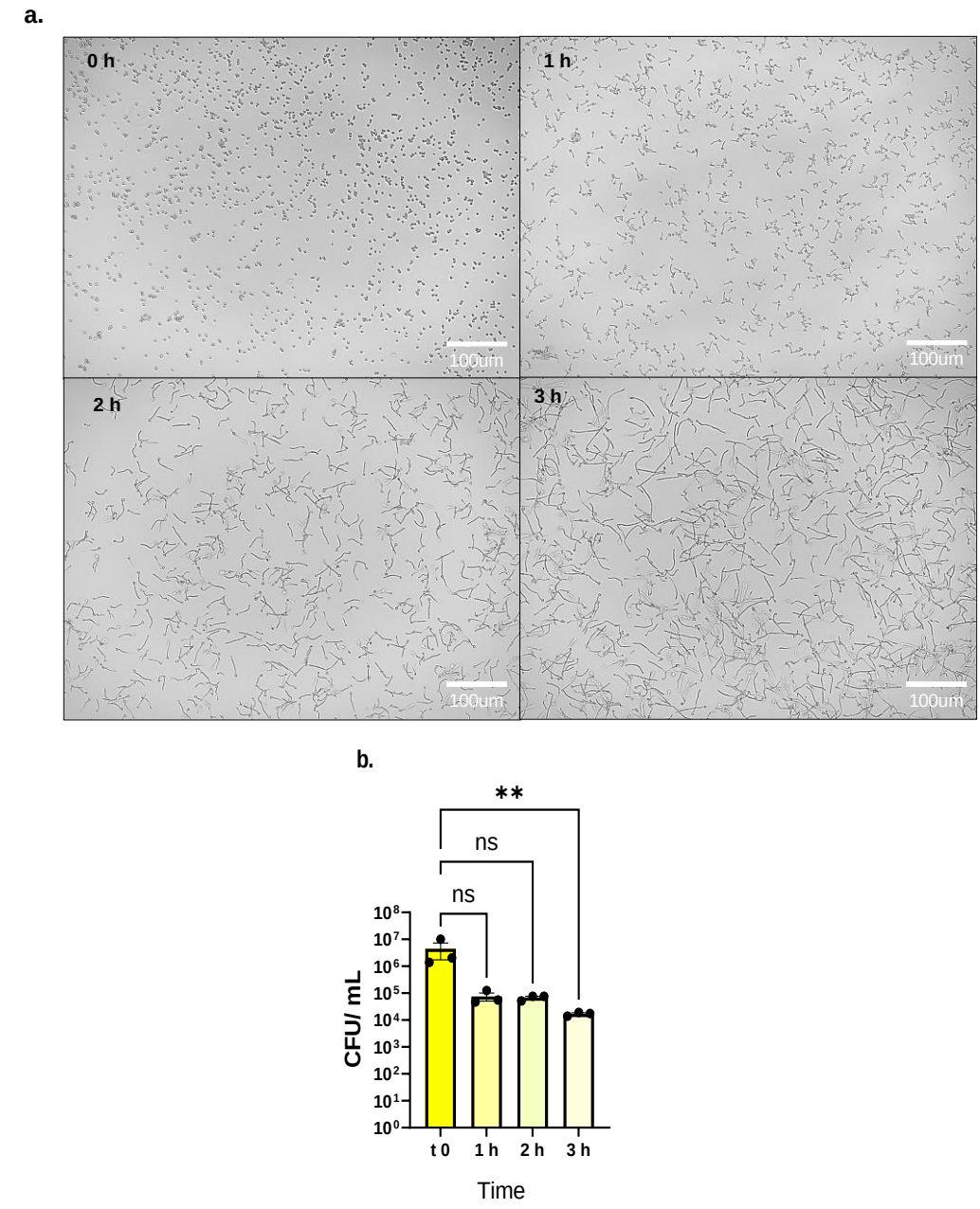

Figure 4.4. Hyphae formation by *C. albicans* correlates with reduced CFU recovery in the presence of serum. Cells from overnight culture were washed in PBS and seeded at a cell density of 10^6 cells/well in RPMI complete media in 24-well tissue culture plates and incubated for up to 3 hours at 37°C, 5% CO_2 (N=3). **a.** Cultures were assessed at time of seeding (0h) then every hour after (1h, 2h and 3h) using bright microscopy (ZOE™ cell imager). Scale bar= 100µm. **b.** CFU quantification. Graphs show mean +/- SEM and individual values. Data were analysed using One-Way ANOVA by GraphPad Prism (**) p<0.001.

Another way to observe *C. albicans* growth in terms of time is to grow cells without serum in RPMI media. In brief, *C. albicans* cells cultured overnight were washed in PBS two times and then adjusted to 10^6 cells/well in RPMI and plated in 4 low-attachment plates. Plates were analysed at the time of infection, 1 hour, 2 hours, and 3 hours of incubation. Cultures were imaged using bright microscopy and processed for CFU counts.

Similar to the behaviour shown in cultures in complete RPMI, images of the cultures showed that hyphae formation within cultures might interfere with CFU quantification. *C. albicans* produced the maximum CFU count at the beginning of the culture (0 h), which was associated with all plated cells being in the yeast state. The yeast cells started to bud after being incubated at 37°C; during the first hour, hyphae had begun to develop. The hyphae were clearly continuing to extend by the second and third hours (Figure 4.5. a).

From three independent repeats, at time 0 (inoculum), CFU counts were at their highest, demonstrating the initial number of viable yeast cells. The variability between replicates at the time of infection was low; therefore, the reduction in CFU between time 0 and the subsequent hour of the cultures was significant up to the third hour (Figure 4.5. b).

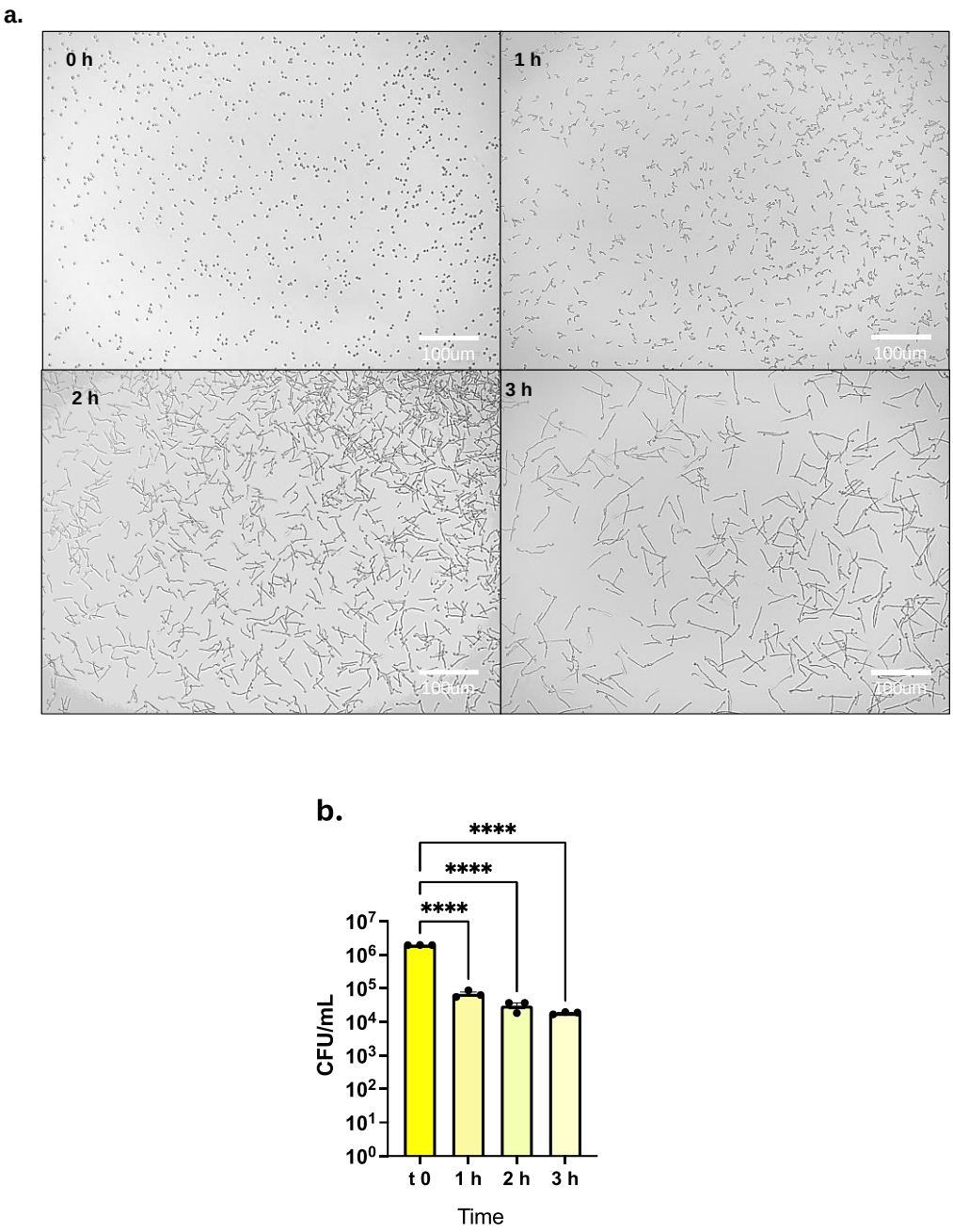

Figure 4.5. Hyphae formation by *C. albicans* correlates with reduced CFU recovery in the absence of serum. Cells from overnight culture, were washed in PBS and seeded at a cell density of 10^6 cells/well in RPMI1460 that doesn't contain AB serum, seeded in 24-well tissue culture plates and incubated for 1, 2 and 3 hours at 37°C, 5% CO_2 **(N=3). a.** Cultures were assessed at time of seeding (0h) then every hour after (1h, 2h and 3h) using bright microscopy (ZOE™ cell imager). Scale bar 100µm. **b.** CFU quantification**.** Graph shows mean +/- SEM and individual values. Data were analysed using One-Way ANOVA by GraphPad Prism (****) p <0.0001.

4.4.3. Effect of GM-CSF monocytes on *C. albicans* hyphae formation

To further confirm that decreased CFU correlates with hypha formation in the presence of monocytes, infection assays were imaged using bright microscopy and hyphae were quantified. Images from infected monocytes suggested that the monocyte treatment conditions influence hyphal length. In brief, monocytes treated with M-CSF or GM-CSF and infected with *C. albicans* at a density of 10^6 cells/well MOI 1, were incubated in complete RPMI for 1, 2 and 3 hours at 37°C, 5% CO_2. Cultures were fixed in 4% PFA and imaged using bright microscopy (ZOE™ cell imager). Hypha length was quantified using Fiji software (Chapter 2, Section 2.3.4. Quantification of *C. albicans* CFU and hyphae formation after incubation with human monocytes).

Figure 4.6. a. shows cell length distribution in cultures from M-CSF monocytes and GM-CSF monocytes infected with *C. albicans* over 3 hours and *C. albicans* only. Five images per well were collected and analysed. Meanwhile, *C. albicans* only cultures showed spread of hyphae throughout the wells, and generation of a network of hyphae by the third hour.

From the first hour of exposure to GM-CSF, monocytes significantly reduced the hyphal length of *C. albicans*. In contrast, M-CSF monocytes showed no notable effect at that time, with high variability observed in both *C. albicans* only and the monocyte conditions. By the second hour, both GM-CSF and M-CSF monocytes reduced hyphal length, but GM-CSF monocytes continued to demonstrate a more significant effect compared to *C. albicans* only and M-CSF-monocyte conditions. At the third hour, hyphae formed in the *C. albicans*-only condition are the longest, up to 200μm, whereas GM-CSF monocytes significantly reduced hyphal length (~100μm) compared to both *C. albicans* alone and M-CSF monocytes, making the impact of GM-CSF particularly evident (Figure 4.6. b).

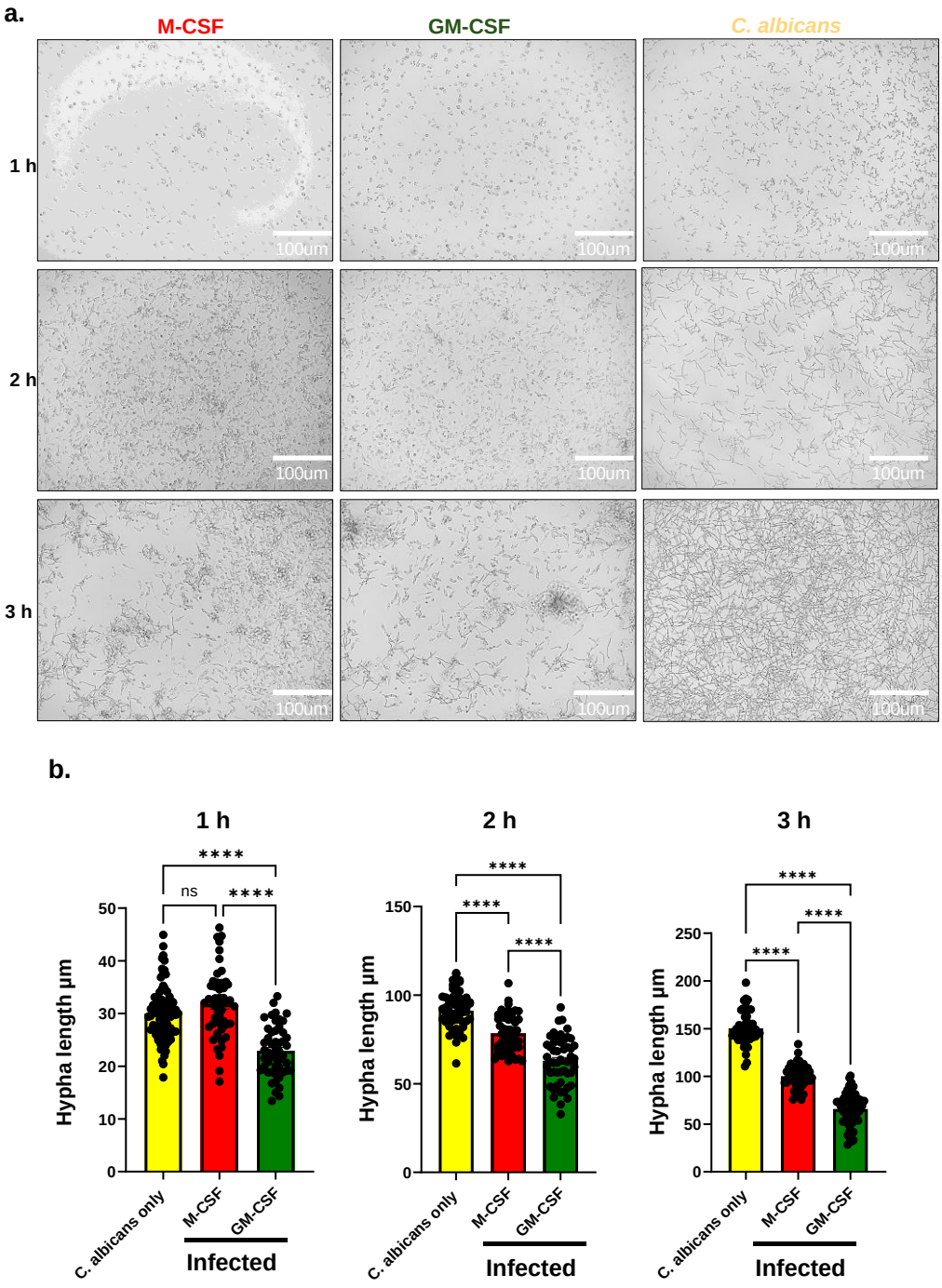

Figure 4.6. GM-CSF monocytes are more efficient at controlling the length of *C. albicans* hyphae compared to M-CSF monocytes. Monocytes treated with either M-CSF or GM-CSF were incubated in the presence of *C. albicans* at MOI1 for 3 hours. Cells were fixed with 4% PFA and bright field images captured at 1 hour, 2 hours and 3 hours post-infection using a ZOE™ imager. Similar fields in wells were investigated. **a.** Representative images of the cultures. Scale bar 100µm **b.** Bar graphs show hyphal lengths in the first, second and third hour. Graphs show mean +/- SEM and individual values. Data were analysed using One-Way ANOVA by GraphPad Prism, ns: not significant, (****) p<0.0001.

4.4.5. Evaluation of the effect of GM-CSF on Monocyte Phagocytosis of *C. albicans*

Phagocytosis is one of the most critical cellular functions in innate immunity during infections [292]. Therefore, it was important to investigate whether GM-CSF influences the uptake of *C. albicans* by monocytes. This was particularly relevant as GM-CSF upregulated surface receptors previously implicated in *C. albicans* uptake, like Dectin-1 and CD11b [293], see (Chapter 3, Section 3.3.4. GM-CSF- and M-CSF-treated monocytes differ in expression of selected surface markers).

M-CSF- and GM-CSF-treated monocytes were infected with GFP-expressing *C. albicans* in complete RPMI media for 1 hour at MOI 10, 37°C, 5% CO_2. After incubation, cells were harvested, incubated in PBS-FBS buffer containing 5% human serum, adjusted to 10^6 cells per FACS tube and labelled for CD11b. To assess phagocytosis, monocytes were gated based on CD11b expression and then queried for presence of GFP (i.e. *C. albicans*). The controls included uninfected cells as well as *C. albicans* only. Phagocytic activity was quantified as the GFP MFI in the CD11b+ gate (E).

Figure 4.7 a-d show the strategy followed to analyse each sample and representative plots. Section 1 shows how live cells (gate A) were selected based on side scatter (SSC) and forward scatter (FSC) characteristics. A singlet gate (G) was created to exclude aggregates and focus on single cells for analysis using SSC Height versus SSC Area. Section 2 shows how a quadrant plot was generated from the singlet gate (G) to represent the distribution of the cells based on two labels: CD11b vs GFP (Section 2b) based on the isotype control (Section 2 a). The (E) region comprised CD11b+ cells that interacted or not with GFP-*C. albicans*, distributed across the C−+ and C++ quadrants, reflecting varying levels of GFP uptake. From gate (E), histograms were generated to calculate the MFI and quantify expression of CD11b and GFP levels.

Figure 4.7 a and b represent the uninfected monocytes, which in both M-CSF and GM-CSF monocytes show expression of CD11b in comparison to isotype control. But compared to M-CSF, the density and colour intensity (from red to yellow) suggest a high number of events in the GM-CSF monocytes (Figure 4.7 a.2.b) and (Figure 4.7 b.2.b).

In infected monocytes on the other hand, the main cell population shifted to $GFP^+/CD11b^+$, indicating CD11b+ cells that associated with GFP-expressing *C. albicans*. This implies that GFP-*C. albicans* had been internalised by a sizable percentage of the cells. The spread into the area is indicative of a population of GFP-positive and receptor-positive cells, which are probably the most functionally active in terms of phagocytosis. However, the difference between M-CSF and GM-CSF for internalised *Candida albicans* is minor, indicating that phagocytosis is unaffected by the presence of GM-CSF under our assay conditions (Figure 4.7 c and d.2).

a. Uninfected M-CSF monocytes

1. Cell population

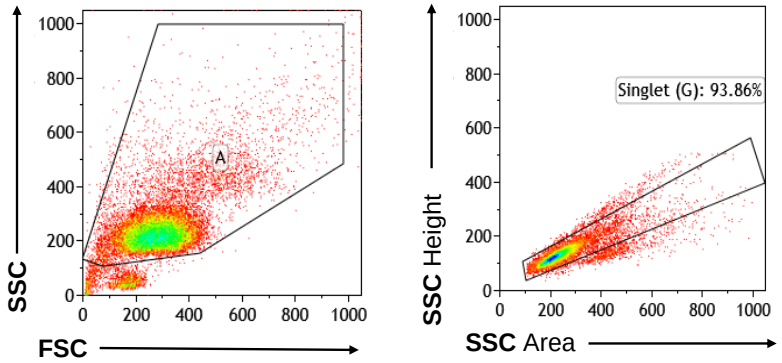

2. Uninfected CD11b+ monocytes

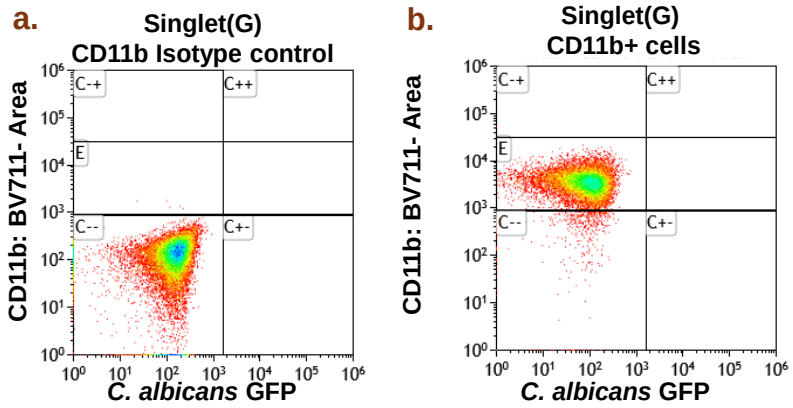

b. Uninfected GM-CSF monocytes

1. Cell population

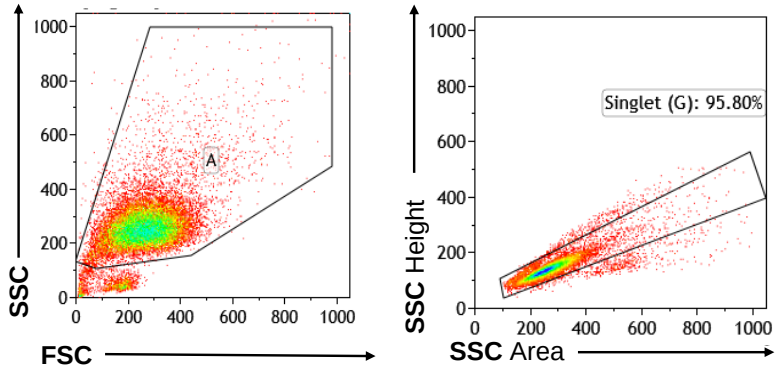

2. Uninfected CD11b+ monocytes

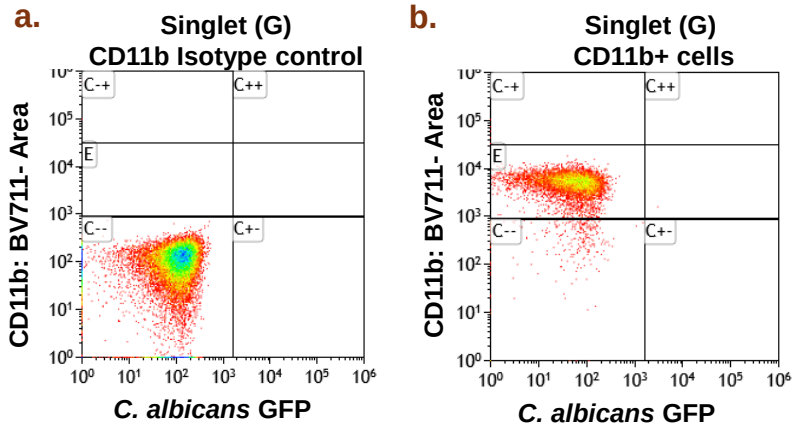

c. Infected M-CSF monocytes

1. Cell population

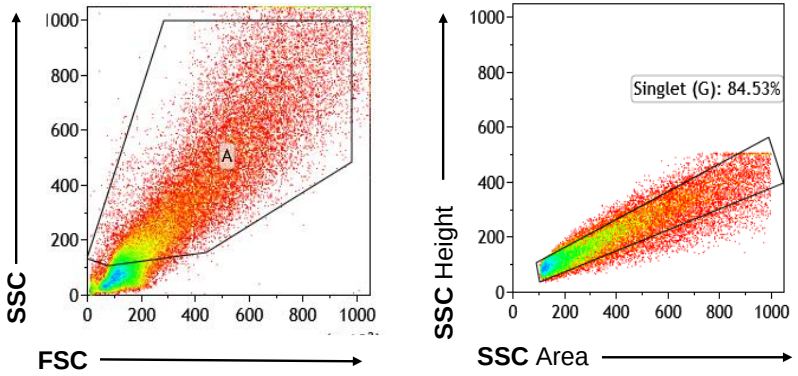

2. Infected CD11b+ monocytes

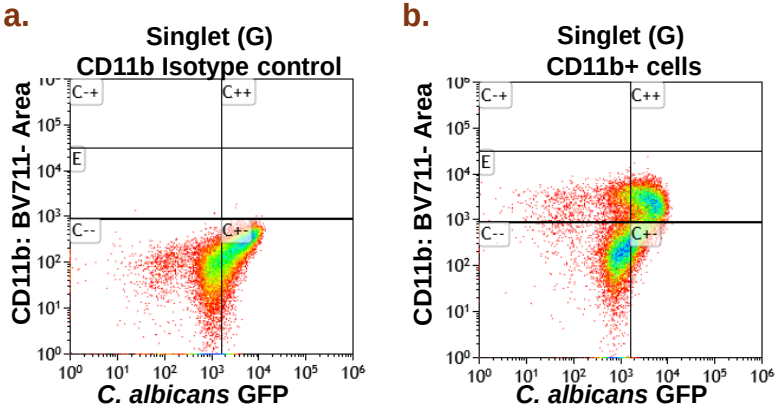

d. Infected GM-CSF monocytes

1. Cell population

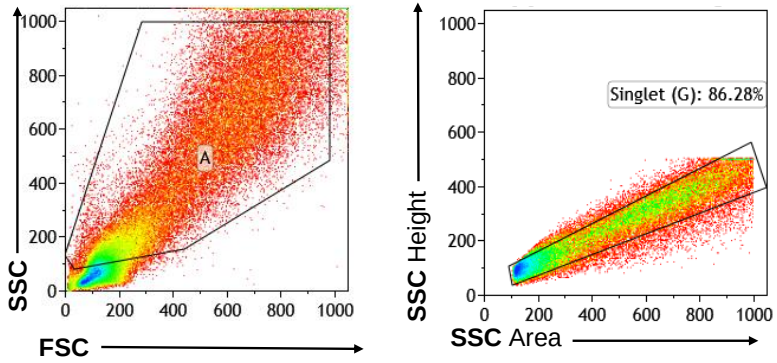

2. Infected CD11b+ monocytes

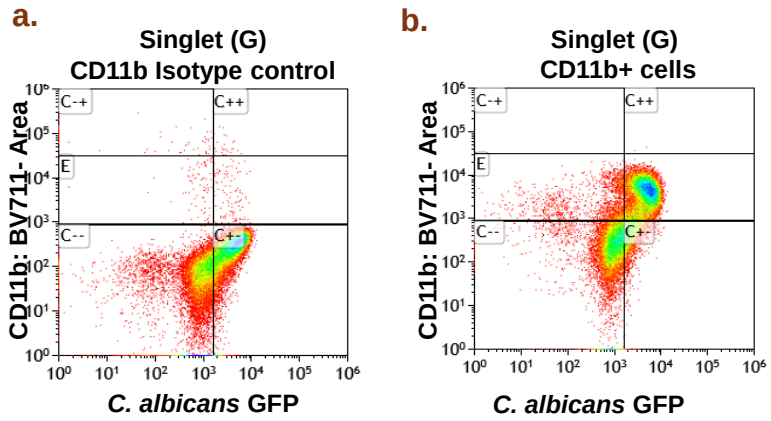

e.

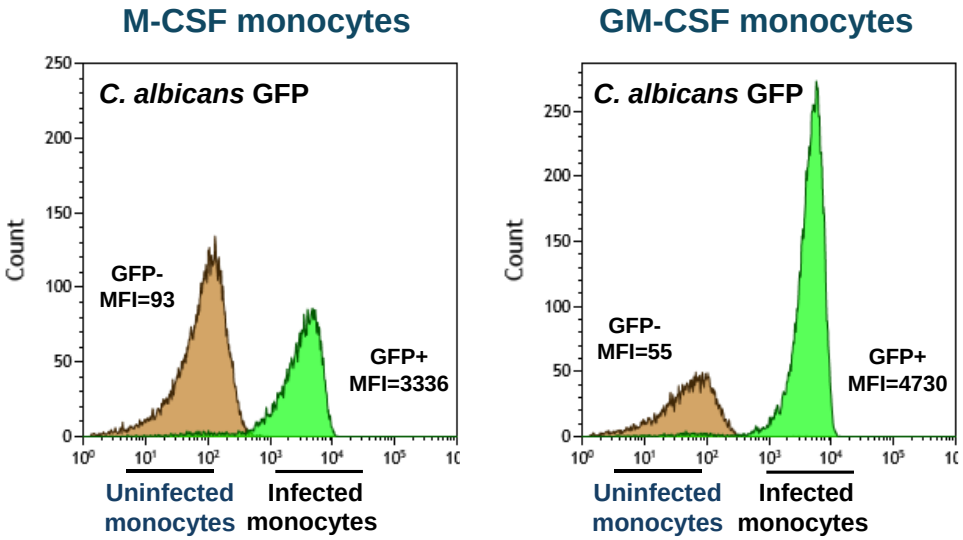

Figure 4.7. Effect of GM-CSF on monocytes phagocytic activity against live *C. albicans*. Monocytes were purified and cultured in the presence of GM-CSF or M-CSF for 40-44 hours. Then, cells were collected and incubated in the presence and absence of *C. albicans* GFP at an MOI 10 for 1 hour. Cells were harvested and labelled for CD11b and its isotype control. **a.** Uninfected M-CSF monocytes**. a.1.** Cell population: shows the unstained population of M-CSF-treated monocytes on a dot plot gate (A) based on SSC and FSC parameters, then a singlet gate (G) was generated from gate (A). **a.2.** Quadrant plots are created from gate (G) on two parameters: CD11b+vs GFP+ positive cells in gate (E). This analysis included the isotype control followed by the CD11b+. **(Note: The same organisation is followed for the remaining conditions). b.** Uninfected GM-CSF monocytes**. c.** Infected M-CSF monocytes. **d.** Infected GM-CSF monocytes. **e.** Histogram from gate (E) of the GFP fluorescence in M-CSF and GM-CSF monocytes **(representative from N=4).** Data were analysed using Kaluza software.

The MFI from relevant gates were plotted and analysed using GraphPad Prism. Figure 4.8. a shows the phagocytic activity of monocytes treated with M-CSF and GM-CSF based on GFP labelling. No significant differences were observed between the two treatments, indicating that treating monocytes with GM-CSF did not affect phagocytosis of *C. albicans* under our experimental conditions. There was variability in the data, particularly in M-CSF monocyte samples. Figure 4.8. b shows surface expression of CD11b on monocytes treated with M-CSF or GM-CSF and infected or left uninfected. GM-CSF monocytes showed significantly higher CD11b expression compared to M-CSF monocytes in the absence of infection, as described in (Chapter 3, 3.3.2. GM-CSF alters expression of selected surface markers in human monocytes compared to untreated monocytes) on (Figure 3.5). However, this difference in CD11b expression disappears upon infection. CD11b expression was reduced in M-CSF- and GM-CSF-monocytes following infection; however, this reduction did not reach statistical significance, probably because of the high variability. In conclusion, although GM-CSF influences receptor expression in monocytes it does not appear to affect their phagocytic activity.

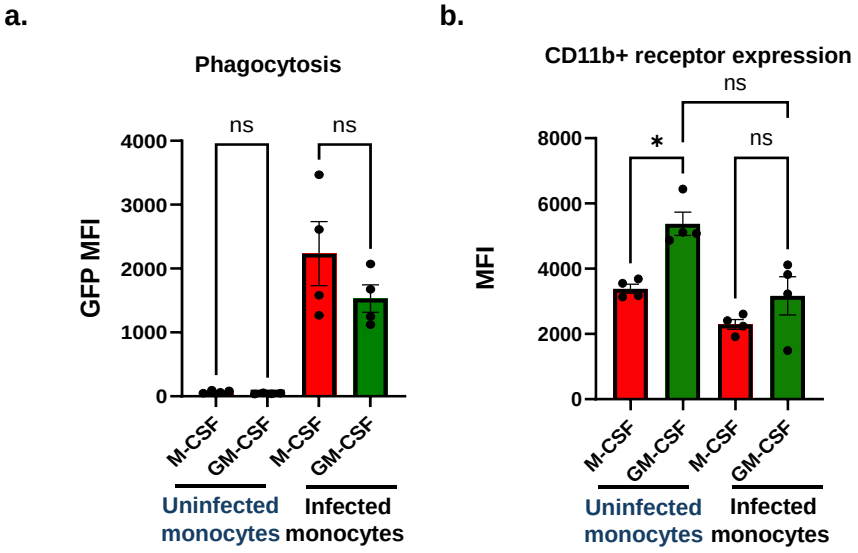

Figure 4.8. Effect of GM-CSF on monocyte phagocytosis. a. Analysis of phagocytic activity of monocytes against *C. albicans*, to assess if GM-CSF influences monocyte phagocytosis, GFP MFI from the CD11b gate was plotted. Data were analysed using paired t-test using GraphPad Prism. **b.** CD11b expression in M-CSF and GM-CSF, both uninfected and infected with GFP-expressing *C. albicans* **(N=4),** Graphs show mean +/- SEM and individual values. Data were analysed using One-Way ANOVA by GraphPad Prism, ns: not significant, (*) $p<0.05$.

To confirm that the GFP fluorescence corresponded to *C. albicans* internalised by the monocytes, flow cytometry samples were subjected to ImageStreamX analysis. Data were analysed using the IDEA 6.2 software as follows: first, a single gate is created to identify the main targeted population. All channels should be selected from that gate based on the labels (i.e. CD11b+ and GFP+). Then, the population is analysed depending on the desired parameters, such as receptor expression and internalisation, in our case. Finally, images are taken and identified as single labels and composites that overlay all channels and the brightfield were generated.

The unstained populations of the uninfected M-CSF- and GM-CSF-treated monocytes show that the cells in the brightfield channel are spherical and healthy under all circumstances. Additionally, it was noted that, in contrast to M-CSF monocytes, GM-CSF increased CD11b expression in uninfected monocytes. This is shown in the quadrant plot, where M-CSF monocytes stay lower on the plot (Figure 4.9. a.2) while GM-CSF monocytes move towards the positive population (Figure 4.9. b.2). Additionally, GM-CSF monocytes have stronger CD11b labelling, as seen by the increased fluorescence intensity of CD11b in the images (Figure 4.9. b.2) when compared to M-CSF monocytes (Figure 4.9. a.2).

In infected monocytes, both conditions display a similar shift towards the upper-right quadrant in the plots, indicating the presence of CD11b+, GFP+ populations (Figure 4.9. c.2) and (Figure 4.9. d.2). Additionally, infected monocytes display clear GFP signals, indicating the engulfment of *C. albicans* by the cells (Figure 4.9. c and d).

a. Uninfected M-CSF monocytes

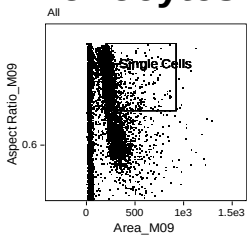

1. Unlabeled cells

Single cells

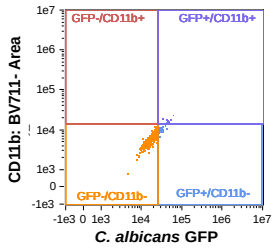

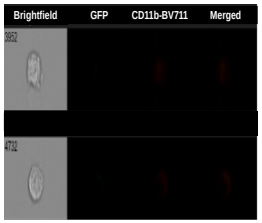

2. CD11b+

Single cells

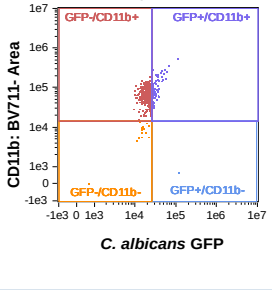

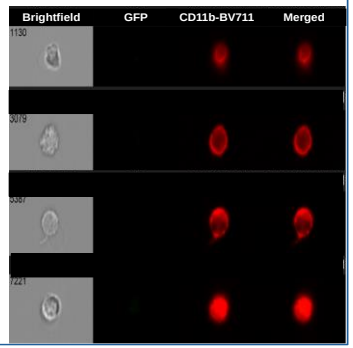

b. Uninfected GM-CSF monocytes

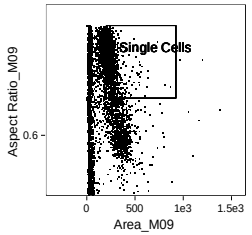

1. Unlabeled cells

Single cells

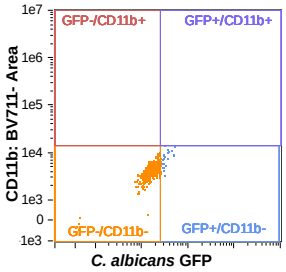

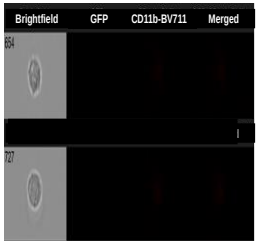

2. CD11b+

Single cells

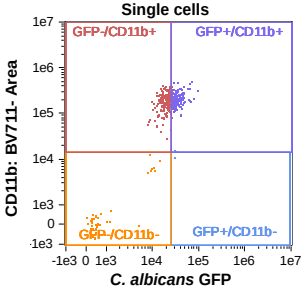

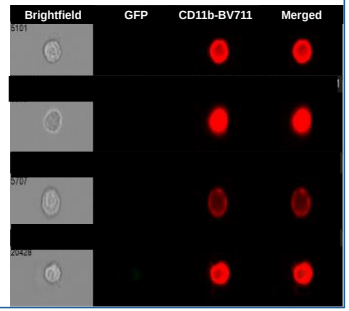

c. Infected M-CSF monocytes

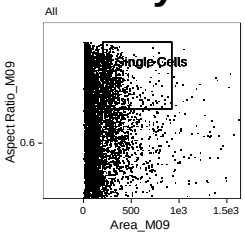

1. Unlabeled cells

Single cells

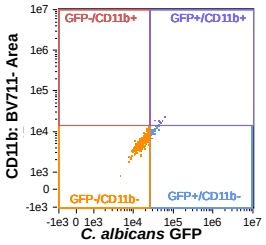

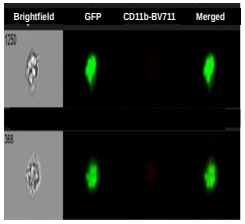

2. CD11b+

Single cells

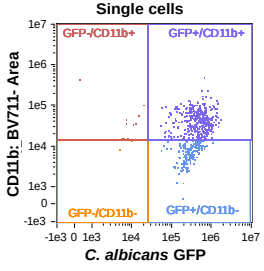

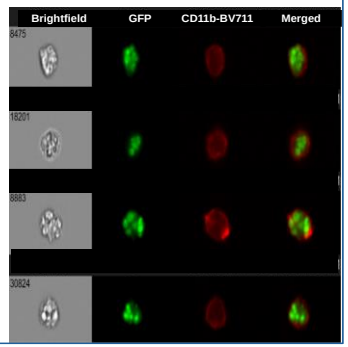

d. Infected GM-CSF monocytes

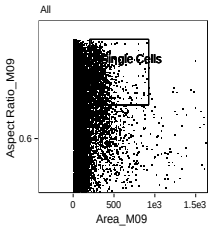

1. Unlabeled cells

Single cells

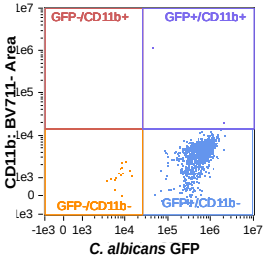

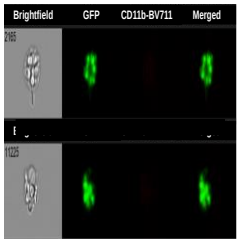

2. CD11b+

Single cells

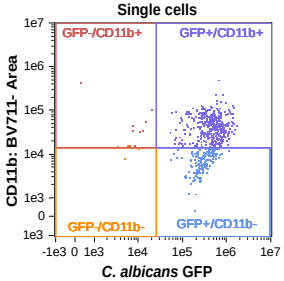

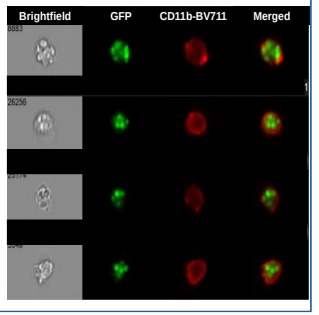

Figure 4.9. Single-cell analysis of *C. albicans* phagocytosis by monocytes using ImageStreamX. ImageStreamX analysis was used to visualise the $CD11b^{+}$ population directly using the same samples that were set up in the flow cytometry experiments. **a.** Uninfected M-CSF monocytes**. a. 1.** Unstained cells, quadrant plot labelled for GFP+ and CD11b+from the main population. Representative images are shown in the brightfield, GFP+, CD11b+ and merged channels. **a. 2.** CD11b+ cells quadrant plot labelled for GFP+ and CD11b+from the main population. Representative images are shown in the brightfield, GFP+, CD11b+ and merged channels. **(Note: The same organisation is followed for the remaining conditions). b.** Uninfected GM-CSF monocytes**. c.** Infected M-CSF monocytes. **d.** Infected GM-CSF monocytes **(N=4).** Data were analysed using IDEA 6.2. software.

Internalisation (phagocytosis) was examined, and the results are consistent with the flow cytometry analysis. No significant differences were observed between

GM-CSF- and M-CSF monocytes, meaning GM-CSF does not affect internalisation of *C. albicans* under these experimental conditions (Figure 4.10. a).

The bar graphs display CD11b expression on monocytes, comparing non-infected and infected cells treated with either M-CSF or GM-CSF. In non-infected monocytes, GM-CSF substantially upregulated CD11b expression compared to non-infected M-CSF monocytes. This finding is consistent with the observed upregulation of CD11b following GM-CSF treatment, as demonstrated by flow cytometry (Chapter 3, Section 3.3.4, which shows that GM-CSF- and M-CSF-treated monocytes differ in the expression of selected surface markers). In infected monocytes, however, there is no significant difference in CD11b expression between M-CSF and GM-CSF conditions (Figure 4.10. b).

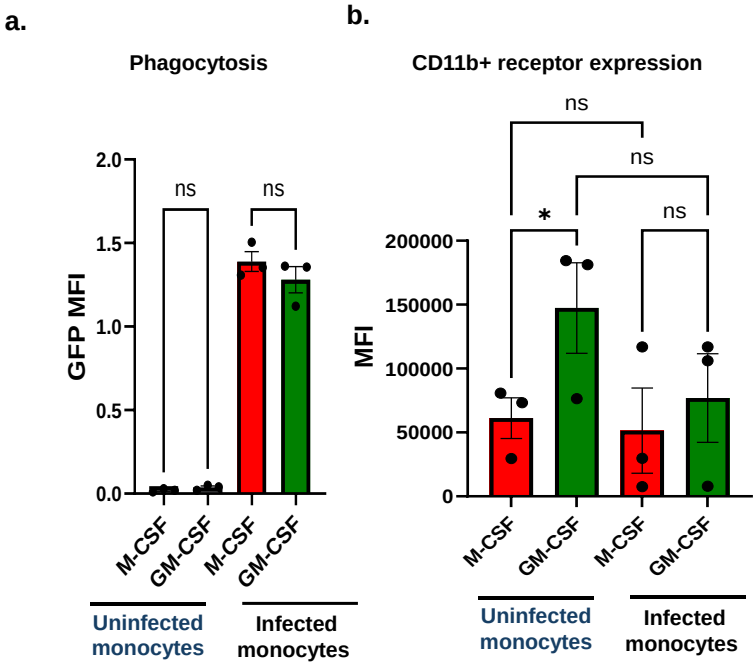

Figure 4.10. Single-cell analysis of *C. albicans* phagocytosis and CD11b expression in monocytes using ImageStreamX. To validate the phagocytosis assay, monocyte samples were analysed using ImageStreamX flow cytometry. **a.** Phagocytosis by infected M-CSF/GM-CSF monocytes (GFP) was analysed using a t-test **(N = 3). b.** Surface expression of CD11b in uninfected and infected monocytes. Significance analysed using One-Way ANOVA**.** Graphs show mean +/- SEM (*) p<0.01, (ns) non-significance.

4.4.6. MR (CD206) expression is reduced in GM-CSF monocytes infected with *C. albicans*

From the phagocytosis assays, the same set of cells was labelled for MR (CD206). The analysis process and sample plots are shown in Figure 53a–d. To eliminate aggregates, Section 1 illustrates the gating of live, single cells based on FSC/SSC and SSC-H vs. SSC-A. Using MR and GFP staining, a quadrant plot was created from singlets in Section 2 (using isotype control as a reference).

In uninfected monocytes, both M-CSF- and GM-CSF-treated cells show positive MR expression. But compared to M-CSF-treated cells, MR expression was considerably higher in GM-CSF-treated monocytes (Figure 4.11. a.2.b) and (Figure 4.11. b.2.b).

However, adding *C. albicans* monocytes significantly reduced MR surface expression, with cells disappearing from the MR+ gate for M-CSF-treated monocytes or displaying reduced MR expression in GM-CSF-treated monocytes.

a. Uninfected M-CSF monocytes

1. Cell population

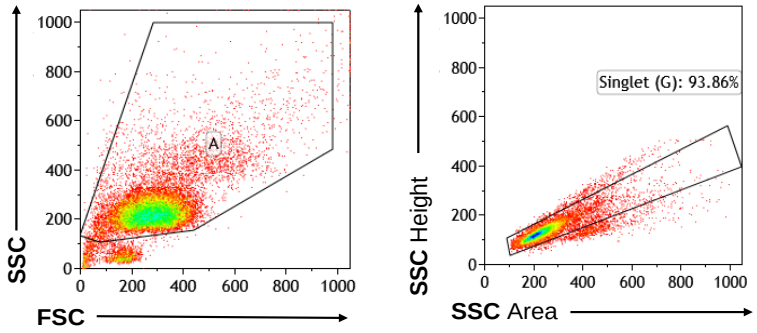

2. Uninfected MR+ monocytes

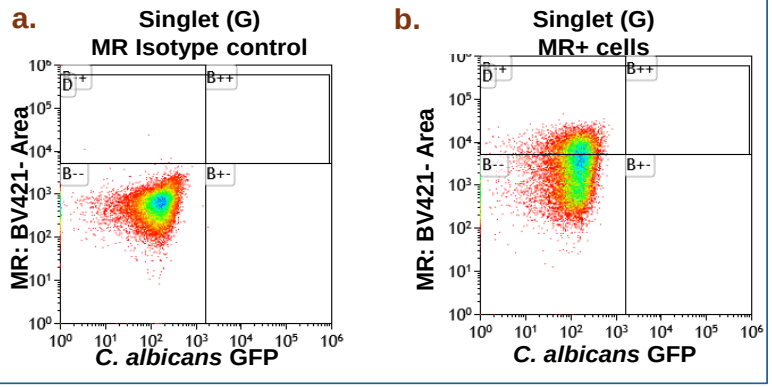

b. Uninfected GM-CSF monocytes

1. Cell population

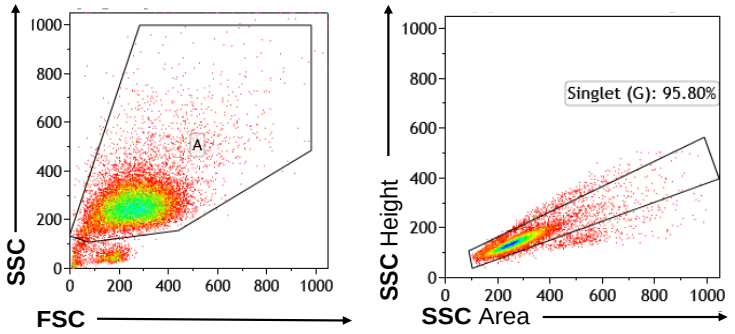

2. Uninfected MR+ monocytes

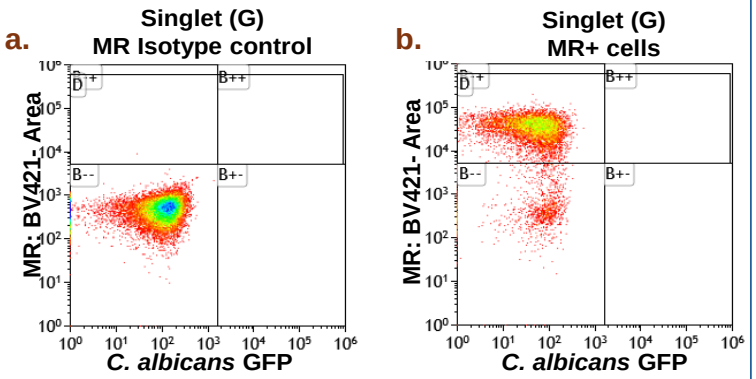

c. Infected M-CSF monocytes

1. Cell population

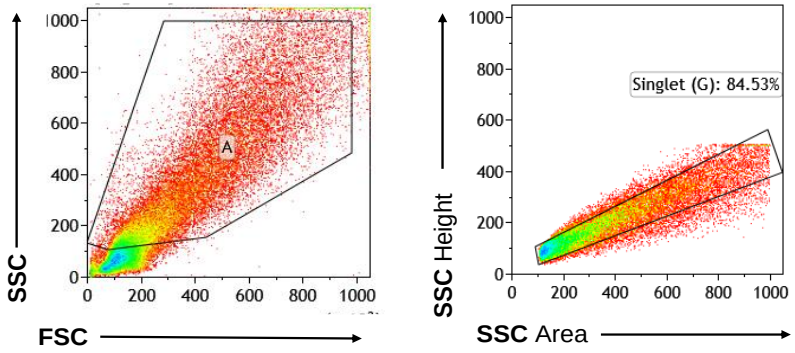

2. Infected MR+ monocytes

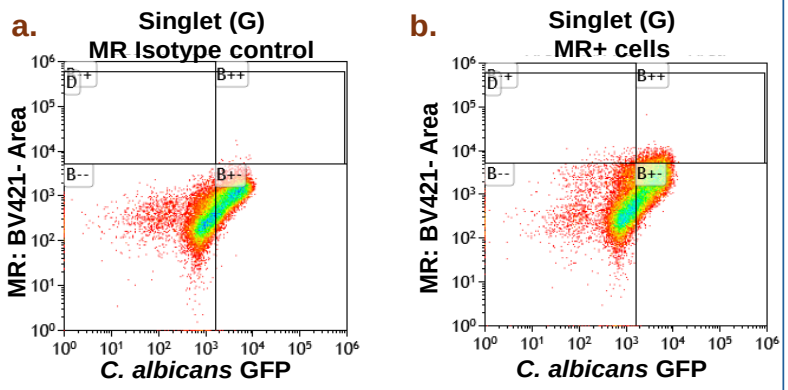

d. Infected GM-CSF monocytes

1. Cell population

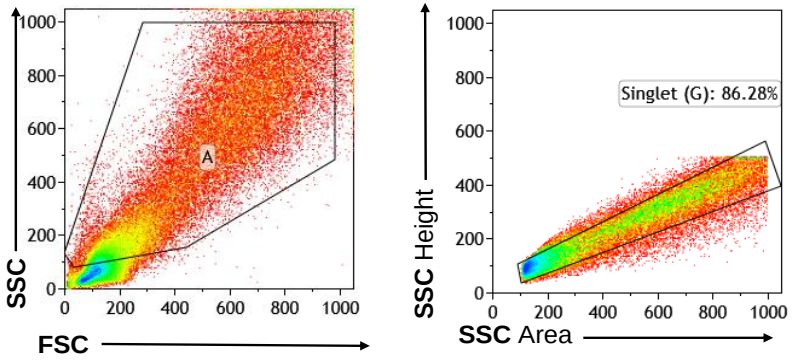

2. Infected MR+ monocytes

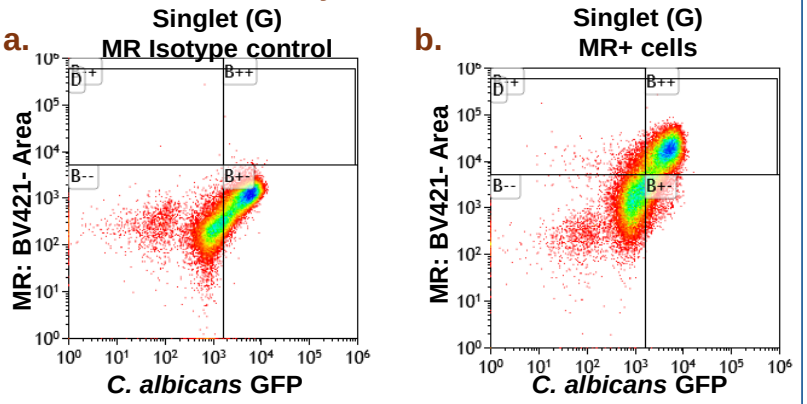

e.

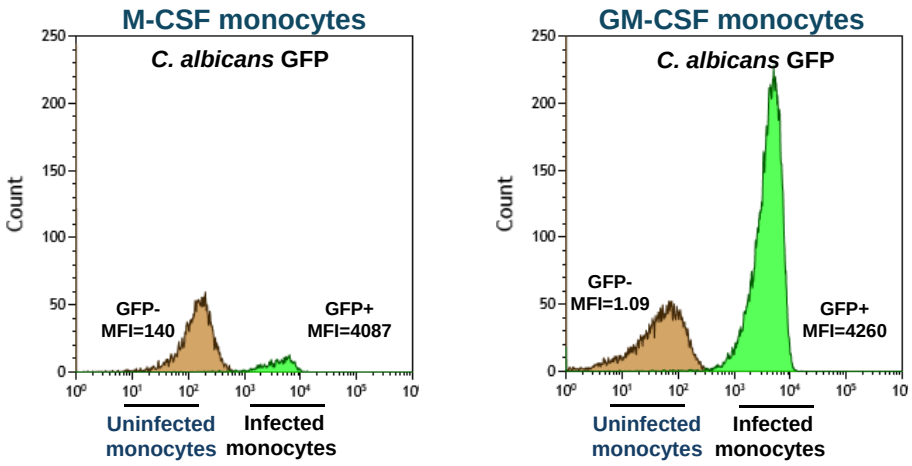

Figure 4.11. MR reduction with GM-CSF treatment in infected monocyte. Monocytes were purified and cultured in the presence of GM-CSF or M-CSF for 40-44 hours. Then, cells were collected and incubated in the presence and absence of *C. albicans* GFP at an MOI 10 for 1 hour. Cells were harvested and labelled for MR and its isotype control. **a.** Uninfected M-CSF monocytes**. a.1. C**ell population: shows the unstained population of M-CSF-treated monocytes on a dot plot gate (A) based on SSC and FSC parameters, then a singlet gate (G) was generated from gate (A). **a.2.** Quadrant plots are created from gate (G) on two parameters: CD11b+Vs GFP+ positive cells in gate (D). This analysis included the isotype control followed by the CD11b+. **(Note: The same organisation is followed for the remaining conditions). b.** Uninfected GM-CSF monocytes**. c.** Infected M-CSF monocytes. **d.** Infected GM-CSF monocytes. **E.** Histogram of the GFP expression internalised M-CSF and GM-CSF monocytes **(N=4).** Data were analysed using KALUSA software.

Data analysis over the multiple repeats demonstrated a significant upregulation of MR expression in the uninfected cells of GM-CSF monocytes compared to M-CSF. However, following infection, MR expression was substantially reduced in GM-CSF monocytes. Due to the high loss of infected MR+ in M-CSF-treated monocytes, we only analyse the receptor expression in GM-CSF monocytes (Figure 4.12. a).

On the other hand, Infected M-CSF monocytes also exhibit MR reduction; however, the cells are leaving the gate due to the extremely low MR labelling. Consequently, we plotted the percentage of positive cells with and without *C. albicans* for M-CSF (Figure 4.12. b).

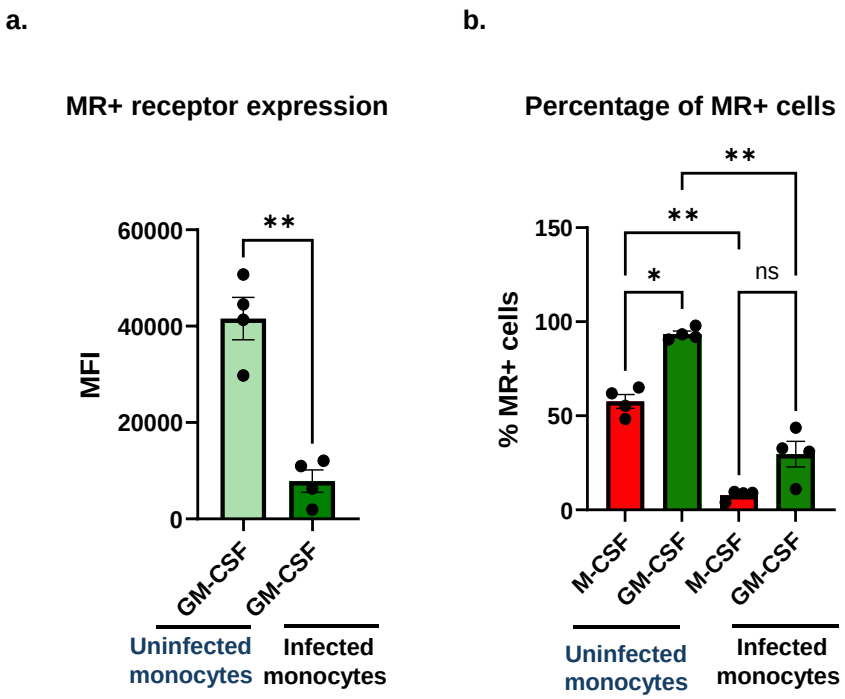

Figure 4.12. Changes in surface expression of MR in monocytes in response to *C. albicans*. Graphs represent **a.** receptor expression for non-infected and infected GM-CSF-monocytes, both uninfected and infected. **b.** the percentage of MR+ cells for M-CSF- and GM-CSF-monocytes, both uninfected and infected**.** Graphs show mean +/- SEM. Significance is analysed using One-Way ANOVA; **(N=4)**, (**) p<0.0001.

From the phagocytosis assays, the same set of cells was labelled for MR (CD206) and validated by performing single-cell analysis by ImageStreamX.
The expression of MR is upregulated in monocytes treated with GM-CSF compared to M-CSF (Figure 4.13. a.1) and (Figure 4.13. b.1). After adding *C. albicans* it is obvious how the brightness of fluorescence is reduced in both GM-CSF and M-CSF (Figure 4.13. b.3) and (Figure 4.13. d.3).

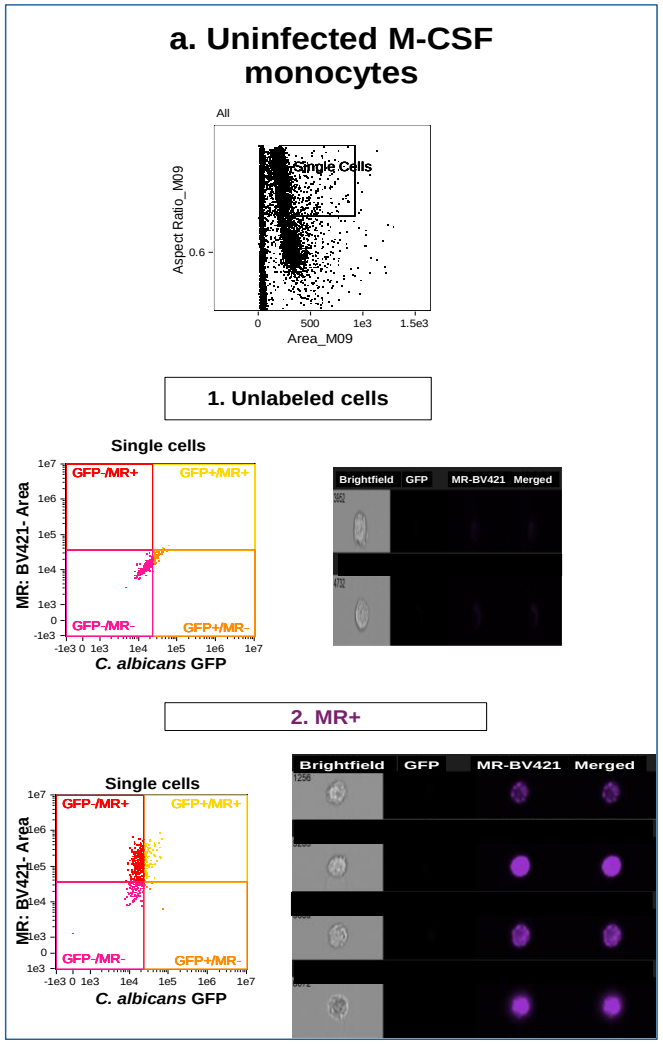
a. Uninfected M-CSF monocytes
All
Single Cells
Aspect Ratio_M09
Area_M09
1. Unlabeled cells
Single cells
GFP-/MR+
GFP+/MR+
GFP-/MR-
GFP+/MR-
MR: BV421- Area
C. albicans GFP
Brightfield
GFP
MR-BV421
Merged
2. MR+

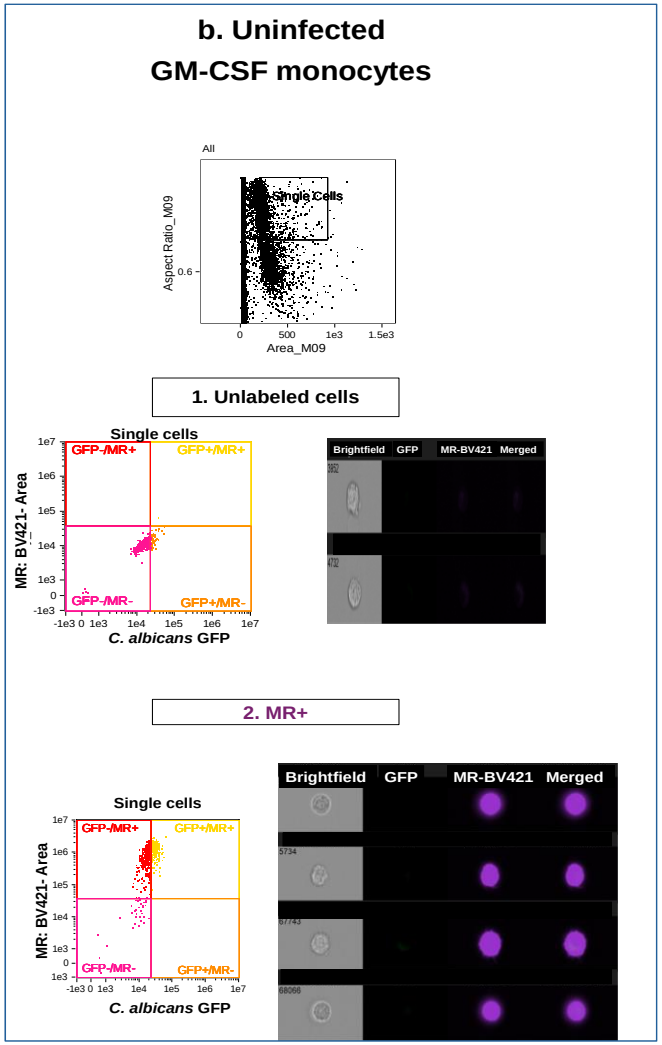
b. Uninfected GM-CSF monocytes
All
Single Cells
Aspect Ratio_M09
Area_M09
1. Unlabeled cells
Single cells
GFP-/MR+
GFP+/MR+
GFP-/MR-
GFP+/MR-
MR: BV421- Area
C. albicans GFP
Brightfield
GFP
MR-BV421
Merged
2. MR+

c. Infected M-CSF monocytes

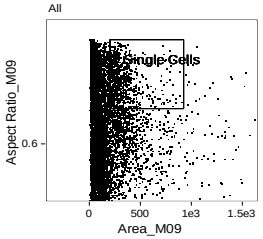

1. Unlabeled cells

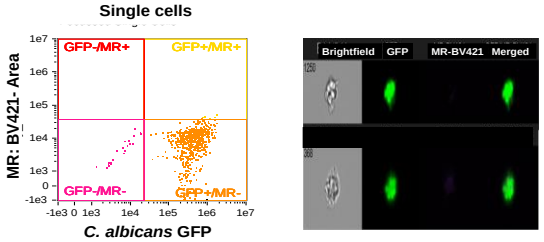

2. MR+

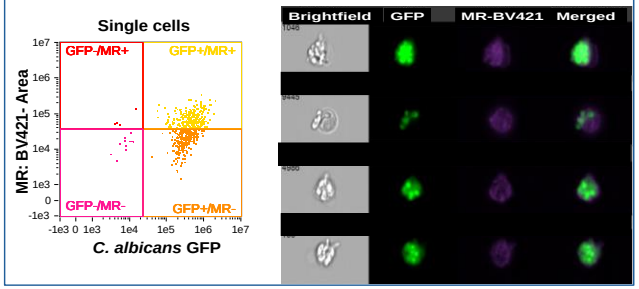

d. Infected GM-CSF monocytes

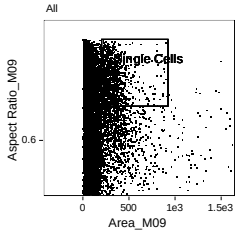

1. Unlabeled cells

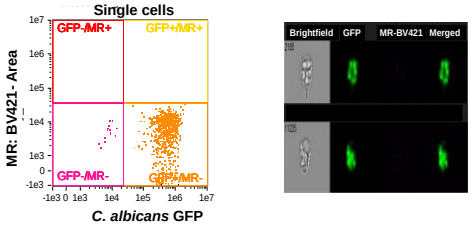

2. MR+

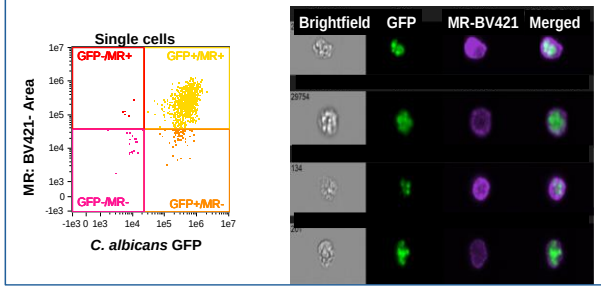

Figure 4.13. Validating MR reduction after phagocytosis using ImageStreamX. ImageStreamX analysis was used to visualise the MR^+ population directly using the same samples used in the flow cytometry analysis. **a.** Uninfected M-CSF monocytes**. a. 1.** Unstained cells, quadrant plot labelled for GFP+ and MR+ from the main population. Representative images are shown in the brightfield, GFP+, MR+ and merged channels. **a. 2.** MR+ cells quadrant plot labelled for GFP+ and MR+ from the main population. Representative images are shown in the brightfield, GFP+, MR+ and merged channels. **(Note: The same organisation is followed for the remaining conditions). b.** Uninfected GM-CSF monocytes**. c.** Infected M-CSF monocytes. **d.** Infected GM-CSF monocytes **(N=4).** Data were analysed using IDEA 6.2. software.

Similarly to flow cytometry data, ImageStreamX data revealed that GM-CSF monocytes had upregulated MR compared to M-CSF, and MR expression was

reduced drastically when *C. albicans* was added. M-CSF monocytes have low MR surface expression and almost lose it when infected with *C. albicans* (Figure 4.14).

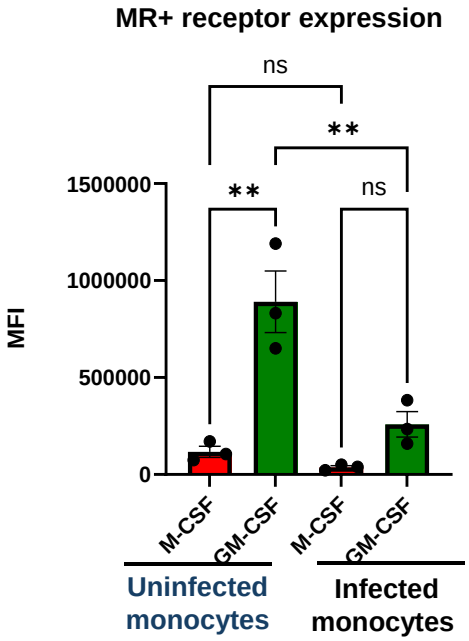

Figure 4.14. Surface expression of MR monocytes in response to *C. albicans* by ImageStreamX. Analysis of the expression of MR receptors, MFI is calculated for M-CSF and GM-CSF-monocytes, both Uninfected and infected**.** Data are collected from ImageStreamX analysis; Graphs show mean +/- SEM. Significance is analysed using One-Way ANOVA; **(N=3)**, (ns)= no significance, (**) p<0.001

4.4.7. Effect of GM-CSF on the production of cytokines and chemokines by human monocytes in response to *C. albicans.*

An essential approach to studying immune responses to infection is investigating cytokine and chemokine secretion [294]. To determine the effect of GM-CSF on cytokine production by human monocytes, purified monocytes were treated with 10 ng/mL of either M-CSF or GM-CSF and incubated for ~ 40 to 44 hours. Cells were collected and infected with *C. albicans* at MOI 1 for 3 hours at 37°C, 5% CO_2. Supernatants from multiple independent repeats were collected and tested for the presence of the proinflammatory cytokines: TNF-α, IL-1β, and IL-6. Additionally, the chemokines CCL-22, CCL-17, CXCL-10, and CXCL-5, as well as VEGF, were also examined.

GM-CSF significantly enhanced the secretion of proinflammatory cytokines in infected monocytes, and in some cases, also in non-infected monocytes. TNF-α is produced in both uninfected and infected monocytes, at notably higher levels in infected cells. Infected M-CSF-monocytes secreted TNF-α only after infection, however, at lower levels compared to GM-CSF-monocytes. IL-1β secretion is observed in infected M-CSF monocytes, but it is markedly increased in GM-CSF monocytes. Interestingly, IL-6 exhibited a distinct secretion profile, being uniquely detected in infected GM-CSF monocytes (Figure 4.15).

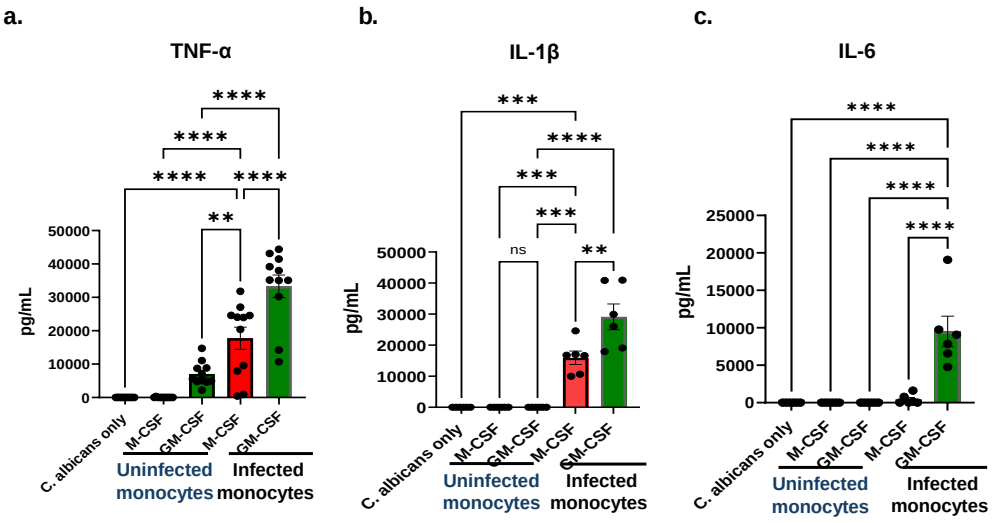

Figure 4.15. Effect of GM-CSF on cytokine secretion by monocytes in response to *C. albicans* infection. Purified monocytes treated with M-CSF or GM-CSF were incubated in the presence and absence of *C. albicans* MOI 1 for 3 hours at 37°C, 5% CO_2. Supernatants were collected, and cytokines quantified using capture ELISA. **a.** TNF-α (N=11), **b.** IL-1β and **c.** IL-6 (N=6)**.** Graphs show mean +/- SEM and individual values. Data were analysed using One-Way ANOVA by GraphPad Prism. (*) p<0.05, (**) p<0.001, (***) p<0.0001, (****) p<0.0001.

The secretion of CCL-22 is significantly influenced by GM-CSF treatment, with higher levels observed in infected GM-CSF-treated monocytes compared to uninfected ones (Figure 4.16.a). However, variability in CCL-22 secretion was noted among donors. Furthermore, CCL22 was detected in cultures of uninfected GM-CSF monocytes; however, no correlation was found between CCL-22 secretion between infected and uninfected GM-CSF monocytes across donors (Figure 4.16. b).

Monocytes treated with M-CSF showed no detectable CCL-22 secretion under either condition (Figure 4.16).

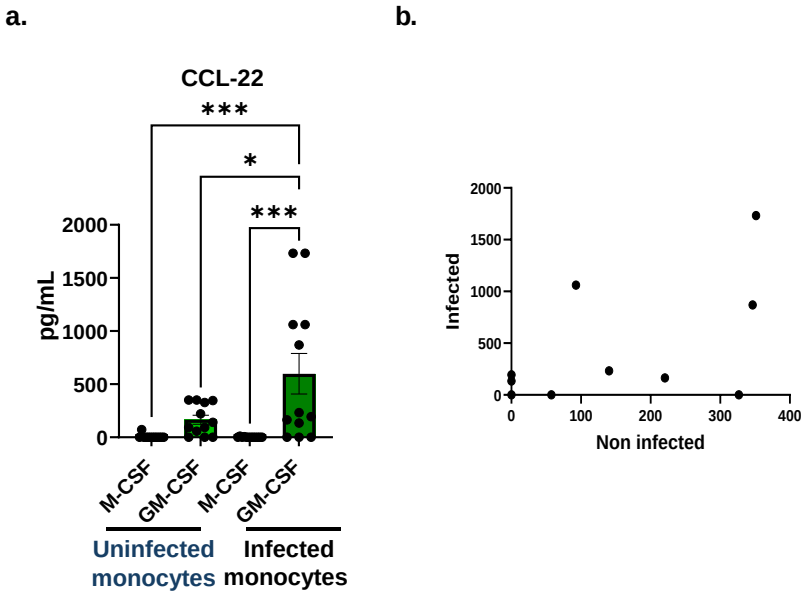

Figure 4.16. Effect of GM-CSF on CCL-22 secretion by monocytes in response to *C. albicans* infection. Monocytes treated with M-CSF or GM-CSF were incubated in the presence and absence of *C. albicans* for 3 hours. Supernatants were collected, and cytokines quantified using capture ELISA. **a.** CCL-22 secretion by monocytes, **b**. XY analysis shows lack of correlation between infected and non-infected samples from the same donor (N=11). Graphs show mean +/- SEM and individual values. Data were analysed using One-Way ANOVA by GraphPad Prism (*) $p<0.05$, (***) $p<0.001$.

ELISA analysis also revealed that among six donors, only two donors demonstrated upregulation of CCL-17 under GM-CSF treatment, both in uninfected and infected conditions with no clear differences in response to infection (Figure 4.17. a).

VEGF secretion was observed in both uninfected and infected M-CSF monocytes with no observed secretion from monocytes treated with GM-CSF (Figure 4.17. b).

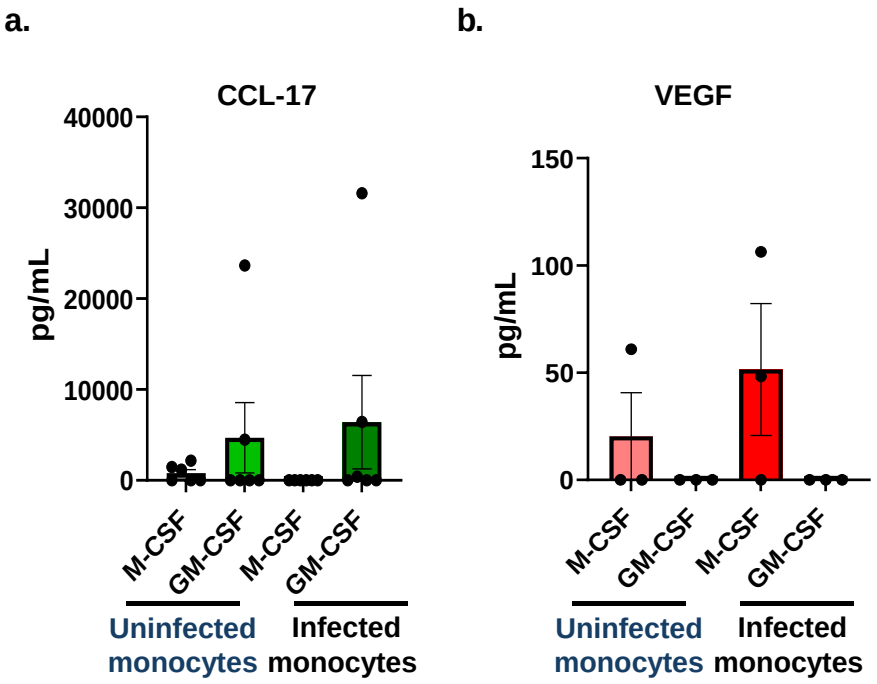

Figure 4.17. Effect of GM-CSF on CCL-17 and VEGF secretion by monocytes in response to *C. albicans* infection. Monocytes treated with M-CSF or GM-CSF were incubated in the presence and absence of *C. albicans* for 3 hours. Supernatants were collected, and cytokines quantified using capture ELISA. **a.** CCL-17 (N=6), **b.** VEGF (N=3). Data analysed using One-Way ANOVA in GraphPad Prism.

4.4.8. Use of confocal microscopy to explore receptor dynamics during *C. albicans* internalisation

Confocal microscopy was used to examine the expression of MR and CLEC5A in non-infected and infected monocytes. M-CSF- and GM-CSF-treated monocytes were infected for 5 and 10 minutes with *C. albicans* wild-type at MOI 10, and labelled for CLEC5A and MR, and examined using confocal microscopy (details in (Chapter 2, Section 2.10.3 Confocal microscopy)). Despite being a single-pilot study, the data provided relevant information about the role of GM-CSF in the recruitment and expression of MR and CLEC5A during *C. albicans* infection.

In uninfected M-CSF monocytes, receptor expression was barely detectable at 5 minutes (Figure 4.18. a). In contrast, uninfected GM-CSF monocytes showed upregulation of both MR and CLEC5A in nearly all observed cells, with a stronger signal evident for CLEC5A (Figure 4.18. b).

In infected M-CSF monocytes, CLEC5A expression was broadly upregulated on the surface of monocytes. Interestingly, CLEC5A also appeared to be recruited to form distinct ring-like structures around phagosomes. In contrast, MR expression was largely absent (Figure 4.18. c). Practically all viable cells in infected GM-CSF exhibit high levels of MR and CLEC5A expression. CLEC5A is clearly co-localised with *C. albicans* while MR, which is largely located in the endosomal compartment in both uninfected and infected monocytes, is also recruited into phagosomes in GM-CSF monocytes (Figure 4.18. d)

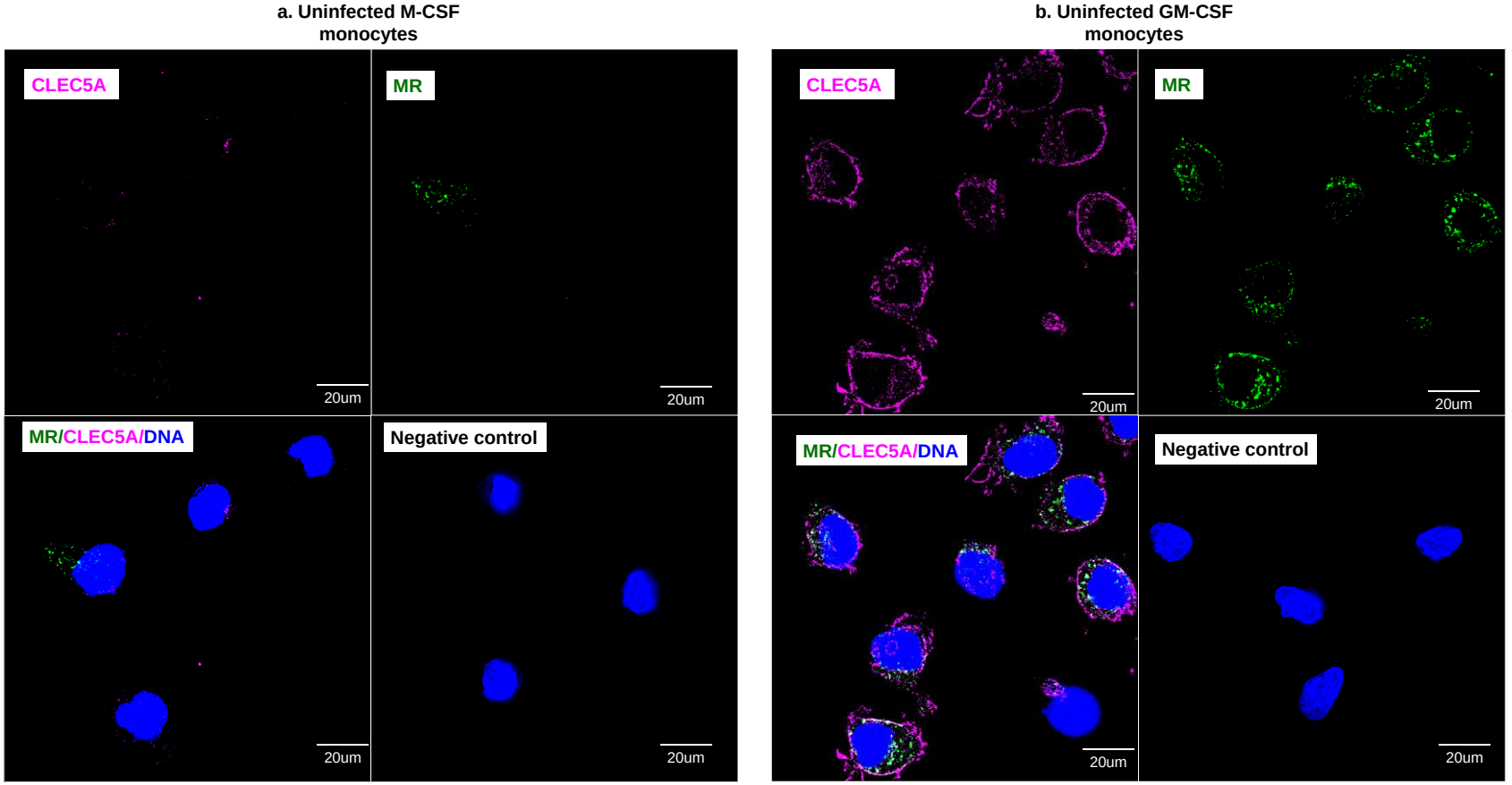
a. Uninfected M-CSF monocytes
b. Uninfected GM-CSF monocytes
CLEC5A
MR
MR/CLEC5A/DNA
Negative control
20um

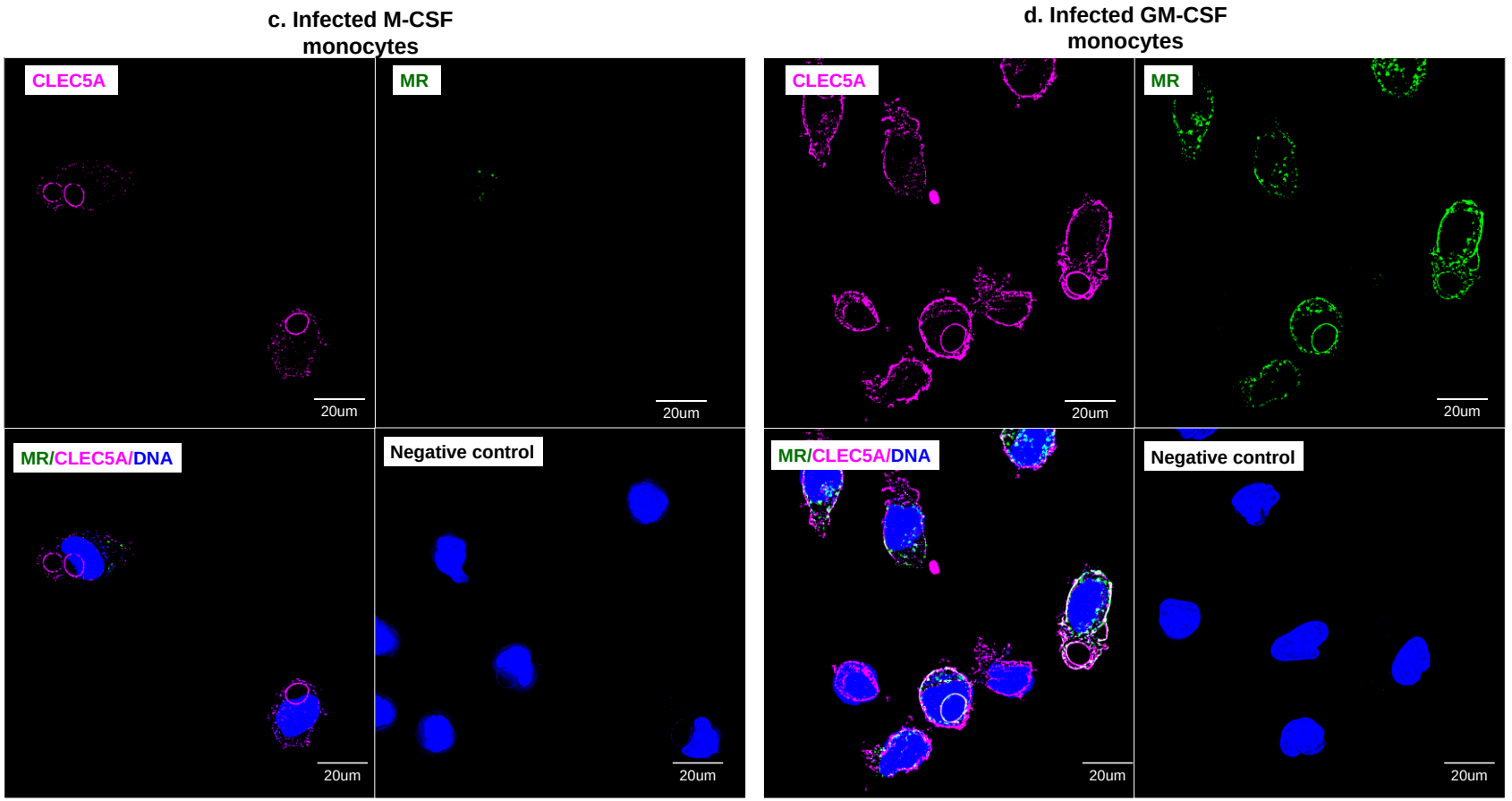
c. Infected M-CSF monocytes
d. Infected GM-CSF monocytes
CLEC5A
MR
CLEC5A
MR
20um
20um
20um
20um
MR/CLEC5A/DNA
Negative control
MR/CLEC5A/DNA
Negative control
20um
20um
20um
20um

Figure 4.18. MR and CLEC5A expression in uninfected and infected monocytes after 5 minutes infection. Monocytes treated with GM-CSF or M-CSF were incubated for ~24h then, cells were collected transferred to 8-well ibidi plates at $1x10^4$ cells/well. Following incubation, cells are washed with complete RPMI and seeded into 8-well ibidi plates at a density of 10^5 cells/well in complete RPMI containing either GM-CSF or M-CSF overnight. The next day, cells were infected with *C. albicans* at MOI 10 for 5 min in complete RPMI to allow the yeast to interact with the cells. Unbound yeast was removed by washing with cold RPMI, and warm complete RPMI was added. Plates are incubated for 5 minutes at 37ºC, 5% CO_2. Cells were then fixed in 4% PFA in PEM and permeabilised. The primary Abs for MR and CLEC5A were added and incubated at 4ºC overnight. The following day, secondary Abs were added, incubated, and then fixed at 4% PFA**. a.** Uninfected M-CSF-treated monocytes**. b.** Uninfected GM-CSF-treated monocytes **c.** Infected M-CSF-treated monocytes. **d.** Infected GM-CSF-treated monocytes. Images show split channels of CLEC5A, MR, merged channels and negative controls (secondary antibody only)**,** scale bar 20µm **(N=1)**. Images are taken by SIM microscopy and analysed by Fiji.

Samples collected after 10 minutes show similar results although not clear presence of MR in phagosomes was observed. This experiment revealed that monocytes rapidly internalise *C. albicans* within just 5 minutes, i.e. before *C. albicans* begins to form hyphae and receptors are recruited to phagosomes, particularly CLEC5A. As observed, GM-CSF treatment resulted in a greater expression of both receptors compared to M-CSF treatment

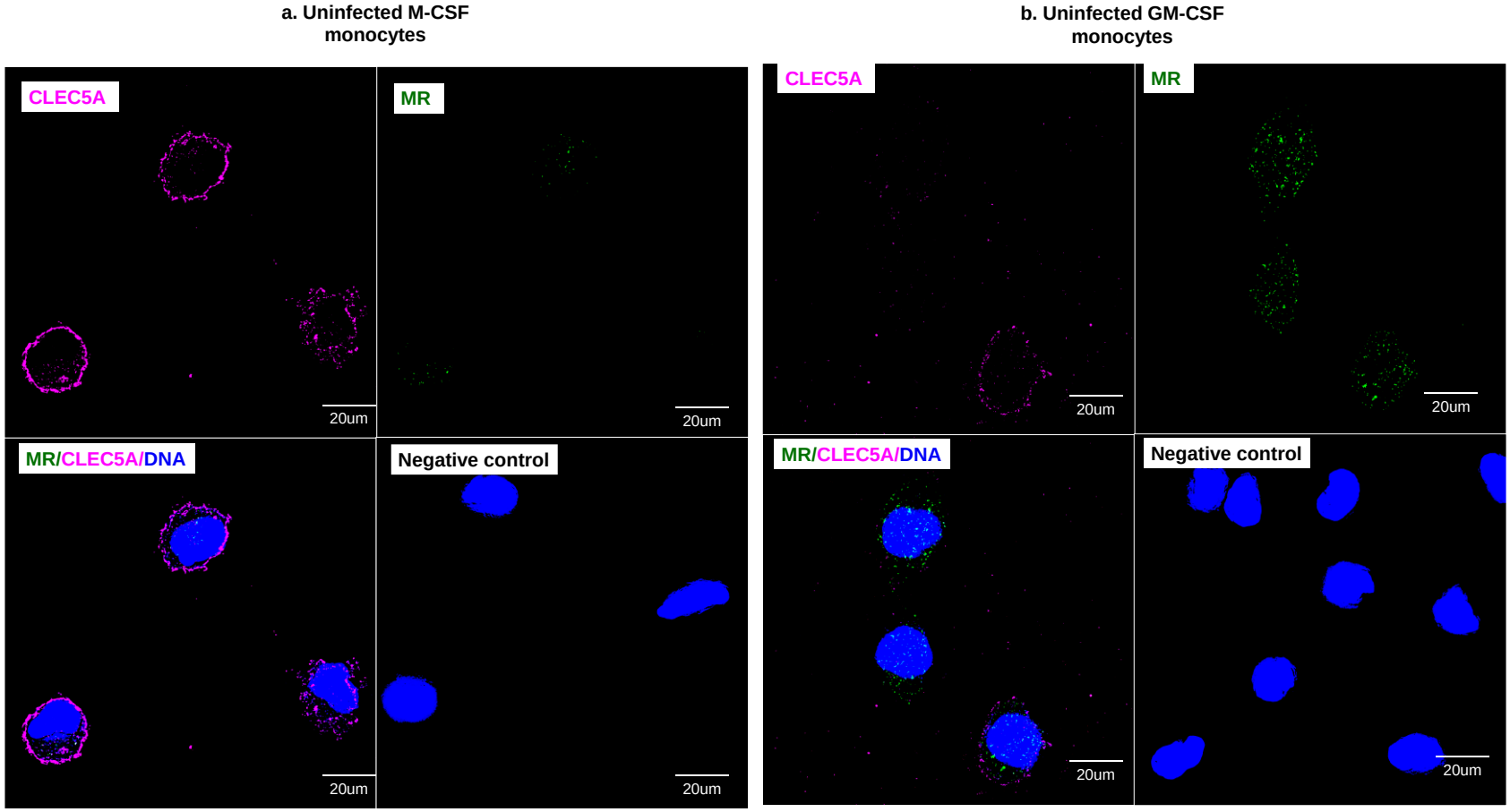
a. Uninfected M-CSF monocytes
b. Uninfected GM-CSF monocytes
CLEC5A
MR
MR/CLEC5A/DNA
Negative control
20um

c. Infected M-CSF monocytes

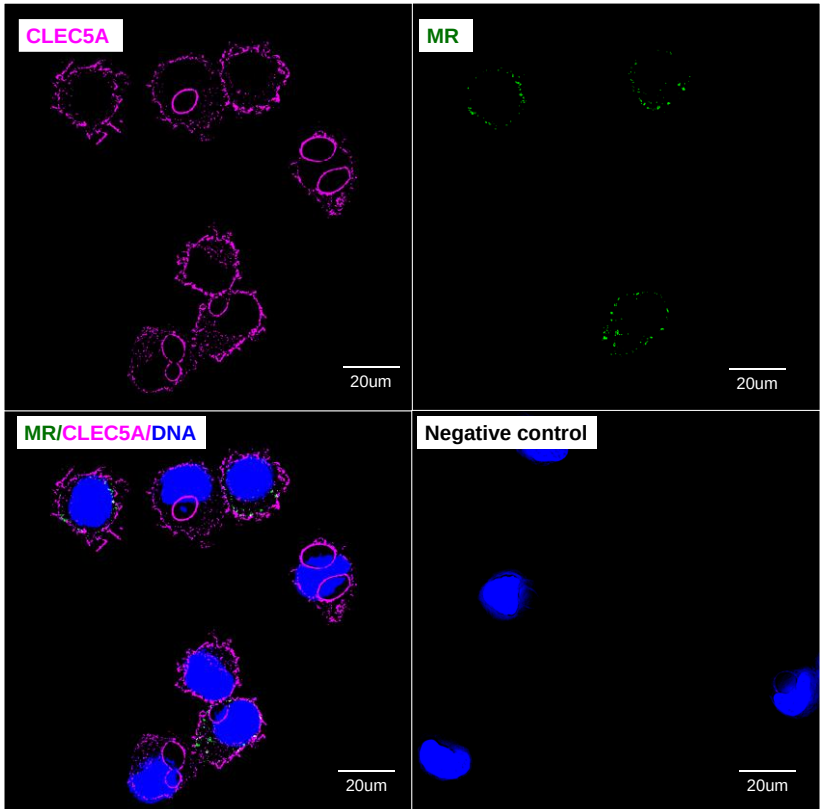

d. Infected GM-CSF monocytes

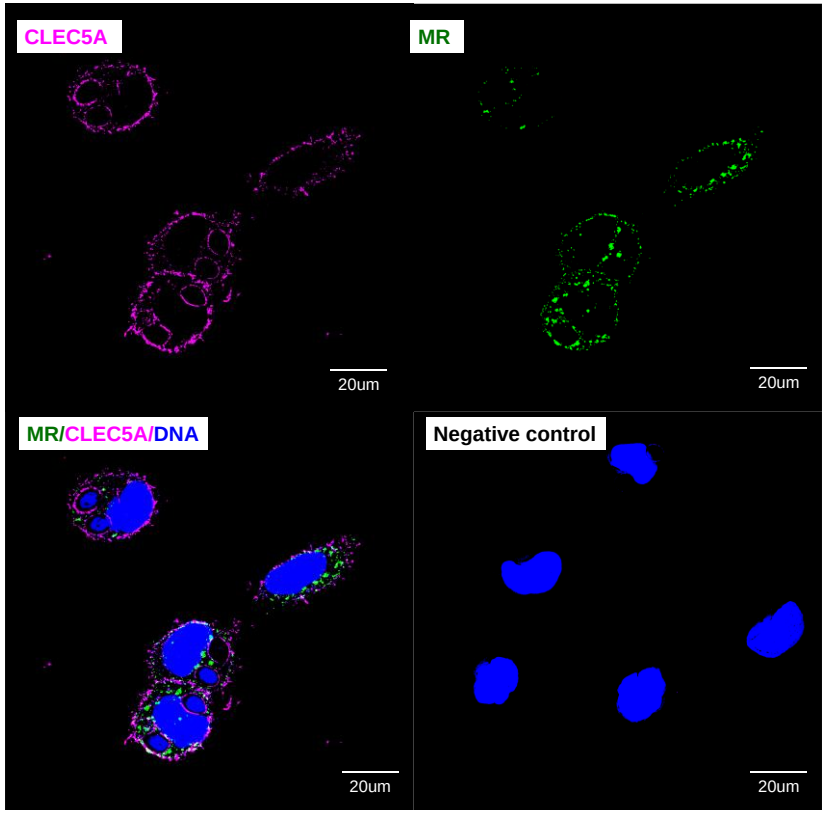

Figure 4.19. MR and CLEC5A expression in uninfected and infected monocytes in 10 minutes culture. Same experiment set up in figure 4.18 was applied here, only cells incubated for 10 minutes**. a.** Uninfected M-CSF-treated monocytes**. b.** Uninfected GM-CSF-treated monocytes **c.** Infected M-CSF-treated monocytes. **d.** Infected GM-CSF-treated monocytes. Figures represent Images, split channels of CLEC5A, MR, merged channels and negative controls**,** scale bar 20µm **(N=1)**. Images were taken by SIM microscopy and analysed by Fiji.

4.5. Summary

- *C. albicans* CFU were reduced after incubation and were not affected by monocytes probably due to hypha formation at 37°C.
- GM-CSF-monocytes restricted the growth of *C. albicans* hypha compared to M-CSF-monocytes and cultures lacking monocytes.
- GM-CSF did not affect monocyte phagocytosis of *C. albicans*. There was a noticeable reduction in expression of CD206 after *C. albicans* uptake.
- GM-CSF increased secretion of proinflammatory cytokines and some chemokines from infected monocytes.
- Confocal microscopy images indicate that the uptake of *C. albicans* is immediate after infection and CLEC5A is recruited phagosomes.

4.6. Discussion

This chapter focuses on the development of an *in vitro* model to study host-pathogen interactions involving co-culturing primary human monocytes with *C. albicans* [295]. We specifically studied on how the phenotypical changes induced by GM-CSF on human monocytes (Chapter 3) affect their response to *C. albicans* infection. Hence, this discussion will cover the following:

1. Selection of infection assay conditions
2. The effect of GM-CSF on hyphae formation
3. The effect of GM-CSF on cellular response against *C. albicans*
4. Future refinements of the infection assay

1. Selection of infection assay conditions

Our protocol involved infecting purified monocytes with *C. albicans* in the presence of 15% AB human serum at 37°C, 5% CO_2, from 1 to 3 hours, and then evaluating host defence mechanisms to test the effect of GM-CSF on the responses of monocytes to infection. Regardless of other factors, such as the type of media or the incubation time, temperature (37°C) plays a crucial role in promoting *C. albicans* hyphae formation, which mimics the human body's normal temperature. Adding serum has been identified in the literature as a critical key in addition to the temperature for hyphal growth; promoting rapid hyphae growth [279]. Despite numerous attempts in the laboratory to manipulate virulence factors, such as growing *C. albicans* in serum-free media or PBS alone (Figure 4.5), hyphae were never developed until the temperature was raised from 30 to 37 ˚C. However, in all experiments of this project, *C. albicans* was cultured in the presence of 15% AB human serum.

Before establishing the infection assay model, the initial objective was to characterise *C. albicans* behaviour. The strains obtained from Prof. Rebecca Drummond (University of Birmingham) were cultured in YPD medium, and CFUs were subsequently quantified in the presence and absence of monocytes (M-CSF and GM-CSF). Cultures were prepared at 10^6 monocytes per well. Generally, in phagocytosis assays, an MOI of 10 and incubation of 1 hour, were selected as reported in the literature; which we also found suitable for our conditions [296]. However, for bright microscopy or cytokine secretion analysis, an MOI of 1 with incubation for 3 hours were deemed appropriate [295].

Following infection, we either labelled the cells for flow cytometry analysis, collected the supernatants for ELISA to assess cytokine production, or fixed cells for imaging, depending on the assay we had to conduct later. Our design yielded promising data that were also reproducible and consistent, as will be discussed in the following section.

Evaluation of the relevance of the infection model.

In our model, monocytes were cultured in RPMI media supplemented with serum to maintain optimal viability and functionality. Monocytes were seeded onto UpCell tissue culture for a better cellular retrieval with higher viability and recovery. Monocytes treated with GM-CSF are primed to improve pathogen recognition and potentiate inflammatory signalling [297]. Cells were incubated then, characterised for cellular behaviours details in (Chapter 3, 3.6. discussion).

Infection assays have been employed previously for different purposes, for example, to develop antifungal treatments. Gow et al investigated the structural and functional features of the fungal cell wall and discovered how its biosynthesis aids in invasion and immune cell evasion [298]. Another approach is to study adhesion and biofilm formation, as seen in Lin's group. They demonstrated that agglutinin-like sequence (Als3), a protein on hyphal surfaces mainly responsible for *C. albicans* adhesion and invasion, is essential for *C. albicans* attachment to human immune cells, exposing the molecular processes that underlie adhesion [299]. Furthermore, Holyt et al provided a thorough analysis of systems biology methods for treating fungal infections, focusing on the integration of in vitro coculture data to understand pathologic strategies and host responses [14].

In our model, we used *C. albicans* co-cultures with monocytes at relevant conditions (37 °C, 5% CO_2) to dissect the dynamics of fungal recognition, phagocytosis, and effector response. Studies in immune cells, including macrophages, demonstrate that maintained MOIs allow assessment of fungal clearance and immune effector pathways. Commonly, MOI 1 is used to mimic physiological conditions, while MOI 10 is used to amplify immune activation. For instance, the production of IL-1β is significantly influenced by infection multiplicity in certain cases involving *C. albicans*-infected macrophages [300]. Nevertheless, we employed both MOIs in our design to address different aspects of the infection, i.e. cellular responses and phagocytosis.

In correlation with literature, our model is thought to be scientifically practical and consistent with established methods by using infection conditions that have been validated across a coculture system that maintains physiological receptor expression and function. This guarantees that any increases in cytokine production or fungal clearance that are seen can be reliably linked to the immunomodulatory effect of GM-CSF rather than to improper assay design or cell handling artefacts.

2. The effect of GM-CSF on hyphal formation.

Hypha formation interferes with CFU quantification.

The significant reduction in CFU over time, compared to the initial inoculum, prompted further investigation into hyphal formation, as imaging revealed that the yeast cells were not eliminated by the host cells as expected because the striking reduction in CFU was even observed in wells that had *C. albicans* alone; instead, over time *C. albicans* transitioned into hyphal form. Baltch *et al*. used a similar experimental design to ours; they investigated the effect of GM-CSF-treated monocyte-derived macrophages (MDMs) on the viability of *C. albicans* (CFU). They found that GM-CSF-MDMs dramatically reduced the *C. albicans* CFU, and that the reduction was substantially greater when GM-CSF was combined with fluconazole. However, their study did not include any hyphal quantification or morphological switching [287]. Hyphae appear to adhere to and invade tissues more effectively than the yeast form, suggesting that morphological switching may play a role in pathogenicity [301]. Hyphal growth begins with the appearance of the germ tube at polarity sites, which is driven by hydrostatic pressure that causes the plastic cell wall at the tip to expand, while the lateral walls remain elastic. In hypertonic media, *C. albicans* hyphal development is considerably slowed [302]. Incubating *C. albicans* with monocytes slightly enhances the CFU as some *C. albicans* cells remain in the yeast form [303]. Monocytes severely shorten hyphal length, particularly GM-CSF-treated monocytes. Hyphae quantification was performed using simple laboratory tools, brightfield microscopy, followed by measuring hyphal lengths with FIJI software. To improve accuracy and reliability, fluorescence microscopy is proposed, along with reducing cellular density, to minimise overlaps and enhance visualisation, thereby clearly distinguishing between intracellular and extracellular *C. albicans*. Furthermore, *C. albicans* hyphae can be shortened by methods that prevent it from maintaining the filamentous form, such as the use

of farnesol, which prevents hyphal formation; adjusting pH by maintaining media acidity to restrict hyphal growth; and lowering the temperature to 25–30 °C so that yeast form is encouraged to sustain rather than hyphae form [304]. Cardini A et al employed the HyLength tool, a semi-automated image analysis that measures fungal hypha and plant roots length in different experimental designs *in vivo* and *in vitro*. They demonstrated that the software eliminates user bias and is reliable, saving a significant amount of time, which in our case was the primary limitation in quantifying hyphae. With these advantages, HyLength may prove to be a valuable instrument for upcoming research projects that evaluate hyphal elongation and network formation in fungi in diverse environmental settings [305].

3. The effect of GM-CSF on cellular response against *C. albicans*

No effect of GM-CSF on monocyte phagocytosis of *C. albicans.*

The immune system has a crucial ability to respond to outside stimuli, and one of these responses is phagocytosis [306]. It is one of the processes studied in this project to determine whether it is affected in monocytes in response to GM-CSF. Phagocytosis assays were designed based on an initial experiment investigating the impact of CARD9 inhibition (data shown in the appendix). This was performed using 40 μM of the CARD9 inhibitor BRD5529, a compound demonstrated to effectively inhibit CARD9–TRIM62 protein-protein interactions in a dose-dependent manner [307]. The experiment focused on evaluating whether GM-CSF monocytes demonstrate altered phagocytic activity when CARD9 is inhibited. This approach was inspired by evidence that administering recombinant GM-CSF to some CARD9-deficient patients significantly reduced mucocutaneous fungal infections, suggesting a potential therapeutic pathway worth exploring [158]. Despite being limited to a single experiment and the lack of effective CARD9 inhibition with the inhibitor, the experiment provided valuable insight, prompting a reassessment of the phagocytosis assay model we used after.

We initiated phagocytosis assays in M-CSF- and GM-CSF-treated monocytes by labelling cells with CD11b to track their interaction with GFP-expressing *C. albicans* using flow cytometry and ImageStreamX. The similar levels of phagocytosis between M-CSF and GM-CSF might be explained by the presence of the anti-*C. albicans* antibodies in the human serum used to prepare

the monocyte culture media for both conditions (DJ, personal communication). These antibodies could opsonise yeast cells, making it easier for the monocytes to uptake opsonised yeast cells through complement or Fc receptors. GM-CSF enhances the BTK-calcineurin-CARD9 antifungal mechanism(s) and boosts phagocytosis through FcγR [116]. The opsonisation of organisms with antibodies significantly increases phagocytic cell clearance [308]. In Chapter 3, we investigated the protein profile of M-CSF and GM-CSF-treated monocytes by proteomics. Data from uninfected GM-CSF-treated monocytes revealed similar expression levels of some of the FcR family compared to M-CSF-treated monocytes (Table 7).

Table 4.1. FcRs that expressed on monocytes treated with M-CSF and GM-CSF. Data represent the mean ± SD from two or three independent replicates for each condition, calculated separately for M-CSF and GM-CSF groups.

Gene	M-CSF monocytes Mean	SD	GM-CSF monocytes Mean	SD
FCRL6	136.37	85.24	93.49	4.71
FCGR2A	182.66	46.12	202.8	38.62
FCGR1A	38.34	7.27	41.46	10.93
FCGR3A	180.12	128.77	139.96	114.26
FCAR	166.78	129.71	145.22	109.88

As *C. albicans* is recognised by a variety of PRRs, including opsonic pathways like complement and immunoglobulin Fc receptors (CRs, FcRs), to initiate immunological responses such as phagocytosis and cytokine secretion [309]. Similarities in FcRs levels suggest the rationale behind the unaffected phagocytosis observed in monocytes treated with GM-CSF. As seen in Wich et al, who investigated the protective function of human serum, i.e. anti-*Candida albicans* antibodies and their ability to neutralise fungus. They found that human anti-*Candida albicans* antibodies improve the ability of monocyte-like cells (THP-1) to recognise the fungus, promoting phagocytosis and prevent *C. albicans* adherence causing subsequent tissue damage [200]. Additionally, they studied the support of antibodies in host defence, even in the absence of neutrophils or macrophages, by assisting in the prevention of fungal adhesion and invasion [200]. However, when monocyte-derived macrophages were treated with GM-CSF and infected with opsonised *C. albicans*, their phagocytic capacity was higher than that observed with other cytokine treatments, such as TNF-α, IL-1β, and IL-6. Additionally, it was noted that, in combination with

fluconazole, the killing mechanism was further enhanced at 48 h of incubation [287].

MR expression is reduced after phagocytosis

Following infection, MR expression was strikingly reduced in GM-CSF–treated monocytes, as determined by flow cytometry and confirmed by ImageStreamX. We initially considered this MR downregulation to be an anticipatory strategy by *C. albicans* to evade immune recognition, for example, by reducing MR-mediated uptake [310]. However, cytokine secretion demonstrates an effective immune response against *C. albicans* by monocytes. Therefore, this suggests that the interaction with *C. albicans* may have triggered mechanisms that reduce MR expression or lead to MR shedding from GM-CSF monocytes, which could reflect a cellular response to infection. sMR production increased through non-opsonic recognition of fungal components such as zymosan and fixed *C. albicans*, and *A. fumigatus*. The shedding process was linked to β-glucan recognition on fungal cell walls. It required Dectin-1 expression, Syk- and PI3K-dependent signalling, and metalloproteinase activity such as ADAM-10 and ADAM-17 [311]. Our proteomics data revealed a significant upregulation of the metalloprotease ADAM-10.

This could partly explain the loss of surface MR on monocytes after infection. In our lab, we have shown that culture supernatants contain soluble MR (sCD206), and in this study, exposure to live *C. albicans*, with or without serum, further increased sCD206 release by monocytes. This effect was most evident in GM-CSF–treated monocyte cultures, which already expressed higher baseline levels of CD206. Chapter 5 provides further analysis of MR (CD206), including its expression profile and modulation under experimental settings used in this study.

GM-CSF effect on cytokine secretion from monocytes.

C. albicans activates the immune system, resulting in many enhanced functions for the recognition and pathogen clearance, one of which is cytokine secretion [312]. Netea M et al, demonstrated that recognition of different elements of *C. albicans* cell wall like mannosylated residues will trigger proinflammatory cytokines secretion like TNF-α and IL-6 through MR and TLR4. Mutant lacking mannosyl residues significantly reduced the secretion of those cytokines,

indicating that these signals are crucial for an effective immune response [282]. GM-CSF-treated monocytes increased the secretion of proinflammatory cytokines like TNF-α, IL-1β [128], and IL-6, most likely to promote cellular responses against infection [313]. The strong IL-1β secretion in our system is consistent with inflammasome formation under the assay conditions because *C. albicans*, especially its hyphae, triggers the NLRP3 inflammasome to induce caspase-1–dependent maturation and release of IL-1β. This conclusion aligns with previous studies showing that pharmacologic or genetic impairment of NLRP3/ASC signalling significantly reduces the induction of IL-1β by *C. albicans* [166, 169].

CCL-22, also known as macrophage-derived chemokine (MDC), is well established as a marker of M2-like macrophage activation [314]. M2 secrets immunomodulatory cytokines like IL-10 and TGF-β, and chemokines like CCL-17 and CC-22, which contribute to the Th2 and Treg cells recruitment [315]. Our data from CCL-22 secretion showed a considerable production by GM-CSF-treated monocytes, particularly in response to infection, although it could also be detected in the absence of infection. CCL-22 is produced constitutively under homeostatic conditions [316]. This indicates an immunomodulatory effect of GM-CSF, Piseddu et al found that isolated DCs need T cell assistance in order to secrete CCL-22. Only when DCs and T cells or their supernatants were cocultured *in vitro* did CCL-22 secretion occur. Additionally, T cell-derived GM-CSF was the primary inducer of DC-derived CCL-22 production [300]. On the other hand, several CCL-22-inducing mechanisms have already been identified in inflammatory immune responses in particular during *C. albicans* infection. IL-4 and IL-13 can increase the production of CCL-22 in macrophages and DCs, which are essential for antigen presentation [317].

Additionally, we investigated the production of vascular endothelial growth factor (VEGF). VEGF-A promotes endothelial cell migration, proliferation, and lumen development by attaching to its receptors, VEGFR-1 and VEGFR-2, which aid in the production of new blood vessels. This process is essential for tissue healing, regeneration, and embryonic development [318]. Various studies have proposed that GM-CSF enhances wound healing. However, GM-CSF monocytes did not exhibit any detectable level of secretion of VEGF, whereas its release was detected in M-CSF-treated monocytes.

The chemokine CCL17 is classified as an M2 cytokine since it was first linked to the preferential attraction of Th2 cells; however, it can also draw

effector/memory Th1 lymphocytes and Tregs [319]. Additionally, Achuthan A et al demonstrated that GM-CSF-treated human monocytes and murine macrophages produced a substantial level of CCL-17, which makes GM-CSF considered a proinflammatory cytokine [320]. The synthesis of CCL17 in response to GM-CSF required the activation of Jumonji Domain–Containing Protein 3 (JMJD3) and Interferon Regulatory Factor 4 (IRF4). Mechanistically, GM-CSF increased JMJD3 demethylase activity, which in turn increased IRF4 expression [320, 321]. These reports are relatively aligned with our data; however, only two out of six donors tested showed an increased CCL-17 level in both infected and uninfected circumstances, with larger levels seen in infected monocytes.

Chemokines are divided into four categories based on variations in the common cysteine motif near the N-terminus: the CCL, CXCL, XCL, and CX3CL families. Tumour cells, leukocytes, fibroblasts, endothelial cells, and epithelial cells all release the tiny proteins in this family. These chemokines are increasingly being discovered to have a significant impact on the development and spread of neoplasms, including ovarian cancer, hepatocellular carcinoma (HCC), kidney renal clear cell carcinoma, breast cancer, and others. In the future, they may be used as therapeutic targets for various illnesses. Similar to this, the CXCL family has a complex role in the development of inflammatory reactions, which supports the treatment of conditions linked to inflammation, including arthritis, chronic obstructive pulmonary disease (COPD), and even certain autoimmune diseases [322]. CXCL-9 or CXCL-10 and CCL-5 are chemokines that play an essential role in attracting immune cells to the site of inflammation, and they are also involved in the chemotactic signals and the activation of M1-like macrophages [323]. During *C. albicans* infection, these chemokines are upregulated to coordinate antifungal immunity by attracting such effector cells to the infection site [324]. Impaired CCL5/CCR5 signalling is linked to decreased immune cell influx and increased susceptibility to *C. albicans* [325]. Finally, no measurable secretion of CXCL-10 or CXCL-9 and CCL-5 (three replicates each) was detected under any experimental conditions. This suggests that these chemokines were either not induced or were present at levels below the assay's detection threshold.

Cellular heterogeneity among and within cultures.

In multiple assays, donor heterogeneity was observed in the GM-CSF response. The secretion of TNF-α and CCL-22, two cytokines produced from both infected and non-infected monocytes, showed no consistent correlation between the two conditions within the same individuals. Furthermore, TNF-α and CCL-22 levels secreted by non-infected GM-CSF monocytes did not show any correlation, indicating that donors with high TNF-α secretion did not necessarily exhibit high CCL-22 secretion. Variability in GM-CSF signalling was discussed in previous studies. For example, a study by Bryson BD*. et al*. showed heterogeneous GM-CSF signalling within macrophage cultures is associated with *Mycobacterium tuberculosis* control in macrophages. They investigate how variability in GM-CSF signalling among macrophages from the same donor influences their ability to control infection. The researchers found that macrophages with active GM-CSF signalling were more effective at restricting *Mycobacterium tuberculosis* growth, while those with diminished signalling were more permissive to bacterial proliferation [326].

4. Future refinements of the infection assay.

Given its established function in boosting antifungal immunity, it would be beneficial to include IL-17A in future infection assays to simulate Th17-driven immune responses [327]. It has been demonstrated that IL-23 induces the production of IL-17A by Th17 cells [328]. Even though fungus-specific Th17 cells are found in peripheral blood in practically all healthy patients [329], it has been proposed that the importance of fungi in causing immunopathology is vastly underestimated, most likely as a result of a lack of suitable diagnostic tools. More than *S. aureus*, *C. albicans* is a potent human fungal pathogen that induces Th17 responses, which is a robust defence against *C. albicans*-induced mucosal damage [330].

On the other hand, human research has demonstrated that, when re-stimulated with *C. albicans, A. fumigatus*-specific T cells can adopt a Th17 phenotype. When Th17 cells invade the lungs, patients with underlying lung conditions are more likely to become colonised by *A. fumigatus* and experience more severe pulmonary disease, suggesting that this subset may have an immunopathological function. These findings suggest that Th17 responses may lead to detrimental cross-reactive immunity against *A. fumigatus*, despite being protective at mucosal sites against *C. albicans*. Furthermore, elevated intestinal

colonisation by *C. albicans*, frequently after the use of antibiotics, has been connected to inflammatory effects at distant locations like the lungs, highlighting the significance of microbiota in immune regulation [330]. To better understand the balance between innate and humoral contributions to antifungal immunity, future assays should be performed both in the presence and absence of antibodies, a hypothesis we are currently testing in the lab. Additionally, incorporate IL-17A to model Th17 conditions more accurately. Neutrophils should be included to reflect their crucial role in fungal clearance, as Th17-produced cytokines, primarily IL-17A, induce IL17R+ cells to secrete chemokines, interleukins, and other inflammatory mediators that help attract neutrophils to the site of inflammation [330].

In conclusion, this chapter demonstrates that our experimental setting for studying *C. albicans* infection of monocytes provides a reliable model. We used various readouts to ensure its reliability and effectiveness, and the results of the experiments supported our original hypothesis, GM-CSF drives changes in monocytes during *C. albicans* infection that could be linked to protection (reduced hypha length) while promoting a over inflammatory response (CCL22 secretion). These findings inform of the suitability of GM-CSF as a therapeutic agent against fungi.

Chapter 5

Mannose Receptor Inhibition as a Strategy to Modulate Monocyte Immune Function During Fungal Infection

5.1. Introduction

Previous chapters focused on the effect of GM-CSF on human monocytes and identified multiple phenotypic changes such as increasing expression of key receptors, promoting motility, and modulating immune responses against *C. albicans*. We extended our investigation to explore how Sulfated Glycopolymers (sGP) specific to the CR domain of MR (CD206) influence monocyte responses to *C. albicans* infection. We decided to focus on CD206 because of its known ability to bind *C. albicans*, its upregulation by GM-CSF and the reduction of surface CD206 after *C. albicans* uptake. These glycopolymers have been shown to inhibit MR function *in vitro* and *in vivo* [331].

Glycopolymers are synthetic polymers containing carbohydrates that mimic natural glycans and affect biological processes [332]. They are obtained from sugar-based monomers that have a ring-shaped sugar structure; therefore, they can imitate the structure of biological materials [333]. Consequently, glycopolymers with cyclic sugar structures have been extensively investigated for their roles in lectin recognition and other functions such as bacterial adhesion, drug delivery and bioimaging [334]. The desire to study glycopolymers effect in modern medicine increased due to the high avidity between multimeric glycans and cellular lectins that is crucial during immune responses and immunotherapy [335]. Many immune cell surface lectins can recognise multivalent carbohydrate ligands, which can either activate the immune system or cause down-regulation, including suppression and resistance against infectious stimuli. As multivalent carbohydrate ligands, glycopolymers can contribute to the modulation of the immune system [336].

Targeting MR has shown remarkable effectiveness in immune therapy, improving treatment specificity and efficacy while reducing side effects by accurately delivering drugs, vaccines, and imaging agents to macrophages and dendritic cells [93]. MR is a PRR capable of directly binding to glycans present in the cell wall of *C. albicans* [337]. The MR is essential for clearing pathogenic species and potentially harmful glycans. It shares structural similarities with other type I transmembrane receptors such as endo180 and DEC205. MR (CD206) efficiently removes molecules bearing glycans with terminal mannose residues from the circulation. This mannose-specific binding activity is mediated by the CTLD1-8 domains and facilitates internalisation and subsequent

lysosomal degradation. CD206 interacts with a wide range of mannose-containing proteins including lysosomal enzymes and tissue plasminogen activator [338]. The CR domain of CD206 binds to carbohydrates terminated in SO_4-3-Gal. Mastrotto et al. evaluated how the interaction of glycopolymers with the MR (CD206) are impacted by sulfation (Figure 5.2). Synthetic compounds called sGP are made to mimic the naturally occurring sulfated sugars that attach to CD206's cysteine-rich (CR) domain. Even while each individual interaction is somewhat weak, they retain CD206 quite firmly overall because they exhibit several sulfate–galactose groups along a single polymer chain. By creating these stable complexes, sGP prevent CD206 from interacting with its typical ligands and from recycling back to the cell surface, which stops its endocytic function and permits the selective modulation of CD206 activity and, consequently, certain immunological responses [331].

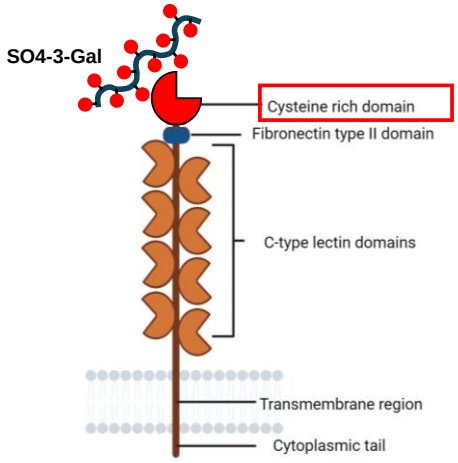

Figure 5.2. MR structure. Glycopolymers with SO4-3-Gal (s) effectively bind to CD206 through its Cystine-rich domain. Created using PowerPoint.

After synthesising glycopolymers with Sulfated galactose (SO_4-3-Gal) side chains, researchers found that these glycopolymers attach to the CR domain of CD206 [97]. They showed that the ability of multivalent glycopolymers to modulate MR depends on their structural and chemical properties, including the type and number of carbohydrate units and the size of the polymer chain. They also revealed that new details about how sugars interact with MR (CD206) and how the receptor is trafficked inside cells. Notably, the researchers discovered a previously unknown way to inhibit CD206-mediated endocytosis using galactose SO_4-3-Gal-based glycopolymers, with this effect confirmed both *in vitro* and *in vivo* [331]. Internalised MR forms persistent intracellular complexes

with these glycopolymers that trap MR inside the cell. This binding effectively inhibits the receptor's endocytic activity by preventing it from recycling back to the cell surface (Figure 5.3). This is because binding of the CR domain to SO_4-3-Gal is Ca^{2+}- and pH- independent. The study suggested possible uses for SO_4-3-Gal glycopolymers in immunotherapy [331].

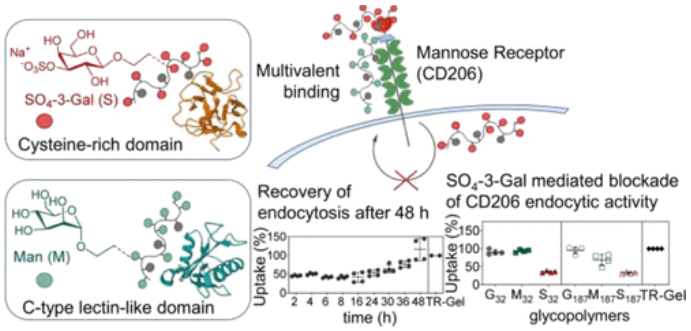

Figure 5.3. SO_4-3-Gal glycopolymers prevent CD206 from returning to the plasma membrane [331].

Taking advantage of these findings, in our lab, we used similar glycopolymers (S100-DP240, kindly provided by Dr. Giuseppe Mantovani, School of Pharmacy, University of Nottingham) to inhibit MR while maintaining the integrity of other pathways. Modulation od MR was analysed alongside CD11b expression, which did not change in sGP-treated monocytes and was used as an internal control. Finally, if MR inhibition alters the immune response, these glycopolymers could represent potential therapeutic agents in inflammatory disorders related to fungal infection.

5.2. Hypothesis

We hypothesise that treating human monocytes with a sulfated glycopolymer will inhibit the surface expression of CD206 and potentially regulate their responses to *C. albicans* infection.

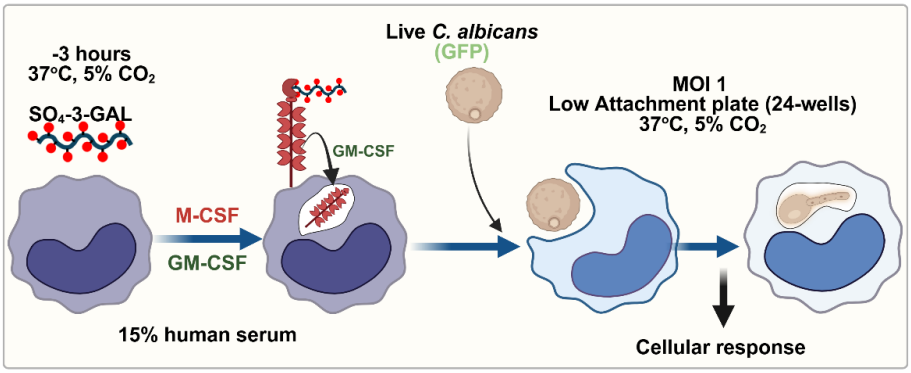

5.3. Specific Objective

To address this hypothesis, purified monocytes were treated with 10 ng/mL of M-CSF or GM-CSF and incubated for approximately 40-44 hours; 2 hours before harvesting, monocytes were treated with sGP, which was subsequently removed through washing. Treated and untreated cells were infected with *C. albicans* at 37°C, 5% CO_2 as before. Cultures were assayed for:

- Changes in surface expression of MR and CD11b in uninfected cultures.
- *C. albicans* phagocytosis
- Cytokine production.

5.4. Results

5.4.1. Evaluating the effect of sGP on MR surface expression in GM-CSF monocytes.

Firstly, we assessed the effect of sGP on its ability to reduce MR surface expression. In the first experiment we determined the optimal dose and timing for use in subsequent experiments. Accordingly, as a preliminary exploratory experiment, only GM-CSF-treated monocytes were used to because of their higher MR expression.

Isolated monocytes were cultured for roughly 44–48 hours at 37°C with 5% CO_2 in the presence of 10 ng/mL GM-CSF. The cells were cultured in two separate plates. At 16 hours before harvesting cells, monocytes in one of the plates were treated with sGP at a concentration of 80 μM or 160 μM. Then, 2 hours before harvesting the cells, the second plate was treated with sGP at the same concentrations (Chapter 2, 2.1.1. Treatment of monocytes with Sulfated Glycopolymers). After total 44 hours of monocyte culture, cells were harvested, the sGP washed off, and cells were adjusted to a concentration of 10^7 cells/mL and prepared for flow cytometry and labelled for CD11b (negative control) and MR.

Figure 5.4. a, demonstrates CD11b expression after 16-h and 2-h of incubation with either 80 μM or 160 μM sGP. Then, CD11b in the unstained gate shows the MFI of zero as the population is yet unlabelled (Figure 5.4. a. 1). After 16 hours of incubation with sGP, the MFI for untreated and treated with 80 μM and 160 μM sGP was 20,245, 17,647 and 17,424, respectively (Figure 5.4. a. 2). Then, at 2 h incubation, untreated monocytes have an CD11b MFI of 19,191. For 80 μM and 160 μM concentrations MFIs were 20,000 for both concentrations (Figure 5.4. a. 3). Hence, we concluded that CD11b expression hadn't been affected by sGP treatment at 80 μM and 160 μM concentrations for 2 h or 16 h of incubation.

Conversely, for MR, while sGP untreated GM-CSF monocytes exhibit an MFI of 126,704, treatment with the sGP reduces MR expression by over 50%. Specifically, MFIs of approximately 41,000 and 43,000 were observed at concentrations of 80 μM and 160 μM, respectively (Figure 5.4. b. 2). The reduction is almost the same at 16 hours of incubation compared to the untreated monocytes (Figure 5.4. b. 3).

Therefore, in the following assays, we treated cells with sGP at a concentration of 80 µM for 2 hours at 37°C with 5% CO_2.

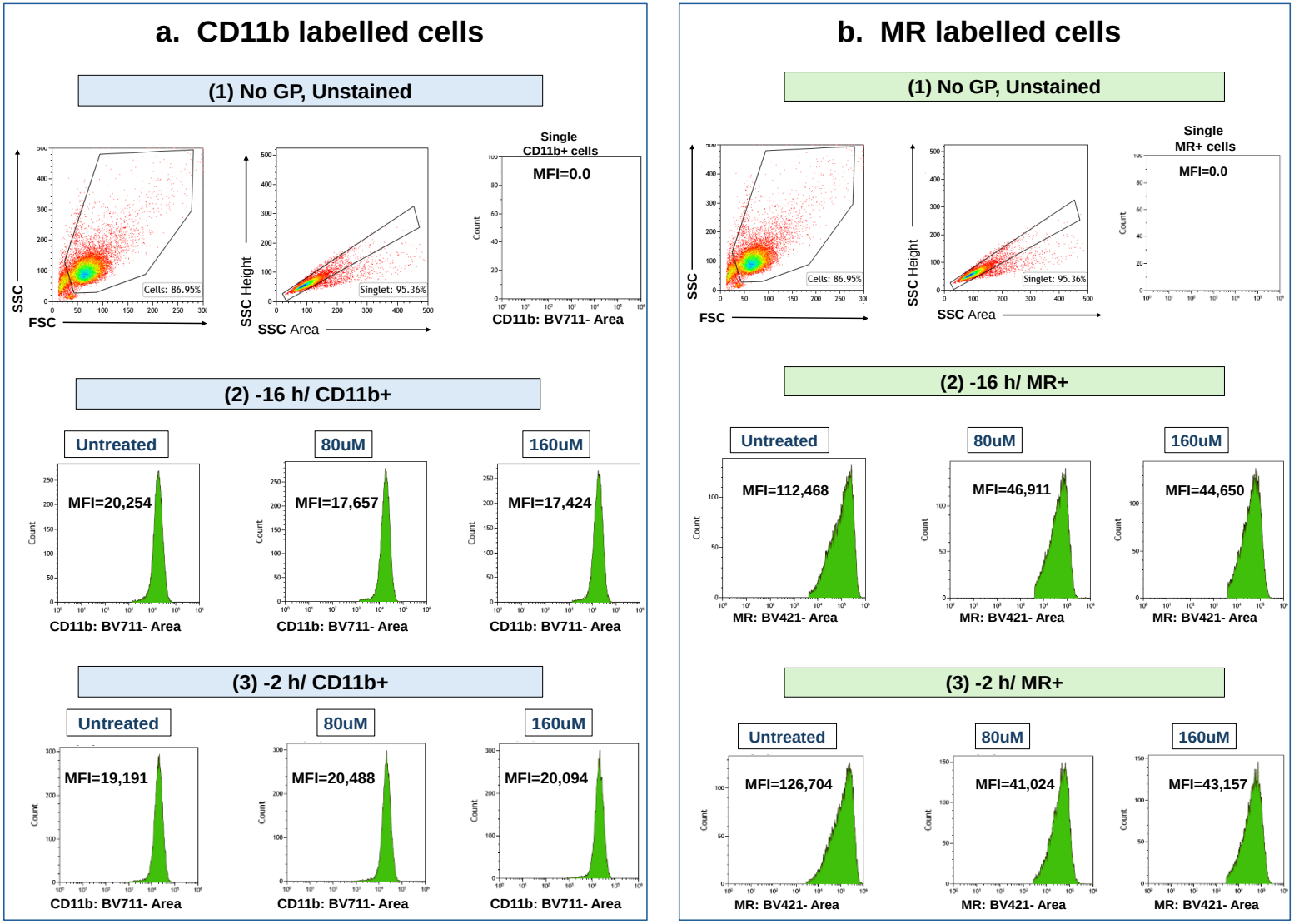
a. CD11b labelled cells
(1) No GP, Unstained
SSC
FSC
Cells: 86.95%
SSC Height
SSC Area
Singlet: 95.36%
Single CD11b+ cells
MFI=0.0
Count
CD11b: BV711- Area
(2) -16 h/ CD11b+
Untreated
80uM
160uM
MFI=20,254
MFI=17,657
MFI=17,424
(3) -2 h/ CD11b+
MFI=19,191
MFI=20,488
MFI=20,094
b. MR labelled cells
(1) No GP, Unstained
Single MR+ cells
(2) -16 h/ MR+
MFI=112,468
MFI=46,911
MFI=44,650
MR: BV421- Area
(3) -2 h/ MR+
MFI=126,704
MFI=41,024
MFI=43,157

Figure 5.4. Testing the effect of sGP on CD11b and MR expression in human monocytes. Monocytes were isolated and cultured with 10 ng/mL GM-CSF for 40-44 hours in the presence or absence of sGP for either 16 h or 2 h and stained for CD11b and MR for flow cytometry analysis. **a.** CD11b. **1.** The gating strategy of the unstained population is based on FSC and SSC, and the singlet gate from the original population is based on the SSC area and height followed by the histogram. **2.** CD11b histograms after 16 hours incubation of monocytes with sGP, Untreated, 80 µM and 160 µM. **3.** CD11b histograms after 2 hours incubation of monocytes with sGP, Untreated, 80 µM and 160 µM. **b.** MR **(N=1)**. Samples read by ID7000 and analysed using Kaluza.

5.4.2. sGP is more efficient at reducing MR expression in GM-CSF-treated monocytes compared to M-CSF-treated monocytes.

After confirming that sGP downregulated the expression of MR on GM-CSF monocytes, we tested if a similar effect could be seen in M-CSF monocytes and if the reduction in MR expression was maintained after incubation without sGP for 3h, the duration of the *C. albicans* infection assay. Using GM-CSF and M-CSF monocytes, we incubated the cells for 2 hours with 80 μM sGP as above before we harvested them. After incubation and washing the monocytes were plated at 10^6 cells/well in a 24-well Ultra-Low attachment plate, and incubated at 37°C, 5% CO_2 for 3 h. Cells were harvested, labelled for CD11b and MR, and prepared for flow cytometry.

Density plots illustrate cell populations for M-CSF monocytes (~87% within the singlet gate) (Figure 5.5. a.1) and a larger population of GM-CSF monocytes (~96% within the singlet gate) (Figure 5.5. b.1). From these singlet gates, histograms representing antibody labelling were generated and compared against their respective isotype controls and unstained population of monocytes untreated and treated with sGP (Figure 5.5. a.2 and 3) and (Figure 5.5. b.2 and 3).

From data, CD11b expression remained unchanged by the treatment with sGP in M-CSF- and GM-CSF-treated monocytes (Figure 5.5. a.2 and b.2). In contrast, the MR expression shifts to the left in both M-CSF and GM-CSF monocytes (Figure 5.5. a.3 and b.3).

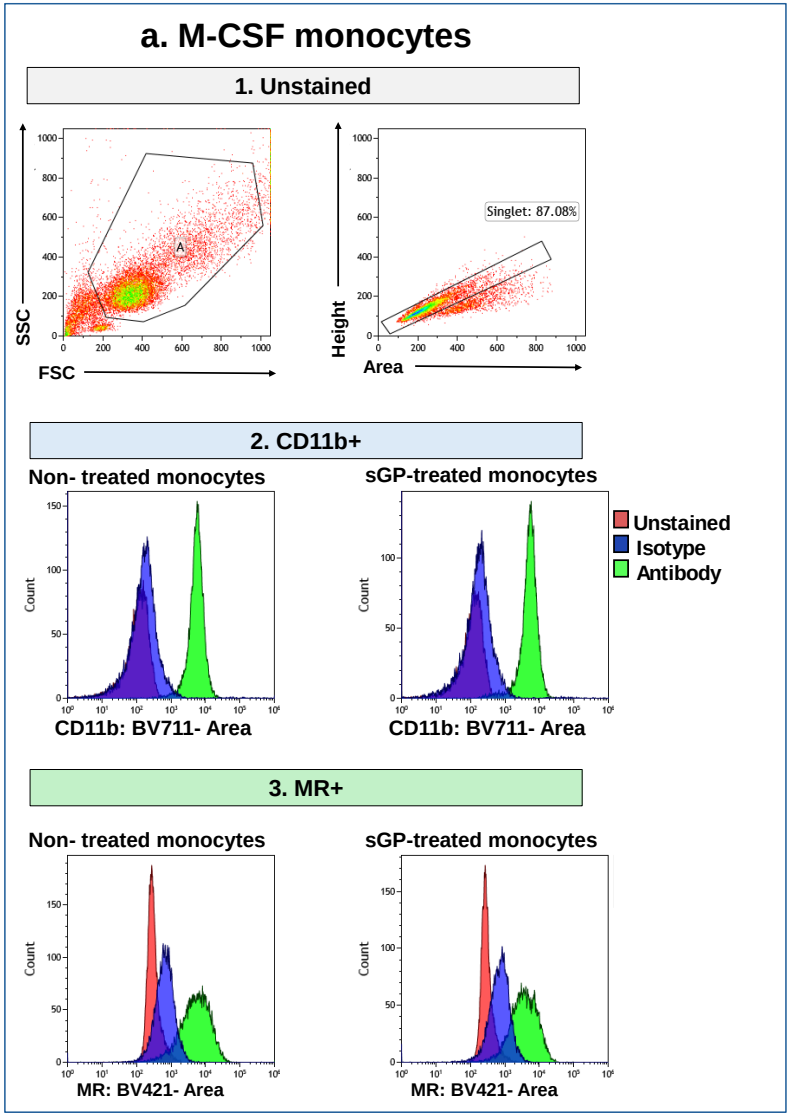
a. M-CSF monocytes
1. Unstained
SSC
FSC
A
Height
Area
Singlet: 87.08%
2. CD11b+
Non- treated monocytes
sGP-treated monocytes
Unstained
Isotype
Antibody
Count
CD11b: BV711- Area
3. MR+
MR: BV421- Area

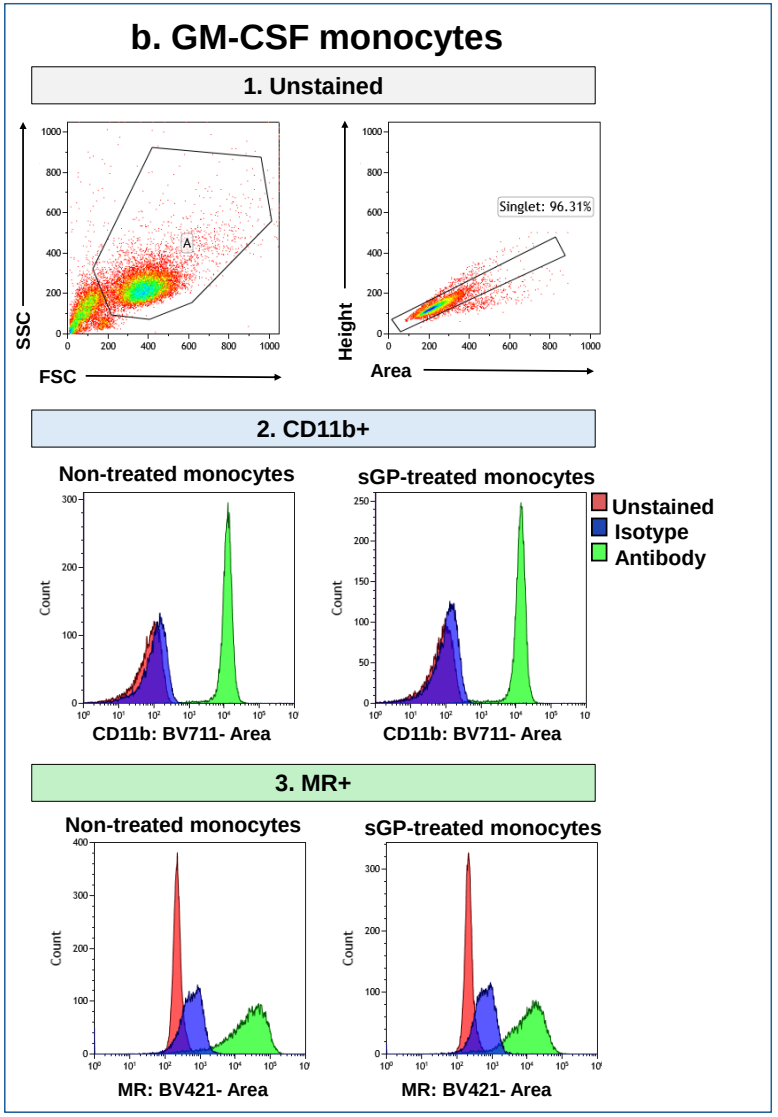
b. GM-CSF monocytes
1. Unstained
SSC
FSC
A
Height
Area
Singlet: 96.31%
2. CD11b+
Non-treated monocytes
sGP-treated monocytes
Unstained
Isotype
Antibody
Count
CD11b: BV711- Area
3. MR+
MR: BV421- Area

Figure 5.5. Effect of sGP on surface receptors expression in human monocytes. Monocytes are isolated and cultured with M-CSF or GM-CSF (both 10 ng/mL) for 40-44 hours absence of treated with 80μM then sGP is removed and cells are stained with CD11b and MR. **a. M-CSF monocytes. a.1.** Gating strategy based on the FSC and SSC axis followed by Singlet gate from original population based on SSC Area and Hight. **a.2. CD11b**, histograms of untreated monocytes followed by sGP treated of CD11b (green population) vs. unstained (red population) and isotype control (blue population**). a.3. MR,** histograms of untreated monocytes followed by sGP treated of CD11b (green population) vs. unstained (red population) and isotype control (blue population**)**. **b. GM-CSF monocytes. (Note: The same organisation is followed for the remaining conditions)**, **(N=7)**. Samples read by ID7000 and analysed using KALUSA.

Finally, MFI was calculated out of 7 biological replicates to compare and conduct statistical analysis. As shown before, CD11b expression was upregulated by GM-CSF. The sGP did not affect the expression of CD11b when comparing monocytes without and with treatment in both M-CSF and GM-CSF monocytes (Figure 5.6. a). MR was upregulated by GM-CSF, and after adding sGP, there is a significant downregulation in the MR expression only in GM-CSF-monocytes. Therefore, data analysis from multiple repeats reveals that sGP only affected the expression of MR in GM-CSF monocytes (Figure 5.6. b).

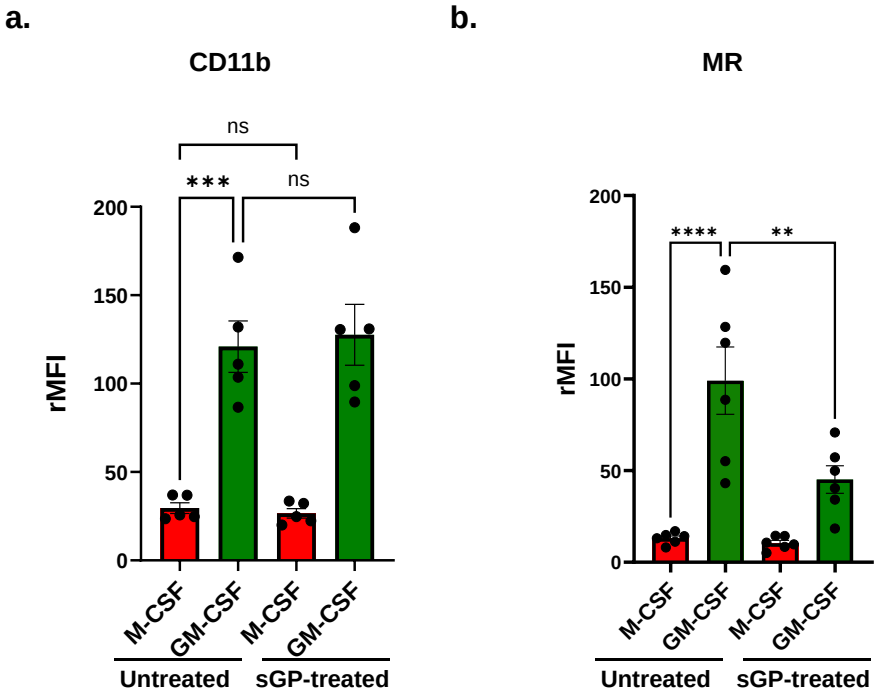

Figure 5.6. sGP inhibits MR surface expression in GM-CSF monocytes. Graphs show MFI values for CD11b and MR in M-CSF and GM-CSF monocytes, untreated and treated with sGP. **a.** CD11b, Data were analysed using One-Way ANOVA **(N=5)**. **b.** MR, Data were analysed using One-Way ANOVA (**N=6).** Graphs show mean +/- SEM and individual values. Data were analysed by GraphPad Prism, ns: not significant, (*) $p<0.05$, (***) $p<0.0001$.

5.4.3. sGP treatment does not affect the binding activity of monocytes against *C. albicans*

To investigate if the phagocytosis of *C. albicans* by monocytes is altered in response to sGP treatment, isolated monocytes were treated with 10 ng/mL M-CSF or GM-CSF and incubated for 40-44 h. At 2 h before cell collection, cells were treated with 80 μM sGP and incubated at 37°C, 5% CO_2. Afterwards, the monocytes were washed to remove the sGP, infected with *C. albicans* at MOI 1 and incubated at 37°C, 5% CO_2 for 3 h. Cells were harvested, labelled for CD11b, and prepared for flow cytometry. MR modulation was assessed in parallel with CD11b, which remained unchanged in sGP-treated monocytes and was used both as an internal control and as a marker in the phagocytosis assays as this receptor was used in previous chapter for phagocytosis assay.

Figure 5.7 shows that the addition of the sGP did not affect the association of GFP-expressing *C. albicans* at this time point, indicating that binding was not affected by the downregulation of MR using the glycopolymers.

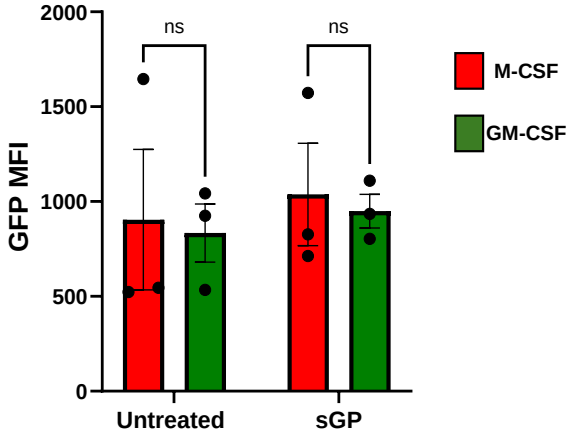

Figure 5.7. Effect of sGP on *C. albicans* association with human monocytes. Monocytes were isolated and cultured with M-CSF or GM-CSF (both 10 ng/mL) for 40-44 hours in the absence or presence of 80μM then sGP for the last 2 h. Monocytes were washed, plated and infected at MOI=1 and stained with CD11b. After plotting data from flow cytometry, MFI is collected from GFP gate, and significance calculated **(N=3).** Graphs show mean +/- SEM and individual values. Data were analysed using Two-Way ANOVA by GraphPad Prism, ns: not significant.

.

5.4.4. Treatment with sGP alters cytokine secretion by GM-CSF monocytes in response to *C. albicans*.

To assess whether MR inhibition using the sGP modulates the response of monocytes to *C. albicans* infection, we quantified cytokine secretion in infected and non-infected monocytes, with and without sGP treatment, under M-CSF and GM-CSF conditions. Isolated monocytes were treated with 10 ng/mL M-CSF or GM-CSF and incubated for 40–44 h at 37°C, 5% CO_2. Two hours before harvesting, they were treated with 80 µM sGP. After removing the sGP, monocytes were infected with *C. albicans* MOI1 for 3 h. After incubation, supernatants were collected and tested for the selected cytokines using capture ELISA.

We found that sGP had a selective effect on cytokine production in infected GM-CSF–treated monocytes. As revealed in the previous chapter, GM-CSF enhanced TNF-α, IL-1β, IL-6 and CCL22 secretion in response to *C. albicans* compared with M-CSF–treated cells; however, pre-treatment with sGP consistently reduced TNF-α production only in infected GM-CSF monocytes (Figure 5.8a).

IL-1β and IL-6 secretion were not significantly affected by sGP treatment in GM-CSF–treated monocytes (Figure 5.8. b and c).

CCL22 showed only a tendency towards reduced levels in sGP-treated infected GM-CSF monocytes (Figure 5.8d), suggesting that sGP imposes a consistent but partial dampening of specific GM-CSF–driven inflammatory outputs rather than broadly suppressing cytokine secretion.

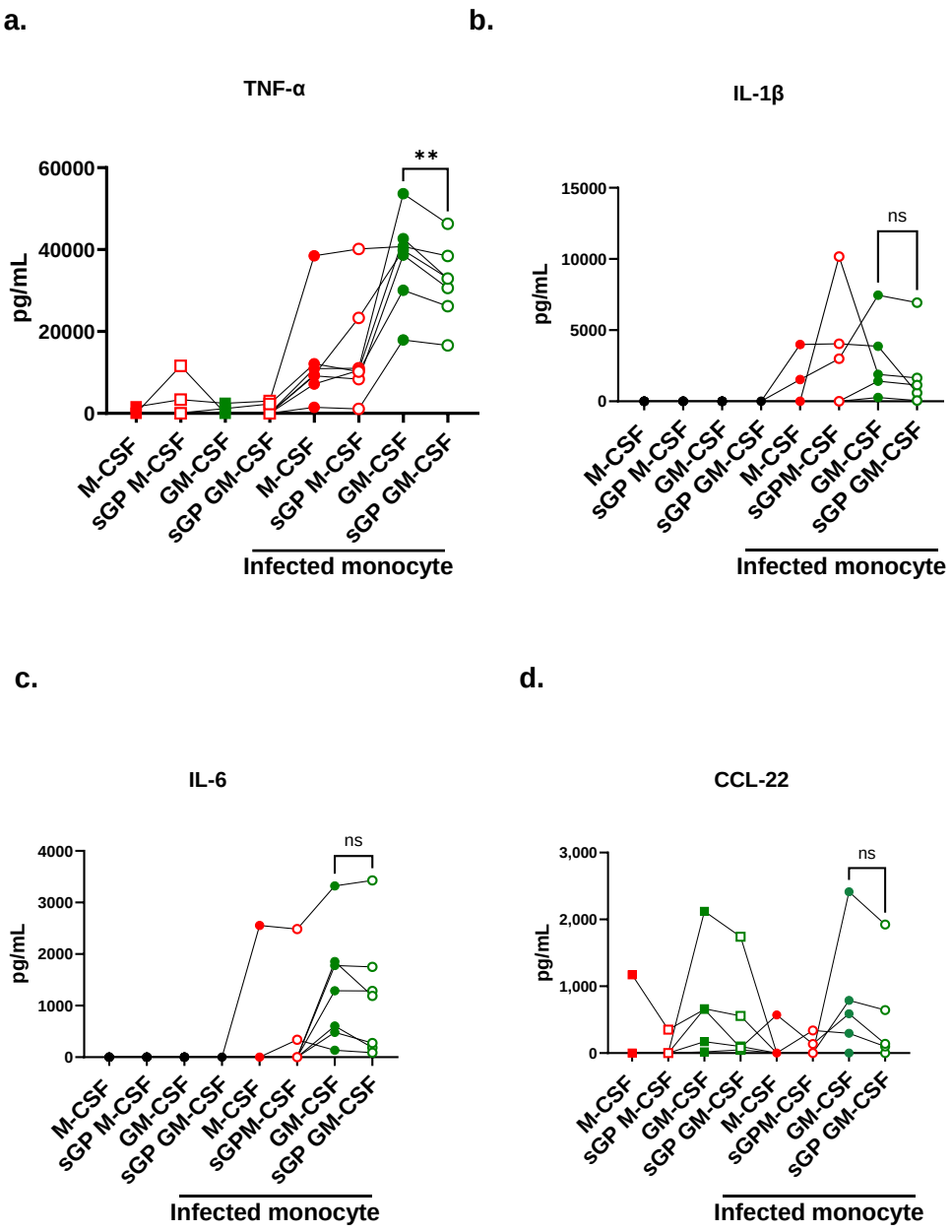

Figure 5.8. Effect of sGP on cytokine secretion by monocytes in response to *C. albicans*. Purified monocytes treated with 10ng/mL M-CSF or GM-CSF were either pretreated with sGP (80 µM) or left untreated and incubated with *C. albicans* for 3 h at 37°C, 5% CO_2. Supernatants were collected, and cytokines quantified using capture ELISA. **a.** TNF-α (N=7), **b.** IL-1β (N=5), **c.** IL-6 (N=7) and d. CCL-22 (N=7). Graphs show mean +/- SEM and individual values. Data were analysed using paired t-test by GraphPad Prism, ns: not significant, (**) p<0.003.

5.5. Summary

- sGP affects the expression of surface MR on GM-CSF-treated monocytes.
- sGP did not change the phagocytic activity in monocytes against *C. albicans*.
- sGP altered cytokine production by monocytes in response to *C. albicans*.

5.6. Discussion

Synthetic glycopolymers have been used extensively in modern medicine for different applications such as drug delivery and vaccine development [339]. In general, they consist of carbohydrate units attached to the side groups of a larger molecular structure, such as proteins or lipids [9], which makes them suitable for targeting immune cells**.** They could selectively deliver therapeutic agents to disease-associated immune cells by distinguishing them from other cell types through their ability to bind selected carbohydrates, enhancing treatment efficacy and minimising systemic side effects [10]. For example, galectin-3 binds to T cells, playing a key role in immune regulation. T cells are essential for maintaining a controlled and consistent immune environment, but galectin-3's inhibitory effect can lead to immunosuppression [10]. Filippova and Bojarova synthesised galectin-3-inhibiting glycopolymers, which proved remarkably effective; they inhibited T-cell apoptosis and suppressed tumour cell migration and proliferation [340]. Another example is the targeting of Siglecs, which offers a strategy to regulate immune responses. Cancer cells frequently display elevated sialylation, suppressing natural killer cell activation by engaging Siglec-7. Studies have shown that targeting Siglec-7 using a high-affinity ligand promotes rapid Siglec-7 endocytosis and potent T cell responses, highlighting the potential of Siglec targeting for precise antigen delivery to specific cells [341, 342].

The CRDs of MR demonstrate a strong binding affinity for both branched and linear oligosaccharides containing terminal mannose, fucose or N-acetyl-glucosamine. Moreover, the multivalent presentation of mannose on diverse platforms, including peptides, proteins, polymers, micelles, and dendrimers, has proven to be an effective strategy for targeting and efficiently delivering therapeutically active agents to MR [343]. Park et al. explore the specific interaction between mannosylated glycopolymers and macrophages, focusing on the MR (CD206) role in eliminating foreign pathogens. They used a glycopolymer PV-MAN, a polystyrene derivative that interacts with the macrophage cell line, which carries mannose receptors and includes mannose moieties. They found that PV-MAN specifically interacted with macrophages through MR, with binding intensity increasing with higher polymer concentration and longer incubation times. Findings suggest that MR-mediated interactions can be leveraged for therapeutic applications, particularly in immunomodulation

and macrophage-targeted treatments [344]. MR undergoes essential pH-dependent changes for efficient ligand dissociation and receptor recycling. When MR binds a mannosylated ligand, it internalises it through endocytosis into acidic endosomal compartments. They lower pH causes structural changes in the receptor, mostly in CTLDs. This shift would reduce the affinity of MR for mannose-containing glycans. Therefore, the ligand dissociates from the receptor in the endosome, allowing the empty receptor to be recycled back to the membrane [96]. Therefore, the sGP in our model, which targets the CR domain of MR and inhibits MR surface expression likely does so because binding to MR by these compounds is pH-independent, resulting in the intracellular trapping of MR. Noted that this study has not tested pH measurement by Mastrotto and colleagues demonstrated sGP binding to MR was not affect by lower pH [331].

In our experimental design, the aim was to add sGP to GM-CSF and M-CSF-treated monocytes, which would lead to reduced surface MR expression, and test how this treatment affects monocyte responses to *C. albicans*. We observed a consistent reduction in surface MR, mostly in GM-CSF monocytes, which correlated with modest changes in cytokine secretion after *C. albicans* infection only in GM-CSF-treated monocytes. Lower TNF-α secretion upon treatment aligns with *in vitro* studies, where targeting MR in M2 macrophages has been shown to reduce TNF-α secretion using a novel peptide. In their study, Gebremedhin et al. used mouse bone marrow-derived macrophages and differentiated them into M1 macrophages (treated with M-CSF and IFN-γ) and M2 macrophages (treated with M-CSF and IL-4). They utilised a novel peptide RP-832c (Polypeptide Laboratories, located in San Diego, California, USA) to specifically target MR, which it did not inhibit the general function of MR; rather, it engages explicitly the MR receptor to induce macrophage apoptosis. RP-832c significantly decreased fibrosis in a dose-dependent manner by binding to CRD5 in MR, RP-832c induced apoptosis in M2 macrophages, resulting in a decline in M2 macrophage numbers and the profibrotic cytokines they produce. Researchers observed that RP-832c selectively inhibited M2 macrophages while exerting minimal effects on M1 macrophages. *In vivo*, this treatment reduced $CD206^{+}$ macrophages and lung fibrosis in mice, accompanied by decreased expression of TNF-α, IL-6, IL-10, and IFN-γ in a lung fibrosis model [291]. Cytokines such as IL-6 and IL-1β showed variable and inconsistent yet promising results in our model. However, supernatants were collected at three

hours, which limited the assessment of temporal cytokine dynamics. To improve the assay, future studies should include multiple time points and increase the number of experimental repeats to enhance data reliability and accuracy.

Although MR plays a crucial role in facilitating the phagocytosis of various pathogens, including *Mycobacterium kansasii*, *Mycobacterium tuberculosis*, *Francisella tularensis and C. albicans* [105]. Conversely, monocytes with inhibited MR showed no impact on phagocytosis compared to untreated monocytes in 3 h in our model. Similarly, MR-knockout (MR-KO) mice exhibited no significant differences in the phagocytosis of *C. albicans*, recruitment of inflammatory cells, or humoral response to *C. albicans* antigens compared to wild-type mice. This study was performed by Lee et al., who studied the immune response during *C. albicans* infection in MR-deficient mice [345]. Heinsbroek et al. also studied the effect of MR, Dectin-1, and CR3 on phagocytosis in mice and human monocytes from healthy donors in *C. albicans* infection. In their study, they found that Dectin-1 is the primary non-opsonic receptor for initiating the recognition and uptake of *C. albicans*. Together with CR3, it is recruited to the phagocytic cup to contribute to phagocytosis in the early stages of infection. On the other hand, MR is recruited to phagosomes at later stages for a subsequent response, such as cytokine secretion, without influencing the phagocytosis [107]. Ideally, phagocytosis would be assessed after 1 h incubation at MOI 1. However, since we were already collecting supernatants for cytokines secretion and at the same time looking at the MR expression by flowcytometry. Therefore, we labelled cells with CD11b as an opportunity to examine phagocytosis.

In parallel to assessing MR expression through flow cytometry and collecting supernatants for cytokine quantification, lysates and supernatants were also collected for western blot analysis to quantify the soluble MR (sMR) in infected monocytes (experiments run by Darryl Jackson). Metalloproteases, such as ADAM10, are known to mediate receptor cleavage [277], are significantly overexpressed in GM-CSF-activated monocytes, as determined by proteomics analysis (M-CSF mean± 62.5 and GM-CSF mean± 85.0).

sMR, lacking the C-terminus, is released by all MR-expressing cells studied [10] and is present in both mouse and human serum, as well as in the bronchoalveolar lavage of HIV patients infected with *Pneumocystis carinii* [100, 346]. Although the exact roles of sMR are unknown, the soluble portion of the receptor retains its ability to bind ligands, which suggests that it could act as a

shuttle to deliver circulating antigens to the lymphoid organs [347]. The MR appears to shed constitutively, and some inflammatory mediators cause increased shedding [10]. For example, Sandahl T and their group demonstrated that sMR is significantly elevated in patients with alcoholic liver diseases, particularly in those who suffer from alcoholic hepatitis. sMR is also increased with disease severity and portal hypertension and correlates with increased long-term mortality. Higher sMR levels were associated with high markers of immune activation, like C-reactive protein, and worsened prognosis, highlighting sMR's potential as a biomarker for disease severity [348]. sMR has also been identified as a potential prognostic marker for pulmonary tuberculosis [349]. Additionally, elevated sMR correlated with macrophage activation and serum proinflammatory cytokines secretion in obesity, promoting meta-inflammation and metabolic dysfunction [350].

The mechanism of MR shedding is partly mediated by Dectin-1, which becomes activated upon encountering β-D-glucan located in the fungal cell wall. This mechanism triggers intracellular pathways, dependent on Syk, leading to MR shedding [311]. sMR shedding has been observed *in vitro* in macrophages upon exposure to various fungal pathogens, including *A. fumigatus, P. carinii* and *C. albicans* [346]. sMR shedding was detected in monocytes cultured in the presence of GM-CSF, infected with *C. albicans*. Remarkably, this shedding was diminished upon pre-treatment with the sGP, suggesting that shedding occurs at the plasma membrane.

sGP are attractive as potential therapies because they allow us to gently “tune” the behaviour of $CD206^+$ myeloid cells instead of simply shutting them down. SO_4-3-Gal–based glycopolymers bind with high overall strength to the cysteine-rich domain of CD206 and form stable complexes inside the cell that block receptor recycling and endocytosis, a mechanism that has now been shown both in vitro and in vivo [331]. Since CD206 is highly expressed on tissue macrophages, Kupffer cells and many tumour-associated macrophages, this offers a way to selectively modulate these cells in diseases such as cancer, chronic inflammation and infection without broadly suppressing the immune system. sGP are synthetic, can be chemically fine-tuned and show low toxicity at concentrations where they are functionally active, which makes them appealing both as direct CD206 inhibitors and as scaffolds for delivering drugs or immunomodulators specifically to $CD206^+$ cells [343]. Taken together, current evidence suggests that SO_4-3-Gal glycopolymers could form the basis of future

macrophage-targeted therapies, using precise control of CD206 function to reshape harmful immune responses rather than simply dampening immunity.

To conclude, this study demonstrates that sGP modulates MR-mediated immune responses in human monocytes treated with GM-CSF. Targeting the mannose receptor with the sGP altered cytokine secretion, indicating its potential to regulate inflammatory responses and reduce sMR shedding. By influencing MR-ligand interactions, the sGP may serve as a valuable tool to modulate monocyte activation and the downstream immune response against *C. albicans* in the presence of GM-CSF. These findings highlight the therapeutic potential of synthetic glycopolymers in controlling MR-driven immune functions.

Chapter 6

Macrophages Induced from Stem Cells: Evaluating GM-CSF-Mediated Immune Responses Against *C. albicans* in a tractable *in vitro* model

6.1 Introduction

The advancement of induced pluripotent stem cell (iPSC) technology has revolutionised *in vitro* modelling of human biology and expanded possibilities for cell therapy applications [351]. Due to their ability to differentiate into distinct cell types and to reflect genetic variables associated with illness risk, human iPSCs are increasingly being employed for disease modelling. It is possible to alter human iPSCs genomes to either introduce or fix mutations linked to disease [352]. Abud et al. (2017) developed a method for transforming human iPSCs into cells that resemble microglia (iMGLs). These iMGLs are useful for researching neurodegenerative diseases like Alzheimer's disease (AD) because they share functional traits and gene expression profiles with primary human microglia. These authors found that blocking complement receptor 3 (CR3), via anti-CD11b, in iMGLs reduces phagocytosis of human synaptosomes, and iMGLs secrete a variety of cytokines in response to IFN-γ, IL-1β and LPS stimulation. In AD, dysregulated cytokine release and microglial phagocytic activity can worsen synaptic loss and neurodegeneration. This indicates that altering these pathways might be a useful treatment approach to improve disease prognosis [353].

There has been significant progress and persistent challenges in developing stem cell therapies. In the case of cardiac and cardiovascular diseases, the potential of cardiomyocytes created from pluripotent stem cells for needs to be balanced with the continuous need to maximise cell sources and obtain a deeper understanding of the mechanisms underlying genuine cardiac regeneration [354]. A significant scientific advance was made in 2006 by Takahashi and Yamanaka, who discovered that somatic cells could be converted into pluripotent stem cells. This allowed generating iPSCs from fibroblasts by introducing particular transcription factors. These iPSCs have characteristics similar to embryonic stem cells, including the ability to differentiate into various cell types [355]. Further developments improved the techniques for directing pluripotent stem cells into specialised adult cells. One important usage has been the effective production of cardiomyocytes through the modification of specific signalling pathways, providing a plentiful supply of heart cells for medical purposes [356]. Transplanting these lab-grown cardiomyocytes into damaged hearts has shown promising results in animal

models, helping restore heart muscle, improve cardiac function, and reduce tissue remodelling after injury [357].

In recent years, protocols have been developed for differentiating iPSCs into various immune cell types, including dendritic cells (DCs), natural killer (NK) cells, and macrophages [234]. In addition to reflecting patient-specific genetic backgrounds, iPSC-derived macrophages (iMacs) provide a useful system for studying innate immune systems under controlled conditions [233]. In the innate immune response, macrophages play a crucial role as first-line defences against pathogens like *C. albicans* [189]. iMacs resemble primary human macrophages in morphology, surface marker expression, and functional capabilities, including phagocytosis and cytokine production[358]. They are also useful tools for investigating the basic pathways that control the biology and development of macrophages [359]. In addition to research, iMacs have shown promise for future cell-based treatment approaches for various illnesses [360]. Lyadova *et al*. outlined several protocols for differentiating iPSCs into macrophages, including OP9-dependent methods that involve co-culturing iPSCs with mouse stromal cells. OP9 is a stromal cell line deficient in M-CSF that has been used successfully to induce mouse embryonic stem cell differentiation into myeloid, lymphoid, erythroid, and megakaryocytic lineage cells [361]. However, these approaches are now seldom used due to limitations because of the absence of the M-CSF pathway in OP9 cells and the challenges posed by the use of a xenogeneic cell line in human immune cell generation [362]. On the other hand, Klepikova *et al*. conducted a comparative study of two protocols for differentiating iMacs, using the same iPSC cell line for both methods. While the resulting macrophages showed similar basic features such as morphology, surface markers, and functional activity, their transcriptomic analyses revealed notable differences influenced by the differentiation method. Genes linked to inflammation, lipid metabolism, and antigen presentation differed between the methods, suggesting that the cell line and method selection influence the immunological traits and macrophage formation pathways. These results emphasise the importance of selecting the appropriate differentiation techniques to produce macrophages with the desired characteristics for both research and medical applications [363].

The KOLF2.1J human iPSC line represents a significant advancement in stem cell research, particularly in generating macrophages [234]. Utilising robust methodology, we adopted the KOLF2.1J line for differentiation into

macrophages following the methodology described by Pantazis *et al.* [234]. This process involved the formation of embryoid bodies (EBs), which were directed towards fully functional immune cells, by culturing under specialised conditions in the presence of growth factors such as human M-CSF and IL-3. This adaptation of KOLF2.1J for macrophage generation would contribute towards understanding innate immune responses and developing potential therapeutic interventions during fungal infection by analysing the effect of GM-CSF on iMacs.

This project's use of iPSC-derived macrophages is strategically driven by both pragmatic and scientific factors. Using iPSCs provides a reliable and renewable source of human macrophages, enabling experiments with consistent biological replicates and reduced donor-to-donor variability. Furthermore, iPSC-based differentiation presents a more economical option than sourcing buffy coats, which can be expensive and scarce. Incorporating iMacs therefore supports the project’s aim to investigate GM-CSF-mediated immune responses under controlled and reproducible conditions while maintaining financial feasibility.

6.2 Hypothesis

We hypothesise that macrophages derived from iPSCs, upon stimulation with GM-CSF, will mount a distinct and measurable immune response against *C. albicans*, providing insights into GM-CSF-mediated immunomodulation.

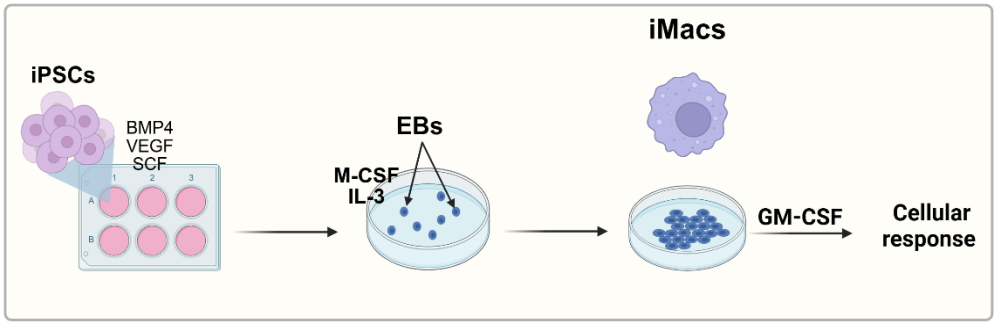

6.3 Specific Objective

In this preliminary study, iMacs were analysed for (i) expression of selected markers, (ii) the effect of GM-CSF on their phenotype and (iii) their influence on *C. albicans* CFUs.

6.4. Results

6.4.1. Characterisation of Macrophages derived from iPSCs (iMacs).

To characterise iMacs, cells generated as described in (Chapter 2, 2.11. Macrophage generation from immortalised pluripotent stem cells (iMacs)), then, Cells were labelled using a cocktail of antibodies targeting CD14, CD45, CD11b, HLA-DR and single label for MR (CD206) and analysed by flow cytometry. Density plots indicate a homogeneous cell population, with 90.38% of events falling within the live cell gate. A gating strategy was applied using SSC-Area versus SSC-Height parameters to ensure the analysis of individual cells while excluding aggregates or doublets (Figure 70. a). Given that the population was dual labelled with CD14 and CD45, quadrant plots were generated to distinguish between positive and negative populations. Despite the substantial background binding of the isotype controls, the cells stained exhibited an upward, rightward shift, corresponding to the expected location of positively labelled cells, indicating that the cells were indeed $CD14^+$ and $CD45^+$. iMacs expressed higher levels of CD14 and CD45 compared to the isotype and unstained populations, as demonstrated by the histograms in Figure 70. b.

CD11b and HLA-DR expression were assessed using quadrant plots in conjunction with $CD14^+$ cells for each antibody. As shown in Figure 70. c, the population positively stained for both CD11b and CD14, and MFI analysis in the histogram confirmed CD11b expression in iMacs (MFI 8881) compared to the isotype control (MFI 414). In contrast, HLA-DR expression was absent, as indicated in Figure 70. d, where the unstained control, isotype control, and HLA-DR-labelled cells were aligned at the same position with MFI=0.10 for all three. Additionally, the mannose receptor (MR) was assessed using single staining of the same cells. The histogram analysis demonstrated that iMacs express MR on their surface, as indicated by the fluorescence shift compared to the isotype control (MFI 26,677 in the positive population versus MFI 446 in the isotype control) (Figure 70. e).

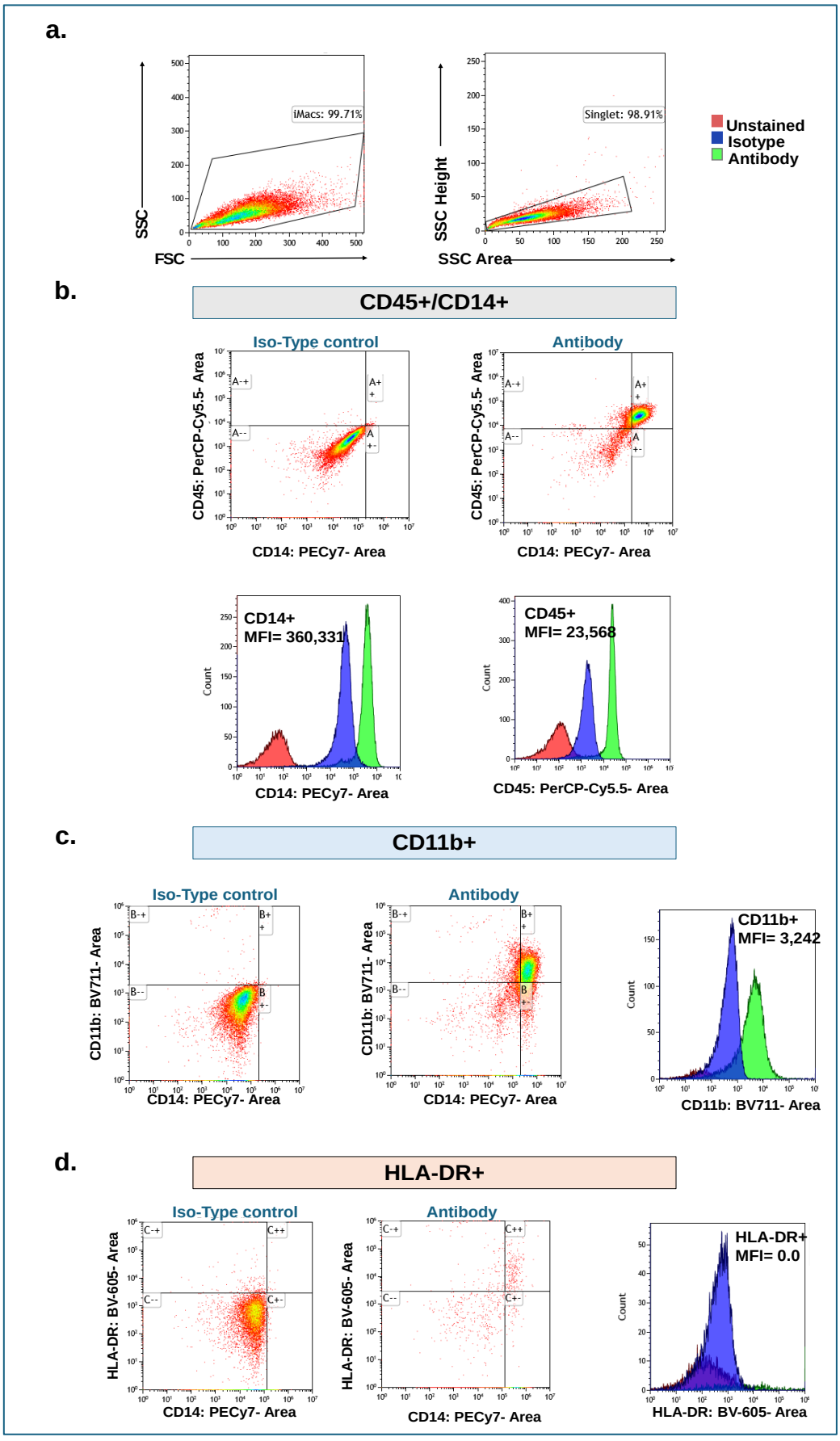
a.
iMacs: 99.71%
SSC
FSC
Singlet: 98.91%
SSC Height
SSC Area
Unstained
Isotype
Antibody
b.
CD45+/CD14+
Iso-Type control
Antibody
CD45: PerCP-Cy5.5- Area
CD14: PECy7- Area
CD14+
MFI= 360,331
Count
CD45+
MFI= 23,568
CD45: PerCP-Cy5.5- Area
c.
CD11b+
Iso-Type control
Antibody
CD11b: BV711- Area
CD14: PECy7- Area
CD11b+
MFI= 3,242
d.
HLA-DR+
Iso-Type control
Antibody
HLA-DR: BV-605- Area
HLA-DR+
MFI= 0.0

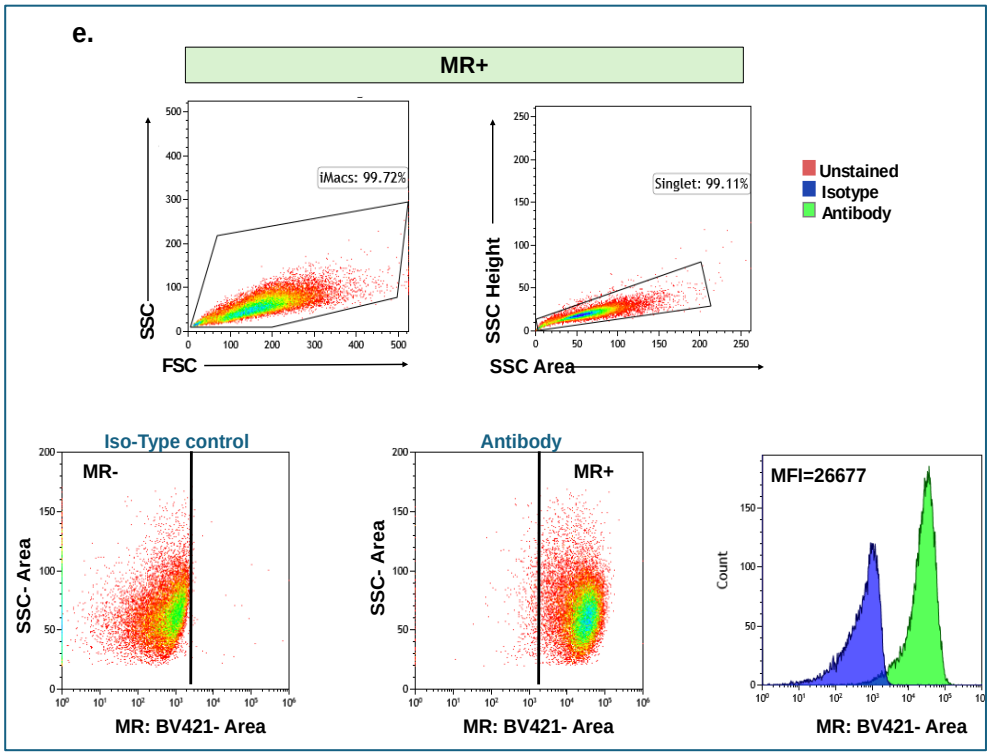

Figure 6.1. Characterisation of macrophages generated from human iPSCs. iMacs were harvested, counted and adjusted to 10^5 / 100µL. Then, cells were processed for FACS and labelled with CD45, CD14, CD11b, HLA-DR antibodies (multiple labelling), and MR (single labelling). **a.** Gating strategy based on the FSC and SSC axis of unstained population, Singlet gate using SSC Area and High**, b.** Dot plot showing CD45, CD14 positive cells, including Isotype controls and specific labelling, followed by histograms of labelled Abs, iso type control and unstained cells. **c.** CD11b expression **d.** HLA-DR expression. **e**. MR expression. MR was labelled in isolation and characterised by normal FSC, SSC gating strategy from the unstained population, then dot plots and histograms were created **(N=1)**. Files were analysed using KALUSA software.

6.4.2. The effect of GM-CSF on receptors expression in iMacs

iMacs were collected, plated, and treated with 10 ng/ml GM-CSF or M-CSF to mimic the conditions used with primary monocytes, and then incubated for ~40-44 hours. iMacs were analysed by flow cytometry for CD45, CD14, CD11b and HLA-DR expression. The gating strategy of dot plots by FSC vs SSC showed a similar percentage of viable cell population, then singlets created from the main population (~90% average of live cells) for M-CSF- and GM-CSF-treated iMacs. Histograms illustrate that GM-CSF-treated iMacs seemed to express more CD45 (MFI 49,726) and CD14 (MFI 990,629) compared to MFI 37,865 and MFI 828,523 for M-CSF-treated cells, although the variable binding of the isotype controls makes comparison difficult. No expression of CD11b or HLA-DR was detected in M-CSF- and GM-CSF-treated cells (Figure 71 a and b).

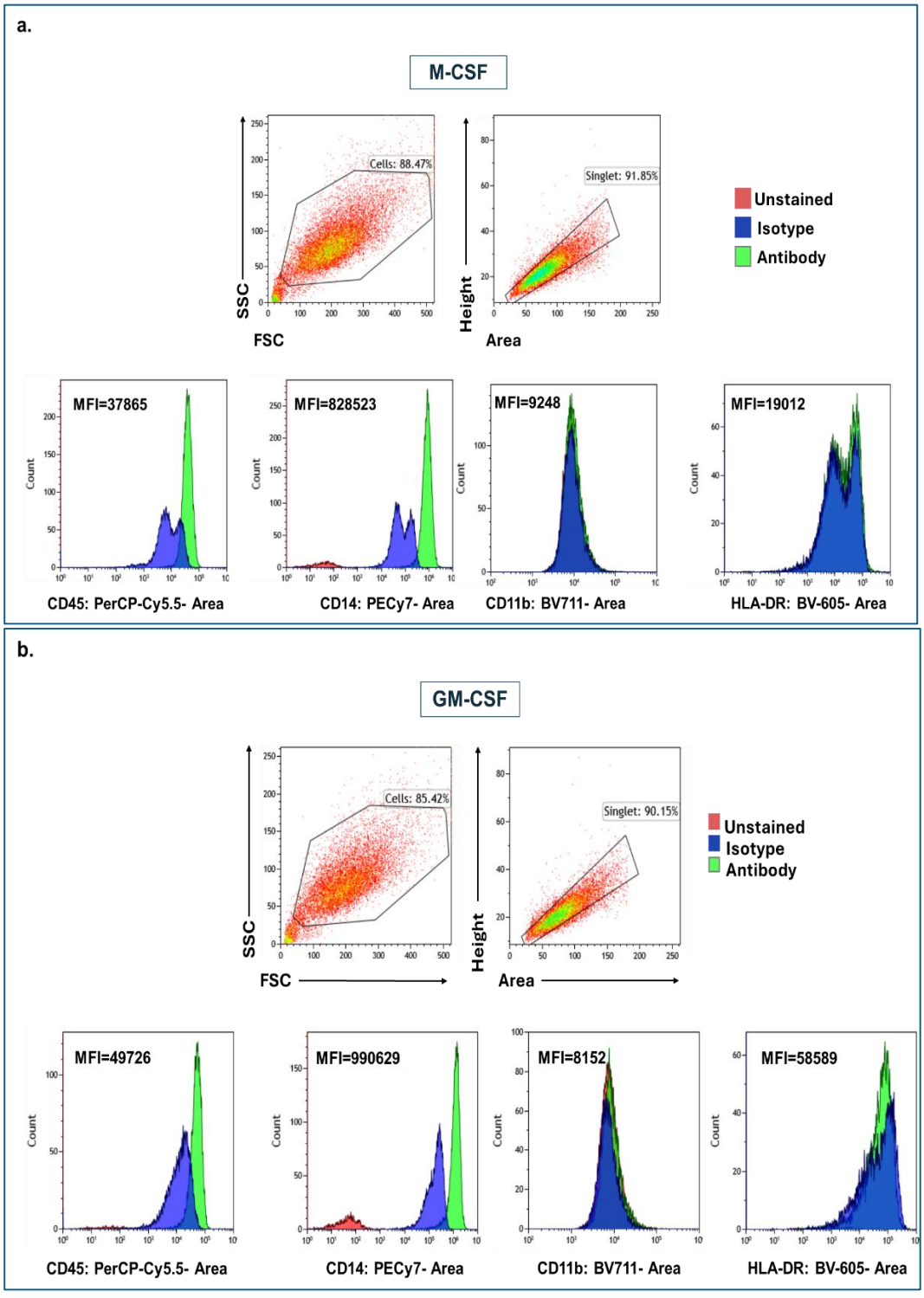

Figure 6.2. iMacs characterisation in the presence of GM-CSF. iMacs were treated with 10ng/mL GM-CSF or M-CSF for 44 h afterwards, harvested and adjusted 10^5/ 100µL, then harvested and set up for FACS, labelled with CD45, CD14, CD11b and HLA-DR. **a.** M-CSF **b.** GM-CSF **(N=1).** Files were analysed using KALUSA software.

Brightfield images show the morphology and distribution of iMacs treated with either M-CSF or GM-CSF (Figure 72). Both M-CSF- and GM-CSF-differentiated cells, plated in 6-well tissue culture plates for ~44 h, display morphological characteristics consistent with human macrophages. M-CSF-treated iMacs displayed a more varied and elongated morphology, and many cells appeared spindle-shaped or flattened. iMacs treated with GM-CSF seem more compact, dense and round.

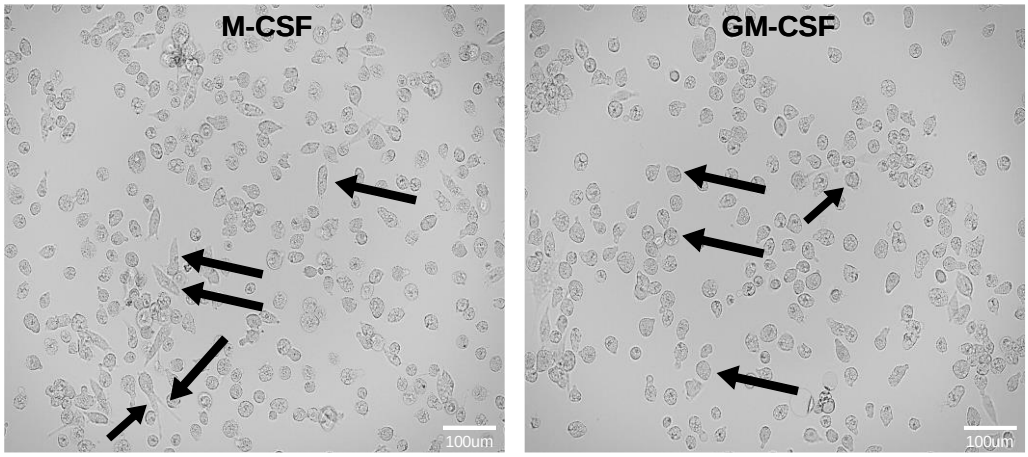

Figure 6.3. iMacs morphology in M-CSF- and GM-CSF-treated iMacs. iMacs were treated with 10ng/mL GM-CSF or M-CSF for 44 h afterwards, harvested and adjusted 10^5/ 100µL, then fixed in 4% PFA and imaged ZOE™ fluorescent microscope **(N=1).** Scale bar=100µm.

Additionally, no cytokine secretion was detected from iMacs in either condition, M-CSF or GM-CSF, in the presence and absence of LPS (Data not shown).

6.4.3. Analysis of MRC1 and CLEC7A gene expression on GM-CSF and M-CSF-treated iMacs

iMacs were treated with 10 ng/ml GM-CSF or M-CSF and incubated for ~40-44 hours. The RNA was extracted from multiple preparations of generated iMacs, and qPCR was performed to assess the expression of MRC1 and CLEC7A genes, which encode for MR and Dectin-1, respectively. Primer sequences are included in detail in (Chapter 2, 2.7. qPCR analysis). GM-CSF-treated iMacs exhibited a significant increase in MR expression compared to M-CSF-treated cells. Dectin-1 was expressed in both M-CSF- and GM-CSF-treated iMacs, and there was no apparent difference in expression levels between the two populations (Figure 73).

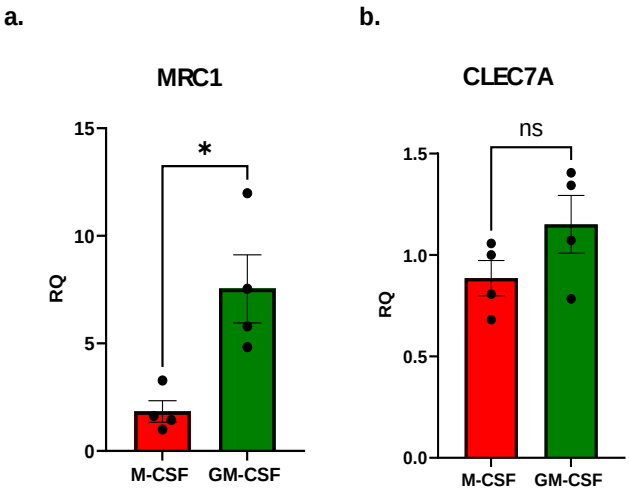

Figure 6.4. Analysis of MRC1 and CLEC7A expression in M-CSF or GM-CSF-treated iMacs. iMacs were treated with 10ng/mL GM-CSF and M-CSF, incubated for 44 h afterwards, harvested and adjusted to 10^5/ 100µL, and then lysed for RNA extraction for the qPCR. **a.** MRC1 **b.** CLEC7A **(N=4)**. Graphs show mean +/- SEM and individual values. Data were analysed using paired t-test by GraphPad Prism, ns= not significant, (*) p<0.01. This experiment was performed by Darryl Jackson.

6.4.4. Analysis of the effect of iMacs on *C. albicans* CFU recovery after infection.

The effect of GM-CSF-treated monocytes on *C. albicans* colony-forming units (CFU) was established in previous chapters. Consequently, we aimed to assess this outcome using iMacs treated with GM-CSF or M-CSF. Both GM-CSF-treated and M-CSF-treated iMacs were exposed to *C. albicans* at a density of 10^6 cells/well (MOI = 1), using 100 µL of monocyte/ *C. albicans* suspension per well (200 µL final volume) and incubated for 1 and 3 hours at 37°C with 5% CO_2. The effect of iMacs on *C. albicans* CFU was consistent with that observed in primary monocytes. CFU quantification following incubation demonstrated a reduction in fungal burden relative to the initial inoculum (stock solution from overnight culture), at 1 and 3 h incubation, regardless of the presence or absence of iMacs, with a slight increase in the iMacs treated with GM-CSF. However, the validity of this experiment remains inconclusive, as it was performed only once and requires multiple repeats for robust interpretation (Figure 74).

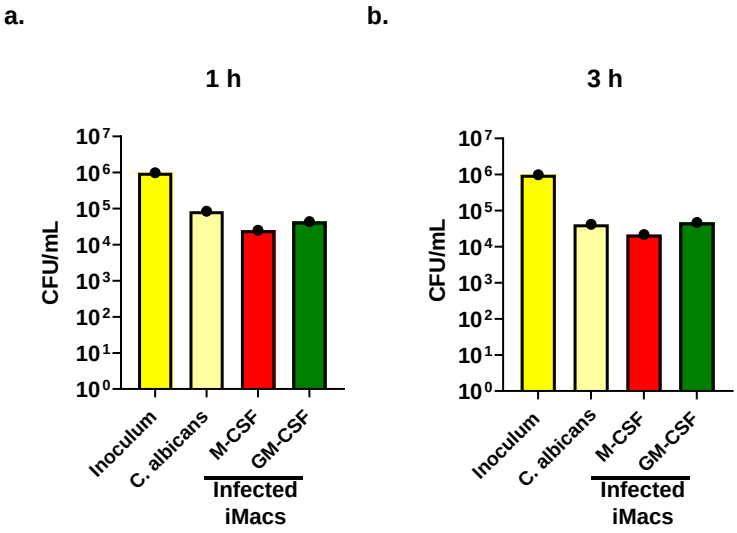

Figure 6.5. Analysis of *C. albicans* CFUs. To test the influence of GM-CSF on the interaction of iMacs with *C. albicans,* M-CSF/GM-CSF-treated iMacs were exposed to *C. albicans* at an MOI of 1, 10^6 cells/well. CFUs were analysed at different time points post-infection. **a**. 1 hour **b**. 3 hours. The graph shows individual values calculated as the means from duplicate wells and was created using GraphPad Prism **(N=1).**

6.6. Summary

- iMacs expressed key myeloid markers, including CD14, CD45, CD11b, and the mannose receptor (MR), but lacked HLA-DR expression.
- GM-CSF-treated iMacs might have higher surface expression of CD14 and CD45 compared to those treated with M-CSF. Additional culture might reduce the expression of CD11b.
- qPCR analysis revealed increased MRC1 transcript levels in GM-CSF-treated iMacs, while Dectin-1 expression showed no significant differences between both conditions.
- Colony-forming unit (CFU) assays are consistent with data from primary monocytes.
- All these findings need to be validated, as in most cases N=1.

6.7. Discussion

The generation of macrophages from iPSCs represents a promising and rapidly advancing area in modern biomedicine. iMacs have been effectively utilised to model rare genetic disorders affecting phagocyte function, for drug screening applications, and to investigate various aspects of macrophage–pathogen interactions [364]. In our study, we effectively produced macrophages from human iPSCs (iMacs) from the line KOLF2.1J that originally was cultured and differentiated into numerous cell types, including three-germ layer cells, cortical glutamatergic neurons, cortical forebrain neurons, skeletal monocytes, motor neurons, astrocytes, microglia and macrophages using established differentiation protocols [234].

At our lab, we used recognised macrophage surface markers to describe iMacs. According to flow cytometry examination, the differentiated cells displayed a high vitality of over 90% and the expression of the important macrophage markers CD14 [365], CD45 [366], and CD11b [367]. These are almost the same surface markers which were also assessed in previous studies. For example, Pouyanfard et al., who characterised human iMac phenotypes and reported consistent and uniform expression of typical macrophage markers, including CD14, CD11b, CD36, CD68, and SIRP-α [368]. Cells treated with M-CSF and GM-CSF exhibit morphological traits common to human macrophages. These include surface adhesion, a distinct cell body, and varying morphologies based on the activation state (rounder for GM-CSF, elongated for M-CSF). This observation is consistent with previous studies on iMacs, which describe them as large, vacuolated cells with pseudopodia that exhibit classical macrophage markers ($CD14^+$, $CD11b^+$, $CD45^+$) and perform key macrophage functions, including phagocytosis and the secretion of pro- and anti-inflammatory cytokines [369]. The iMacs generated in this study may resemble an immature or alternatively activated macrophage phenotype rather than a classically activated, pro-inflammatory state, as indicated by their lack of HLA-DR expression. This observation is supported by findings from Lyadova et al., who reported that patient-derived iMacs showed impaired upregulation of HLA-DR and other surface receptors, including CD64, CD38, and CD282, following IFN-γ stimulation [11]. In contrast, Pouyanfard et al. demonstrated that human iPSC-derived macrophages stimulated with LPS and IFN-γ, expressed HLA-DR along with other macrophage markers such as CD14, CD11b, CD68, and CD86. Flow

cytometric analysis in that study confirmed that these cells possessed antigen-presenting features typical of functional macrophages [358]. Crucially, in our study, the status of the iMacs as macrophages with tissue-resident or anti-inflammatory characteristics is further supported by the expression of the MR (CD206) [370].

Next, we evaluated the effects of GM-CSF and M-CSF on the expression of surface markers in iMacs. In comparison to cells treated with M-CSF, iMacs treated with GM-CSF exhibited a slight increase in CD45 and CD14 expression, indicating that GM-CSF might promote the maturation and myeloid commitment of macrophages produced from iPSCs [371]. Nevertheless, neither condition resulted in the expression of CD11b or HLA-DR, supporting the idea that these iMacs might not completely mimic the phenotype of traditionally activated (M1) macrophages in the absence of further stimulation. Stimulation with GM-CSF was used to produce the engineered chimeric antigen receptor-iPSC-derived (CAR-iMac). Zhang et al. employed M-CSF and GM-CSF to drive macrophage differentiation from iPSCs, specifically to generate CAR-iMac cells. Their protocol began with the formation of EBs in APEL II medium supplemented with BMP-4, bFGF, VEGF, and SCF. To initiate myeloid differentiation, BMP-4 was later replaced with IGF-1, IL-3, M-CSF, and GM-CSF (exact concentrations of M-CSF and GM-CSF were not reported); these cytokines were essential for steering the cells toward the myeloid lineage. The resulting macrophages expressed the CAR and exhibited antigen-specific phagocytosis of tumour cell lines, underscoring their promise for adoptive cell therapy applications [372].

At the transcriptional level, iMacs treated with GM-CSF showed a notable elevation of MR, while the expression of Dectin-1 was similar in groups treated with GM-CSF and M-CSF. This pattern is significant since MR is a crucial receptor for fungus detection [370], suggesting that GM-CSF treatment could prime iMacs for more effective antifungal responses. Dectin-1 expression remained constant under both conditions, suggesting that its regulation may be less responsive to GM-CSF stimulation under these conditions or may need other parameters to be modulated.

By infecting cells with *C. albicans* and measuring fungal survival using CFU assays, the functional ability of iMacs to respond to fungal infection was further investigated. Following one and three hours of infection, iMacs treated with GM-CSF and M-CSF showed a decrease in fungal burden, which is in line with earlier findings in primary monocytes (Chapter 4, 4.4.1. Effect of GM-CSF

monocytes on *C. albicans* CFU.) Given that *C. albicans* rapidly forms hyphae upon transitioning to its pathogenic state at 37ºC in the presence of human serum, this morphological shift likely contributes to the observed reduction in CFUs [24]. Multiple biological replicates are necessary to validate the validity of these results and to describe how GM-CSF affects iMacs antifungal activity more thoroughly.

To determine whether the produced iMacs have functional traits similar to those of primary monocytes and macrophages, the study measured the release of TNF-α, CCL-22, and CCL-17. However, regardless of whether iMacs were activated with LPS or left unstimulated, none of these cytokines were found in the supernatants of either condition (M-CSF and GM-CSF). This lack of cytokine release contrasts with results from several investigations, where the proinflammatory and anti-inflammatory cytokine profiles of iMacs were regularly assessed to evaluate their immunological competence and activation state [363, 373]. This implies that the iMacs might have an immature phenotype, which probably contributes to their inability to release cytokines. Alternatively, perhaps we required a costimulatory signal such as IFN-γ.

These results demonstrate that in our hands, human iPSCs can successfully differentiate cells with macrophage characteristics. Treatment with GM-CSF appears to improve certain macrophage-associated traits, such as MR expression, which may influence the identification and elimination of fungi. The incomplete maturation profile, which is highlighted by the lack of CD11b and HLA-DR in GM-CSF- and M-CSF-treated iMacs, suggests that more activation steps or further optimisation of differentiation protocols are required to achieve a fully mature and functional macrophage phenotype suitable for mimicking complex immune responses. This work is now being followed by another PhD student who has reduced the binding of isotype control antibodies using Fc block, has extended the range of cell surface markers and is incorporating IFN-γ alongside LPS to stimulate these cells. To enable data integration across genetic variants, cell types, and analysis modalities, the stem cell field requires a standard reference cell line (a reference human induced pluripotent stem cell line for large-scale collaborative studies) [234].

Chapter 7
General discussion

Introduction

Fungal infections, particularly those caused by *Candida albicans (C. albicans),* can be extremely costly and cause major damage, especially to immunocompromised patients [219]. In essence, *C. albicans* is an innocuous microorganism that resides in the microbiota; however, in some cases, it becomes pathogenic by multiplying and forming hyphae, which can penetrate tissues and cause a systemic and lethal infection [17]. Immunity to *C. albicans* begins with neutrophils migrating from the periphery, recruited in response to activation of resident immune (i.e. macrophages) and non-immune cells. Trafficking monocytes arrive at the infection site, differentiate into macrophages and DCs, and contribute to shaping the adaptive immune system in collaboration with key cytokines involved during fungal infection, such as TNF-α and IL-23, which help in inducing Th17 maturation and secreting IL-17 [374]. Other immune cells, like mast cells and innate lymphoid cells (ILCs), contribute to stopping infection. For example, mast cells degranulate, releasing leukotriene C4 (LTC4) when fungal β-glucan binds to Dectin-1 [375]. LTC4 is a lipid mediator that is released into the vasculature during inflammation, causing vasodilation and increasing vascular permeability. They also aid in the recruitment and migration of leukocytes to the site of an inflammatory reaction [376]. Despite the general assumption that Th cells are the primary source of IL-17 in response to *C. albicans*, it has been shown that ILCs that secrete IL-17 influence fungal control [377]. All these integrated mechanisms can create a system capable of controlling the infection and eliminating the pathogen [378]. However, studies on mice showed how monocytes on their own can protect against *C. albicans* [379]. Granulocyte colony-stimulating factor (GM-CSF) is a potent cytokine known for its modulatory effect during infections. It has been used in clinical and research practice to provide immune system stimulation by enhancing the proliferation, differentiation and activation of myeloid cells, including monocytes, thereby improving host defence against infection [220]. Hence, our study aimed to explore the effector function of human monocytes when treated with GM-CSF during *C. albicans* infection. This chapter discusses the findings of our project from a variety of perspectives, including clinical and immunological, and is structured in the following sections:

1. Clinical use of GM-CSF.
2. GM-CSF as an antifungal agent.

3. Overview of the immunological responses of monocytes treated with GM-CSF during *C. albicans* infection
4. Macrophage colony-stimulating factor (M-CSF) as a homeostatic cytokine.
5. Generating an infection assay model involving iMacs treated with GM-CSF.
6. Limitations and future directions.
7. General discussion.

1. Clinical use of GM-CSF.

GM-CSF has been utilised in a variety of clinical and research settings to boost the immune system, aid in the recovery of immune cells following chemotherapy, increase the efficacy of cancer vaccines and immunotherapies, and support the immune system following haematological transplantations [380].

Cancer chemotherapy.

Recombinant human GM-CSF (rhGM-CSF) has significantly improved myeloid recovery following cytotoxic chemotherapy, which has led to significant improvements in the supportive treatment of cancer patients [381]. There is increasing interest in using GM-CSF as primary immunotherapy as a result of recent findings on its effects on DCs. It has been shown that GM-CSF can produce type 1 DCs (DC1), which can bias T-cells towards a Th-1 phenotype as a desirable strategy for producing anti-tumour effects [382]. GM-CSF may play a part in cell-mediated immunity treatment, given its ability to skew the immune system towards Th1 effects *in vitro* [383].

Cancer vaccines.

Cancer vaccine effectiveness requires optimal choice of vectors, co-stimulatory molecules to overcome immune tolerance and tumour antigens. GM-CSF was introduced as an adjuvant therapy to recruit DCs to the vaccination site and enhance antigen presentation to promote tumour-specific immunity. Pioneering studies demonstrated that engineered tumour cells expressing GM-CSF stimulate powerful, long-lasting immunity that is less toxic to the body when it's used as an adjuvant therapy. Clinical studies on a variety of malignancies, such as lymphoma and melanoma, have demonstrated that vaccinations containing GM-CSF boost DCs infiltration, trigger anti-tumour immunity, and occasionally eradicate residual disease. Therefore, by promoting strong and targeted T-cell

responses, GM-CSF significantly contributes to increasing the effectiveness of cancer vaccines [380].

Support hematopoietic cell recovery following transplantation.

Clinical studies examined whether the administration of GM-CSF and G-CSF after autologous hematopoietic stem cell transplantation may affect the post-transplant reconstitution of cellular immunity, particularly on the DC subsets in the peripheral blood. Fattorossi et al. carried out a randomised, prospective clinical trial to examine potential variations in immunological recovery in 39 patients with breast and ovarian cancer who received either GM-CSF or G-CSF following high-dose myeloablative chemotherapy and autologous transplantation. GM-CSF was more effective at day 12 at up-regulating membrane molecules on phagocytic cells. By day 80, a significantly higher percentage of mitogen-stimulated T cells from GM-CSF-treated patients expressed IL-2 receptor, and a higher percentage of these T cells were actively proliferating [384].

2. GM-CSF as an antifungal agent

A serious issue with patients on mechanical ventilation and in the clinical setting of the intensive care unit is a pathogenic mycobiome. Airway colonisation by *C. albicans* may promote the growth of *Escherichia coli (E. coli), Staphylococcus aureus (S. aureus),* and *Pseudomonas aeruginosa (P. aeruginosa)* [294]. Even with recent advances in the management of patients infected with *C. albicans*, therapeutic options remain limited and clinical outcomes are sometimes unsatisfactory [385]. Two potential strategies to address this include reversing underlying immunological deficiencies or employing immunomodulatory therapies to enhance host immune responses. Effective therapies, however, need a thorough understanding of the underlying immunology because immune responses against fungal infections vary widely [386].

GM-CSF is one of the earliest hematopoietic growth factors identified in the late 1970s [387]. It has since been discovered to be comparatively redundant for the production of granulocytes and other cells in this lineage. Mice with this gene knocked out do not experience cell deficiencies; instead, because alveolar macrophages are unable to remove surfactants, these animals die from alveolar proteinosis [388]. Surfactant is a complex mixture of proteins (surfactant proteins A, B, C, and D) and phospholipids (mainly dipalmitoyl-phosphatidylcholine and phosphatidyl-glycerol). Its primary function in the

alveolus is to lower surfactant tension at the air-liquid interface, though it may also aid in lung defence [388]. Therefore, GM-CSF is necessary to generate lung alveolar macrophages, which are essential for maintaining surfactant homeostasis [389].

According to the literature, GM-CSF may help treat a range of invasive fungal infections (IFI), such as zygomycotic, aspergillosis, and candidiasis, when combined with antifungal medications [386]. GM-CSF is thought to work by enhancing the antifungal pathways of calcineurin, Bruton's tyrosine kinase (BTK), and CARD9 through signal convergence. The link between CARD9 and GM-CSF is illustrated by a case report of a 41-year-old individual with a spontaneous CARD9 deficiency who developed central nervous system candidiasis and was successfully treated with sargramostim (a rhGM-CSF prescribed as an immunostimulatory medication to boost white blood cells) [390]. However, the results of GM-CSF acting as an immunotherapy in CARD9-deficient patients are thought to be influenced by subtle differences in genetic deficiencies displayed by these patients. This may explain the variations in GM-CSF responses that we observed across several experiments, including cytokine secretion. In fact, we don't expect all healthy donors to have a complete deficiency in CARD9, as this is a rare condition associated with serious disorders such as inflammatory bowel diseases (IBD), cardiovascular diseases (CVD) and tumour formation and metastasis, and this is typically linked to severe fungal infections as well [205]. However, an allelic series of CARD9 variations, such as those identified in some IBD patients, has both a rare protective function, such as the splice-site variant c. IVS11+1G>C (rs141992399) whereas the common variant S12N (rs4077515) confers increased disease risk [391]. Additionally, there is the heterogeneity in GM-CSF response among individuals that was discussed in detail in (Chapter 4, 4.6. discussion, 4. Cellular heterogeneity among and within cultures).

More comprehensive research is required to elucidate the mechanisms underlying how GM-CSF interacts with downstream signalling pathways to impact fungal infection in patients lacking CARD9 [161]. According to research by Vora and associates, monocytes treated with sargramostim and voriconazole exhibited increased activity against *A. fumigatus*. Research in mice suggests that GM-CSF, when combined with conventional antifungal treatments, may be a useful treatment for *A. fumigatus*. These scientists demonstrated that mice lacking the β chain of the GM-CSF receptor

(GMCSFRβ−/−) exhibited poorer survival rates than wild-type controls when challenged with *A. fumigatus*. The scientists demonstrated that NADPH oxidase activity is decreased when the GM-CSFR-β chain is depleted [392]. GM-CSFR comprises an α chain that specifically binds GM-CSF and a β chain, which shares activity with IL-3 and IL-5 receptors, which is essential for downstream signalling activation [393]. Deficiency of GM-CSFRβ could be the mechanism behind increased mortality in response to infection. Interestingly, these authors also demonstrated that administering rhGM-CSF to wild-type mice may increase neutrophil NADPH oxidase activity, suggesting the potential use of GM-CSF as a therapeutic agent for inhibiting fungal infections [392]. Additionally, to improve the immune response against fungal infection in cancer patients with neutropenia, Bodey G et al administered GM-CSF as an adjuvant therapy to promote the production of neutrophils and monocytes/macrophages. Neutrophil count improved, along with a reduction in fungal pathogenesis, when GM-CSF was administered in conjunction with antifungal therapy; nevertheless, the high dosage of GM-CSF resulted in toxicity, indicating that it was probably overdosed, and the GM-CSF concentration needs consideration [394].

Fungal infections that affect healthy individuals, including pneumonia, sinus infections, and vaginal infections, are easily treated. However, fungal infections in immunocompromised hosts, such as *A. fumigatus*, *C. albicans* and *Zygomycetes*, represent considerable danger [294]. Over the past decade, clinical evidence, although limited to small case reports and studies, has indicated that adjunctive GM-CSF could be beneficial in certain fungal infections, particularly in those immunocompromised patients [395]. According to these studies, GM-CSF appears to increase host immunity against fungi overall, and clinical use (as sargramostim) has been well tolerated. Thereby, understanding how GM-CSF influences monocyte responses to *C. albicans* infections provides further insights for therapeutic development [294].

3. Overview of the immunological response in monocytes treated with GM-CSF during *C. albicans* infection.

Monocytes characterisation.

In our cultures, we have selected $CD14^+$ cells using CD14 microbeads, but we have not investigated monocyte subpopulations. Monocytes can be broadly divided into $CD14^{++}CD16^-$ "classical" monocytes, which represent ~90-95% of

all circulating monocytes and are considered mature or proinflammatory, and $CD14^{+}CD16^{-}$ "non-classical" monocytes [396, 397]. These subsets differ in their functional properties; for example, classical $CD14^{++}CD16^{-}$ monocytes are thought to be potent inducers for Th17 in response to *C. albicans* infection [397]. This is because of the high secretion of IL-1β, IL-6 [398] and the significant expression of MR (CD206) [397]. In our study, we did not assess the phenotype of monocytes or the expression of CD14/CD16 in detail, nor did we consider subset-specific responses. However, based on the substantial secretion of IL-1β and the expression of MR that we observed in GM-CSF-treated monocytes, it is possible that our cultures were enriched in classical $CD14^{++}CD16^{-}$ monocytes. In addition, proteomics data showed comparable CD14 expression levels between M-CSF– and GM-CSF–treated cells (M-CSF mean: 803; GM-CSF mean: 767).

Moreover, GM-CSF significantly upregulates surface activation receptors, such as HLA-DR (MHC II), which is expressed on many immune cells, including CD4+ T cells, and plays a crucial role in immune response induction by presenting and recognising antigens [399]. CD11b is also highly expressed in response to GM-CSF, which is essential for adhesion and trafficking, indicating the proinflammatory state of these monocytes. The role of CD11b in response to *A. fumigatus* was investigated. *(*CD11b−/−) mice were used and compared to wild-type mice after intratracheal infection. Researchers found that (CD11b−/−) mice survived the infection similarly to wild-type, but they exhibited a higher pulmonary fungal burden and increased infiltrated neutrophils, indicating impaired fungal clearance. Moreover, they detected lower proinflammatory cytokine secretion. In vitro, neutrophils lacking CD11b showed reduced phagocytic activity against fungal infection, suggesting that CD11b is crucial for effective fungal killing [400].

GM-CSF-treated monocytes also upregulated C-type lectin receptors (CLRs), like Dectin-1, which is the primary receptor in recognising essential yeast form molecules like β-glucan (a significant component of the *C. albicans* cell wall) [401]. According to studies of Dectin-1 activation, only particulate β-glucans can trigger downstream signalling by clustering Dectin-1, displacing regulatory phosphatases CD45 and CD148, and phosphorylating the intracellular ITAM-like motif of Dectin-1 in an SRC-dependent pathway [402]. Recent evidence suggests that pharmacological impairment of phagocytosis (e.g., by using actin polymerisation inhibitors, such as cytochalasin D and latrunculin) enhances

human and mouse cell activation upon stimulation with β-glucans, highlighting the intricate relationship between membrane dynamics and Dectin-1 signalling [403]. GM-CSF also upregulated MR (CD206), which is known for its activity in cytokine secretion enhancement [337] and CLEC5A, which, along with other CLRs, is known for the general function in sugar recognition because of its carbohydrate recognition domain [404]. Additionally, the motility of GM-CSF-treated monocytes was measured, and the expression of various proteins, including CD11b and GTPases and inflammatory receptors, provided a rationale for the high cellular motility. Details about the GTPase family and monocyte cellular migration and motility are well explained in (Chapter 3, 3.6. Discussion). On the other hand, in our study, GM-CSF did not affect other cellular characteristics, such as Dectin-2 expression (monocytes) and the production of extracellular vesicles (EVs, macrophages). It is commonly known that GM-CSF increases human Dectin-2 expression to improve Dectin-2's capacity to recognise and react to various stimuli, such as fungal infections [405]. Dectin-2 is the most thoroughly studied member of this receptor family. It was found to be an over-expressed transcript in macrophages, neutrophils, and pluripotent myeloid progenitors, as well as in a mouse model of myeloid leukaemia [406]. Human Dectin-2 seems to be elevated in inflammatory environments, just like mouse Dectin-2, following the treatment with GM-CSF, TGF-β1, and TNF-α, which could increase gene expression in CD14+ monocytes [407]. Although Dectin-2 is a fungal PRR, the receptor seems to recognise hyphal rather than yeast forms preferentially [408] since yeasts have Dectin-1 as a PRR for β-glucan, as mentioned before [31]. In our model, however, we tested expression in monocytes treated with M-CSF or GM-CSF without additional stimulation like LPS and in the absence of *C. albicans*, which could explain the very low or even absent levels of Dectin-2 expression. Moreover, the incubation time (~44 h) may not have been sufficient for detectable transcriptional induction. Monocyte differentiation depends on several critical factors, among which time plays a key role, especially when cells integrate multiple signals such as IL-4, GM-CSF, or their combination [409].

Monocytes/ *C. albicans* infection.

In brief, our cocultures revealed distinct findings that could enhance our understanding of how monocytes integrate stimulatory cues and translate them into specific functional outcomes. For example, the secretion of proinflammatory cytokines by monocytes treated with GM-CSF, in particular following infection

with *C. albicans*. This indicates that cellular pathways (such as NFkB) are activated, which *in vivo* would be expected to trigger the activation of other immune cells, promote their recruitment, and amplify cytokine release [410].

Furthermore, in infected GM-CSF monocytes, we demonstrated that while incubation with monocytes did not alter *C. albicans* viability (CFU), it significantly affected hyphal length, especially in GM-CSF–treated monocytes. This is noteworthy because hyphae represent the most pathogenic form of *C. albicans*, and limiting their growth not only weakens fungal virulence but also supports infection control in coordination with other immune mechanisms. According to a study by Bain J. and associates, hyphal folding is a mechanism that can both promote and hinder hyphal growth and damage. This mechanism is an additional tactic in the immune cell's toolbox that probably helps with efficient fungal removal [303]. This suggests that GM-CSF-boosted effector functions will increase hyphal damage by monocytes, particularly those treated with GM-CSF. Clinically, hyphal development can be suppressed through genetic deletion or mutation in some *C. albicans'* key transcriptional regulators, such as EFG1, CPH1 and RAS1 or by acidifying the media that hosts *C. albicans* to reduce hyphal growth [411]. Chapter 4 focused on the effectiveness of our model and the outcomes from infected monocytes with *C. albicans* in the presence and absence of GM-CSF.

The role of sGP in antifungal response in collaboration with GM-CSF.

Additionally, we found that GM-CSF-treated monocytes downregulate MR expression in response to *C. albicans* infection. This could correlate with Dectin-1 activation upon β-glucan engagement, which contributes to activating cleavage metalloproteases that mediate MR shedding from the membrane and release into the plasma [311]. Therefore, we extended this study to investigate what could result from MR inhibition in response to sulfated glycopolymer (sGP). The use of sulfated glycopolymer (sGP) that binds the CR domain of MR facilitates the inhibition of MR in both infected and non-infected GM-CSF-treated monocytes, making it a valuable tool for studying the contribution of MR to antifungal therapy. MR inhibition is essential to consider for study because clinically, MR (CD206) is implicated in a variety of medical conditions. For example, MR mediates the entry of the hepatitis B virus into intrahepatic DCs and the dengue virus and HIV-1 infection of macrophages. MR overexpression on alveolar macrophages in the lungs of patients with severe chronic obstructive pulmonary disease suggested its involvement in the pathogenesis of this

condition. Furthermore, tumour-associated macrophages (TAMs) have been shown to express MR robustly. These cells cause immunosuppression, metastasis, and angiogenesis [331]. Therefore, inhibiting MR could modulate the immune response during fungal infections and help reduce pathological risk. However, it is challenging to use glycosylated multivalent ligands *in vivo* because many lectins have overlapping sugar ligand specificities that can cause off-target effects. For instance, many other animal lectins, such as mannose-binding lectin and DC-specific intercellular adhesion molecule-3-grabbing non-integrin (DC-SIGN, CD209), recognise mannose-based molecular patterns in addition to MR [412]. Therefore, it may be challenging to target MR selectively *in vivo* with mannosylated ligands unless disease-specific delivery methods, such as local injection, are employed. In contrast, lectins that exhibit strong avidity and selective recognition of SO4-3-Gal (sGP) motifs are considerably less common [331]. Mastrotto et al. injected sGP labelled with Oregon Green intraperitoneally into mice. They incubated for 4 hours, followed by treatment with TR-gelatin (fluorescent MR ligand). After 2 hours, they collected liver tissues and investigated the presence of gelatin using confocal microscopy, finding that gelatin uptake by hepatic cells was significantly downregulated. These findings indicate the effective inhibition of MR *in vivo* and the capability of sGP to specifically target MR, which highlights its potential for therapeutic applications [331].

From sGP-treated monocytes, we had an interesting finding in which inhibiting MR led to the downregulation of different cytokines. Still, TNF-α has a consistent decrease when comparing untreated and sGP-treated GM-CSF monocytes among all donors, which means that the treatment is working and could help to reduce inflammation [413]. This suggests that sGP may have therapeutic potential as an antifungal agent in the context of GM-CSF–treated monocytes, particularly if future studies confirm the role of MR in anti-*C. albicans* immunity. Hence, the soluble mannose receptor (sMR), which thought to be cleaved from immune cells' surface, is essential in contributing to the immune system by activating macrophages and secreting TNF-α, IL-6, IL-1β, and IL-12 [414]. Clinically, critically ill patients with IFI, like candidemia, have a substantially higher sMR concentration than those with sterile inflammation. This suggests that testing serum sMR may aid in the identification of fungal infections during systemic inflammation, although its diagnostic performance alone is moderate [415].

GM-CSF and sulfated glycopolymers together reveal a possible therapeutic pathway for specifically modifying myeloid cell activity. In patients at risk of invasive *C. albicans* infection or with compromised monocyte/macrophage function, carefully timed or local GM-CSF delivery may be helpful. GM-CSF is already used clinically to increase myeloid cell numbers and function, and our data support its role in enhancing antifungal responses. Concurrently, the sGP, which is intended to interact with CD206, seems to regulate MR-mediated signalling without significantly reducing phagocytosis or cell viability. This offers sGP as a candidate immunomodulatory tool to change cytokine profiles or reduce excessive MR-dependent responses, for example in chronic inflammation, tissue fibrosis, or contexts where alternatively activated/macrophage-like phenotypes are harmful. In the longer run, sGP-like compounds could also be produced as targeted delivery platforms to MR-expressing cells, linking receptor specificity with regulated immune regulation.

4. Macrophage colony-stimulating factor (M-CSF) as a homeostatic cytokine

At the beginning of this project, we used untreated monocytes as a negative control for GM-CSF-treated monocytes. We found that they had reduced viability after incubation, leading to significant cell loss. In contrast, M-CSF supported monocyte survival, making them a reliable and physiologically appropriate negative control for GM-CSF in all experiments of this thesis.

Although M-CSF and GM-CSF were initially identified as hematopoietic growth factors, they have been shown to have distinct functions in controlling mature myeloid cell populations in both homeostatic and inflammatory settings [416]. The effects of M-CSF and GM-CSF on myeloid populations are diverse, including activation, differentiation, mobilisation, and survival. However, while GM-CSF is necessary for the maturation of alveolar macrophages and the differentiation of natural killer cells into effector cells, studies employing gene-deficient mice have demonstrated a critical function for M-CSF in maintaining various myeloid lineage populations. Numerous cells and tissues in the body produce M-CSF under homeostatic conditions, polarising macrophages towards an anti-inflammatory phenotype [281]. Indeed, M-CSF and GM-CSF induce macrophages to react in opposing ways; M-CSF polarises macrophages towards an anti-inflammatory phenotype (M2-like), whereas GM-CSF encourages a proinflammatory phenotype (M1-like) [417]. The biologic activities

of M-CSF are mediated by signalling via the colony-stimulating factor receptor 1 (CSF-1R), a type III tyrosine kinase transmembrane receptor [418]. After attaching to its receptor, M-CSF dimerises and activates the phospholipase C, ERK, and PI3K pathways, which leads to the subsequent nuclear localisation of the transcription factor Sp1 [250]. Mutations in CSF-1R have been linked to myelodysplastic syndromes, the development of acute myeloid leukaemia, and hereditary diffuse leukoencephalopathy in humans [419]. Under homeostatic circumstances, CSF-1R-mediated endocytosis and subsequent intracellular degradation control the availability of M-CSF [420].

There have been limited clinical uses for M-CSF as a therapy; it has been demonstrated that M-CSF can be used as an adjuvant therapy in conjunction with other traditional antifungal medications to treat fungal infections. When *A. fumigatus* was introduced to transplant-mouse models, Kandalla et al observed that the mice's survival increased from 10% in controls to 60% in M-CSF-treated animals [421]. In human studies, Hume and McDonald used M-CSF in 46 stem cell transplantation patients with IFD; they all received rhM-CSF combined with their routine antifungal therapy. Patients who received M-CSF showed an improved survival rate compared to the controls [422]. However, rhM-CSF was administered to cancer patients and was found to accelerate the disease progression by boosting the macrophage population [423]. Consequently, unlike GM-CSF, M-CSF hasn’t been pursued further in human therapy, and there isn't a pharmaceutical product for it [395].

5. Generating an infection assay model involves iMacs treated with GM-CSF.

In parallel with this work, we generated macrophages from induced pluripotent stem cells (iPSCs). The benefits of using iMacs in research include creating a cell line that is useful for genetic manipulation, opening avenues to explore host-pathogen interactions in a controlled and genetically feasible system [424]. Reprogramming macrophages has been explored as a therapeutic strategy for various diseases, including atherosclerosis [425]. M2-like macrophages are often described as anti-inflammatory cells, promoting tissue repair and healing wounds [426]. However, their anti-inflammatory phenotype is unstable once transferred into the human body, which limits their clinical utility. In contrast, iMacs provide a more reliable and physiologically relevant mode, making them a better option for therapeutic or experimental applications [427]—for example,

the safety of genetic modification. Since macrophages have developed the ability to identify foreign nucleic acids and mount an immune response in reaction to them, they are regarded as difficult-to-transfect cells. Although macrophages such as CAR-macrophages can be genetically engineered, the process is technically challenging and often inefficient. By contrast, iMacs may provide a more beneficial and feasible regulated substitute for macrophages in anti-tumour treatments [428]. Also, Zhang et al. developed CAR-iMac cells that exhibited antigen-specific and active function in the optimisation of macrophage-based therapeutics. Their research showed that the produced cells were highly effective in providing antigen-dependent macrophage capabilities, including cytokine production like TNF-α, IL-1β and IL-6, and release, proinflammatory/anti-tumour polarisation, improved tumour cell phagocytosis, and *in vivo* anti-cancer cell activity. In addition, CAR-iMac were safe, and had the potential to be used as an anti-tumour agent *in vivo* [372]. Incomplete understanding of plasticity and phenotype stability, limited clinical and experimental reproducibility and elucidating the underlying role of macrophages in tissue repair and inflammation resolution highlight key gaps that iMacs would be better equipped to tackle [369].

At the initial stage of characterising the generated iMacs, our model showed expression of CD11b, Dectin-1, and MR. Upon treatment with 10 ng/mL GM-CSF, flow cytometry confirmed the successful differentiation of iPSCs into macrophages through the expression of CD14 and CD45. Unfortunately, due to overlapping experiments and limited time, we were not able to assess CLR expression (such as MR and Dectin-1) by flow cytometry. Nevertheless, qPCR analysis of GM-CSF–treated iMacs revealed increased transcripts for MR and Dectin-1, supporting the acquisition of an inflammatory phenotype in the generated iMacs. However, we did have the opportunity to infect the iMacs and assess cytokine secretion. The CFU readout showed no noticeable differences compared to primary monocytes, although this was based on a single experiment. Interestingly, we did not detect any secreted proinflammatory cytokines in iMacs cultures, regardless of whether they were infected or not.

Although the central focus of this thesis is to study primary monocytes, the findings generated potential value for transitioning studies with iMacs. Only by addressing the limitations identified in this preliminary study, with the minimal amount of work on these cells. However, working with iMacs treated with GM-CSF and infected with *C. albicans* would represent an important next step in

validating and expanding on the observations made in this thesis. This offers consistency and flexibility in studying innate immunity to fungal pathogens.

6. Limitations and future directions

This study offers valuable insights into how GM-CSF affects the response of monocytes to *C. albicans*; however, several limitations should be acknowledged. While treating monocytes with GM-CSF influenced cytokine secretion and fungal control, some molecular pathways, such as the expression of other PRRs, signalling cascades, or metabolic changes, were not thoroughly investigated. Additionally, because each infection assay took a week, the limited number of donors may not adequately account for the variety of individual immunological diversity. Furthermore, this study focused on the cellular responses of GM-CSF–treated monocytes during early-stage infection with *C. albicans* (up to 3 hours). It did not assess either long-term infection or kinetic effects. The study includes planktonic cell forms of *C. albicans* (hypha and yeast), while biofilm cells are far more hazardous and harmful [429]. Thus, running a study involving biofilm formation will provide a new approach for biofilm immunotherapy. Throughout the project, we conducted all experiments in the presence of human serum to maintain physiological relevance. It would be of interest to perform studies in the absence of serum, thereby eliminating the potential interference of serum proteins, such as immunoglobulins. X-vivo-15 would provide a convenient environment as well as serum-free media. Another limitation of this study is that CD45, CD14, and CD16 were not investigated in either uninfected or infected monocytes. Including these markers alongside CD11b in the phagocytosis assays would have provided stronger support for the interpretation of CD11b expression.

CLEC5A expression has not yet been studied in relation to fungal infection; nevertheless, it has been demonstrated that it is highly expressed in GM-CSF monocytes and differentiated macrophages [430]. Our model's detection of CLEC5A expression provided a valuable opportunity to initiate investigating its potential function in the response to *C. albicans*, in conjunction with CD11b. A better understanding of the molecular mechanisms underlying antifungal immunity may be gained by investigating this receptor in relation to GM-CSF-driven monocyte activation.

7. General conclusion.

In conclusion, this thesis highlights the modulatory effect of GM-CSF on monocytes during *C. albicans* infection, shedding light on how this cytokine shapes the antifungal response of human monocytes. The findings from this study suggest that GM-CSF activates monocytes by enhancing cytokine and chemokine secretion, upregulating key inflammatory receptors, and regulating hyphal length. Overall, this study aims to gain a deeper understanding of this cytokine, thereby opening new avenues for exploring strategic adjuvants and immunotherapies.

References

1. Reddy, G.K.K., A.R. Padmavathi, and Y.V. Nancharaiah, *Fungal infections: Pathogenesis, antifungals and alternate treatment approaches.* Current research in microbial sciences, 2022. **3**: p. 100137-100137.
2. Perlroth, J., B. Choi, and B. Spellberg, *Nosocomial fungal infections: epidemiology, diagnosis, and treatment.* Medical mycology (Oxford), 2007. **45**(4): p. 321-346.
3. Wilson, L.S., et al., *The Direct Cost and Incidence of Systemic Fungal Infections.* Value in health, 2002. **5**(1): p. 26-34.
4. Haque, M., et al., *Health care-associated infections – An overview.* Infection and drug resistance, 2018. **11**: p. 2321-2333.
5. Keenan, J.E., et al., *The Preventive Surgical Site Infection Bundle in Colorectal Surgery: An Effective Approach to Surgical Site Infection Reduction and Health Care Cost Savings.* JAMA surgery, 2014. **149**(10): p. 1045-1052.
6. Turner, S.A. and G. Butler, *The Candida pathogenic species complex.* Cold Spring Harbor perspectives in medicine, 2014. **4**(9): p. a019778-a019778.
7. Marunaka, Y., *The Proposal of Molecular Mechanisms of Weak Organic Acids Intake-Induced Improvement of Insulin Resistance in Diabetes Mellitus via Elevation of Interstitial Fluid pH.* International journal of molecular sciences, 2018. **19**(10): p. 3244.
8. Fukuda, T., et al., *Effect of Brazilian green propolis in patients with type 2 diabetes: A double-blind randomized placebo-controlled study.* Biomedical reports, 2015. **3**(3): p. 355-360.
9. Sherrington, S.L., et al., *Adaptation of Candida albicans to environmental pH induces cell wall remodelling and enhances innate immune recognition.* PLoS Pathog, 2017. **13**(5): p. e1006403.
10. Jordens, R., et al., *Human dendritic cells shed a functional, soluble form of the mannose receptor.* International immunology, 1999. **11**(11): p. 1775-1780.
11. Gunsalus, K.T.W., et al., *Manipulation of host diet to reduce gastrointestinal colonization by the opportunistic pathogen Candida albicans.* mSphere, 2016. **1**(1).
12. Fisher, M.C., et al., *Tackling the emerging threat of antifungal resistance to human health.* Nature reviews. Microbiology, 2022. **20**(9): p. 557-571.
13. Nash, A.K., et al., *The gut mycobiome of the Human Microbiome Project healthy cohort.* Microbiome, 2017. **5**(1): p. 153-153.
14. d'Enfert, C., et al., *The impact of the Fungus-Host-Microbiota interplay upon Candida albicans infections: current knowledge and new perspectives.* FEMS microbiology reviews, 2021. **45**(3): p. 1.
15. Suryana, K., H. Suharsono, and I.G.P.J. Antara, *Factors associated with oral candidiasis in people living with HIV/AIDS: A case control study.* HIV/AIDS (Auckland), 2020. **12**: p. 33-39.
16. Vila, T., et al., *Oral Candidiasis: A Disease of Opportunity.* Journal of fungi (Basel), 2020. **6**(1): p. 15.
17. Talapko, J., et al., *Candida albicans—The Virulence Factors and Clinical Manifestations of Infection.* Journal of fungi (Basel), 2021. **7**(2): p. 79-19.

18. Spinillo, A., et al., *Epidemiologic characteristics of women with idiopathic recurrent vulvovaginal candidiasis.* Obstetrics and gynecology (New York. 1953), 1993. **81**(5 I): p. 721-727.
19. Swamiappan, M., *Anogenital Pruritus – An Overview.* Journal of clinical and diagnostic research, 2016. **10**(4): p. WE01-WE03.
20. Dadar, M., et al., *Candida albicans - Biology, molecular characterization, pathogenicity, and advances in diagnosis and control – An update.* Microbial pathogenesis, 2018. **117**: p. 128-138.
21. Jabra-Rizk, M.A., et al., *Candida albicans pathogenesis: Fitting within the host-microbe damage response framework.* Infection and immunity, 2016. **84**(10): p. 2724-2739.
22. Li, Y., et al., *A pharmacokinetic/pharmacodynamic mathematical model accurately describes the activity of voriconazole against Candida spp. in vitro.* International journal of antimicrobial agents, 2007. **31**(4): p. 369-374.
23. Lionakis, M.S. and M.G. Netea, *Candida and host determinants of susceptibility to invasive candidiasis.* PLoS pathogens, 2013. **9**(1): p. e1003079-e1003079.
24. Sudbery, P.E., *Growth of Candida albicans hyphae.* Nature reviews. Microbiology, 2011. **9**(10): p. 737-748.
25. Bourgeois, C. and K. Kuchler, *Fungal pathogens-a sweet and sour treat for toll-like receptors.* Frontiers in cellular and infection microbiology, 2012. **2**: p. 142-142.
26. Wilson, D., et al., *Identifying infection-associated genes of Candida albicans in the postgenomic era.* FEMS yeast research, 2009. **9**(5): p. 688-700.
27. Gow, N.A.R. and B. Hube, *Importance of the Candida albicans cell wall during commensalism and infection.* Current opinion in microbiology, 2012. **15**(4): p. 406-412.
28. Phan, Q.T., et al., *Als3 Is a Candida albicans Invasin That Binds to Cadherins and Induces Endocytosis by Host Cells.* PLoS biology, 2007. **5**(3): p. e64-0557.
29. Lowman, D.W., et al., *Novel Structural Features in Candida albicans Hyphal Glucan Provide a Basis for Differential Innate Immune Recognition of Hyphae Versus Yeast.* The Journal of biological chemistry, 2014. **289**(6): p. 3432-3443.
30. Davidson, L., M.G. Netea, and B.J. Kullberg, *Patient Susceptibility to Candidiasis-A Potential for Adjunctive Immunotherapy.* Journal of fungi (Basel), 2018. **4**(1): p. 9.
31. Brown, G.D., et al., *Dectin-1 is a major β-glucan receptor on macrophages.* The Journal of experimental medicine, 2002. **196**(3): p. 407-412.
32. Brown, G.D. and S. Gordon, *Immune recognition of fungal β-glucans.* Cellular microbiology, 2005. **7**(4): p. 471-479.
33. Wheeler, R.T., et al., *Dynamic, Morphotype-Specific Candida albicans β-Glucan Exposure during Infection and Drug Treatment.* PLoS pathogens, 2008. **4**(12): p. e1000227-e1000227.
34. Wani, S.M., et al., *β-Glucan: A dual regulator of apoptosis and cell proliferation.* International journal of biological macromolecules, 2021. **182**: p. 1229-1237.
35. Cheng, S.C., et al., *The dectin-1/inflammasome pathway is responsible for the induction of protective T-helper 17 responses that discriminate*

between yeasts and hyphae of Candida albicans. Journal of leukocyte biology, 2011. **90**(2): p. 357-366.
36. Braun, P.C. and R.A. Calderone, *Chitin Synthesis in Candida albicans: Comparison of Yeast and Hyphal Forms.* Journal of Bacteriology, 1978. **133**(3): p. 1472-1477.
37. Shibata, N., et al., *Chemical structure of the cell-wall mannan of Candida albicans serotype A and its difference in yeast and hyphal forms.* Biochemical journal, 2007. **404**(3): p. 365-372.
38. Garcia-Rubio, R., et al., *The Fungal Cell Wall: Candida, Cryptococcus, and Aspergillus Species.* Frontiers in microbiology, 2020. **10**: p. 2993-2993.
39. Verma-Gaur, J. and A. Traven, *Post-transcriptional gene regulation in the biology and virulence of Candida albicans.* Cellular microbiology, 2016. **18**(6): p. 800-806.
40. Lu, Y., C. Su, and H. Liu, *Candida albicans hyphal initiation and elongation.* Trends in microbiology (Regular ed.), 2014. **22**(12): p. 707-714.
41. Dalle, F., et al., *Cellular interactions of Candida albicans with human oral epithelial cells and enterocytes.* Cellular microbiology, 2010. **12**(2): p. 248-271.
42. Lorenz, M.C., J.A. Bender, and G.R. Fink, *Transcriptional Response of Candida albicans upon Internalization by Macrophages.* Eukaryotic Cell, 2004. **3**(5): p. 1076-1087.
43. Laprade, D., et al., *Filamentation protects Candida albicans from amphotericin B-induced programmed cell death via a mechanism involving the yeast metacaspase, MCA1.* Microbial cell, 2016. **3**(7): p. 285-292.
44. Ghannoum, M., et al., *The Role of Echinocandins in Candida Biofilm–Related Vascular Catheter Infections: In Vitro and In Vivo Model Systems.* Clinical infectious diseases, 2015. **61**(suppl_6): p. S618-S621.
45. Lohse, M.B., et al., *Development and regulation of single-and multi-species Candida albicans biofilms.* Nature reviews. Microbiology, 2018. **16**(1): p. 19-31.
46. Winter, M.B., et al., *Global Identification of Biofilm-Specific Proteolysis in Candida albicans.* mBio, 2016. **7**(5).
47. Wolcott, R., et al., *The polymicrobial nature of biofilm infection.* Clinical microbiology and infection, 2013. **19**(2): p. 107-112.
48. Fourie, R., et al., *Candida albicans and Pseudomonas aeruginosa interaction, with focus on the role of eicosanoids.* Frontiers in physiology, 2016. **7**: p. 64-64.
49. Rajendran, R., et al., *Biofilm formation is a risk factor for mortality in patients with Candida albicans bloodstream infection—Scotland, 2012–2013.* Clinical microbiology and infection, 2016. **22**(1): p. 87-93.
50. Lohse, M.B., et al., *Development and regulation of single- and multi-species Candida albicans biofilms.* Nature reviews. Microbiology, 2018. **16**(1): p. 19-31.
51. Pereira, R., et al., *Biofilm of Candida albicans: formation, regulation and resistance.* Journal of applied microbiology, 2021. **131**(1): p. 11-22.
52. Thomas, R.E. and B.C. Thomas, *Reducing biofilm infections in burn patients' wounds and biofilms on surfaces in hospitals, medical facilities and medical equipment to improve burn care: A systematic*

review. International journal of environmental research and public health, 2021. **18**(24): p. 13195.
53. Gulati, M. and C.J. Nobile, *Candida albicans biofilms: development, regulation, and molecular mechanisms.* Microbes and infection, 2016. **18**(5): p. 310-321.
54. Fox, E., et al., *Biofilms and Antifungal Resistance*. 2015. p. 71-90.
55. Akins, R.A., *An update on antifungal targets and mechanisms of resistance in Candida albicans.* Medical mycology (Oxford), 2005. **43**(4): p. 285-318.
56. Peman, J., E. Canton, and A. Espinel-Ingroff, *Antifungal drug resistance mechanisms.* Expert review of anti-infective therapy, 2009. **7**(4): p. 453-460.
57. Pappas, P.G., et al., *Clinical Practice Guideline for the Management of Candidiasis: 2016 Update by the Infectious Diseases Society of America.* Clinical infectious diseases, 2016. **62**(4): p. 409-417.
58. Kritikos, A., et al., *Accuracy of Sensititre YeastOne echinocandins epidemiological cut-off values for identification of FKS mutant Candida albicans and Candida glabrata: a ten year national survey of the Fungal Infection Network of Switzerland (FUNGINOS).* Clinical Microbiology and Infection, 2018. **24**(11): p. 1214.e1-1214.e4.
59. Hart, A.R., et al., *The role of extracellular vesicles in endometrial receptivity and their potential in reproductive therapeutics and diagnosis.* Reproductive biology, 2022. **22**(2): p. 100645.
60. Hokken, M.W.J., et al., *Facilitators of adaptation and antifungal resistance mechanisms in clinically relevant fungi.* Fungal genetics and biology, 2019. **132**: p. 103254-103254.
61. Silva, S.C., et al., *Candida species biofilms' antifungal resistance.* Journal of fungi (Basel), 2017. **3**(1, 8): p. 1-17.
62. Nobile, C.J., A.D. Johnson, and S. Gottesman, *Candida albicans Biofilms and Human Disease.* Annual review of microbiology, 2015. **69**(1): p. 71-92.
63. Mukaremera, L., et al., *Candida albicans yeast, pseudohyphal, and hyphal morphogenesis differentially affects immune recognition.* Frontiers in immunology, 2017. **8**: p. 629-629.
64. Dobbs, K.R., J.N. Crabtree, and A.E. Dent, *Innate immunity to malaria—The role of monocytes.* Immunological reviews, 2020. **293**(1): p. 8-24.
65. Maza, P.K., et al., *Candida albicans: The ability to invade epithelial cells and survive under oxidative stress is unlinked to hyphal length.* Frontiers in microbiology, 2017. **8**: p. 1235-1235.
66. Gow, N.A., et al., *Candida albicans morphogenesis and host defence: discriminating invasion from colonization.* Nature reviews. Microbiology, 2011. **10**(2): p. 112-22.
67. Marchiando, A.M., et al., *Caveolin-1—dependent occludin endocytosis is required for TNF-induced tight junction regulation in vivo.* The Journal of cell biology, 2010. **189**(1): p. 111-126.
68. Coates, M., S. Blanchard, and A.S. MacLeod, *Innate antimicrobial immunity in the skin: A protective barrier against bacteria, viruses, and fungi.* PLoS pathogens, 2018. **14**(12): p. e1007353-e1007353.
69. Draelos, Z.D.M.D., *New treatments for restoring impaired epidermal barrier permeability: Skin barrier repair creams.* Clinics in dermatology, 2012. **30**(3): p. 345-348.

70. Constant, D.A., T.J. Nice, and I. Rauch, *Innate immune sensing by epithelial barriers.* Current opinion in immunology, 2021. **73**: p. 1-8.
71. Carroll, M.C., *The complement system in regulation of adaptive immunity.* Nature immunology, 2004. **5**(10): p. 981-986.
72. Sego, T.J., et al., *A modular framework for multiscale, multicellular, spatiotemporal modeling of acute primary viral infection and immune response in epithelial tissues and its application to drug therapy timing and effectiveness.* PLoS computational biology, 2020. **16**(12): p. e1008451-e1008451.
73. Alvarez-Rueda, N., et al., *In vitro immune responses of human PBMCs against Candida albicans reveals fungal and leucocyte phenotypes associated with fungal persistence.* Sci Rep, 2020. **10**(1): p. 6211.
74. Wang, Y., et al., *Innate immune responses against the fungal pathogen Candida auris.* Nature Communications, 2022. **13**(1): p. 3553.
75. Netea, M.G. and L. Maródi, *Innate immune mechanisms for recognition and uptake of Candida species.* Trends in immunology, 2010. **31**(9): p. 346-353.
76. Drummond, R.A., et al., *Innate defense against fungal pathogens.* Cold Spring Harbor perspectives in medicine, 2015. **5**(6): p. 1-19.
77. Zindel, J. and P. Kubes, *DAMPs, PAMPs, and LAMPs in Immunity and Sterile Inflammation.* Annual review of pathology, 2020. **15**(1): p. 493-518.
78. Weng, J., C. Couture, and S. Girard, *Innate and Adaptive Immune Systems in Physiological and Pathological Pregnancy.* Biology (Basel, Switzerland), 2023. **12**(3): p. 402.
79. Schmidt, A., S. Endres, and S. Rothenfusser, *Pattern recognition of viral nucleic acids by RIG-I-like helicases.* Journal of molecular medicine (Berlin, Germany), 2010. **89**(1): p. 5-12.
80. Gurung, P. and T.-D. Kanneganti, *Novel Roles for Caspase-8 in IL-1β and Inflammasome Regulation.* American Journal of Pathology, 2015. **185**(1): p. 17-25.
81. Chen, R., et al., *Pattern recognition receptors: function, regulation and therapeutic potential.* Signal Transduction and Targeted Therapy, 2025. **10**(1): p. 216.
82. Girardi, G., et al., *Essential Role of Complement in Pregnancy: From Implantation to Parturition and Beyond.* Frontiers in immunology, 2020. **11**: p. 1681-1681.
83. Cheng, S.C., et al., *Complement plays a central role in Candida albicans-induced cytokine production by human PBMCs.* European journal of immunology, 2012. **42**(4): p. 993-1004.
84. Harpf, V., et al., *Candida and Complement: New Aspects in an Old Battle.* Frontiers in immunology, 2020. **11**: p. 1471.
85. Mödinger, Y., et al., *Role of the Complement System in the Response to Orthopedic Biomaterials.* International journal of molecular sciences, 2018. **19**(11): p. 3367.
86. Van Bruggen, R., et al., *Complement receptor 3, not Dectin-1, is the major receptor on human neutrophils for b-glucan-bearing particles.* Molecular immunology, 2009. **47**(2-3): p. 575-581.
87. Kashem, S.W., et al., *Candida albicans morphology and dendritic cell subsets determine T helper cell differentiation.* Immunity (Cambridge, Mass.), 2015. **42**(2): p. 356-366.
88. Zelensky, A.N. and J.E. Gready, *The C-type lectin-like domain superfamily.* The FEBS journal, 2005. **272**(24): p. 6179-6217.

89. Sancho, D., C. Reis e Sousa, and W.E. Paul, *Signaling by Myeloid C-Type Lectin Receptors in Immunity and Homeostasis.* Annual Review of Immunology, 2012. **30**(1): p. 491-529.
90. Kalia, N., J. Singh, and M. Kaur, *The ambiguous role of mannose-binding lectin (MBL) in human immunity.* Open medicine (Warsaw, Poland), 2021. **16**(1): p. 299-310.
91. Miller, A., et al., *Near-planar Solution Structures of Mannose-binding Lectin Oligomers Provide Insight on Activation of Lectin Pathway of Complement.* The Journal of biological chemistry, 2012. **287**(6): p. 3930-3945.
92. Drickamer, K., *C-type lectin-like domains.* Current Opinion in Structural Biology, 1999. **9**(5): p. 585-590.
93. He, L.-Z., et al., *Antigenic Targeting of the Human Mannose Receptor Induces Tumor Immunity.* Journal of Immunology, 2007. **178**(10): p. 6259-6267.
94. Ariizumi, K., et al., *Cloning of a Second Dendritic Cell-associated C-type Lectin (Dectin-2) and Its Alternatively Spliced Isoforms.* The Journal of biological chemistry, 2000. **275**(16): p. 11957-11963.
95. Kingeter, L.M. and X. Lin, *C-type lectin receptor-induced NF-κB activation in innate immune and inflammatory responses.* Cellular & molecular immunology, 2012. **9**(2): p. 105-112.
96. Martinez-Pomares, L., G. Mantovani, and P.D. Stahl, *The Mannose Receptor (CD206) and Its Siblings-The Back Story*, in *Encyclopedia of Cell Biology (Second Edition)*, R.A. Bradshaw, G.W. Hart, and P.D. Stahl, Editors. 2023, Academic Press: Oxford. p. 525-542.
97. Luisa, M.-P., *The mannose receptor.* Journal of leukocyte biology, 2012. **92**(6): p. 1177-1186.
98. van der Zande, H.J., et al., *The mannose receptor: from endocytic receptor and biomarker to regulator of (meta) inflammation.* Frontiers in Immunology, 2021. **12**: p. 765034.
99. Martinez-Pomares, L., et al., *Carbohydrate-independent recognition of collagens by the macrophage mannose receptor.* European Journal of Immunology, 2006. **36**(5): p. 1074-1082.
100. Martínez-Pomares, L., et al., *A Functional Soluble Form of the Murine Mannose Receptor Is Produced by Macrophages in Vitro and Is Present in Mouse Serum.* The Journal of biological chemistry, 1998. **273**(36): p. 23376-23380.
101. Llorca, O., *Extended and bent conformations of the mannose receptor family.* Cellular and Molecular Life Sciences, 2008. **65**(9): p. 1302-1310.
102. Harris, N., et al., *Characterization of the Murine Macrophage Mannose Receptor: Demonstration That the Downregulation of Receptor Expression Mediated by Interferon-γ Occurs at the Level of Transcription.* Blood, 1992. **80**(9): p. 2363-2373.
103. Forsyth, C.B., E.F. Plow, and L. Zhang, *Interaction of the Fungal Pathogen Candida albicans with Integrin CD11b/CD18: Recognition by the I Domain Is Modulated by the Lectin-Like Domain and the CD18 Subunit.* The Journal of immunology (1950), 1998. **161**(11): p. 6198-6205.
104. Veerdonk, F.L.v.d., et al., *The macrophage mannose receptor induces IL-17 in response to Candida albicans.* Cell host & microbe, 2009. **5**(4): p. 329-40.

105. Gazi, U. and L. Martinez-Pomares, *Influence of the mannose receptor in host immune responses.* Immunobiology (1979), 2009. **214**(7): p. 554-561.
106. Polando, R.E., et al., *Mannose receptor (MR) and Toll-like receptor 2 (TLR2) influence phagosome maturation during Leishmania infection.* Parasite immunology, 2018. **40**(4): p. e12521-n/a.
107. Heinsbroek, S.E.M., et al., *Stage-specific sampling by pattern recognition receptors during Candida albicans phagocytosis.* PLoS pathogens, 2008. **4**(11): p. e1000218-e1000218.
108. Takahara, K., et al., *C-type lectin SIGNR1 enhances cellular oxidative burst response against C. albicans in cooperation with Dectin-1.* European journal of immunology, 2011. **41**(5): p. 1435-1444.
109. Khoo, U.-S., et al., *DC-SIGN and L-SIGN: the SIGNs for infection.* Journal of Molecular Medicine, 2008. **86**(8): p. 861-874.
110. Ayodele, S., et al., *Advances in immunomodulatory strategies for host-directed therapies in combating tuberculosis.* Biomedicine & pharmacotherapy, 2023. **162**: p. 114588.
111. Sainz, J., et al., *Dectin-1 and DC-SIGN Polymorphisms Associated with Invasive Pulmonary Aspergillosis Infection.* PloS one, 2012. **7**(2): p. e32273-e32273.
112. Rogers, N.C., et al., *Syk-Dependent Cytokine Induction by Dectin-1 Reveals a Novel Pattern Recognition Pathway for C Type Lectins.* Immunity (Cambridge, Mass.), 2005. **22**(6): p. 773-774.
113. Ortiz, M.A., et al., *Src family kinases, adaptor proteins and the actin cytoskeleton in epithelial-to-mesenchymal transition.* Cell communication and signaling, 2021. **19**(1): p. 67-19.
114. Strasser, D., et al., *Syk Kinase-Coupled C-type Lectin Receptors Engage Protein Kinase C-δ to Elicit Card9 Adaptor-Mediated Innate Immunity.* Immunity (Cambridge, Mass.), 2012. **36**(1): p. 32-42.
115. Sato, K., et al., *Dectin-2 Is a Pattern Recognition Receptor for Fungi That Couples with the Fc Receptor γ Chain to Induce Innate Immune Responses.* The Journal of biological chemistry, 2006. **281**(50): p. 38854-38866.
116. Bertin, J., et al., *CARD9 Is a Novel Caspase Recruitment Domain-containing Protein That Interacts With BCL10/CLAP and Activates NF-κB.* The Journal of biological chemistry, 2000. **275**(52): p. 41082-41086.
117. Hughes, C.E., et al., *Critical Role for an Acidic Amino Acid Region in Platelet Signaling by the HemITAM (Hemi-immunoreceptor Tyrosine-based Activation Motif) Containing Receptor CLEC-2 (C-type Lectin Receptor-2).* The Journal of biological chemistry, 2013. **288**(7): p. 5127-5135.
118. Gringhuis, S.I., et al., *Dectin-1 directs T helper cell differentiation by controlling noncanonical NF-kappaB activation through Raf-1 and Syk.* Nature immunology, 2009. **10**(2): p. 203-213.
119. del Fresno, C., et al., *Interferon-β production via Dectin-1-Syk-IRF5 signaling in dendritic cells is crucial for immunity to C. albicans.* Immunity, 2013. **38**(6): p. 1176-1186.
120. Chen, S.M., et al., *The critical role of dectin-1 in host controlling systemic candida krusei infection.* American journal of translational research, 2019. **11**(2): p. 721-732.

121. Ferwerda, G., et al., *Human Dectin-1 Deficiency and Mucocutaneous Fungal Infections.* The New England journal of medicine, 2009. **361**(18): p. 1760-1767.
122. Cunha, C., et al., *Dectin-1 Y238X polymorphism associates with susceptibility to invasive aspergillosis in hematopoietic transplantation through impairment of both recipient- and donor-dependent mechanisms of antifungal immunity.* Blood, 2010. **116**(24): p. 5394-5402.
123. Taylor, P.R., et al., *Dectin-2 is predominantly myeloid restricted and exhibits unique activation-dependent expression on maturing inflammatory monocytes elicited in vivo.* European journal of immunology, 2005. **35**(7): p. 2163-2174.
124. Gringhuis, S.I., et al., *Selective C-Rel Activation via Malt1 Controls Anti-Fungal T-H-17 Immunity by Dectin-1 and Dectin-2.* PLoS pathogens, 2011. **7**(1).
125. Drummond, R., et al., *The role of Syk/CARD9 coupled C-type lectins in antifungal immunity.* European journal of immunology, 2011. **41**: p. 276-81.
126. Robinson, M.J., et al., *Dectin-2 is a Syk-coupled pattern recognition receptor crucial for Th17 responses to fungal infection.* Journal of Experimental Medicine, 2009. **206**(9): p. 2037-2051.
127. McGreal, E.P., et al., *The carbohydrate-recognition domain of Dectin-2 is a C-type lectin with specificity for high mannose.* Glycobiology (Oxford), 2006. **16**(5): p. 422-430.
128. Gow, N.A.R., et al., *Immune Recognition of Candida albicans β-glucan by Dectin-1.* The Journal of infectious diseases, 2007. **196**(10): p. 1565-1571.
129. Wells, C.A., et al., *The Macrophage-Inducible C-Type Lectin, Mincle, Is an Essential Component of the Innate Immune Response to Candida albicans.* The Journal of immunology (1950), 2008. **180**(11): p. 7404-7413.
130. Vijayan, D., et al., *Mincle polarizes human monocyte and neutrophil responses to Candida albicans.* Immunology and cell biology, 2012. **90**(9): p. 889-895.
131. Bates, E.E.M., et al., *APCs Express DCIR, a Novel C-Type Lectin Surface Receptor Containing an Immunoreceptor Tyrosine-Based Inhibitory Motif.* The Journal of immunology (1950), 1999. **163**(4): p. 1973-1983.
132. Yoshikawa, F.S.Y., et al., *The C-type lectin receptor Dcir (Clec4a2) restrains Aspergillus fumigatus elimination by limiting the degranulatory activity of neutrophils.* Frontiers in immunology, 2025. **16**.
133. Trimaglio, G., et al., *The C-type lectin DCIR contributes to the immune response and pathogenesis of colorectal cancer.* Scientific reports, 2024. **14**(1): p. 7199-7199.
134. Colonna, M., *DAP12 signaling: from immune cells to bone modeling and brain myelination.* The Journal of clinical investigation, 2003. **111**(3): p. 313-314.
135. Watson, A.A. and C.A. O'Callaghan, *Crystallization and X-ray diffraction analysis of human CLEC5A (MDL-1), a dengue virus receptor.* Acta crystallographica. Section F, Structural biology and crystallization communications, 2010. **66**(1): p. 29-31.
136. Chen, S.-T., et al., *CLEC5A is critical for dengue-virus-induced lethal disease.* Nature, 2008. **453**(7195): p. 672-676.

137. Wu, M.-F., et al., *CLEC5A is critical for dengue virus–induced inflammasome activation in human macrophages.* Blood, 2013. **121**(1): p. 95-106.
138. Chen, S.-T., et al., *CLEC5A Regulates Japanese Encephalitis Virus-Induced Neuroinflammation and Lethality.* PLoS pathogens, 2012. **8**(4): p. e1002655-e1002655.
139. Teng, O., et al., *CLEC5A-Mediated Enhancement of the Inflammatory Response in Myeloid Cells Contributes to Influenza Virus Pathogenicity In Vivo.* Journal of virology, 2017. **91**(1).
140. Fitzgerald, K.A. and J.C. Kagan, *Toll-like Receptors and the Control of Immunity.* Cell, 2020. **180**(6): p. 1044-1066.
141. Randow, F. and B. Seed, *Endoplasmic reticulum chaperone gp96 is required for innate immunity but not cell viability.* Nature cell biology, 2001. **3**(10): p. 891-896.
142. Choteau, L., et al., *Role of TLR1, TLR2 and TLR6 in the modulation of intestinal inflammation and Candida albicans elimination.* Gut pathogens, 2017. **9**(1): p. 9-9.
143. Herscovics, A., *Importance of glycosidases in mammalian glycoprotein biosynthesis.* Biochimica et Biophysica Acta (BBA) - General Subjects, 1999. **1473**(1): p. 96-107.
144. von Bernuth, H., et al., *Pyogenic Bacterial Infections in Humans with MyD88 Deficiency.* Science (American Association for the Advancement of Science), 2008. **321**(5889): p. 691-696.
145. Fitzgerald, K.A., et al., *LPS-TLR4 signaling to IRF-3/7 and NF-kappaB involves the toll adapters TRAM and TRIF.* J Exp Med, 2003. **198**(7): p. 1043-55.
146. Liu, S., et al., *Phosphorylation of innate immune adaptor proteins MAVS, STING, and TRIF induces IRF3 activation.* Science (American Association for the Advancement of Science), 2015. **347**(6227): p. 1217-1217.
147. Yamamoto, M., et al., *TRAM is specifically involved in the Toll-like receptor 4–mediated MyD88-independent signaling pathway.* Nature immunology, 2003. **4**(11): p. 1144-1150.
148. Anwar, M.A., S. Basith, and S. Choi, *Negative regulatory approaches to the attenuation of Toll-like receptor signaling.* Experimental & molecular medicine, 2013. **45**(2): p. e11-e11.
149. Bishu, S., et al., *The Adaptor CARD9 Is Required for Adaptive but Not Innate Immunity to Oral Mucosal Candida albicans Infections.* Infection and Immunity, 2014. **82**(3): p. 1173-1180.
150. Wang, Y., et al., *The adaptor protein CARD9, from fungal immunity to tumorigenesis.* Am J Cancer Res, 2020. **10**(8): p. 2203-2225.
151. Li, X., et al., *PKC-δ activation in neutrophils promotes fungal clearance.* Journal of leukocyte biology, 2016. **100**(3): p. 581-588.
152. Németh, T., et al., *Neutrophil-specific deletion of the CARD9 gene expression regulator suppresses autoantibody-induced inflammation in vivo.* Nature communications, 2016. **7**(1): p. 11004-11004.
153. Drummond, R.A., et al., *CARD9-Dependent Neutrophil Recruitment Protects against Fungal Invasion of the Central Nervous System: e1005293.* PLoS pathogens, 2015. **11**(12).
154. Wu, W., et al., *CARD9 facilitates microbe-elicited production of reactive oxygen species by regulating the LyGDI-Rac1 complex.* Nature immunology, 2009. **10**(11): p. 1208-1214.

155. Rivas, M.A., et al., *Deep resequencing of GWAS loci identifies independent rare variants associated with inflammatory bowel disease.* Nature genetics, 2011. **43**(11): p. 1066-1073.
156. Drummond, R.A. and M.S. Lionakis, *Mechanistic insights into the role of C-type lectin receptor/CARD9 signaling in human antifungal immunity.* Frontiers in cellular and infection microbiology, 2016. **6**: p. 39-39.
157. Roth, S., et al., *Vav Proteins Are Key Regulators of Card9 Signaling for Innate Antifungal Immunity.* Cell reports (Cambridge), 2016. **17**(10): p. 2572-2583.
158. Glocker, E.-O., et al., *A Homozygous CARD9 Mutation in a Family with Susceptibility to Fungal Infections.* The New England journal of medicine, 2009. **361**(18): p. 1727-1735.
159. Gavino, C.M., et al., *Impaired RASGRF1/ERK–mediated GM-CSF response characterizes CARD9 deficiency in French-Canadians.* Journal of allergy and clinical immunology, 2015. **137**(4): p. 1178-1188.e7.
160. Rodriguez, R.M., et al., *Signal Integration and Transcriptional Regulation of the Inflammatory Response Mediated by the GM-/M-CSF Signaling Axis in Human Monocytes.* Cell reports (Cambridge), 2019. **29**(4): p. 860-872.e5.
161. Drummond, R.A., et al., *GM-CSF therapy in human caspase recruitment domain–containing protein 9 deficiency.* Journal of allergy and clinical immunology, 2018. **142**(4): p. 1334-1338.e5.
162. Drummond, R.A., L.M. Franco, and M.S. Lionakis, *Human CARD9: A critical molecule of fungal immune surveillance.* Frontiers in immunology, 2018. **9**: p. 1836-1836.
163. Martinon, F., K. Burns, and J. Tschopp, *The inflammasome: a molecular platform triggering activation of inflammatory caspases and processing of proIL-beta.* Mol Cell, 2002. **10**(2): p. 417-26.
164. Kummer, J.A., et al., *Inflammasome components NALP 1 and 3 show distinct but separate expression profiles in human tissues suggesting a site-specific role in the inflammatory response.* J Histochem Cytochem, 2007. **55**(5): p. 443-52.
165. Saxena, M. and G. Yeretssian, *NOD-Like Receptors: Master Regulators of Inflammation and Cancer.* Frontiers in immunology, 2014. **5**: p. 327.
166. Joly, S., et al., *Cutting Edge: Candida albicans Hyphae Formation Triggers Activation of the Nlrp3 Inflammasome.* The Journal of immunology (1950), 2009. **183**(6): p. 3578-3581.
167. Wellington, M., et al., *Candida albicans Triggers NLRP3-Mediated Pyroptosis in Macrophages.* Eukaryotic Cell, 2014. **13**(2): p. 329-340.
168. Kanazawa, N., K. Tashiro, and Y. Miyachi, *Signaling and immune regulatory role of the dendritic cell immunoreceptor (DCIR) family lectins: DCIR, DCAR, dectin-2 and BDCA-2.* Immunobiology, 2004. **209**(1): p. 179-190.
169. Hise, A.G., et al., *An Essential Role for the NLRP3 Inflammasome in Host Defense against the Human Fungal Pathogen Candida albicans.* Cell host & microbe, 2009. **5**(5): p. 487-497.
170. Silvis, M.J.M., et al., *Immunomodulation of the NLRP3 Inflammasome in Atherosclerosis, Coronary Artery Disease, and Acute Myocardial Infarction.* Journal of cardiovascular translational research, 2021. **14**(1): p. 23-34.

171. Andreu, Z. and M. Yáñez-Mó, *Tetraspanins in extracellular vesicle formation and function.* Frontiers in immunology, 2014. **5**: p. 442-442.
172. Lee, Y., S. El Andaloussi, and M.J.A. Wood, *Exosomes and microvesicles: extracellular vesicles for genetic information transfer and gene therapy.* Human molecular genetics, 2012. **21**(R1): p. R125-R134.
173. Kulig, K., M. Rapala-Kozik, and J. Karkowska-Kuleta, *Extracellular vesicle production: A bidirectional effect in the interplay between host and Candida fungi.* Current research in microbial sciences, 2024. **7**: p. 100255.
174. Kulig, K., et al., *Host cell responses to Candida albicans biofilm-derived extracellular vesicles.* Frontiers in cellular and infection microbiology, 2025. **14**: p. 1499461.
175. Sabatke, B., et al., *Extracellular vesicles biogenesis and uptake concepts: A comprehensive guide to studying host–pathogen communication.* Molecular microbiology, 2024. **122**(5): p. 613-629.
176. Moyes, D.L. and J.R. Naglik, *Mucosal Immunity and Candida albicans Infection.* Clinical & developmental immunology, 2011. **2011**: p. 1-9.
177. Tkalcevic, J., et al., *Impaired Immunity and Enhanced Resistance to Endotoxin in the Absence of Neutrophil Elastase and Cathepsin G.* Immunity (Cambridge, Mass.), 2000. **12**(2): p. 201-210.
178. Karlsson, M., et al., *Nanoporous aluminum oxide affects neutrophil behaviour.* Microscopy research and technique, 2004. **63**(5): p. 259-265.
179. Feehan, K.T. and D.W. Gilroy, *Is Resolution the End of Inflammation?* Trends in molecular medicine, 2019. **25**(3): p. 198-214.
180. Gazendam, R.P., et al., *Two independent killing mechanisms of Candida albicans by human neutrophils: evidence from innate immunity defects.* Blood, 2014. **124**(4): p. 590-597.
181. Shi, C. and E.G. Pamer, *Monocyte recruitment during infection and inflammation.* Nature reviews. Immunology, 2011. **11**(11): p. 762-774.
182. Domínguez-Andrés, J., et al., *Inflammatory Ly6Chigh Monocytes Protect against Candidiasis through IL-15-Driven NK Cell/Neutrophil Activation.* Immunity (Cambridge, Mass.), 2017. **46**(6): p. 1059-1072.e4.
183. Olingy, C.E., H.Q. Dinh, and C.C. Hedrick, *Monocyte heterogeneity and functions in cancer.* J Leukoc Biol, 2019. **106**(2): p. 309-322.
184. Passlick, B., D. Flieger, and H.W. Ziegler-Heitbrock, *Identification and characterization of a novel monocyte subpopulation in human peripheral blood.* Blood, 1989. **74**(7): p. 2527-34.
185. Chimma, P., et al., *A distinct peripheral blood monocyte phenotype is associated with parasite inhibitory activity in acute uncomplicated Plasmodium falciparum malaria.* PLoS pathogens, 2009. **5**(10): p. e1000631-e1000631.
186. Heung, L.J., *Monocytes and the Host Response to Fungal Pathogens.* Frontiers in cellular and infection microbiology, 2020. **10**: p. 34-34.
187. Lauvau, G., P.n. Loke, and T.M. Hohl, *Monocyte-mediated defense against bacteria, fungi, and parasites.* Seminars in immunology, 2016. **27**(6): p. 397-409.
188. Osterholzer, J.J., et al., *Accumulation of CD11b+ Lung Dendritic Cells in Response to Fungal Infection Results from the CCR2-Mediated Recruitment and Differentiation of Ly-6Chigh Monocytes.* The Journal of immunology (1950), 2009. **183**(12): p. 8044-8053.

189. Zhang, F.-y., N. Lian, and M. Li, *Macrophage pyroptosis induced by Candida albicans.* Pathogens and disease, 2024. **82**.
190. van Lookeren Campagne, M., C. Wiesmann, and E.J. Brown, *Macrophage complement receptors and pathogen clearance.* Cellular Microbiology, 2007. **9**(9): p. 2095-2102.
191. Urb, M. and D.C. Sheppard, *The Role of Mast Cells in the Defence against Pathogens.* PLoS pathogens, 2012. **8**(4): p. e1002619.
192. Figueiredo, R.T. and J.S. Neves, *Eosinophils in fungal diseases: An overview.* J Leukoc Biol, 2018. **104**(1): p. 49-60.
193. Patente, T.A., et al., *Human Dendritic Cells: Their Heterogeneity and Clinical Application Potential in Cancer Immunotherapy.* Frontiers in immunology, 2018. **9**: p. 3176-3176.
194. Ramirez-Ortiz, Z.G. and T.K. Means, *The role of dendritic cells in the innate recognition of pathogenic fungi (A. fumigatus, C. neoformans and C. albicans).* Virulence, 2012. **3**(7): p. 635-646.
195. Bojang, E., et al., *Immune sensing of Candida albicans.* Journal of fungi (Basel), 2021. **7**(2): p. 1-16.
196. Richardson, J.P. and D.L. Moyes, *Adaptive immune responses to Candida albicans infection.* Virulence, 2015. **6**(4): p. 327-337.
197. Shah, H., et al., *Behind the scenes with basophils: an emerging therapeutic target.* Immunother Adv, 2021. **1**(1): p. ltab008.
198. Sutton, C.E., et al., *Interleukin-1 and IL-23 induce innate IL-17 production from gammadelta T cells, amplifying Th17 responses and autoimmunity.* Immunity (Cambridge, Mass.), 2009. **31**(2): p. 331-341.
199. Ouederni, M., et al., *Clinical Features of Candidiasis in Patients With Inherited Interleukin 12 Receptor β1 Deficiency.* Clinical infectious diseases, 2014. **58**(2): p. 204-213.
200. Wich, M., et al., *Functionality of the human antibody response to Candida albicans.* Virulence, 2021. **12**(1): p. 3137-3148.
201. Li, R., et al., *Antibody-Independent Function of Human B Cells Contributes to Antifungal T Cell Responses.* The Journal of immunology (1950), 2017. **198**(8): p. 3245-3254.
202. Li, F.-q., et al., *Diagnostic value of immunoglobulin G antibodies against Candida enolase and fructose-bisphosphate aldolase for candidemia.* BMC infectious diseases, 2013. **13**(1): p. 253-253.
203. Mochon, A.B., et al., *Serological Profiling of a Candida albicans Protein Microarray Reveals Permanent Host-Pathogen Interplay and Stage-Specific Responses during Candidemia.* PLoS pathogens, 2010. **6**(3): p. e1000827.
204. Rudkin, F.M., et al., *Single human B cell-derived monoclonal anti-Candida antibodies enhance phagocytosis and protect against disseminated candidiasis.* Nature communications, 2018. **9**(1): p. 5288-16.
205. Liu, X., et al., *CARD9 Signaling, Inflammation, and Diseases.* Frontiers in immunology, 2022. **13**: p. 880879.
206. Burgess, A.W. and D. Metcalf, *The Nature and Action of Granulocyte-Macrophage Colony Stimulating Factors.* Blood, 1980. **56**(6): p. 947-958.
207. Hamilton, J.A., *Colony-stimulating factors in inflammation and autoimmunity.* Nature reviews. Immunology, 2008. **8**(7): p. 533-544.
208. Mathias, B., et al., *A review of GM-CSF therapy in sepsis.* Medicine (Baltimore), 2015. **94**(50): p. e2044-e2044.

209. Bär, E., et al., *IL-17 Regulates Systemic Fungal Immunity by Controlling the Functional Competence of NK Cells.* Immunity (Cambridge, Mass.), 2014. **40**(1): p. 117-127.
210. Van Overmeire, E., et al., *M-CSF and GM-CSF Receptor Signaling Differentially Regulate Monocyte Maturation and Macrophage Polarization in the Tumor Microenvironment.* Cancer Res, 2016. **76**(1): p. 35-42.
211. Hansen, G., et al., *The Structure of the GM-CSF Receptor Complex Reveals a Distinct Mode of Cytokine Receptor Activation.* Cell, 2008. **134**(3): p. 496-507.
212. Hamilton, J.A., *GM-CSF-Dependent Inflammatory Pathways.* Frontiers in immunology, 2019. **10**: p. 2055-2055.
213. Becher, B., S. Tugues, and M. Greter, *GM-CSF: From Growth Factor to Central Mediator of Tissue Inflammation.* Immunity (Cambridge, Mass.), 2016. **45**(5): p. 963-973.
214. Fischer, H.G., et al., *Granulocyte-macrophage colony-stimulating factor activates macrophages derived from bone marrow cultures to synthesis of MHC class II molecules and to augmented antigen presentation function.* The Journal of immunology (1950), 1988. **141**(11): p. 3882-3888.
215. Hayes, M.P. and K.C. Zoon, *Priming of human monocytes for enhanced lipopolysaccharide responses: expression of alpha interferon, interferon regulatory factors, and tumor necrosis factor.* Infection and Immunity, 1993. **61**(8): p. 3222-3227.
216. Lendemans, S., et al., *GM-CSF priming of human monocytes is dependent on ERK1/2 activation.* Journal of endotoxin research, 2006. **12**(1): p. 10-20.
217. Fang, Y., et al., *Impaired cutaneous wound healing in granulocyte/ macrophage colony-stimulating factor knockout mice.* British journal of dermatology (1951), 2007. **157**(3): p. 458-465.
218. Hamilton, J.A., *GM-CSF as a target in inflammatory/autoimmune disease: current evidence and future therapeutic potential.* Expert Rev Clin Immunol, 2015. **11**(4): p. 457-65.
219. Giri, S. and A.J. Kindo, *A review of Candida species causing blood stream infection.* Indian journal of medical microbiology, 2012. **30**(3): p. 270-278.
220. Dong, Q., W. Wu, and R. Zhang, *Mechanistic insights into granulocyte-macrophage colony-stimulating factor in combating fungal infections: Diverse fungal pathogens.* Medical mycology (Oxford), 2025. **63**(5).
221. Nguyen, N.Z.N., et al., *CCR5-mediated Recruitment of NK Cells to the Kidney Is a Critical Step for Host Defense to Systemic Candida albicans Infection.* Immune Netw, 2020. **20**(6): p. e49.
222. Knooihuizen, S.A.I., et al., *Loss of Coordinated Neutrophil Responses to the Human Fungal Pathogen, Candida albicans, in Patients With Cirrhosis.* Hepatology communications, 2021. **5**(3): p. 502-515.
223. Neofytos, D., et al., *Epidemiology and Outcome of Invasive Fungal Infection in Adult Hematopoietic Stem Cell Transplant Recipients: Analysis of Multicenter Prospective Antifungal Therapy (PATH) Alliance Registry.* Clinical infectious diseases, 2009. **48**(3): p. 265-273.
224. Sam, Q.H., et al., *Immunomodulation as Therapy for Fungal Infection: Are We Closer?* Frontiers in microbiology, 2018. **9**: p. 1612.
225. Chen, T.K., et al., *Recombinant Human Granulocyte-Macrophage Colony-Stimulating Factor (rhu GM-CSF) as Adjuvant Therapy for*

Invasive Fungal Diseases. Open Forum Infect Dis, 2022. **9**(11): p. ofac535.
226. Bennett, C.L., et al., *Economic analysis of a randomized placebo-controlled phase III study of granulocyte macrophage colony stimulating factor in adult patients (> 55 to 70 years of age) with acute myelogenous leukemia. Eastern Cooperative Oncology Group (E1490).* Ann Oncol, 1999. **10**(2): p. 177-82.
227. McCormick, T.S., et al., *GM-CSF: Orchestrating the Pulmonary Response to Infection.* Frontiers in pharmacology, 2022. **12**: p. 735443-735443.
228. Lew, K., *3.05 - Blood Sample Collection and Handling*, in *Comprehensive Sampling and Sample Preparation*, J. Pawliszyn, Editor. 2012, Academic Press: Oxford. p. 95-121.
229. Mohammadi, Z., S. Shalavi, and H. Jafarzadeh, *Ethylenediaminetetraacetic acid in endodontics.* European journal of dentistry, 2013. **7**(S 01): p. S135-S142.
230. Klinder, A., et al., *Comparison of different cell culture plates for the enrichment of non-adherent human mononuclear cells.* Experimental and therapeutic medicine, 2019. **17**(3): p. 2004-2012.
231. Gomez, N.E., et al., *PBMC-derived extracellular vesicles in a smoking-related inflammatory disease model.* European journal of immunology, 2023. **53**(6): p. e2250143-n/a.
232. Babania, O., et al., *The expansion of CD14+ CD163+ subpopulation of monocytes and myeloid cells-associated cytokine imbalance candidate diagnostic biomarkers for celiac disease (CD).* Journal of clinical laboratory analysis, 2021. **35**(10): p. e23984-n/a.
233. van Wilgenburg, B., et al., *Efficient, Long Term Production of Monocyte-Derived Macrophages from Human Pluripotent Stem Cells under Partly-Defined and Fully-Defined Conditions.* PloS one, 2013. **8**(8): p. e71098-e71098.
234. Pantazis, C.B., et al., *A reference human induced pluripotent stem cell line for large-scale collaborative studies.* Cell stem cell, 2022. **29**(12): p. 1685-1702.e22.
235. Ansari, M.A., et al., *Low monocytic HLA-DR expression in critically ill patients of sepsis: An indicator for antimicrobial and/or immunomodulatory intervention.* Transplant immunology, 2023. **81**: p. 101942-101942.
236. Thompson, A., et al., *The protective effect of inflammatory monocytes during systemic C. Albicans infection is dependent on collaboration between C-type lectin-like receptors.* PLoS pathogens, 2019. **15**(6): p. e1007850-e1007850.
237. Tripathi, S., et al., *Passive blood plasma separation at the microscale: a review of design principles and microdevices.* Journal of micromechanics and microengineering, 2015. **25**(8): p. 83001-24.
238. Lee, D.-H., et al., *An integrated microfluidic platform for size-selective single-cell trapping of monocytes from blood.* Biomicrofluidics, 2018. **12**(5): p. 054104-054104.
239. Delirezh, N. and E. Shojaeefar, *Phenotypic and functional comparison between flask adherent and magnetic activated cell sorted monocytes derived dendritic cells.* Iranian journal of immunology, 2012. **9**(2): p. 98-108.
240. Tang, J., et al., *Regulation of C-Type Lectin Receptor-Mediated Antifungal Immunity.* Frontiers in Immunology, 2018. **9**.

241. Farzam-kia, N., et al., *GM-CSF distinctly impacts human monocytes and macrophages via ERK1/2-dependent pathways.* Immunology Letters, 2023. **261**: p. 47-55.
242. Lacey, D.C., et al., *Defining GM-CSF– and Macrophage-CSF–Dependent Macrophage Responses by In Vitro Models.* The Journal of Immunology, 2012. **188**(11): p. 5752-5765.
243. Hahm, J., J. Kim, and J. Park, *Strategies to Enhance Extracellular Vesicle Production.* Tissue Eng Regen Med, 2021. **18**(4): p. 513-524.
244. Ullah, A., et al., *Characteristics and potential clinical applications of the extracellular vesicles of human pathogenic Fungi.* BMC microbiology, 2023. **23**(1): p. 1-227.
245. Muntaka, S., et al., *Gamma Interferon and Interleukin-17A Differentially Influence the Response of Human Macrophages and Neutrophils to Pseudomonas aeruginosa Infection.* Infect Immun, 2019. **87**(2).
246. Bischoff, F.Z., et al., *Intact fetal cell isolation from maternal blood: improved isolation using a simple whole blood progenitor cell enrichment approach (RosetteSep™).* Clinical genetics, 2003. **63**(6): p. 483-489.
247. Chen, Y.-C., et al., *Withholding of M-CSF Supplement Reprograms Macrophages to M2-Like via Endogenous CSF-1 Activation.* International journal of molecular sciences, 2021. **22**(7): p. 3532.
248. Deville, S., et al., *Macrophages Release Extracellular Vesicles of Different Properties and Composition Following Exposure to Nanoparticles.* International journal of molecular sciences, 2022. **24**(1): p. 260.
249. Lee, K.M.C., A.A. Achuthan, and J.A. Hamilton, *GM-CSF: A Promising Target in Inflammation and Autoimmunity.* Immunotargets Ther, 2020. **9**: p. 225-240.
250. Ushach, I. and A. Zlotnik, *Biological role of granulocyte macrophage colony-stimulating factor (GM-CSF) and macrophage colony-stimulating factor (M-CSF) on cells of the myeloid lineage.* J Leukoc Biol, 2016. **100**(3): p. 481-9.
251. Van Nguyen, T. and A.C. Alfaro, *Applications of flow cytometry in molluscan immunology: Current status and trends.* Fish & shellfish immunology, 2019. **94**: p. 239-248.
252. Lescoat, A., et al., *Distinct Properties of Human M-CSF and GM-CSF Monocyte-Derived Macrophages to Simulate Pathological Lung Conditions In Vitro: Application to Systemic and Inflammatory Disorders with Pulmonary Involvement.* International Journal of Molecular Sciences, 2018. **19**(3): p. 894.
253. Lo, Y.L., et al., *Dengue Virus Infection Is through a Cooperative Interaction between a Mannose Receptor and CLEC5A on Macrophage as a Multivalent Hetero-Complex.* PLoS One, 2016. **11**(11): p. e0166474.
254. Mata-Martínez, P., M. Bergón-Gutiérrez, and C. del Fresno, *Dectin-1 Signaling Update: New Perspectives for Trained Immunity.* Frontiers in Immunology, 2022. **13**.
255. Ifrim, D.C., et al., *The Role of Dectin-2 for Host Defense Against Disseminated Candidiasis.* J Interferon Cytokine Res, 2016. **36**(4): p. 267-76.
256. Yu, P.C., et al., *Altered Membrane Expression and Function of CD11b Play a Role in the Immunosuppressive Effects of Morphine on*

Macrophages at the Nanomolar Level. Pharmaceuticals (Basel), 2023. **16**(2).
257. Affandi, A.J., et al., *CD169 Defines Activated CD14+ Monocytes With Enhanced CD8+ T Cell Activation Capacity.* Frontiers in Immunology, 2021. **12**.
258. Couture, A., et al., *HLA-Class II Artificial Antigen Presenting Cells in CD4+ T Cell-Based Immunotherapy.* Frontiers in Immunology, 2019. **10**.
259. Sunderkötter, C., et al., *Subpopulations of Mouse Blood Monocytes Differ in Maturation Stage and Inflammatory Response1.* The Journal of Immunology, 2004. **172**(7): p. 4410-4417.
260. Yang, J., et al., *Monocyte and macrophage differentiation: circulation inflammatory monocyte as biomarker for inflammatory diseases.* Biomark Res, 2014. **2**(1): p. 1.
261. Simanshu, D.K., D.V. Nissley, and F. McCormick, *RAS Proteins and Their Regulators in Human Disease.* Cell, 2017. **170**(1): p. 17-33.
262. Phee, H., et al., *Regulation of thymocyte positive selection and motility by GIT2.* Nature immunology, 2010. **11**(6): p. 503-511.
263. Yang, C., et al., *Transcriptomic Analysis Identified ARHGAP Family as a Novel Biomarker Associated With Tumor-Promoting Immune Infiltration and Nanomechanical Characteristics in Bladder Cancer.* Frontiers in Cell and Developmental Biology, 2021. **9**.
264. Shereck, E.B., C. van de Ven, and M.S. Cairo, *Chapter 78 - Neonatal Leukocyte Physiology and Disorders*, in *Avery's Diseases of the Newborn (Ninth Edition)*, C.A. Gleason and S.U. Devaskar, Editors. 2012, W.B. Saunders: Philadelpia. p. 1108-1122.
265. Roskoski, R., *RAF protein-serine/threonine kinases: Structure and regulation.* Biochemical and Biophysical Research Communications, 2010. **399**(3): p. 313-317.
266. Duan, S., et al., *Selection of novel human scFvs against cancer antigen IL1RAP by phage and yeast surface display technology.* Biotechnology & Biotechnological Equipment, 2020. **34**(1): p. 287-293.
267. Chen, T., et al., *The nucleotide receptor STING translocates to the phagosomes to negatively regulate anti-fungal immunity.* Immunity, 2023. **56**(8): p. 1727-1742.e6.
268. Ridley, A.J., *Rho proteins, PI 3-kinases, and monocyte/macrophage motility.* FEBS Lett, 2001. **498**(2-3): p. 168-71.
269. Lucas, B. and J. Hardin, *Mind the (sr)GAP - roles of Slit-Robo GAPs in neurons, brains and beyond.* J Cell Sci, 2017. **130**(23): p. 3965-3974.
270. Que, F., et al., *RHOA G17V induces T follicular helper cell specification and involves angioimmunoblastic T-cell lymphoma via upregulating the expression of PON2 through an NF-κB-dependent mechanism.* Oncoimmunology, 2022. **11**(1): p. 2134536.
271. Franco, J.H., S. Chattopadhyay, and Z.K. Pan, *How Different Pathologies Are Affected by IFIT Expression.* Viruses, 2023. **15**(2): p. 342.
272. Liu, D., *The adaptor protein Crk in immune response.* Immunol Cell Biol, 2014. **92**(1): p. 80-9.
273. Heitzer, E., et al., *Current and future perspectives of liquid biopsies in genomics-driven oncology.* Nature Reviews Genetics, 2019. **20**(2): p. 71-88.

274. Charrin, S., et al., *Lateral organization of membrane proteins: Tetraspanins spin their web.* Biochemical journal, 2009. **420**(2): p. 133-154.
275. Boucheix, C., et al., *Tetraspanins and malignancy.* Expert reviews in molecular medicine, 2001. **3**(4): p. 1-17.
276. Brosseau, C., et al., *CD9 Tetraspanin: A New Pathway for the Regulation of Inflammation?* Front Immunol, 2018. **9**: p. 2316.
277. Dornier, E., et al., *Correction to TspanC8 tetraspanins regulate ADAM10/Kuzbanian trafficking and promote Notch activation in flies and mammals [Journal of Cell Biology, 199, 3, (2012) 481-496].* The Journal of cell biology, 2016. **213**(4): p. 495-496.
278. Pols, M.S. and J. Klumperman, *Trafficking and function of the tetraspanin CD63.* Experimental cell research, 2009. **315**(9): p. 1584-1592.
279. Sudbery, P., N. Gow, and J. Berman, *The distinct morphogenic states of Candida albicans.* Trends in microbiology (Regular ed.), 2004. **12**(7): p. 317-324.
280. Chen, H., et al., *The regulation of hyphae growth in Candida albicans.* Virulence, 2020. **11**(1): p. 337-348.
281. Fleetwood, A.J., et al., *GM-CSF- and M-CSF-dependent macrophage phenotypes display differential dependence on Type I interferon signaling.* Journal of leukocyte biology, 2009. **86**(2): p. 411-421.
282. Netea, M.G., *Immune sensing of Candida albicans requires cooperative recognition of mannans and glucans by lectin and Toll-like receptors.* The Journal of clinical investigation, 2006. **116**(6): p. 1642-1650.
283. Muñoz-Soriano, V., S. López-Domenech, and N. Paricio, *Why mammalian wound-healing researchers may wish to turn to Drosophila as a model.* Experimental dermatology, 2014. **23**(8): p. 538-542.
284. Olivier, F.A.B. and A. Traven, *Quantitative live-cell imaging of Candida albicans escape from immune phagocytes.* STAR protocols, 2023. **4**(4): p. 102737-102737.
285. Saijo, S., et al., *Dectin-1 is required for host defense against Pneumocystis carinii but not against Candida albicans.* Nature Immunology, 2007. **8**(1): p. 39-46.
286. Netea, M.G. and L.A.B. Joosten, *Trained innate immunity: Concept, nomenclature, and future perspectives.* Journal of Allergy and Clinical Immunology, 2024. **154**(5): p. 1079-1084.
287. Baltch, A.L., et al., *Effects of Cytokines and Fluconazole on the Activity of Human Monocytes against Candida albicans.* Antimicrobial Agents and Chemotherapy, 2001. **45**(1): p. 96-104.
288. Roy, René M. and Bruce S. Klein, *Dendritic Cells in Antifungal Immunity and Vaccine Design.* Cell host & microbe, 2012. **11**(5): p. 436-446.
289. Puel, A., et al., *Chronic Mucocutaneous Candidiasis in Humans with Inborn Errors of Interleukin-17 Immunity.* Science (American Association for the Advancement of Science), 2011. **332**(6025): p. 65-68.
290. Valladao, A.C., et al., *STAT6 Regulates the Development of Eosinophilic versus Neutrophilic Asthma in Response to Alternaria alternata.* The Journal of Immunology, 2016. **197**(12): p. 4541-4551.

291. Ghebremedhin, A., et al., *A Novel CD206 Targeting Peptide Inhibits Bleomycin-Induced Pulmonary Fibrosis in Mice.* Cells (Basel, Switzerland), 2023. **12**(9): p. 1254.
292. Aderem, A., et al., *The Toll-like receptor 2 is recruited to macrophage phagosomes and discriminates between pathogens.* Nature (London), 1999. **401**(6755): p. 811-815.
293. Francisco-Cruz, A., et al., *Granulocyte–macrophage colony-stimulating factor: not just another haematopoietic growth factor.* Medical oncology (Northwood, London, England), 2014. **31**(1): p. 1-14.
294. Damiani, G., et al., *Recombinant human granulocyte macrophage-colony stimulating factor expressed in yeast (sargramostim): A potential ally to combat serious infections.* Clinical Immunology, 2020. **210**: p. 108292.
295. Du, C., et al., *Phagocytosis and Killing Assays for Candida Species.* Candida albicans, 2009. **499**: p. 17-26.
296. Dongari-Bagtzoglou, A. and H. Kashleva, *Granulocyte-macrophage colony-stimulating factor responses of oral epithelial cells to Candida albicans.* Oral microbiology and immunology, 2003. **18**(3): p. 165-170.
297. Shibata, Y., et al., *GM-CSF Regulates Alveolar Macrophage Differentiation and Innate Immunity in the Lung through PU.1.* Immunity (Cambridge, Mass.), 2001. **15**(4): p. 557-567.
298. Gow, N.A.R., et al., *The fungal cell wall: Structure, biosynthesis, and function.* Microbiology spectrum, 2017. **5**(3).
299. Lin, J., et al., *The Peptide-binding Cavity Is Essential for Als3-mediated Adhesion of Candida albicans to Human Cells.* The Journal of biological chemistry, 2014. **289**(26): p. 18401-18412.
300. Piseddu, I., et al., *Constitutive Expression of CCL22 Is Mediated by T Cell-Derived GM-CSF.* J Immunol, 2020. **205**(8): p. 2056-2065.
301. Moron, L.S. and E.C. Cabrera, *ABC genotyping and putative virulence factors of Candida albicans clinical isolates.* Malaysian Journal of Microbiology, 2019. **15**(5): p. 400-407.
302. Desai, J.V., *Candida albicans Hyphae: From Growth Initiation to Invasion.* J Fungi (Basel), 2018. **4**(1).
303. Bain, J.M., et al., *Immune cells fold and damage fungal hyphae.* Proc Natl Acad Sci U S A, 2021. **118**(15).
304. Diamond, R.D. and C.C. Haudenschild, *Monocyte-mediated serum-independent damage to hyphal and pseudohyphal forms of Candida albicans in vitro.* The Journal of clinical investigation, 1981. **67**(1): p. 173-182.
305. Cardini, A., et al., *HyLength: a semi-automated digital image analysis tool for measuring the length of roots and fungal hyphae of dense mycelia.* Mycorrhiza, 2020. **30**(2-3): p. 229-242.
306. She, X., et al., *The mitochondrial complex I proteins of Candida albicans moderate phagocytosis and the production of pro-inflammatory cytokines in murine macrophages and dendritic cells.* The FASEB journal, 2022. **36**(11): p. e22575-n/a.
307. Leshchiner, E.S., et al., *Small-molecule inhibitors directly target CARD9 and mimic its protective variant in inflammatory bowel disease.* Proceedings of the National Academy of Sciences - PNAS, 2017. **114**(43): p. 11392-11397.
308. Kottom, T.J., et al., *The importance of Fcγ and C-type lectin receptors in host immune responses during Pneumocystis pneumonia.* Infection and immunity, 2025. **93**(2): p. e0027624.

309. Ferwerda, G., et al., *The role of Toll-like receptors and C-type lectins for vaccination against Candida albicans.* Vaccine, 2010. **28**(3): p. 614-622.
310. Larcombe, D.E., et al., *Glucose-enhanced oxidative stress resistance—A protective anticipatory response that enhances the fitness of Candida albicans during systemic infection.* PLoS pathogens, 2023. **19**(7): p. e1011505.
311. Gazi, U., et al., *Fungal recognition enhances mannose receptor shedding through dectin-1 engagement.* J Biol Chem, 2011. **286**(10): p. 7822-7829.
312. Turvey, S.E.M.B.B.S.D. and D.H.M.B.C. Broide, *Innate immunity.* Journal of allergy and clinical immunology, 2010. **125**(2): p. S24-S32.
313. Zhang, J.M. and J. An, *Cytokines, inflammation, and pain.* Int Anesthesiol Clin, 2007. **45**(2): p. 27-37.
314. Wang, Q., et al., *CCL22-Polarized TAMs to M2a Macrophages in Cervical Cancer In Vitro Model.* Cells, 2022. **11**(13).
315. Strizova, Z., et al., *M1/M2 macrophages and their overlaps - myth or reality?* Clin Sci (Lond), 2023. **137**(15): p. 1067-1093.
316. Ren, G., et al., *CCL22 induces pro-inflammatory changes in fibroblast-like synoviocytes.* iScience, 2021. **24**(1): p. 101943.
317. Piseddu, I., et al., *Constitutive expression of CCL22 is mediated by T cell–Derived GM-CSF.* The Journal of immunology (1950), 2020. **205**(8): p. 2056-2065.
318. Lee, C., et al., *Vascular endothelial growth factor signaling in health and disease: from molecular mechanisms to therapeutic perspectives.* Signal Transduct Target Ther, 2025. **10**(1): p. 170.
319. Alferink, J., et al., *Compartmentalized production of CCL17 in vivo: strong inducibility in peripheral dendritic cells contrasts selective absence from the spleen.* J Exp Med, 2003. **197**(5): p. 585-99.
320. Achuthan, A., et al., *Granulocyte macrophage colony-stimulating factor induces CCL17 production via IRF4 to mediate inflammation.* The Journal of clinical investigation, 2016. **126**(9): p. 3453-3466.
321. Satoh, T., et al., *The Jmjd3-Irf4 axis regulates M2 macrophage polarization and host responses against helminth infection.* Nat Immunol, 2010. **11**(10): p. 936-44.
322. Zhou, C., et al., *The role of CXCL family members in different diseases.* Cell death discovery, 2023. **9**(1): p. 212-12.
323. Lee, J.S. and C. Kim, *Role of CARD9 in Cell- and Organ-Specific Immune Responses in Various Infections.* International journal of molecular sciences, 2024. **25**(5): p. 2598.
324. Liu, M., et al., *CXCL10/IP-10 in infectious diseases pathogenesis and potential therapeutic implications.* Cytokine Growth Factor Rev, 2011. **22**(3): p. 121-30.
325. Kang, S.W., et al., *CCR5-mediated recruitment of NK cells to the kidney is a critical step for host defense to systemic Candida albicans infection.* The Journal of immunology (1950), 2019. **202**(1_Supplement): p. 190-190.55.
326. Bryson, B.D., et al., *Heterogeneous GM-CSF signaling in macrophages is associated with control of Mycobacterium tuberculosis.* Nature communications, 2019. **10**(1): p. 2329-2329.
327. Acosta-Rodriguez, E.V., et al., *Surface phenotype and antigenic specificity of human interleukin 17–producing T helper memory cells.* Nature Immunology, 2007. **8**(6): p. 639-646.

328. Aggarwal, S., et al., *Interleukin-23 Promotes a Distinct CD4 T Cell Activation State Characterized by the Production of Interleukin-17 *.* Journal of Biological Chemistry, 2003. **278**(3): p. 1910-1914.
329. Bacher, P., et al., *Antigen-specific expansion of human regulatory T cells as a major tolerance mechanism against mucosal fungi.* Mucosal Immunol, 2014. **7**(4): p. 916-28.
330. Paroli, M., et al., *The Double Game Played by Th17 Cells in Infection: Host Defense and Immunopathology.* Pathogens (Basel), 2022. **11**(12): p. 1547.
331. Mastrotto, F., et al., *Sulfation at Glycopolymer Side Chains Switches Activity at the Macrophage Mannose Receptor (CD206) In Vitro and In Vivo.* Journal of the American Chemical Society, 2022. **144**(50): p. 23134-23147.
332. González-Cuesta, M., C. Ortiz Mellet, and J.M. García Fernández, *Carbohydrate supramolecular chemistry: beyond the multivalent effect.* Chemical communications (Cambridge, England), 2020. **56**(39): p. 527-5222.
333. Gregory, G.L., E.M. López-Vidal, and A. Buchard, *Polymers from sugars: cyclic monomer synthesis, ring-opening polymerisation, material properties and applications.* Chemical communications (Cambridge, England), 2017. **53**(14): p. 2198-2217.
334. Wang, J., et al., *Glycopolymers based on carbohydrate or vinyl backbones and their biomedical applications.* Polymer chemistry, 2023. **14**(2): p. 2414-2434.
335. Medzhitov, R., *Recognition of microorganisms and activation of the immune response : Host-Microbe Interactions.* Nature (London), 2007. **449**(7164): p. 819-826.
336. Qin, Q., S. Lang, and X. Huang, *Synthetic linear glycopolymers and their biological applications.* Journal of carbohydrate chemistry, 2021. **40**(1-3): p. 1-44.
337. Stahl, P.D. and R.A.B. Ezekowitz, *The mannose receptor is a pattern recognition receptor involved in host defense.* Current opinion in immunology, 1998. **10**(1): p. 50-55.
338. Radhakrishnan, A., et al., *Back2Basics: animal lectins: an insight into a highly versatile recognition protein.* Journal of proteins and proteomics, 2023. **14**(1): p. 43-59.
339. Stenzel, M.H., *Glycopolymers for Drug Delivery: Opportunities and Challenges.* Macromolecules, 2022. **55**(12): p. 4867-4890.
340. Filipová, M., et al., *Glycopolymers for Efficient Inhibition of Galectin-3: In Vitro Proof of Efficacy Using Suppression of T Lymphocyte Apoptosis and Tumor Cell Migration.* Biomacromolecules, 2020. **21**(8): p. 3122-3133.
341. Karsten, C.B., et al., *Exclusive decoration of simian immunodeficiency virus env with high-mannose type N-glycans is not compatible with mucosal transmission in rhesus macaques.* Journal of virology, 2015. **89**(22): p. 11727-11733.
342. Hudak, J.E., S.M. Canham, and C.R. Bertozzi, *Glycocalyx engineering reveals a Siglec-based mechanism for NK cell immunoevasion.* Nature chemical biology, 2014. **10**(1): p. 69-75.
343. Paurević, M., M. Šrajer Gajdošik, and R. Ribić, *Mannose Ligands for Mannose Receptor Targeting.* International journal of molecular sciences, 2024. **25**(3): p. 1370.

344. Park, K.-H., et al., *Specific interaction of mannosylated glycopolymers with macrophage cells mediated by mannose receptor.* Journal of bioscience and bioengineering, 2005. **99**(3): p. 285-289.
345. Lee, S.J., et al., *Normal Host Defense during Systemic Candidiasis in Mannose Receptor-Deficient Mice.* Infection and Immunity, 2003. **71**(1): p. 437-445.
346. Fraser, I.P., et al., *Pneumocystis carinii enhances soluble mannose receptor production by macrophages.* Microbes and infection, 2000. **2**(11): p. 1305-1310.
347. Su, Y., et al., *Glycosylation Influences the Lectin Activities of the Macrophage Mannose Receptor.* The Journal of biological chemistry, 2005. **280**(38): p. 32811-32820.
348. Sandahl, T.D., et al., *The soluble mannose receptor (sMR) is elevated in alcoholic liver disease and associated with disease severity, portal hypertension, and mortality in cirrhosis patients.* PloS one, 2017. **12**(12): p. e0189345-e0189345.
349. Suzuki, Y., et al., *Macrophage mannose receptor, CD206, predict prognosis in patients with pulmonary tuberculosis.* Scientific reports, 2018. **8**(1): p. 13129-9.
350. Embgenbroich, M., et al., *Soluble mannose receptor induces proinflammatory macrophage activation and metaflammation.* Proceedings of the National Academy of Sciences - PNAS, 2021. **118**(31): p. 1-10.
351. Rowe, R.G. and G.Q. Daley, *Induced pluripotent stem cells in disease modelling and drug discovery.* Nat Rev Genet, 2019. **20**(7): p. 377-388.
352. Kwart, D., et al., *A Large Panel of Isogenic APP and PSEN1 Mutant Human iPSC Neurons Reveals Shared Endosomal Abnormalities Mediated by APP β-CTFs, Not Aβ.* Neuron (Cambridge, Mass.), 2019. **104**(2): p. 256-270.e5.
353. Abud, E.M., et al., *iPSC-Derived Human Microglia-like Cells to Study Neurological Diseases.* Neuron (Cambridge, Mass.), 2017. **94**(2): p. 278-293.e9.
354. Kasai-Brunswick, T.H., A.B. Carvalho, and A.C. Campos de Carvalho, *Stem cell therapies in cardiac diseases: Current status and future possibilities.* World J Stem Cells, 2021. **13**(9): p. 1231-1247.
355. Takahashi, K. and S. Yamanaka, *Induction of Pluripotent Stem Cells from Mouse Embryonic and Adult Fibroblast Cultures by Defined Factors.* Cell, 2006. **126**(4): p. 663-676.
356. Lian, X., et al., *Robust cardiomyocyte differentiation from human pluripotent stem cells via temporal modulation of canonical Wnt signaling.* Proceedings of the National Academy of Sciences - PNAS, 2012. **109**(27): p. E1848-E1857.
357. Laflamme, M.A., et al., *Cardiomyocytes derived from human embryonic stem cells in pro-survival factors enhance function of infarcted rat hearts.* Nature biotechnology, 2007. **25**(9): p. 1015-1024.
358. Buchrieser, J., W. James, and M.D. Moore, *Human Induced Pluripotent Stem Cell-Derived Macrophages Share Ontogeny with MYB-Independent Tissue-Resident Macrophages.* Stem cell reports, 2017. **8**(2): p. 334-345.
359. Zhang, H., et al., *CRISPR/Cas9-Mediated Gene Editing in Human iPSC-Derived Macrophage Reveals Lysosomal Acid Lipase Function in Human Macrophages—Brief Report.* Arteriosclerosis, thrombosis, and vascular biology, 2017. **37**(11): p. 2156-2160.

360. Ackermann, M., et al., *Bioreactor-based mass production of human iPSC-derived macrophages enables immunotherapies against bacterial airway infections.* Nature communications, 2018. **9**(1): p. 5088-13.
361. Vodyanik, M.A., et al., *Human embryonic stem cell–derived CD34+ cells: efficient production in the coculture with OP9 stromal cells and analysis of lymphohematopoietic potential.* Blood, 2005. **105**(2): p. 617-626.
362. Lyadova, I., T. Gerasimova, and T. Nenasheva, *Macrophages Derived From Human Induced Pluripotent Stem Cells: The Diversity of Protocols, Future Prospects, and Outstanding Questions.* Front Cell Dev Biol, 2021. **9**: p. 640703.
363. Klepikova, A., et al., *iPSC-Derived Macrophages: The Differentiation Protocol Affects Cell Immune Characteristics and Differentiation Trajectories.* International journal of molecular sciences, 2022. **23**(24): p. 16087.
364. Panicker, L.M., et al., *Induced pluripotent stem cell model recapitulates pathologic hallmarks of Gaucher disease.* Proceedings of the National Academy of Sciences - PNAS, 2012. **109**(44): p. 18054-18059.
365. Wynn, T.A., A. Chawla, and J.W. Pollard, *Macrophage biology in development, homeostasis and disease.* Nature (London), 2013. **496**(7446): p. 445-455.
366. St-Pierre, J. and H.L. Ostergaard, *A Role for the Protein Tyrosine Phosphatase CD45 in Macrophage Adhesion through the Regulation of Paxillin Degradation.* PloS one, 2013. **8**(7): p. e71531-e71531.
367. Zhang, Y.-L., et al., *CD11b mediates hypertensive cardiac remodeling by regulating macrophage infiltration and polarization.* Journal of advanced research, 2024. **55**: p. 17-31.
368. Pouyanfard, S., et al., *Human induced pluripotent stem cell-derived macrophages ameliorate liver fibrosis.* Stem cells (Dayton, Ohio), 2021. **39**(12): p. 1701-1717.
369. Lyadova, I. and A. Vasiliev, *Macrophages derived from pluripotent stem cells: prospective applications and research gaps.* Cell & bioscience, 2022. **12**(1): p. 1-96.
370. Jaynes, J.M., et al., *Mannose receptor (CD206) activation in tumor-associated macrophages enhances adaptive and innate antitumor immune responses.* Science translational medicine, 2020. **12**(530): p. 1.
371. Lambert, C., et al., *Monocytes and macrophages in flow: an ESCCA initiative on advanced analyses of monocyte lineage using flow cytometry.* Cytometry. Part B, Clinical cytometry, 2017. **92**(3): p. 180-188.
372. Zhang, L., et al., *Pluripotent stem cell-derived CAR-macrophage cells with antigen-dependent anti-cancer cell functions.* Journal of hematology and oncology, 2020. **13**(1): p. 153-5.
373. Schinke, M., et al., *Polarization of human iPSC-derived macrophages directs their immunological response to secondary pro-inflammatory stimuli.* Journal of immunology and regenerative medicine, 2022. **17**: p. 100061.
374. Gaffen, S.L., et al., *The IL-23–IL-17 immune axis: from mechanisms to therapeutic testing.* Nature reviews. Immunology, 2014. **14**(9): p. 585-600.

375. Olynych, T.J., D.L. Jakeman, and J.S. Marshall, *Fungal zymosan induces leukotriene production by human mast cells through a dectin-1-dependent mechanism.* J Allergy Clin Immunol, 2006. **118**(4): p. 837-43.
376. Lata Kanyal, B., et al., *Leukotrienes and Inflammation –A Review.* Indian journal of forensic medicine toxicology, 2021. **15**(2): p. 295-301.
377. Gladiator, A., et al., *Cutting Edge: IL-17–Secreting Innate Lymphoid Cells Are Essential for Host Defense against Fungal Infection.* The Journal of immunology (1950), 2013. **190**(2): p. 521-525.
378. Gazendam, R.P., et al., *How neutrophils kill fungi.* Immunol Rev, 2016. **273**(1): p. 299-311.
379. Quintin, J., et al., *Candida albicans Infection Affords Protection against Reinfection via Functional Reprogramming of Monocytes.* Cell host & microbe, 2012. **12**(2): p. 223-232.
380. Arellano, M. and S. Lonial, *Clinical uses of GM-CSF, a critical appraisal and update.* Biologics, 2008. **2**(1): p. 13-27.
381. Cashen, A.F., et al., *Cytokines and stem cell mobilization for autologous and allogeneic transplantation.* Curr Hematol Rep, 2004. **3**(6): p. 406-12.
382. Ferlazzo, G., et al., *Dendritic Cells Generated From CD34+ Progenitor Cells With flt3 Ligand, c-Kit Ligand, GM-CSF, IL-4, and TNF-α Are Functional Antigen-Presenting Cells Resembling Mature Monocyte-Derived Dendritic Cells.* Journal of immunotherapy (1997), 2000. **23**(1): p. 48-58.
383. Matzinger, P., *Tolerance, Danger, and the Extended Family.* Annual Review of Immunology, 1994. **12**(1): p. 991-1045.
384. Fattorossi, A., et al., *Effects of granulocyte-colony-stimulating factor and granulocyte/macrophage-colony-stimulating factor administration on T cell proliferation and phagocyte cell-surface molecules during hematopoietic reconstitution after autologous peripheral blood progenitor cell transplantation.* Cancer Immunol Immunother, 2001. **49**(12): p. 641-8.
385. Nicola, A.M., et al., *Antifungal drugs: New insights in research & development.* Pharmacology & Therapeutics, 2019. **195**: p. 21-38.
386. Scriven, J.E., et al., *Modulating host immune responses to fight invasive fungal infections.* Curr Opin Microbiol, 2017. **40**: p. 95-103.
387. Burgess, A.W., J. Camakaris, and D. Metcalf, *Purification and properties of colony-stimulating factor from mouse lung-conditioned medium.* The Journal of biological chemistry, 1977. **252**(6): p. 1998-2003.
388. Dranoff, G., et al., *Involvement of Granulocyte-Macrophage Colony-Stimulating Factor in Pulmonary Homeostasis.* Science (American Association for the Advancement of Science), 1994. **264**(5159): p. 713-716.
389. Ríos, I., et al., *Reprogramming of GM-CSF-dependent alveolar macrophages through GSK3 activity modulation.* eLife, 2025. **14**: p. RP102659.
390. Gavino, C., et al., *CARD9 Deficiency and Spontaneous Central Nervous System Candidiasis: Complete Clinical Remission With GM-CSF Therapy.* Clinical Infectious Diseases, 2014. **59**(1): p. 81-84.
391. Luo, P., et al., *The multifaceted role of CARD9 in inflammatory bowel disease.* J Cell Mol Med, 2020. **24**(1): p. 34-39.

392. Kasahara, S., et al., *Role of Granulocyte-Macrophage Colony-Stimulating Factor Signaling in Regulating Neutrophil Antifungal Activity and the Oxidative Burst During Respiratory Fungal Challenge.* The Journal of Infectious Diseases, 2016. **213**(8): p. 1289-1298.
393. Perugini, M., et al., *Alternative modes of GM-CSF receptor activation revealed using activated mutants of the common beta-subunit.* Blood, 2010. **115**(16): p. 3346-53.
394. Bodey, G.P., et al., *Role of Granulocyte-Macrophage Colony-Stimulating Factor as Adjuvant Therapy for Fungal Infection in Patients with Cancer.* Clinical infectious diseases, 1993. **17**(4): p. 705-707.
395. Ademe, M., *Immunomodulation for the Treatment of Fungal Infections: Opportunities and Challenges.* Frontiers in cellular and infection microbiology, 2020. **10**: p. 469.
396. Patel, A.A., et al., *The fate and lifespan of human monocyte subsets in steady state and systemic inflammation.* J Exp Med, 2017. **214**(7): p. 1913-1923.
397. Smeekens, S.P., et al., *The classical CD14^{++}CD16^{-} monocytes, but not the patrolling CD14^{+}CD16^{+} monocytes, promote Th17 responses to Candida albicans.* Eur J Immunol, 2011. **41**(10): p. 2915-24.
398. Hadadi, E., et al., *Differential IL-1β secretion by monocyte subsets is regulated by Hsp27 through modulating mRNA stability.* Sci Rep, 2016. **6**: p. 39035.
399. Perry, S.E., et al., *HLA-DR regulation and the influence of GM-CSF on transcription, surface expression and shedding.* Int J Med Sci, 2004. **1**(3): p. 126-136.
400. Teschner, D., et al., *CD11b Regulates Fungal Outgrowth but Not Neutrophil Recruitment in a Mouse Model of Invasive Pulmonary Aspergillosis.* Frontiers in immunology, 2019. **10**: p. 123-123.
401. Ma, J. and D.M. Underhill, *β-Glucan signaling connects phagocytosis to autophagy.* Glycobiology, 2013. **23**(9): p. 1047-51.
402. Goodridge, H.S., et al., *Activation of the innate immune receptor Dectin-1 upon formation of a 'phagocytic synapse'.* Nature (London), 2011. **472**(7344): p. 471-475.
403. Camilli, G., et al., *Impaired phagocytosis directs human monocyte activation in response to fungal derived β-glucan particles.* Eur J Immunol, 2018. **48**(5): p. 757-770.
404. Shiomi, A. and T. Usui, *Pivotal roles of GM-CSF in autoimmunity and inflammation.* Mediators Inflamm, 2015. **2015**: p. 568543.
405. Graham, L.M. and G.D. Brown, *The Dectin-2 family of C-type lectins in immunity and homeostasis.* Cytokine (Philadelphia, Pa.), 2009. **48**(1-2): p. 148-155.
406. Fernandes, M.J., et al., *Characterization of a novel receptor that maps near the natural killer gene complex: demonstration of carbohydrate binding and expression in hematopoietic cells.* Cancer Res, 1999. **59**(11): p. 2709-17.
407. Gavino, A.C.P., et al., *Identification and expression profiling of a human C-type lectin, structurally homologous to mouse dectin-2.* Experimental dermatology, 2005. **14**(4): p. 281-288.
408. Sato, K., et al., *Dectin-2 is a pattern recognition receptor for fungi that couples with the Fc receptor gamma chain to induce innate immune responses.* J Biol Chem, 2006. **281**(50): p. 38854-66.
409. Sander, J., et al., *Cellular Differentiation of Human Monocytes Is Regulated by Time-Dependent Interleukin-4 Signaling and the*

Transcriptional Regulator NCOR2. Immunity, 2017. **47**(6): p. 1051-1066.e12.
410. Kany, S., J.T. Vollrath, and B. Relja, *Cytokines in Inflammatory Disease.* Int J Mol Sci, 2019. **20**(23).
411. Money, N.P., *Physical forces supporting hyphal growth.* Fungal genetics and biology, 2025. **177**: p. 103961.
412. Eddie Ip, W.K., et al., *Mannose-binding lectin and innate immunity.* Immunological reviews, 2009. **230**(1): p. 9-21.
413. Cruceriu, D., et al., *The dual role of tumor necrosis factor-alpha (TNF-α) in breast cancer: molecular insights and therapeutic approaches.* Cellular oncology (Dordrecht), 2020. **43**(1): p. 1-18.
414. Embgenbroich, M., et al., *Soluble mannose receptor induces proinflammatory macrophage activation and metaflammation.* Proc Natl Acad Sci U S A, 2021. **118**(31).
415. De Vlieger, G., et al., *The soluble mannose receptor (sMR/sCD206) in critically ill patients with invasive fungal infections, bacterial infections or non-infectious inflammation: A secondary analysis of the EPaNIC RCT.* Critical care (London, England), 2019. **23**(1): p. 270-270.
416. Hamilton, J.A. and A. Achuthan, *Colony stimulating factors and myeloid cell biology in health and disease.* Trends in immunology, 2013. **34**(2): p. 81-89.
417. Murray, Peter J., et al., *Macrophage Activation and Polarization: Nomenclature and Experimental Guidelines.* Immunity (Cambridge, Mass.), 2014. **41**(1): p. 14-20.
418. Pixley, F.J. and E.R. Stanley, *CSF-1 regulation of the wandering macrophage: complexity in action.* Trends in cell biology, 2004. **14**(11): p. 628-638.
419. Rademakers, R., et al., *Mutations in the colony stimulating factor 1 receptor (CSF1R) gene cause hereditary diffuse leukoencephalopathy with spheroids.* Nature genetics, 2012. **44**(2): p. 200-205.
420. Bartocci, A., et al., *Macrophages Specifically Regulate the Concentration of Their Own Growth Factor in the Circulation.* Proceedings of the National Academy of Sciences - PNAS, 1987. **84**(17): p. 6179-6183.
421. Kandalla, P.K., et al., *M-CSF improves protection against bacterial and fungal infections after hematopoietic stem/progenitor cell transplantation.* J Exp Med, 2016. **213**(11): p. 2269-2279.
422. Hume, D.A. and K.P. MacDonald, *Therapeutic applications of macrophage colony-stimulating factor-1 (CSF-1) and antagonists of CSF-1 receptor (CSF-1R) signaling.* Blood, 2012. **119**(8): p. 1810-20.
423. Medina-Echeverz, J., F. Aranda, and P. Berraondo, *Myeloid-derived cells are key targets of tumor immunotherapy.* Oncoimmunology, 2014. **3**(4): p. e28398.
424. Lee, C.Z.W., T. Kozaki, and F. Ginhoux, *Studying tissue macrophages in vitro: are iPSC-derived cells the answer?* Nature reviews. Immunology, 2018. **18**(11): p. 716-725.
425. Bi, Y., et al., *M2 Macrophages as a Potential Target for Antiatherosclerosis Treatment.* Neural Plast, 2019. **2019**: p. 6724903.
426. Poltavets, A.S., et al., *Macrophage Modification Strategies for Efficient Cell Therapy.* Cells (Basel, Switzerland), 2020. **9**(6): p. 1535-19.
427. Alagesan, S. and M.D. Griffin, *Alternatively activated macrophages as therapeutic agents for kidney disease: in vivo stability is a key factor.* Kidney international, 2014. **85**(4): p. 730-733.

428. Keller, A.-A., et al., *Transfecting Macrophages.* Macrophages, 2018. **1784**: p. 187-195.
429. Nobile, Clarissa J., et al., *A Recently Evolved Transcriptional Network Controls Biofilm Development in Candida albicans.* Cell, 2012. **148**(1-2): p. 126-138.
430. González-Domínguez, é., et al., *CD163L1 and CLEC5A discriminate subsets of human resident and inflammatory macrophages in vivo.* Journal of leukocyte biology, 2015. **98**(4): p. 453-466.

Appendix

a. Effect of GM-CSF on the expression of MR and CLEC5A

Samples are collected and handed to the MSc student (Maria Vergara) for western blot analysis. The data showed that GM-CSF upregulated MR but there was no detectable effect on the expression of CLEC5A.

b. Proteomics raw data from monocytes treated with GM-CSF/ M-CSF, showing 500 proteins out of a total of 2820 identified.

Samples are collected from 3 different donors and run based on our assay conditions. Then sent to the proteomic facility for analysis, details about the method in (Chapter 2, 2.8. Proteomic analysis).

c. Using CARD9 inhibitor (BRD5529) in GM-CSF-treated monocytes only.

Cells (uninfected and infected) were treated with DMSO (negative control) and BRD5592 (positive control) to analyse phagocytic activity, N=1.

1. Non-labelled No *C. albicans* No Treatment
2. CD11b No *C. albicans* No Treatment
3. Non-labelled With *C. albicans* (wild type) No Treatment
4. CD11b With *C. albicans* (wild type) No Treatment
5. Non-labelled With GFP No Treatment
6. CD11b With GFP No Treatment
7. Non-labelled With *C. albicans* (wild type) treated with BRD5529
8. CD11b With *C. albicans* (wild type) treated with BRD5529
9. Histograms of GFP and CD11n in BRD5529-untreated monocytes, uninfected and infected with *C. albicans* (WT) and GFP.

a.

1.

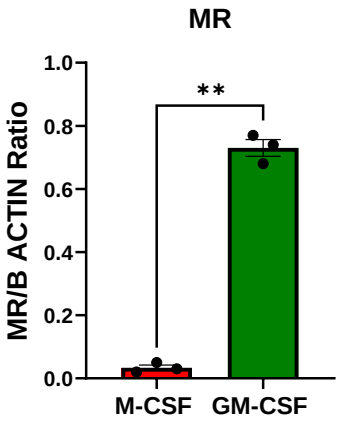
MR
MR/B ACTIN Ratio
1.0
0.8
0.6
0.4
0.2
0.0
**
M-CSF
GM-CSF

2.

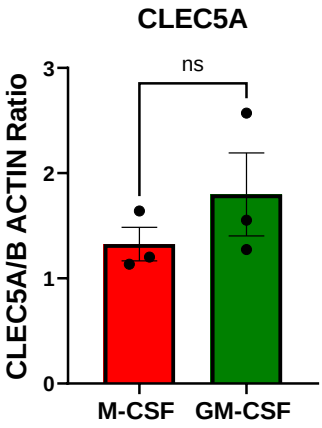
CLEC5A
CLEC5A/B ACTIN Ratio
3
2
1
0
ns
M-CSF
GM-CSF

b.

Genes	First.Protein.Description	GM-CSF 1	GM-CSF 2	GM-CSF 3	Average	M-CSF 1	M-CSF 2	M-CSF 3	Average2	T.test	Log10 Test	Log2
ANKHD1;ANKRD17	Ankyrin repeat domain-containing protein 17	7.42975		7.3865	7.408125	5.83954		5.86695	5.853245	0.00027101	3.56701907	0.339871774927372
CUL1	Cullin-1	31.2785	32.9077	33.4344	32.5402	16.0336		15.7292	15.8814	0.00028556	3.54430006	1.03488502157931
CRK	Adapter molecule crk	34.6904	37.8222		36.2563	58.1994	56.7949	55.2428	56.7457	0.00103783	2.9838731	-0.646279370133049
RPS6KA1	Ribosomal protein S6 kinase alpha-1	59.1872	56.7727	57.8495	57.9364667	43.4205	47.5986	43.0614	44.6935	0.00120521	2.91893594	0.374406674309317
RPL9	Large ribosomal subunit protein uL6	405.016	381.398	406.012	397.475333	330.072	317.172	313.927	320.390333	0.00122184	2.91298528	0.311034711803087
TOR4A	Torsin-4A	73.0354	80.5416	73.4918	75.6896	56.1791	54.7767	56.1208	55.6922	0.00126972	2.89629282	0.442619798474332
DDX42	ATP-dependent RNA helicase DDX42	98.3601	102.188	104.634	101.727367	68.0467		72.373	70.20985	0.00159314	2.79774616	0.534962493936791
PPIA	Peptidyl-prolyl cis-trans isomerase A	3025.9	2957.93	2862.32	2948.71667	3667.17	3885.02	3589.15	3713.78	0.00159493	2.79725846	-0.332801149408107
CHID1	Chitinase domain-containing protein 1	40.0647	40.8397	46.3386	42.4143333	77.505		72.9403	75.22265	0.00174307	2.7586853	-0.826615245732585
ITPR2	Inositol 1,4,5-trisphosphate receptor type 2	51.6172	51.6962	49.4934	50.9356	36.9662		33.8237	35.39495	0.00190484	2.72014092	0.525130802381108
TCP1	T-complex protein 1 subunit alpha	417.171	418.175	429.719	421.688333	365.022	376.868	382.314	374.734667	0.00194905	2.71017695	0.17030766034133
IFIT1	Interferon-induced protein with tetratricopeptide repeats 1	28.8272	40.3424		34.5848	167.844	172.547		170.1955	0.00209665	2.67847447	-2.29898287379239
ARAF	Serine/threonine-protein kinase A-Raf	65.0268	75.906	67.3331	69.4219667	49.4455	48.3094	49.5028	49.0859	0.00364847	2.43788914	0.500083568409966
COLGALT2	Procollagen galactosyltransferase 2	132.352	132.6	127.889	130.947	151.698	167.716	160.911	160.108333	0.00396228	2.40205501	-0.290065391456092
RAB33B	Ras-related protein Rab-33B	139.429	197.73	143.89	160.349667	278.559	280.658	262.42	273.879	0.00441626	2.35494509	-0.772317295193511
ISOC1	Isochorismatase domain-containing protein 1	42.1983	40.2783	40.3248	40.9338	28.5126		23.7977	26.15515	0.00467821	2.32992049	0.646197558536335
PSIP1	PC4 and SFRS1-interacting protein	15.2133	19.8936	18.065	17.7239667	25.216	28.5615	27.0423	26.9399333	0.00526694	2.27844131	-0.60404476197904
EIF3J	Eukaryotic translation initiation factor 3 subunit J	113.341	102.263	122.58	112.728	81.5967	67.0915	69.4027	72.6969667	0.00565202	2.24779623	0.632878831519228
POLR2E	DNA-directed RNA polymerases I, II, and III subunit RPABC1	10.8138	9.95396	12.0654	10.9443867	7.75665	7.50218	6.96715	7.40866	0.00572066	2.24255354	0.562906575017676
ALDOA	Fructose-bisphosphate aldolase A	3549.85	3463.2	3258.5	3423.85	3889.74	3905.05	4026.09	3940.29333	0.00588827	2.23001236	-0.202683536274387
RHEB	GTP-binding protein Rheb	84.1143	95.3335	97.8256	92.4244667	66.3233	71.0866	69.5031	68.971	0.00617738	2.20919574	0.42228492905278
EIF2B3	Translation initiation factor eIF-2B subunit gamma	36.6387	39.1732	36.3609	37.3909333	45.2716	52.3129	48.6328	48.7391	0.00694213	2.15850746	-0.382391127520247
STING1	Stimulator of interferon genes protein	303.184	333.977	354.515	330.558667	231.868	196.467	245.428	224.587667	0.0070909	2.1492989	0.557627636445135
ADPRS	ADP-ribosylhydrolase ARH3	23.4146	23.1936	22.4276	23.0119333	25.9886	24.9639	24.9608	25.3044333	0.00725431	2.13940366	-0.137007971257396
TXNDC12	Thioredoxin domain-containing protein 12	231.491	268.822	239.393	246.568667	189.1	193.508	182.281	188.296333	0.0078689	2.10408586	0.388984570450111
IL1RAP	Interleukin-1 receptor accessory protein	39.0698	35.5098	45.3411	39.9735667	19.7895	20.4114	26.6786	22.2931667	0.00813068	2.08987324	0.842444742916582
MYO1E	Unconventional myosin-Ie	174.116	217.635	173.32	188.357	121.817	110.559	114.444	115.606667	0.00835576	2.07801419	0.704245053991981
RALYL	RNA-binding Raly-like protein	197.754	168.906	173.248	179.969333	225.433	237.821	222.026	228.426667	0.00891131	2.05005857	-0.343979988494192
EML4	Echinoderm microtubule-associated protein-like 4	105.04	80.9974	88.0552	91.3642	61.4436	53.2841	54.8362	56.5213	0.009968	2.00139177	0.692834324425193
UMPS	Uridine 5'-monophosphate synthase	41.9874	40.5449	36.8688	39.8003667	46.589	47.2693	49.4531	47.7704667	0.01041734	1.98224331	-0.263337248606557
RAD23B	UV excision repair protein RAD23 homolog B	164.386	160.677	180.662	168.575	130.2	142.214	137.088	136.500667	0.0104509	1.98084614	0.304482600408445
EIF4G1	Eukaryotic translation initiation factor 4 gamma 1	169.419	145.821	154.383	156.541	118.9	127.651	124.193	123.581333	0.01096137	1.96013511	0.341079722061239
COPG2	Coatomer subunit gamma-2	63.7168	65.836	58.7656	62.7728	47.3404	47.6342	53.7375	49.5707	0.01110375	1.95453022	0.340651930608877
EIF4A1	Eukaryotic initiation factor 4A-I	1345.64	1408.12	1351.86	1368.54	1138.81	966.726	1153.72	1086.41867	0.01112996	1.95350655	0.333057429682699
SNX17	Sorting nexin-17	53.9372	58.0153	55.8648	55.9391	42.4317	34.9071	45.559	40.9659333	0.01134595	1.94515901	0.449432358240204
GGCT	Gamma-glutamylcyclotransferase	73.2004	81.5019	78.2788	77.6603667	68.082	62.8933	65.1491	65.3748	0.01246616	1.90426745	0.248443891067395
PDIA3	Protein disulfide-isomerase A3	1816.54	1743.66	1592.85	1717.68333	2085.47	1982.93	2016.4	2028.26667	0.01278148	1.89341889	-0.239783253064665
LRPPRC	Leucine-rich PPR motif-containing protein, mitochondrial	428.761	420.902	405.596	418.419667	381.298	369.287	345.966	365.517	0.01299946	1.88607461	0.195012156382393
PSMA5	Proteasome subunit alpha type-5	386.815	394.07	386.98	389.288333	361.727	324.449	329.507	338.561	0.01308796	1.883128	0.201423315065123
PPP2R1A	ohine-protein phosphatase 2A 65 kDa regulatory subunit A alp	606.744	572.736	645.311	608.263667	458.079	501.476	397.997	452.517333	0.01310196	1.8826637	0.426723775877234
CCT4	T-complex protein 1 subunit delta	420.685	439.568	395.827	418.693333	343.477	359.033	368.61	357.04	0.01354357	1.86826697	0.229808235170865
UBQLN1	Ubiquilin-1	66.1321	71.6185	73.6561	70.4689	46.9385	54.1565	58.7602	53.2850667	0.01389582	1.85711583	0.403255425068761
MICOS13	MICOS complex subunit MIC13	24.9098	18.8239	26.7294	23.4877	11.0959	11.3895	14.7538	12.4130667	0.01415679	1.84903517	0.920045866915176
SMC1A	Structural maintenance of chromosomes protein 1A	57.7811	51.71	59.2131	56.2347333	47.8768	44.2497	44.311	45.4791667	0.0142951	1.84481284	0.306255665681172
EIF3E	Eukaryotic translation initiation factor 3 subunit E	252.082	277.114	251.517	260.237667	211.847	229.938	216.557	219.447333	0.01526025	1.81643839	0.24595505305998
MAP1S	Microtubule-associated protein 1S	82.8687	84.6929	95.3361	87.6325667	60.168		63.577	61.8725	0.01559926	1.80689609	0.502168786349939
FXR1	RNA-binding protein FXR1	55.6473	60.2313	56.317	57.3985333	48.7918	38.7669	45.1724	44.2437	0.01568151	1.80461223	0.375541833219459
RAPGEF1	Rap guanine nucleotide exchange factor 1	19.7622		19.6712	19.7167		7.91613	4.42981	6.17297	0.01617543	1.79114422	1.67538142174582
NACA	polypeptide-associated complex subunit alpha, muscle-spec	290.267	310.981	356.403	319.217	243.52	245.432	228.456	239.136	0.01676746	1.7755327	0.416706152251302

ACTB	Actin, cytoplasmic 1	32594.7	32062.3	30025.7	31560.9	35201.7	38565.8	35975.9	36581.1333	0.01737615	1.76004652	-0.212961426177984
PRPF31	U4/U6 small nuclear ribonucleoprotein Prp31	32.4105	40.6496	38.6653	37.2418	49.3961	45.8215	47.9766	47.7314	0.01757812	1.75502751	-0.358015848351464
CSNK2B	Casein kinase II subunit beta	128.388	149.513	135.296	137.732333	100.253	113.632	111.87	108.585	0.01776525	1.75042866	0.343042456782605
YWHAE	14-3-3 protein epsilon	2137.28	1935.46	1956.12	2009.62	1755.06	1457.41	1495.25	1569.24	0.01779381	1.74973101	0.356856711943089
TMEM123	Porimin	41.3088	55.1261	37.4223	44.6190667	108.125		85.2443	96.68465	0.01783759	1.74866379	-1.11562652459894
LACC1	Purine nucleoside phosphorylase LACC1	24.9684	26.8507	24.0038	25.2743	46.2589		37.3076	41.78325	0.01813141	1.74156852	-0.7252535773724
ELOC	Elongin-C	245.986	215.829	167.031	209.615333	104.201	130.368	118.989	117.852667	0.01928579	1.71476257	0.830759850688771
MACF1	Microtubule-actin cross-linking factor 1, isoforms 1/2/3/4/5	29.9628	29.7959		29.87935	25.941		26.9212	26.4311	0.02016017	1.69550582	0.17691229606602
SLC30A7	Zinc transporter 7	116.497	110.727	101.754	109.659333	93.8599	86.295	93.7901	91.315	0.02099676	1.67784766	0.264104836679289
COPZ1	Coatomer subunit zeta-1	101.618	102.906	107.516	104.013333	83.9387	52.6849	72.5721	69.7319	0.02114144	1.67486551	0.57687778072022
ATP6V1H	V-type proton ATPase subunit H	163.875	155.718	170.535	163.376	180.691	182.8	176.81	180.100333	0.02250963	1.64763168	-0.140604784848004
VAC14	Protein VAC14 homolog	39.1393	46.7867	41.6267	42.5175667	35.2308	30.5523	33.3079	33.0303333	0.02260196	1.64585383	0.364267503005008
TSNAX	Translin-associated protein X	43.9094	48.2545	50.4778	47.5472333	35.3331	32.3692	40.9613	36.2212	0.02339225	1.63092803	0.392527053111751
GIT2	ARF GTPase-activating protein GIT2	91.8831	115.303	109.887	105.691033	74.0385	79.543	55.5791	69.7202	0.02378257	1.62374125	0.600204372746918
SAR1B	GTP-binding protein SAR1b	57.3288	70.8379	70.9076	66.3581	43.2131		36.6942	39.95365	0.02492073	1.60343932	0.731945271064317
RAP1B	Ras-related protein Rap-1b	209.264	239.76	248.604	232.542667	197.817	170.635	164.176	177.542667	0.02510281	1.60027759	0.389329672957915
RDH14	Retinol dehydrogenase 14	26.4837		25.0548	25.76925		35.0358	38.2748	36.6553	0.02543492	1.59456965	-0.50837126416327
IPO5	Importin-5	93.7007	86.0975	96.3735	92.0572333	68.9886	61.4798	80.4241	70.2975	0.02608549	1.58360103	0.389057701351335
EIF3B	Eukaryotic translation initiation factor 3 subunit B	167.501	172.258	158.916	166.225	146.518	146.989	155.474	149.660333	0.02722926	1.56496415	0.151445484180261
ROCK1	Rho-associated protein kinase 1	57.3445	62.3958	63.0288	60.9230333	54.5193	48.0449	43.9974	48.8538667	0.02735729	1.56292696	0.318515022245894
COPS4	COP9 signalosome complex subunit 4	56.3378	67.5865	65.2574	63.0605667	46.4268	53.3531	48.8575	49.5458	0.02745894	1.56131622	0.347975368975486
SSR4	Translocon-associated protein subunit delta	334.69	335.811	369.581	346.694	261.415	249.85	309.565	273.61	0.02758719	1.5592926	0.34154190966144
COPG1	Coatomer subunit gamma-1	520.291	497.579	538.476	518.782	460.926	399.765	459.232	439.974333	0.02784586	1.5552394	0.237709059681559
LACTB2	Endoribonuclease LACTB2	39.7952	48.0457	43.2235	43.6881333	31.3608	8.83658	21.3268	20.50806	0.02884222	1.53997137	1.09105044122613
CHMP3	Charged multivesicular body protein 3	74.5009	68.4804	62.6431	68.5414667	56.8861	54.7222	58.3159	56.6414	0.02924314	1.53397596	0.27512013850503
CLIP1	CAP-Gly domain-containing linker protein 1	28.8875	23.5219	22.7963	25.0685667	6.14273	13.7254	17.4627	12.44361	0.03038587	1.51732837	1.01047442562263
MTCH1	Mitochondrial carrier homolog 1	57.0924	57.2518	54.4426	56.2622667	59.4335	63.712	65.4988	62.8814333	0.03044935	1.51642197	-0.160466426666699
PEA15	Astrocytic phosphoprotein PEA-15	43.1526	42.5897	40.1165	41.9529333	35.7836	24.0498	21.1962	27.0098667	0.03058526	1.51448788	0.635285168839824
ARHGAP17	Rho GTPase-activating protein 17	28.8344	32.8623	30.069	30.5885667	25.0841	23.9283	17.8034	22.2719333	0.03118788	1.50601416	0.457765708121436
PYGL	Glycogen phosphorylase, liver form	377.957	400.895	406.134	394.995333	311.991	304.7	364.831	327.174	0.03119082	1.50597319	0.271777504547501
EIF3H	Eukaryotic translation initiation factor 3 subunit H	134.325	145.207	123.278	134.27	109.772	113.197	115.767	112.912	0.0312668	1.50491655	0.249938178622022
TRAPPC1	Trafficking protein particle complex subunit 1	47.5588	63.2464	51.1448	53.9833333	68.0504	70.3969	78.4669	72.3047333	0.03243301	1.4890127	-0.421576032083232
NDUFA8	ADH dehydrogenase [ubiquinone] 1 alpha subcomplex subuni	89.9223	83.4034	102.784	92.0365667	76.2423	59.3227	68.6263	68.0637667	0.03310729	1.48007634	0.435320173616965
STX7	Syntaxin-7	79.8422	76.7043	79.1999	78.5821333	69.2366	47.3562	58.4056	58.3328	0.03386945	1.47019187	0.429894008539582
USO1	General vesicular transport factor p115	174.055	187.026	170.595	177.225333	156.032	138.473	159.506	151.337	0.03439273	1.46353331	0.227820091983061
MANF	Mesencephalic astrocyte-derived neurotrophic factor	152.962	174.114	159.453	162.176333	127.993	146.717	126.511	133.740333	0.03446746	1.46259078	0.278128681790239
GMPS	GMP synthase [glutamine-hydrolyzing]	76.0848	88.3408	67.9981	77.4745667	63.3303	50.5763	50.8619	54.9228333	0.03593788	1.44444756	0.496316728024942
CNN2	Calponin-2	73.8045	89.9837	99.0501	87.6127667	47.8136	68.3043	58.9029	58.3402667	0.0364776	1.43797374	0.586649129646204
TKT	Transketolase	3196.67	3141.4	2947.65	3095.24	3457.54	3285.69	3377.83	3373.68667	0.03688132	1.43319358	-0.12427471054966
TAOK3	Serine/threonine-protein kinase TAO3	46.2017	62.1569	51.3659	53.2415	30.8187	35.2619	41.6348	35.9051333	0.0373928	1.42721202	0.568361097650565
TUBB6	Tubulin beta-6 chain	190.121	168.279	209.064	189.154667	137.423	137.414	161.497	145.444667	0.03744612	1.42659317	0.379095974801884
GORASP2	Golgi reassembly-stacking protein 2	43.1323	50.0879	39.6109	44.2770333	35.3009	17.7232	25.0562	26.0267667	0.03748052	1.4261944	0.766562466043766
SEPTIN10	Septin-10	29.5004	22.7306	25.0936	25.7748667	17.7914	4.79636	14.6643	12.4173533	0.03829408	1.41686833	1.05360725796601
YKT6	Synaptobrevin homolog YKT6	118.051	107.662	117.749	114.487333	92.6792	68.2588	96.3457	85.7612333	0.03844531	1.41515664	0.416790431569925
FLII	Protein flightless-1 homolog	339.378	332.534	355.665	342.525667	323.129	322.584	315.196	320.303	0.03858592	1.41357114	0.0967747877479962
MT-ND4	NADH-ubiquinone oxidoreductase chain 4	25.5882	23.2933		24.44075	15.545	17.7389		16.64195	0.0390228	1.40868161	0.554464067635161
NIPSNAP1	Protein NipSnap homolog 1	45.8652		59.1193	52.49225		84.9433	84.027	84.48515	0.04051084	1.39242872	-0.686593342609411
SLC22A18	Solute carrier family 22 member 18	28.6161	19.9521	22.4079	23.6587	34.3839		39.5129	36.9484	0.04056516	1.3918468	-0.643141089244053
NUTF2	Nuclear transport factor 2	294.813	311.599	288.035	298.149	240.341	265.703	275.536	260.526667	0.04058347	1.39165077	0.194602448272752
TUBA4A	Tubulin alpha-4A chain	2418.33	2292.16	2765.9	2492.13	2037.2	1982.93	2133.7	2051.27667	0.04107512	1.38642121	0.280857238430508

EIF3A	Eukaryotic translation initiation factor 3 subunit A	799.66	802.085	786.563	796.102667	642.486	754.394	700.501	699.127	0.04121211	1.3849751	0.187399942665154
DNM1	Dynamin-1	51.0574	47.4363	71.9149	56.8028667	25.2794	37.5493	32.8315	31.8867333	0.04163966	1.38049277	0.833007433068988
AASDHPPT	dipate-semialdehyde dehydrogenase-phosphopantetheinyl tra	23.5211	23.4907	21.7122	22.908		17.6087	20.0464	18.82755	0.04175999	1.37923962	0.283006232086935
PSMC3	26S proteasome regulatory subunit 6A	131.558	146.885	145.062	141.168333	118.213	126.277	101.532	115.340667	0.04181112	1.37870822	0.291515235455818
IDI1	Isopentenyl-diphosphate Delta-isomerase 1	38.8312	37.798	33.529	36.7194	43.6551		48.1972	45.92615	0.04189863	1.37780021	-0.322773362051133
PSME3	Proteasome activator complex subunit 3	133.893	168.786	168.885	157.188	128.394	119.914	110.416	119.574667	0.0419914	1.37683967	0.394579314411698
STX12	Syntaxin-12	109.989	139.236	104.405	117.876667	90.774	77.6702	84.0014	84.1485333	0.04208649	1.37585727	0.486268137976385
MIF	Macrophage migration inhibitory factor	697.308	801.623	804.975	767.968667	461.982	541.509	673.507	558.999333	0.04241534	1.37247709	0.458200887290869
SLC66A3	Solute carrier family 66 member 3	29.5728	25.4403	13.7519	22.9216667	42.3736		46.1836	44.2786	0.04241647	1.37246549	-0.949897659436947
DDAH2	N(G),N(G)-dimethylarginine dimethylaminohydrolase 2	34.5949	41.7088	36.4564	37.5867	55.6067		47.4152	51.51095	0.04280512	1.36850424	-0.454656890845173
PEX11B	Peroxisomal membrane protein 11B	56.3909	45.7684	44.2299	48.7964	39.4205	31.4495	36.3551	35.7417	0.04329781	1.36353403	0.449166459916763
ADAM10	Disintegrin and metalloproteinase domain-containing protein 1	77.0843	91.9354	85.7997	84.9398	58.3081	75.1693	53.8825	62.4533	0.04464838	1.35019431	0.443662906601416
DERA	Deoxyribose-phosphate aldolase	61.3707	76.5714	65.1431	67.6950667	49.4639	55.5942	37.6526	47.5702333	0.04471359	1.34956048	0.508991598272872
CSTF1	Cleavage stimulation factor subunit 1	18.2663	20.4654	24.5716	21.1011	10.9174	13.8363		12.37685	0.04479716	1.34874956	0.769674023866927
UBE2Z	Ubiquitin-conjugating enzyme E2 Z	38.2734	33.3107	29.6462	33.7434333	24.0725		21.4724	22.77245	0.04727939	1.32532812	0.567317258890277
PPP1CA	erine/threonine-protein phosphatase PP1-alpha catalytic subu	353.43	299.847	314.866	322.714333	271.478	224.091	276.774	257.447667	0.04776549	1.32088572	0.325978461869402
KPNA3	Importin subunit alpha-4	62.0928	66.6926	74.1335	67.6396333	58.773	39.2936	49.0792	49.0486	0.04856128	1.31370988	0.463656881068597
CTBP1	C-terminal-binding protein 1	93.8498	104.256	91.0971	96.4009667	77.736	37.4791	67.1523	60.7891333	0.0485835	1.31351124	0.665234162718609
RBX1	E3 ubiquitin-protein ligase RBX1	46.9019	34.9305	29.2378	37.0234	58.327	47.9116	55.6801	53.9729	0.04923351	1.30773919	-0.543797816882979
SAR1A	GTP-binding protein SAR1a	536.845	642.77	557.503	579.039333	444.541	345.806	493.406	427.917667	0.04935102	1.30670391	0.436328109657722
MAGOH;MAGOHB	Protein mago nashi homolog	88.7703	105.475	94.9299	96.3917333	119.488	106.434	114.802	113.574667	0.05011825	1.3000041	-0.236659741520723
ARHGDIB	Rho GDP-dissociation inhibitor 2	1915.83	2185.09	1950.41	2017.11	1526.41	1287.37	1806.11	1539.96333	0.05021631	1.29915519	0.389393760628094
ARFIP1	Arfaptin-1	38.8924	53.0263	38.6499	43.5228667	26.8264	19.1334	32.9884	26.3160667	0.05043946	1.29722958	0.725829711283471
	14-3-3 protein eta	344.363	245.447	269.583	286.464333	188.634	203.781	213.477	201.964	0.05096659	1.29271443	0.50425736918229
DDRGK1	DDRGK domain-containing protein 1	23.7524	36.4904	26.6385	28.9604333	14.5685	9.57366	20.9506	15.03092	0.05152124	1.28801369	0.946149874317143
NUMB	Protein numb homolog	60.8467	76.9413	78.9758	72.2546	96.0582		119.111	107.5846	0.0526618	1.27850431	-0.574310237690923
CANX	Calnexin	1058.61	998.111	1302.27	1119.66367	923.19	821.843	749.799	831.610667	0.05269037	1.27826878	0.429085261156771
DDX3X	ATP-dependent RNA helicase DDX3X	356.286	332.079	319.361	335.908667	303.31	294.445	312.265	303.34	0.05318388	1.27421997	0.147133266717643
STXBP2	Syntaxin-binding protein 2	178.595	170.749	190.642	179.995333	149.952	168.619	156.848	158.473	0.05364861	1.27044156	0.183722442211833
ILF3	Interleukin enhancer-binding factor 3	426.932	385.228	455.776	422.645333	375.109	310.811	355.298	347.072667	0.05383808	1.26891046	0.284209768641354
VARS1	Valine--tRNA ligase	119.257	105.295	104.107	109.553	100.163	91.2772	91.0809	94.1737	0.05452773	1.26338261	0.21823287358025
GCN1	Stalled ribosome sensor GCN1	66.9299	62.6685	57.3229	62.3071	55.9381	35.4533	42.4356	44.609	0.0556942	1.25419005	0.482061762592209
PPP3CB	e/threonine-protein phosphatase 2B catalytic subunit beta iso	20.8702	16.9816	17.7356	18.5291333	13.7692		9.02246	11.39583	0.05569604	1.25417569	0.701289398305467
TARDBP	TAR DNA-binding protein 43	168.963	146.813	146.206	153.994	185.439	169.924	176.459	177.274	0.05606245	1.25132795	-0.203106817070847
PDS5A	Sister chromatid cohesion protein PDS5 homolog A	31.9731	29.0668	34.3065	31.7821333	22.6155	28.9991	21.1671	24.2605667	0.05726695	1.24209598	0.389602718288146
ANKRD44	threonine-protein phosphatase 6 regulatory ankyrin repeat su	110.931	106.985	117.151	111.689	106.075	101.15	98.3358	101.8536	0.05753108	1.24009747	0.13299013196562
DDX24	ATP-dependent RNA helicase DDX24	10.6691		9.19694	9.93302	17.4745		22.23	19.85225	0.05758306	1.23970524	-0.998998206347088
CAPRIN1	Caprin-1	75.7052	67.2052	56.0809	66.3304333	55.41	47.8967	43.0672	48.7913	0.05945874	1.22578428	0.443047027880295
CCT8	T-complex protein 1 subunit theta	493.67	509.329	544.595	515.864667	480.638	438.418	473.269	464.108333	0.06005956	1.22141785	0.152531032598728
PREB	Prolactin regulatory element-binding protein	33.77	39.528	44.2106	39.1695333	45.0873	48.5033	50.0226	47.8710667	0.06037803	1.21912109	-0.28942201256284
TRAPPC3	Trafficking protein particle complex subunit 3	66.0573	82.7723	60.6298	69.8198	43.7968	58.0744	44.1934	48.6882	0.06051838	1.21811268	0.520064059033318
PNPO	Pyridoxine-5'-phosphate oxidase	64.8858	68.8705		66.87815	49.7144		55.823	52.7687	0.0607736	1.21628502	0.341852497783317
S100A11	Protein S100-A11	539.354	634.981	410.852	528.395667	350.124	370.57	358.909	359.867667	0.0610224	1.21451073	0.554152150150084
HIBCH	3-hydroxyisobutyryl-CoA hydrolase, mitochondrial	61.3459	77.799	65.9102	68.3517	95.4308	120	82.6663	99.3657	0.06107746	1.214119	-0.53977071441617
VPS45	Vacuolar protein sorting-associated protein 45	19.3959	12.6308	14.1428	15.3898333	31.9698		23.2579	27.61385	0.06158132	1.21055103	-0.843414438663018
ELOB	Elongin-B	67.4295	59.7141	83.1448	70.0961333	56.8637	44.0537	31.1379	44.0184333	0.06174846	1.2093739	0.671227065030441
RPS6KA3	Ribosomal protein S6 kinase alpha-3	152.294	151.676	151.788	151.919333	123.161	86.2837	134.371	114.605233	0.06207108	1.2071107	0.406632554819413
MFSD1	Major facilitator superfamily domain-containing protein 1	50.1343	49.3859	41.0809	46.8670333	34.6689		19.3377	27.0033	0.06211936	1.20677301	0.795437749725118
RPL35A	Large ribosomal subunit protein eL33	660.106	569.302	578.548	602.652	549.677	357.553	400.623	435.951	0.06223871	1.20593941	0.467159173511866
SH3BP1	SH3 domain-binding protein 1	72.9943	78.4748	99.5795	83.6828667	60.3165	61.4195	65.7164	62.4841333	0.06241658	1.20470006	0.421442382751392

PANK4	4'-phosphopantetheine phosphatase	22.9483		24.7563	23.8523	31.039		35.7074	33.3732	0.06269172	1.20278985	-0.484561639083649
PKN1	Serine/threonine-protein kinase N1	93.5015	91.1251	84.0112	89.5459333	82.4619	48.7328	56.7732	62.6559667	0.06360274	1.19652417	0.515176012168454
COPS5	COP9 signalosome complex subunit 5	71.2262	68.8109	55.9484	65.3285	51.7009	55.2889	41.8504	49.6134	0.06475218	1.18874559	0.396982686241965
GSPT1	aryotic peptide chain release factor GTP-binding subunit ER	83.6797	91.949	84.7911	86.8066	67.5348	64.333	82.2822	71.3833333	0.06490244	1.18773899	0.28221746511428
NUDT3	Diphosphoinositol polyphosphate phosphohydrolase 1	49.4548	47.8872	43.1956	46.8458667	36.6404		20.9401	28.79025	0.06509594	1.18644607	0.702341444151921
SNAP29	Synaptosomal-associated protein 29	22.4666	30.1951	29.4317	27.3644667	11.9145	10.6934	23.4752	15.3610333	0.06512981	1.18622016	0.833028469597972
UBE2N	Ubiquitin-conjugating enzyme E2 N	386.186	356.385	393.296	378.622333	330.749	205.313	301.216	279.092667	0.06543857	1.18416619	0.440015294849724
LILRB1	eukocyte immunoglobulin-like receptor subfamily B member	92.0296	72.0916	64.5555	76.2255667	120.417	88.832	118.003	109.084	0.06544914	1.18409606	-0.517092633012096
CBFB	Core-binding factor subunit beta	100.921	93.1548	124.291	106.122267	79.9705	58.5109	85.6459	74.7091	0.0656062	1.18305513	0.506371508126339
SH3BGRL	Adapter SH3BGRL	315.7	309.102	306.393	310.398333	297.665	229.123	250.469	259.085667	0.0660092	1.18039554	0.260691607215915
STAT3	Signal transducer and activator of transcription 3	139.922	145.898	119.293	135.037667	121.221	94.8201	105.241	107.094033	0.06602177	1.18031284	0.334483777242937
EIF5B	Eukaryotic translation initiation factor 5B	211.791	197.838	211.754	207.127667	185.117	172.952	128.065	162.044667	0.06604394	1.18016704	0.354128733158067
FDX1	Adrenodoxin, mitochondrial	20.4233	35.1089	27.0644	27.5322	16.4392	17.8297	16.1132	16.7940333	0.0660639	1.1800358	0.713171138905073
ACTBL2	Beta-actin-like protein 2	3132.17	3757.79	5091.15	3993.70333	8280.27	7523.94	4935.2	6913.13667	0.06648842	1.17725396	-0.791613278567686
EIF3K	Eukaryotic translation initiation factor 3 subunit K	262.566	309.038	203.218	258.274	190.343	174.201	178.743	181.095667	0.0674984	1.17070653	0.512150391846722
HDAC1	Histone deacetylase 1	194.763	178.269	167.649	180.227	154.712	118.108	156.919	143.246333	0.06750081	1.17069104	0.331316948144775
CTBS	Di-N-acetylchitobiase	50.1971	39.0906	42.7561	44.0146	65.7111	79.6672	51.5961	65.6581333	0.06842203	1.16480405	-0.576991577753344
STX4	Syntaxin-4	45.0931	51.1217	54.812	50.3422667	37.4238	46.0286	38.4319	40.6281	0.06854456	1.16402702	0.309292277922977
TXNIP	Thioredoxin-interacting protein	29.3417	18.0993	28.184	25.2083333	16.6499	6.37253	16.2324	13.0849433	0.06869618	1.16306739	0.945993060000582
PTGES3	Prostaglandin E synthase 3	1149.06	1100.91	911.583	1053.851	919.491	846.579	768.146	844.738667	0.0688882	1.16185517	0.319093909318454
PAIP1	Polyadenylate-binding protein-interacting protein 1	39.9799	38.5883	31.8848	36.8176667	27.987		27.8026	27.8948	0.06984792	1.15584651	0.400401990654315
PSMC5	26S proteasome regulatory subunit 8	138.591	194.692	174.526	169.269667	109.662	140.983	119.338	123.327667	0.07131263	1.14683357	0.456826981153032
ALG5	Dolichyl-phosphate beta-glucosyltransferase	36.4703	46.6939	33.1784	38.7808667	33.0808	20.1796	19.9414	24.4006	0.07299988	1.13667786	0.668428421391316
VTA1	Vacuolar protein sorting-associated protein VTA1 homolog	128.412	201.066	210.003	179.827	129.881	98.1848	112.695	113.586933	0.07304626	1.13640201	0.662812768057947
WARS1	Tryptophan--tRNA ligase, cytoplasmic	331.202	414.711	370.682	372.198333	299.562	308.738	325.393	311.231	0.07339085	1.13435807	0.258085828806799
GGH	Gamma-glutamyl hydrolase	95.6523	120.496	101.894	106.0141	132.999	118.567	128.597	126.721	0.073673	1.13269164	-0.257399467702118
FKBP2	Peptidyl-prolyl cis-trans isomerase FKBP2	299.219	250.887	215.933	255.346333	310.263	380.481	314.725	335.156333	0.07369281	1.13257487	-0.392378853510537
NUCB1	Nucleobindin-1	77.509	79.966	88.4382	81.9710667	57.5825	77.1697	54.0999	62.9507	0.07390434	1.13133004	0.380892350875467
TXLNA	Alpha-taxilin	48.5625	43.2757	38.3286	43.3889333	34.2399		25.5764	29.90815	0.07394557	1.13108784	0.536788445802545
MYL6	Myosin light polypeptide 6	926.918	890.578	896.462	904.652667	694.113	877.179	735.805	769.032333	0.0744288	1.128259	0.234319732201332
IFIT5	Interferon-induced protein with tetratricopeptide repeats 5	10.1295		8.19107	9.160285	17.9349		14.3693	16.1521	0.07489274	1.12556027	-0.8182573576622
SRSF9	Serine/arginine-rich splicing factor 9	74.7397	103.369	103.147	93.7519	77.9216	60.2882	65.0277	67.7458333	0.07494363	1.12526525	0.46871571171335
PSMC6	26S proteasome regulatory subunit 10B	90.8675	81.8215	94.9757	89.2215667	67.4656	81.9141	77.0361	75.4719333	0.07519167	1.12383026	0.241452249419179
NFKB2	Nuclear factor NF-kappa-B p100 subunit	36.036	18.9211	33.0168	29.3246333	45.0512		55.353	50.2021	0.07563709	1.1212652	-0.775634645369989
CCT3	T-complex protein 1 subunit gamma	380.741	405.674	448.038	411.484333	330.703	381.597	345.373	352.557667	0.07624418	1.11779332	0.222978249612937
S100A4	Protein S100-A4	5501.62	5043.58	4587.29	5044.16333	4051.89	3514.71	4619.02	4061.87333	0.07655114	1.11604831	0.312469740934695
NFIA;NFIB;NFIC;NFIX	Nuclear factor 1 B-type	21.9944	17.8506	19.2566	19.7005333	24.7989		23.3841	24.0915	0.07697637	1.11364256	-0.290289535464688
NIT2	Omega-amidase NIT2	73.3543	61.7065	61.0074	65.3560667	76.0084	73.8244	75.0055	74.9461	0.07717493	1.11252373	-0.197532245852939
FMNL1	Formin-like protein 1	192.746	178.285	201.952	190.994333	175.128	143.35	169.637	162.705	0.07760908	1.11008747	0.231271248777001
TECR	Very-long-chain enoyl-CoA reductase	69.1841	92.9213	56.7046	72.9366667	29.7107		40.9302	35.32045	0.07873817	1.10381467	1.04614054374025
PNPT1	Polyribonucleotide nucleotidyltransferase 1, mitochondrial	32.0245	24.3596	15.986	24.1233667	42.2221	37.5518	31.6312	37.1350333	0.07911923	1.10171797	-0.622349608925985
1A;TUBA3C;TUBA3D;TU	Tubulin alpha-3C chain	109.497	118.735	74.0897	100.7739	71.3899	72.2664	58.5664	67.4075667	0.08008103	1.09647033	0.580139583792463
C12;H2AC14;H2AC18;H	Histone H2A type 1	3841.73	4478.46	3720.18	4013.45667	4446.94	6206.29	7130.14	5927.79	0.08019322	1.09586236	-0.562649018225312
PI4KA	Phosphatidylinositol 4-kinase alpha	42.7191		52.995	47.85705	32.4276	38.3503	37.5388	36.1055667	0.08022175	1.0957079	0.406510183736153
NRDC	Nardilysin	84.2541	90.4359	75.6027	83.4309	77.1827	69.2654	65.5072	70.6517667	0.08115106	1.09070578	0.23985617238246
GSK3A	Glycogen synthase kinase-3 alpha	38.5985	55.517	34.2468	42.7874333	21.4972		20.7245	21.11085	0.0813138	1.08983576	1.01920247135712
ARPC3	Actin-related protein 2/3 complex subunit 3	1899.04	1928.12	1679.68	1835.61333	1698.98	1335.17	1557.09	1530.41333	0.08144174	1.08915294	0.262340843234378
RAN	GTP-binding nuclear protein Ran	1402.67	1356.42	1531.35	1430.14667	1355.49	1246.41	1255.13	1285.67667	0.08342075	1.07872591	0.153635241559272
CYP1B1	Cytochrome P450 1B1	92.48	56.761	86.8317	78.6909	29.4922	59.3938	49.7592	46.2150667	0.08355221	1.07804204	0.767833544512587
TMCO1	Calcium load-activated calcium channel	232.648	236.476	282.99	250.704667	174.001	185.779	230.248	196.676	0.08357065	1.07794622	0.350167932022988

S100A8	Protein S100-A8	6044.97	5536.81	6463	6014.92667	4811.06	4584.77	5689.87	5028.56667	0.0837346	1.07709506	0.258399912823961
PPP6R1	Serine/threonine-protein phosphatase 6 regulatory subunit 1	86.2177	71.0913	77.1399	78.1496333	50.6871	68.9021	65.8034	61.7975333	0.08384435	1.07652621	0.338689850643149
EIF3L	Eukaryotic translation initiation factor 3 subunit L	225.848	246.687	222.638	231.724333	211.993	185.307	214.966	204.088667	0.08394225	1.07601941	0.183213479629945
NHERF1	Na(+)/H(+) exchange regulatory cofactor NHE-RF1	61.9243	62.7467	79.49	68.0536667	38.3955	50.1851	58.9673	49.1826333	0.08442341	1.0735371	0.468523913171095
COPB1	Coatomer subunit beta	241.778	254.952	239.387	245.372333	189.697	170.464	237.101	199.087333	0.08566498	1.06719669	0.301571154375215
ARHGAP18	Rho GTPase-activating protein 18	203.693	129.641	154.613	162.649	115.76	120.938	89.319	108.672333	0.08640898	1.06344114	0.581777258078921
RK1;MARK2;MARK3;MAI	MAP/microtubule affinity-regulating kinase 3	38.4419	36.3474	27.2274	34.0055667	49.9953		43.4815	46.7384	0.08660815	1.06244125	-0.458837414070982
KIF5B	Kinesin-1 heavy chain	126.496	128.289	118.246	124.343667	106.801	121.031	107	111.610667	0.0867129	1.06191628	0.155858114469084
RAB31	Ras-related protein Rab-31	186.391	155.852	163.746	168.663	128.375	131.532	157.691	139.199333	0.08675409	1.06171004	0.276991219210764
WDR26	WD repeat-containing protein 26	24.4284		24.2528	24.3406	41.4942		33.2469	37.37055	0.08728244	1.05907311	-0.618537065525626
BABAM2	BRISC and BRCA1-A complex member 2	18.3562	28.5796	25.1259	24.0205667	15.8111		10.1046	12.95785	0.08754299	1.05777861	0.890443823527118
CAND1	Cullin-associated NEDD8-dissociated protein 1	114.849	121.619	134.456	123.641333	74.6928	93.8454	114.897	94.4784	0.08755519	1.05771808	0.38810467935584
RPL17	Large ribosomal subunit protein uL22	183.933	207.615	183.204	191.584	148.171	182.225	134.531	154.975667	0.08793524	1.05583703	0.305935370354967
DAD1	diphosphooligosaccharide--protein glycosyltransferase subur	75.3211	64.356	60.9354	66.8708333	44.299	24.7136	58.8917	42.6347667	0.08843302	1.05338554	0.649346735059042
SELENOF	Selenoprotein F	64.39	60.9577	63.1444	62.8307	56.9051	31.8832	49.6187	46.1356667	0.08993793	1.0460571	0.44558714933641
PREP	Prolyl endopeptidase	134.488	128.856	117.223	126.855667	112.523	89.813	115.025	105.787	0.09071988	1.04229754	0.262025618508725
MYL12A;MYL12B	Myosin regulatory light chain 12B	637.565	768.444	605.785	670.598	524.916	592.547	537.884	551.782333	0.09227505	1.03491573	0.281348914420669
ETF1	Eukaryotic peptide chain release factor subunit 1	128.173	115.451	132.54	125.388	115.611	112.512	96.858	108.327	0.09231252	1.03473939	0.211006411809391
H2AZ1;H2AZ2	Histone H2A.Z	71.1481	80.4326	95.3389	82.3065333	64.1581	50.0236	70.9234	61.7017	0.09243751	1.03415175	0.415696714599085
CCT5	T-complex protein 1 subunit epsilon	580.477	585.798	620.316	595.530333	519.703	502.633	583.015	535.117	0.09260649	1.03335858	0.154320631332379
RAP1GDS1	Rap1 GTPase-GDP dissociation stimulator 1	50.9277	66.1939	59.6975	58.9397	41.4042	24.8235	51.5164	39.2480333	0.09263435	1.03322795	0.586619352949277
PIN1	Peptidyl-prolyl cis-trans isomerase NIMA-interacting 1	75.0951	106.321	93.8632	91.7597667	105.386	138.684	118.753	120.941	0.09266246	1.03309617	-0.398369785185168
MGST2	Microsomal glutathione S-transferase 2	221.759	291.286	325.743	279.596	172.678	199.369	233.889	201.978667	0.09305731	1.03124953	0.469140800053492
FCER1G	High affinity immunoglobulin epsilon receptor subunit gamma	337.004	786.147	905.957	676.369333	282.292	199.765	365.381	282.479333	0.0934268	1.02952854	1.2596659278896
PRKDC	DNA-dependent protein kinase catalytic subunit	234.367	231.132	229.775	231.758	208.606	171.641	219.476	199.907667	0.09365872	1.02845178	0.213285337764893
SEPTIN7	Septin-7	109.118	111.373	124.27	114.920333	94.5825	107.957	102.169	101.5695	0.09402971	1.02673491	0.178166838029603
UBE2I	SUMO-conjugating enzyme UBC9	784.324	888.828	971.764	881.638667	729.796	638.841	804.222	724.286333	0.09513469	1.0216611	0.28362734548923
UBE2V2	Ubiquitin-conjugating enzyme E2 variant 2	57.2801	62.4623	66.6607	62.1343667	49.0458	58.5019	40.2706	49.2727667	0.09561705	1.01946465	0.334600966002729
TRIM28	Transcription intermediary factor 1-beta	171.743	138.1	151.397	153.746667	139.112	127.893	108.739	125.248	0.09705728	1.01297187	0.295767565981558
GRHPR	Glyoxylate reductase/hydroxypyruvate reductase	221.866	248.964	244.516	238.448667	262.232	249.828	274.365	262.141667	0.09713313	1.0126326	-0.136667968497349
RPS10	Small ribosomal subunit protein eS10	206.592	263.015	301.091	256.899333	140.467	222.761	172.655	178.627667	0.09811033	1.00828528	0.524247597432597
EHD4	EH domain-containing protein 4	230.389	201.32	201.263	210.990667	200.825	173.572	169.901	181.432667	0.09811154	1.00827991	0.217744947396997
GNB1	uanine nucleotide-binding protein G(I)/G(S)/G(T) subunit beta	373.822	384.905	376.028	378.251667	381.458	422.209	428.608	410.758333	0.09845513	1.00676166	-0.118943405093595
RPL6	Large ribosomal subunit protein eL6	831.369	786.355	826.105	814.609667	787.155	679.156	577.505	681.272	0.09858351	1.00619571	0.257878020553111
CAMK1	Calcium/calmodulin-dependent protein kinase type 1	77.6924	46.3634	58.9846	61.0134667	47.767	37.4029	33.2104	39.4601	0.09920369	1.00347218	0.628733091982638
COPE	Coatomer subunit epsilon	83.8614	70.2421	82.5726	78.8920333	60.9919	37.7165	70.1247	56.2777	0.09935767	1.00279862	0.487316252904392
NFKB1	Nuclear factor NF-kappa-B p105 subunit	56.2778	46.5868	44.2746	49.0464	59.2207	57.2787	55.295	57.2648	0.09952899	1.00205042	-0.223501357044075
SMAP1	Stromal membrane-associated protein 1	67.4635	79.0067	68.09	71.5200667	98.0044	76.9774	85.4572	86.813	0.09974201	1.0011219	-0.279563017014157
FAH	Fumarylacetoacetase	89.4579	117.407	97.6646	101.509833	87.3654	64.7922	83.3185	78.4920333	0.1005148	0.99777001	0.3710013510755
SMS	Spermine synthase	105.582	123.095	97.9922	108.889733	128.925	123.224	123.349	125.166	0.10100926	0.9956388	-0.200974786880473
U2AF2	Splicing factor U2AF 65 kDa subunit	1363.77	1247.35	1209.3	1273.47333	1137.61	1029.17	1208.9	1125.22667	0.10132687	0.99427539	0.178553101243774
STIM1	Stromal interaction molecule 1	41.0871	44.7705	53.9785	46.6120333	49.2938	77.6423	77.3483	68.0948	0.10179905	0.99225629	-0.546842184084205
ARFGEF1	Brefeldin A-inhibited guanine nucleotide-exchange protein 1	30.7844	29.2277	35.7231	31.9117333	18.524		26.7659	22.64495	0.10218933	0.99059446	0.494897618951686
SETD3	Actin-histidine N-methyltransferase	43.436		42.2055	42.82075	24.1368		33.7663	28.95155	0.10376696	0.9839409	0.564669475678757
PSMC4	26S proteasome regulatory subunit 6B	159.284	165.137	223.075	182.498667	133.649	136.125	147.05	138.941333	0.10399577	0.98298434	0.393410076561673
VCAN	Versican core protein	33.0949	23.9519	24.2278	27.0915333	36.726	30.4451	38.1893	35.1201333	0.10400998	0.982925	-0.374456272201952
SH3KBP1	SH3 domain-containing kinase-binding protein 1	67.4145	103.4	96.4129	89.0758	53.5872	76.415	52.0105	60.6709	0.10405009	0.98275756	0.554028822771847
SKIC8	Superkiller complex protein 8	40.8003	66.6176	42.5955	50.0044667	31.194	29.6319	35.7551	32.1936667	0.10486293	0.97937802	0.635280069351949
SAP18	Histone deacetylase complex subunit SAP18	131.903	151.904	132.689	138.832	133.437	105.039	108.842	115.772667	0.10508723	0.97845005	0.262045458765465
CSRP1	Cysteine and glycine-rich protein 1	142.219	125.062	116.566	127.949	116.338	95.4738	110.756	107.5226	0.10521176	0.97793573	0.250928942467471

MAP2K1	Dual specificity mitogen-activated protein kinase kinase 1	336.74	250.343	330.34	305.807667	237.391	222.579	266.39	242.12	0.10609072	0.97432259	0.336902319679017
PPP1CB	erine/threonine-protein phosphatase PP1-beta catalytic subur	150.872	187.231	131.379	156.494	117.261	122.531	126.33	122.040667	0.10620484	0.97385569	0.358745379102402
SDHC	ccinate dehydrogenase cytochrome b560 subunit, mitochond	54.3893	51.6	41.0812	49.0235	29.0991	28.6554	45.9411	34.5652	0.1072346	0.96966507	0.504153214786582
FUS	RNA-binding protein FUS	221.565	192.577	230.106	214.749333	202.818	178.051	170.223	183.697333	0.10748689	0.96864451	0.22532296914837
SRI	Sorcin	189.612	193.425	189.81	190.949	151.507	136.166	188.544	158.739	0.1078047	0.96736229	0.266530742434929
PGRMC1	Membrane-associated progesterone receptor component 1	63.1394	111.031	96.3352	90.1685333	47.1075	57.9471	69.2657	58.1067667	0.10809971	0.96617546	0.633917876593592
CXCL8	Interleukin-8	51.5354	99.5373	216.027	122.366567		265.473	265.08	265.2765	0.10825886	0.96553654	-1.11628744274737
STK4	Serine/threonine-protein kinase 4	78.0565	70.6862	88.5246	79.0891	56.0863	43.2569	74.0802	57.8078	0.10842153	0.96488448	0.452214708716955
DDX46	Probable ATP-dependent RNA helicase DDX46	86.1857	90.5839	92.0581	89.6092333	115.573	96.5695	96.9335	103.025333	0.10865684	0.96394292	-0.201279831075436
ARF1;ARF3	ADP-ribosylation factor 3	729.541	767.255	839.787	778.861	845.988	834.587	860.209	846.928	0.1095727	0.96029763	-0.12087344711992
PTBP3	Polypyrimidine tract-binding protein 3	67.3168	76.9146	57.2597	67.1637	58.8414	54.1928	50.658	54.5640667	0.10982073	0.95931567	0.299730536888142
QARS1	Glutamine--tRNA ligase	167.014	168.883	133.595	156.497333	140.043	125.443	128.403	131.296333	0.10982076	0.95931557	0.253311447130562
THOP1	Thimet oligopeptidase	37.5121	58.3078	30.7796	42.1998333	17.8955		18.3521	18.1238	0.10987365	0.95910643	1.21935182546931
RPL23	Large ribosomal subunit protein uL14	566.252	464.993	556.298	529.181	468.115	413.927	474.822	452.288	0.10996366	0.9587508	0.226519544017833
IL4I1	L-amino-acid oxidase	38.0475	30.8022	30.3818	33.0771667	48.9416		39.1083	44.02495	0.11029008	0.95746356	-0.412485704540086
ACAA2	3-ketoacyl-CoA thiolase, mitochondrial	372.304	373.644	367.851	371.266333	361.374	355.182	322.17	346.242	0.11149988	0.95272558	0.100673758871724
HTT	Huntingtin	28.3409	24.7788	26.6236	26.5811	23.3863	6.06672	18.3452	15.93274	0.11218867	0.95005101	0.738406415896743
CIAO2A	Cytosolic iron-sulfur assembly component 2A	51.1743	60.5826	43.8213	51.8594	66.4337	75.1819	57.186	66.2672	0.11259881	0.9484662	-0.353689447572402
RPLP2	Large ribosomal subunit protein P2	181.793	88.9875	216.323	162.367833	71.5622	50.8864	110.57	77.6728667	0.11303202	0.94679852	1.06378323124409
USP14	Ubiquitin carboxyl-terminal hydrolase 14	84.5812	76.9264	76.6944	79.4006667	77.5266	67.7454	67.2675	70.8465	0.1131768	0.94624258	0.164454538581636
EIF6	Eukaryotic translation initiation factor 6	227.045	191.648	200.054	206.249	274.751	248.878	216.304	246.644333	0.11350346	0.94499089	-0.258045017261477
SUCLA2	uccinate--CoA ligase [ADP-forming] subunit beta, mitochondr	105.745	107.425	116.236	109.802	107.52	91.445	95.0365	98.0005	0.11419229	0.94236323	0.164033317691288
TMED5	Transmembrane emp24 domain-containing protein 5	251.308	260.098	261.725	257.710333	247.919	141.434	197.172	195.508333	0.11458039	0.94088969	0.398520283489948
COX6B1	Cytochrome c oxidase subunit 6B1	157.072	102.434	137.059	132.188333	108.731	98.3879	65.1616	90.7601667	0.11561267	0.93699459	0.542463689801924
HSPA13	Heat shock 70 kDa protein 13	29.3514	18.2112	19.4672	22.3432667	17.5165	9.93664	14.5959	14.0163467	0.11571385	0.93661467	0.672729765785208
PRPF3	U4/U6 small nuclear ribonucleoprotein Prp3	56.5436	69.9683	49.1164	58.5427667	51.2246	30.7574	42.5402	41.5074	0.11585557	0.93608306	0.496122362363805
CEPT1	Choline/ethanolaminephosphotransferase 1	130.652	133.491	110.732	124.958333	130.041	166.472	156.535	151.016	0.11590921	0.93588205	-0.273254293427785
XPOT	Exportin-T	57.3963	46.3903	58.1448	53.9771333	41.353	42.2847	50.0934	44.5770333	0.1162734	0.93451964	0.276047752548913
ATP6V0D1	V-type proton ATPase subunit d 1	197.301	203.6	191.347	197.416	165.429	109.553	183.187	152.723	0.11753232	0.92984271	0.370321573245535
FASN	Fatty acid synthase	114.656	94.7762	81.5752	97.0024667	82.0691	77.8857	70.1096	76.6881333	0.11809656	0.92776276	0.339018080519478
TM9SF2	Transmembrane 9 superfamily member 2	118.094	93.9631	96.0812	102.712767	86.9046	73.8788	91.7261	84.1698333	0.11915071	0.92390336	0.287240346609694
PARP4	Protein mono-ADP-ribosyltransferase PARP4	30.3013	28.1067	21.8444	26.7508	38.9865		32.303	35.64475	0.11920915	0.92369042	-0.41410756553874
ACTR1A	Alpha-centractin	204.421	269.06	216.242	229.907667	160.42	207.655	178.317	182.130667	0.11930722	0.92333329	0.336080716168333
PMPCB	Mitochondrial-processing peptidase subunit beta	64.1585	56.5506	74.6047	65.1046	106.792	169.929	79.832	118.851	0.11941586	0.922938	-0.868322655530847
PSMD13	26S proteasome non-ATPase regulatory subunit 13	148.023	155.637	147.782	150.480667	114.999	125.956	149.083	130.012667	0.11970069	0.92190334	0.210925958792753
THOC6	THO complex subunit 6 homolog	18.8917	13.6497	12.3986	14.98	30.4961		19.853	25.17455	0.11984928	0.92136459	-0.748928366210142
HNRNPA0	Heterogeneous nuclear ribonucleoprotein A0	78.985	85.6809	103.425	89.3636333	65.7229	77.1315	76.8127	73.2223667	0.12037486	0.91946421	0.287403439234703
GAR1	H/ACA ribonucleoprotein complex subunit 1	35.0326	27.9787	21.5164	28.1759	37.3948		56.5263	46.96055	0.12052964	0.91890616	-0.736987611355857
UBA2	SUMO-activating enzyme subunit 2	63.5452	76.5739	73.454	71.1910333	62.8727	54.0581	65.6669	60.8659	0.12112116	0.91677999	0.226061354610981
YWHAB	14-3-3 protein beta/alpha	1034.52	939.699	1275.06	1083.093	908.555	510.195	876.102	764.950667	0.12118116	0.91656491	0.501718512192071
RAB7A	Ras-related protein Rab-7a	1589.91	1572.46	1451.89	1538.08667	1436.77	1057.59	1379.97	1291.44333	0.12145309	0.91559143	0.25215245574705
RPL35	Large ribosomal subunit protein uL29	1009.36	1262.3	1002.77	1091.47667	1225.02	1900.29	1427.89	1517.73333	0.12161016	0.91503014	-0.475637041565449
MAPK14	Mitogen-activated protein kinase 14	209.897	207.741	243.035	220.224333	192.81	176.859	206.802	192.157	0.1217055	0.91468981	0.19668835333691
SGTB	all glutamine-rich tetratricopeptide repeat-containing protein b	27.5692	71.682	43.4969	47.5827	8.71335		14.5459	11.629625	0.12171901	0.91464158	2.0326325598614
SART1	U4/U6.U5 tri-snRNP-associated protein 1	34.2851	58.4549		46.37	22.0184	28.2578	28.5883	26.2881667	0.12281367	0.91075329	0.818778194613272
RIN3	Ras and Rab interactor 3	40.118	26.8661	27.1732	31.3857667	20.3362		18.1881	19.26215	0.12312057	0.90966938	0.704341707659077
EIF3I	Eukaryotic translation initiation factor 3 subunit I	148.759	143.551	130.689	140.999667	126.525	135.411	123.377	128.437667	0.12401832	0.90651414	0.134623391090004
SKP1	S-phase kinase-associated protein 1	67.1908	52.8399	56.417	58.8159	42.8021		49.1641	45.9831	0.12412095	0.9061549	0.355102488673882
API5	Apoptosis inhibitor 5	87.1503	89.7703	111.809	96.2432	83.2083	76.9703	81.7692	80.6492667	0.12457178	0.90458034	0.255023196424965
SNX5	Sorting nexin-5	128.018	128.197	97.6004	117.938467	103.554	86.1928	97.9551	95.9006333	0.12495897	0.90323255	0.298422094699605

RNF181	E3 ubiquitin-protein ligase RNF181	53.5111		34.9021	44.2066	19.5494		21.2506	20.4	0.12564839	0.90084307	1.11569262638912
MAPKAPK5	MAP kinase-activated protein kinase 5	129.222	90.7634	106.876	108.9538	66.1804	101.523	65.3783	77.6939	0.12794353	0.89298167	0.48784327692216
TBC1D15	TBC1 domain family member 15	27.0729	33.4901	34.3111	31.6247	17.0942	30.7982	11.3508	19.7477333	0.12817994	0.89217992	0.679364725436778
VCP	Transitional endoplasmic reticulum ATPase	794.227	848.25	686.22	776.232333	715.893	628.655	674.855	673.134333	0.12826338	0.89189733	0.205594085215662
UBXN4	UBX domain-containing protein 4	39.3652	23.8971	25.2011	29.4878	51.5408		39.7592	45.65	0.12855365	0.89091558	-0.630496669125069
HMOX2	Heme oxygenase 2	41.245	37.0421	50.4805	42.9225333	37.4656	33.7104	33.8435	35.0065	0.1294792	0.88779999	0.294112401734578
FLOT2	Flotillin-2	46.3811	63.6919	59.6843	56.5857667	39.5763	42.1856	51.6184	44.4601	0.13031197	0.8850157	0.347928016273798
PMM2	Phosphomannomutase 2	56.3095	57.7977	52.2218	55.443	64.2049	59.8785	57.2142	60.4325333	0.13089189	0.88308728	-0.124320097841574
SF1	Splicing factor 1	112.91	98.3752	108.943	106.742733	111.376	126.308	117.421	118.368333	0.1309288	0.88296481	-0.14914531379343
NDUFA13	DH dehydrogenase [ubiquinone] 1 alpha subcomplex subunit	231.03	203.238	186.518	206.928667	157.632	191.879	178.292	175.934333	0.13106143	0.88252511	0.234096471276093
H2AC25;H2AC4	Histone H2A type 1-B/E	89.3686	126.258	90.2784	101.968333	108.746	168.37	150.189	142.435	0.13188245	0.87981298	-0.482182510586217
GCDH	Glutaryl-CoA dehydrogenase, mitochondrial	72.5779		56.1734	64.37565	85.3341		84.0688	84.70145	0.13211472	0.87904879	-0.395871573067495
LYPLA2	Acyl-protein thioesterase 2	96.4375	103.423	92.452	97.4375	93.5032	30.4621	63.6913	62.5522	0.13221224	0.87872835	0.639416492040034
ATP6V1A	V-type proton ATPase catalytic subunit A	768.592	760.118	651.171	726.627	663.445	589.212	669.046	640.567667	0.13299696	0.87615829	0.181863996013778
EIF3F	Eukaryotic translation initiation factor 3 subunit F	183.839	230.082	213.178	209.033	161.338	127.566	198.989	162.631	0.133001	0.87614511	0.362128434521446
UBE2D1;UBE2D4	Ubiquitin-conjugating enzyme E2 D1	155.837		116.37	136.1035	90.2753		83.6047	86.94	0.13335415	0.87499346	0.646612166537354
OXSR1	Serine/threonine-protein kinase OSR1	119.515	141.381	122.867	127.921	103.649	115.344	118.753	112.582	0.13453503	0.87116462	0.184276939213626
MCU	Calcium uniporter protein, mitochondrial	30.5017		33.334	31.91785	43.6326		37.2528	40.4427	0.13458853	0.87099194	-0.341515842115349
NELFB	Negative elongation factor B	15.1136	25.2272	22.835	21.0586	13.4146		12.6303	13.02245	0.13479635	0.87032187	0.693408629684454
MSN	Moesin	3293.5	3201.31	3153.75	3216.18667	3712.78	3203.11	3716.35	3544.08	0.13484772	0.87015638	-0.140060027400007
FAF2	FAS-associated factor 2	18.8776	15.9031		17.39035	12.8599	5.79674	13.2683	10.6416467	0.13510758	0.86932028	0.708565560971502
PSMC1	26S proteasome regulatory subunit 4	91.2643	123.157	149.035	121.1521	87.3652	99.7448	73.6666	86.9255333	0.13520013	0.86902288	0.478967493303729
UBE2A	Ubiquitin-conjugating enzyme E2 A	50.3804	75.6935	54.1047	60.0595333	44.1657		27.465	35.81535	0.13522557	0.8689412	0.745815224465362
CASP7	Caspase-7	48.9598		33.2797	41.11975	58.5822		64.0471	61.31465	0.13549999	0.86806072	-0.576400327106649
PPA1	Inorganic pyrophosphatase	206.847	179.44	250.465	212.250667	184.472	137.947	174.277	165.565333	0.13571028	0.86738726	0.358368457437887
YWHAQ	14-3-3 protein theta	120.044	114.235	149.146	127.808333	111.295	103.762	106.889	107.315333	0.13642427	0.86510836	0.252125680981841
BABAM1	BRISC and BRCA1-A complex member 1	51.5275	53.0103	61.6191	55.3856333	47.9371	31.508	49.8236	43.0895667	0.13648268	0.86492246	0.362173209303493
DOCK8	Dedicator of cytokinesis protein 8	191.369	183.357	196.754	190.493333	169.894	114.945	176.264	153.701	0.13743348	0.86190745	0.309613957386689
PSTPIP2	Proline-serine-threonine phosphatase-interacting protein 2	31.2122	45.0517	21.9422	32.7353667	14.4265	8.93138	27.0563	16.8047267	0.13743487	0.86190307	0.96198306152869
PRKRA	n-inducible double-stranded RNA-dependent protein kinase ac	28.8341	17.3308	6.4663	17.5437333	27.4894	27.8537	37.5459	30.963	0.13780306	0.86074115	-0.819589472572497
GALNT2	Polypeptide N-acetylgalactosaminyltransferase 2	49.7604	74.3521	57.4322	60.5149	47.454	49.3739	43.282	46.7033	0.13870033	0.8579225	0.373765914343347
DBI	Acyl-CoA-binding protein	621.036	1194.5	1092.9	969.478667	638.696	640.143	651.226	643.355	0.13871815	0.85786671	0.591594123227198
MEMO1	Protein MEMO1	43.6237	28.5602	27.9005	33.3614667	58.6836		43.2355	50.95955	0.1387376	0.85780582	-0.611169822656106
FKBP1A	Peptidyl-prolyl cis-trans isomerase FKBP1A	815.569	740.578	856.855	804.334	700.926	773.716	712.865	729.169	0.1393727	0.85582229	0.141541477760245
GPAT3	Glycerol-3-phosphate acyltransferase 3	46.0355	44.7004	38.8614	43.1991	56.9601	48.8993	45.7828	50.5474	0.13953625	0.85531294	-0.22663563039171
IARS1	Isoleucine--tRNA ligase, cytoplasmic	119.729	128.864	143.152	130.581667	123.909	113.074	95.075	110.686	0.13991462	0.85413692	0.238479604469672
SARS1	Serine--tRNA ligase, cytoplasmic	211.579	256.776	264.689	244.348	222.134	196.603	214.176	210.971	0.14028112	0.85300077	0.211892595900818
AP2B1	AP-2 complex subunit beta	208.178	233.2	207.691	216.356333	205.782	138.223	185.565	176.523333	0.14057765	0.85208371	0.293550457504827
HP1BP3	Heterochromatin protein 1-binding protein 3	141.182	172.019	197.554	170.251667	136.062	131.243	149.152	138.819	0.14082048	0.85133419	0.294463879993726
EIF3M	Eukaryotic translation initiation factor 3 subunit M	109.358	88.6389	95.5701	97.8556667	82.699	87.4532	88.535	86.2290667	0.1409577	0.85091119	0.182481132929144
MSRA	Mitochondrial peptide methionine sulfoxide reductase	91.0102	57.5965	75.1138	74.5735	62.9827	52.399	51.6895	55.6904	0.14119199	0.85018995	0.421234399005407
ATP5F1B	ATP synthase subunit beta, mitochondrial	1169.62	1221.78	1665.92	1352.44	985.538	1060.63	1122.41	1056.19267	0.14210734	0.8473835	0.356691561704904
CAST	Calpastatin	70.0917	59.0289	97.3544	75.4916667	57.5393	55.5824	50.469	54.5302333	0.1445686	0.83992601	0.469261069064015
GLRX	Glutaredoxin-1	147.368	153.59	97.1562	132.704733	75.0747	116.81	88.9453	93.61	0.14559364	0.8368576	0.503485269126013
DNM1L	Dynamin-1-like protein	164.526	154.474	143.673	154.224333	145.278	128.006	144.7	139.328	0.14587991	0.83600452	0.146545192181995
EIF3G	Eukaryotic translation initiation factor 3 subunit G	277.429	352.89	343.482	324.600333	326.433	147.333	170.75	214.838667	0.14641451	0.83441588	0.595410808426583
RBM12	RNA-binding protein 12	60.9523	64.7169	49.1533	58.2741667	51.9544	41.684	50.5388	48.0590667	0.14671208	0.83353412	0.278047837833037
RSU1	Ras suppressor protein 1	295.164	322.825	350.079	322.689333	285.816	200.987	296.916	261.239667	0.14672714	0.83348955	0.304771917035988
SRP72	Signal recognition particle subunit SRP72	64.0211	55.2396	58.3917	59.2174667	59.3082	42.129	43.2964	48.2445333	0.14685331	0.83311627	0.295657295579043
LRCH4	ne-rich repeat and calponin homology domain-containing pro	56.23	61.6103	68.2925	62.0442667	52.3789		54.032	53.20545	0.14709574	0.83239991	0.221723868146645

PRKACA	[illegible]	[illegible]	[illegible]	[illegible]	[illegible]	[illegible]	[illegible]	[illegible]	[illegible]	[illegible]	[illegible]	[illegible]
UAP1L1	[illegible]	[illegible]	[illegible]	[illegible]	[illegible]	[illegible]	[illegible]	[illegible]	[illegible]	[illegible]	[illegible]	[illegible]
RARS1	[illegible]	[illegible]	[illegible]	[illegible]	[illegible]	[illegible]	140.197	[illegible]	[illegible]	[illegible]	[illegible]	[illegible]
SAE1	[illegible]	[illegible]	[illegible]	[illegible]	[illegible]	[illegible]	84.0583	[illegible]	[illegible]	[illegible]	[illegible]	[illegible]
MTPN	[illegible]	[illegible]	[illegible]	[illegible]	[illegible]	[illegible]	50.0558	[illegible]	[illegible]	[illegible]	[illegible]	[illegible]
CFL1	[illegible]	[illegible]	[illegible]	[illegible]	[illegible]	[illegible]	3297.27	[illegible]	[illegible]	[illegible]	[illegible]	[illegible]
CCT2	[illegible]	[illegible]	[illegible]	[illegible]	[illegible]	[illegible]	[illegible]	[illegible]	[illegible]	[illegible]	[illegible]	[illegible]
CYB5R3	[illegible]	[illegible]	[illegible]	[illegible]	[illegible]	[illegible]	[illegible]	[illegible]	[illegible]	[illegible]	[illegible]	[illegible]
SF3B2	[illegible]	[illegible]	[illegible]	[illegible]	[illegible]	[illegible]	[illegible]	[illegible]	[illegible]	[illegible]	[illegible]	[illegible]
MYO5A	[illegible]	[illegible]	[illegible]	[illegible]	[illegible]	[illegible]	[illegible]	[illegible]	[illegible]	[illegible]	[illegible]	[illegible]
CLIC4	[illegible]	[illegible]	[illegible]	[illegible]	[illegible]	[illegible]	[illegible]	[illegible]	[illegible]	[illegible]	[illegible]	[illegible]
GOLPH3	[illegible]	[illegible]	[illegible]	[illegible]	[illegible]	[illegible]	[illegible]	[illegible]	[illegible]	[illegible]	[illegible]	[illegible]
RPL36	[illegible]	[illegible]	[illegible]	162.383	[illegible]	[illegible]	[illegible]	[illegible]	[illegible]	[illegible]	[illegible]	[illegible]
CDA	[illegible]	[illegible]	[illegible]	[illegible]	[illegible]	[illegible]	[illegible]	[illegible]	[illegible]	[illegible]	[illegible]	[illegible]
PSME2	[illegible]	[illegible]	[illegible]	[illegible]	[illegible]	[illegible]	439.063	[illegible]	[illegible]	[illegible]	[illegible]	[illegible]
NASP	[illegible]	[illegible]	[illegible]	[illegible]	[illegible]	[illegible]	[illegible]	[illegible]	[illegible]	[illegible]	[illegible]	[illegible]
TSN	[illegible]	[illegible]	[illegible]	[illegible]	[illegible]	[illegible]	[illegible]	[illegible]	[illegible]	[illegible]	[illegible]	[illegible]
COX5B	[illegible]	[illegible]	[illegible]	[illegible]	[illegible]	[illegible]	[illegible]	[illegible]	[illegible]	[illegible]	[illegible]	[illegible]
RPN1	[illegible]	[illegible]	554.462	[illegible]	[illegible]	[illegible]	[illegible]	463.298	[illegible]	[illegible]	[illegible]	[illegible]
MDH1	[illegible]	[illegible]	[illegible]	[illegible]	[illegible]	[illegible]	915.763	[illegible]	[illegible]	[illegible]	[illegible]	[illegible]
SPCS2	[illegible]	[illegible]	[illegible]	[illegible]	[illegible]	[illegible]	[illegible]	[illegible]	[illegible]	[illegible]	[illegible]	[illegible]
IGF2BP2	[illegible]	[illegible]	[illegible]	[illegible]	[illegible]	[illegible]	331.679	[illegible]	[illegible]	[illegible]	[illegible]	[illegible]
BCLAF1	[illegible]	[illegible]	[illegible]	[illegible]	[illegible]	[illegible]	[illegible]	[illegible]	[illegible]	[illegible]	[illegible]	[illegible]
GMPPA	[illegible]	[illegible]	[illegible]	[illegible]	[illegible]	[illegible]	[illegible]	[illegible]	[illegible]	[illegible]	[illegible]	[illegible]
ARL6IP5	[illegible]	[illegible]	[illegible]	[illegible]	[illegible]	[illegible]	[illegible]	[illegible]	[illegible]	[illegible]	[illegible]	[illegible]
TRMT6	[illegible]	[illegible]	1272.08	[illegible]	[illegible]	[illegible]	969.699	[illegible]	[illegible]	[illegible]	[illegible]	[illegible]
COMMD4	[illegible]	[illegible]	[illegible]	[illegible]	[illegible]	[illegible]	94.8433	[illegible]	[illegible]	[illegible]	[illegible]	[illegible]
UQCRQ	[illegible]	[illegible]	[illegible]	[illegible]	[illegible]	[illegible]	[illegible]	[illegible]	[illegible]	[illegible]	[illegible]	[illegible]
ST13	[illegible]	[illegible]	[illegible]	[illegible]	[illegible]	[illegible]	[illegible]	[illegible]	[illegible]	[illegible]	[illegible]	[illegible]
NADK	[illegible]	[illegible]	[illegible]	10.566	[illegible]	[illegible]	12.629	[illegible]	[illegible]	[illegible]	[illegible]	[illegible]
PPM1B	[illegible]	[illegible]	[illegible]	[illegible]	[illegible]	[illegible]	[illegible]	[illegible]	[illegible]	[illegible]	[illegible]	[illegible]
SPR	[illegible]	[illegible]	11.5628	[illegible]	[illegible]	[illegible]	13.1183	[illegible]	[illegible]	[illegible]	[illegible]	[illegible]
NDUFA4	[illegible]	[illegible]	[illegible]	[illegible]	[illegible]	[illegible]	[illegible]	[illegible]	[illegible]	[illegible]	[illegible]	[illegible]
EIF2B5	[illegible]	[illegible]	[illegible]	[illegible]	[illegible]	[illegible]	310.858	[illegible]	[illegible]	[illegible]	[illegible]	[illegible]
IGHV1-45	[illegible]	[illegible]	[illegible]	[illegible]	[illegible]	[illegible]	[illegible]	[illegible]	[illegible]	[illegible]	[illegible]	[illegible]
DDX39A	[illegible]	[illegible]	[illegible]	[illegible]	[illegible]	[illegible]	[illegible]	[illegible]	[illegible]	[illegible]	[illegible]	[illegible]
EIF3C;EIF3CL	[illegible]	[illegible]	[illegible]	[illegible]	[illegible]	[illegible]	[illegible]	[illegible]	[illegible]	[illegible]	[illegible]	[illegible]
ATP5F1E;ATP5F1EP2	[illegible]	[illegible]	[illegible]	[illegible]	[illegible]	[illegible]	[illegible]	[illegible]	[illegible]	[illegible]	[illegible]	[illegible]
PGGT1B	[illegible]	[illegible]	36.1289	[illegible]	[illegible]	[illegible]	[illegible]	35.6638	[illegible]	[illegible]	[illegible]	[illegible]
EIF4G2	[illegible]	[illegible]	[illegible]	[illegible]	[illegible]	[illegible]	[illegible]	[illegible]	[illegible]	[illegible]	[illegible]	[illegible]
PGD	[illegible]	[illegible]	[illegible]	[illegible]	[illegible]	[illegible]	[illegible]	[illegible]	[illegible]	[illegible]	[illegible]	[illegible]
CDK5RAP3	[illegible]	[illegible]	[illegible]	[illegible]	[illegible]	[illegible]	[illegible]	[illegible]	[illegible]	[illegible]	[illegible]	[illegible]
MPST	[illegible]	[illegible]	[illegible]	[illegible]	[illegible]	[illegible]	[illegible]	[illegible]	[illegible]	[illegible]	[illegible]	[illegible]
SHMT2	[illegible]	[illegible]	[illegible]	[illegible]	[illegible]	[illegible]	[illegible]	[illegible]	[illegible]	[illegible]	[illegible]	[illegible]
TUBA1C	[illegible]	[illegible]	[illegible]	[illegible]	[illegible]	[illegible]	[illegible]	[illegible]	[illegible]	[illegible]	[illegible]	[illegible]
PIGS	[illegible]	[illegible]	[illegible]	[illegible]	[illegible]	[illegible]	33.4504	[illegible]	[illegible]	[illegible]	[illegible]	[illegible]
TCIRG1	[illegible]	[illegible]	[illegible]	[illegible]	[illegible]	[illegible]	[illegible]	[illegible]	[illegible]	[illegible]	[illegible]	[illegible]
SUPT16H	[illegible]	[illegible]	[illegible]	[illegible]	[illegible]	[illegible]	[illegible]	[illegible]	[illegible]	[illegible]	[illegible]	[illegible]
MOGS	[illegible]	[illegible]	[illegible]	[illegible]	[illegible]	[illegible]	[illegible]	[illegible]	[illegible]	[illegible]	[illegible]	[illegible]
CTNNBL1	[illegible]	[illegible]	[illegible]	[illegible]	[illegible]	[illegible]	46.838	[illegible]	[illegible]	[illegible]	[illegible]	[illegible]

RABGGTA	Geranylgeranyl transferase type-2 subunit alpha	54.0745	65.7289	56.2322	58.6785333	53.5128	52.0246	53.5644	53.0339333	0.19346746	0.71339206	0.14591705950587
PLIN3	Perilipin-3	190.111	185.16	230.316	201.862333	186.952	171.952	176.635	178.513	0.19381473	0.71261321	0.177342594269214
HNRNPM	Heterogeneous nuclear ribonucleoprotein M	481.319	428.7	519.179	476.399333	445.579	375.106	444.584	421.756333	0.19456858	0.7109273	0.17576166130987
RBPJ	Recombining binding protein suppressor of hairless	52.7291		32.0774	42.40325		25.4692	9.8526	17.6609	0.1961384	0.70743737	1.26361597984363
DAB2	Disabled homolog 2	189.9	219.529	138.467	182.632	166.216	140.283	91.3665	132.621833	0.19630369	0.70707153	0.461621266619711
DNM2	Dynamin-2	180.873	154.133	195.845	176.950333	147.953	147.4	169.592	154.981667	0.19727311	0.70493212	0.191246915410009
EXOC2	Exocyst complex component 2	24.4152	18.5062	23.7561	22.2258333	29.8761	43.0369	22.6878	31.8669333	0.19748003	0.70447681	-0.519822677853028
HNRNPH2	Heterogeneous nuclear ribonucleoprotein H2	164.215	128.599	121.468	138.094	131.126	110.322	94.5999	112.015967	0.19837602	0.70251083	0.301946250241365
SPTBN1	Spectrin beta chain, non-erythrocytic 1	14.6024		20.5203	17.56135	16.0336	9.65504	8.20632	11.29832	0.19855214	0.70212543	0.636295486432808
S100A10	Protein S100-A10	272.433	137.66	141.401	183.831333	134.862	106.224	99.9098	113.665267	0.19870168	0.70179846	0.693591220170751
PRKCD	Protein kinase C delta type	193.603	140.492	186.799	173.631333	146.615	142.024	153.828	147.489	0.19967946	0.69966661	0.23541995890614
LARS1	Leucine--tRNA ligase, cytoplasmic	98.5779	107.909	108.443	104.976633	104.755	85.8427	95.2496	95.2824333	0.20039857	0.69810539	0.139786072774907
OVCA2	Esterase OVCA2	52.0448	75.9657	51.4505	59.8203333	48.5099	31.4661	52.2064	44.0608	0.20058035	0.69771161	0.441140259625263
APEH	Acylamino-acid-releasing enzyme	116.745	138.8	143.262	132.935667	158.487	136.568	151.729	148.928	0.2006539	0.69755238	-0.163886789043212
ATG3	Ubiquitin-like-conjugating enzyme ATG3	156.36	134.113	175.09	155.187667	149.52	124.693	125.656	133.289667	0.20195818	0.69473855	0.219448966544961
YWHAZ	14-3-3 protein zeta/delta	6210.12	6842.86	6467.38	6506.78667	6222.74	5240.47	6291.76	5918.32333	0.20209181	0.69445128	0.136756737050445
NAP1L1	Nucleosome assembly protein 1-like 1	218.031	240.496	217.909	225.478667	223.72	168.223	203.044	198.329	0.20289255	0.69273389	0.18509529517533
NPEPL1	Probable aminopeptidase NPEPL1	34.1157	45.9998	23.9274	34.6809667	30.9602	22.8195	9.51366	21.0977867	0.20289713	0.69272409	0.717052455369551
ZNF207	BUB3-interacting and GLEBS motif-containing protein ZNF207	97.7322	62.0253	81.1993	80.3189333	77.76	38.1552	55.0087	56.9746333	0.20487732	0.68850612	0.495420374970669
NAA15	N-alpha-acetyltransferase 15, NatA auxiliary subunit	98.2528	99.212	78.3279	91.9309	78.0331	85.0472	80.4926	81.1909667	0.20545052	0.68729275	0.179230642983167
ARHGAP4	Rho GTPase-activating protein 4	55.6274	75.4575	69.1956	66.7601667	58.6034	55.136	59.4907	57.7433667	0.20740216	0.68318672	0.209332331538024
CCT7	T-complex protein 1 subunit eta	320.439	335.785	321.591	325.938333	351.583	323.11	350.699	341.797333	0.20789734	0.68215107	-0.0685421050981315
CSE1L	Exportin-2	240.518	232.91	190.538	221.322	214.838	154.673	189.364	186.291667	0.20812186	0.68168229	0.248583725974053
RPA3	Replication protein A 14 kDa subunit	116.969	129.885	94.4067	113.753567	74.4997	98.7435	105.245	92.8294	0.20838544	0.68113262	0.293258081960973
QKI	KH domain-containing RNA-binding protein QKI	129.867	124.579	195.551	149.999	134.892	94.4651	104.569	111.3087	0.20891854	0.68002301	0.430386523139085
WAS	Actin nucleation-promoting factor WAS	232.853	296.187	278.832	269.290667	244.752	153.841	247.501	215.364667	0.20963501	0.67853619	0.322382651714805
MGAT2	1,6-mannosyl-glycoprotein 2-beta-N-acetylglucosaminyltrans	42.4771	40.1847	41.7634	41.4750667	19.6486		39.5832	29.6159	0.21106624	0.67558124	0.485872371182323
CNOT1	CCR4-NOT transcription complex subunit 1	41.3998	37.6926	31.4681	36.8535	33.4356		24.208	28.8218	0.21209329	0.67347307	0.354641200913952
BRCC3	Lys-63-specific deubiquitinase BRCC36	45.3189	30.5504	50.4567	42.1086667	40.3695	23.6045	27.5267	30.5002333	0.21209419	0.67347122	0.465296914935317
SORT1	Sortilin	61.7298	33.2882	61.3601	52.1260333	35.489	44.4121	31.1279	37.0096667	0.21242127	0.67280201	0.494101936624458
CSDE1	Cold shock domain-containing protein E1	142.199	131.866	119.859	131.308	100.996	128.226	119.028	116.083333	0.21262863	0.67237826	0.177793963658806
ZNF507	Zinc finger protein 507	76.7194	66.8034	73.8932	72.472	42.0937		69.0432	55.56845	0.21361133	0.67037572	0.383157709734179
GARS1	Glycine--tRNA ligase	167.902	201.643	193.484	187.676333	167.304	167.162	179.829	171.431667	0.21368288	0.67023028	0.13061310547007
NAPG	Gamma-soluble NSF attachment protein	21.2288	23.8159	22.1723	22.4056667	21.6059	17.4512		19.52855	0.21399429	0.66959782	0.198278820908885
TMX2	Thioredoxin-related transmembrane protein 2	45.8154	36.4142		41.1148	21.522	28.6345	38.6892	29.6152333	0.21430499	0.66896772	0.473318358091256
HGS	Hepatocyte growth factor-regulated tyrosine kinase substrate	44.2447	46.728	42.7271	44.5666	33.1376	46.8933	31.3617	37.1308667	0.2144976	0.66857756	0.26334391214758
CMAS	N-acylneuraminate cytidylyltransferase	55.716	45.4757	87.8354	63.0090333	62.9081	109.571	101.675	91.3847	0.21456974	0.66843152	-0.536393967194825
IDE	Insulin-degrading enzyme	81.8022	86.5694	70.8937	79.7551	68.9009	47.8226	78.0408	64.9214333	0.21505068	0.66745919	0.296881924036786
BAX	Apoptosis regulator BAX	159.277	206.832	154.293	173.467333	152.115	150.826	142.414	148.451667	0.21552504	0.66650226	0.22467071533511
VPS39	Vam6/Vps39-like protein	23.8307	27.353	24.231	25.1382333	27.8177	12.6394	9.96864	16.80858	0.21565731	0.66623582	0.580685413602642
TMOD3	Tropomodulin-3	253.002	366.691	248.625	289.439333	177.599	268.039	216.943	220.860333	0.21572696	0.66609559	0.390126657166809
SH3BGRL3	SH3 domain-binding glutamic acid-rich-like protein 3	1962.09	2010.93	1684.78	1885.93333	1517.6	1851.67	1671.88	1680.38333	0.21627523	0.66499321	0.166488296646081
RUFY1	RUN and FYVE domain-containing protein 1	59.9626	64.559	48.5687	57.6967667	59.7369	34.5217	38.6825	44.3137	0.21689811	0.66374422	0.38073768176808
GAK	Cyclin-G-associated kinase	53.9808	42.6871	48.5038	48.3905667	32.7253	44.739	44.932	40.7987667	0.21731634	0.66290762	0.24620029300594
GPD2	Glycerol-3-phosphate dehydrogenase, mitochondrial	131.353	137.293	130.732	133.126	130.726	130.713	127.856	129.765	0.21752702	0.66248678	0.0368910479466449
SNX1	Sorting nexin-1	77.8894	84.3971	69.9251	77.4038667	80.1954	35.3904	57.0367	57.5408333	0.21784099	0.66186039	0.427819522175294
RRAS;RRAS2	Ras-related protein R-Ras	49.5666		26.9816	38.2741	62.714		55.7118	59.2129	0.21856541	0.66041857	-0.629543058922554
IDH3G	Isocitrate dehydrogenase [NAD] subunit gamma, mitochondria	43.7829	47.7185	54.4083	48.6365667	54.1477		55.6749	54.9113	0.21857062	0.66040821	-0.175061676617469
PRKCSH	Glucosidase 2 subunit beta	319.603	405.835	479.824	401.754	272.602	387.247	290.746	316.865	0.21965786	0.65825326	0.342444075376324
LIMS1	LIM and senescent cell antigen-like-containing domain protein	126.191	155.117	146.321	142.543	148.534	159.292	160.489	156.105	0.22123163	0.65515278	-0.131119554015268

c.

1. **Non-labelled No *C. albicans* No Treatment**

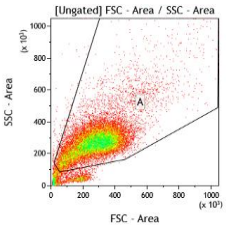

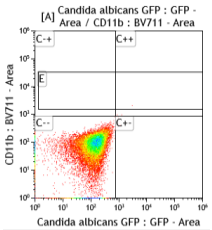

Gate	%Gated	X-Med
All	100.00	130.25
C--	99.97	130.22
C-+	0.00	N/A
C+-	0.02	993.28
C++	0.01	1,266.31
E	0.00	2,992.39

2. **CD11b No *C. albicans* No Treatment**

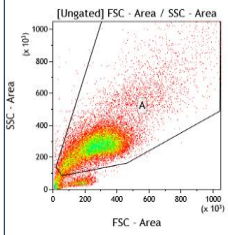

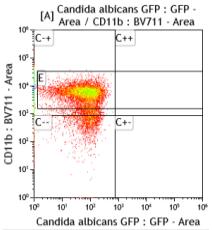

Gate	%Gated	X-Med
All	100.00	1.01
C--	8.05	70.13
C-+	91.95	1.01
C+-	0.00	N/A
C++	0.00	N/A
E	35.67	67.85

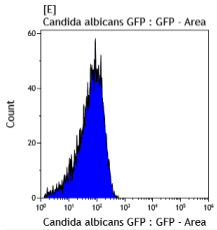

Gate	X-Med
All	67.85

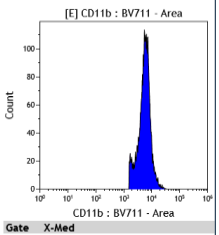

Gate	X-Med
All	5,717.77

3. **Non-labelled With *C. albicans* (wild-type) No Treatment**

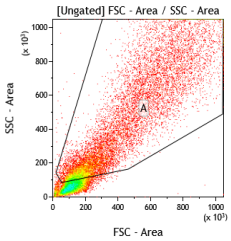

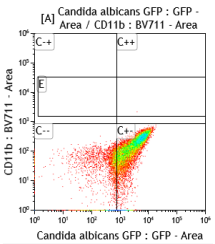

Gate	%Gated	X-Med
All	100.00	1,744.97
C--	21.51	512.94
C-+	0.00	N/A
C+-	78.49	2,601.06
C++	0.01	3,873.19
E	0.01	3,873.19

4. **CD11b With *C. albicans* (wild-type) No Treatment**

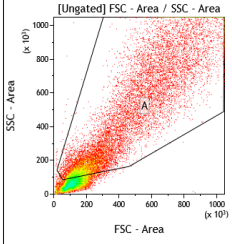

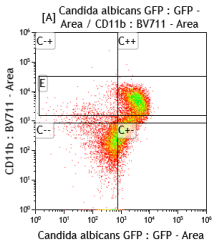

Gate	%Gated	X-Med
All	100.00	1,242.70
C--	29.31	465.31
C-+	5.96	101.13
C+-	21.18	1,172.62
C++	43.54	3,344.35
E	39.18	3,408.75

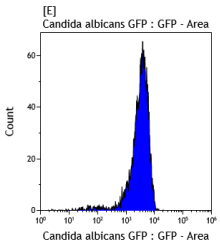

Gate	X-Med
All	3,408.75

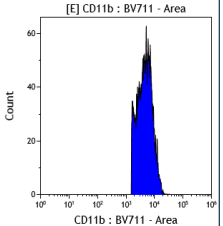

Gate	X-Med
All	4,627.94

5. Non-labelled With GFP No Treatment

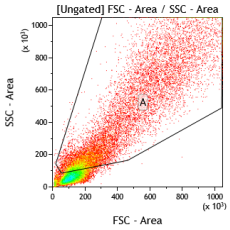

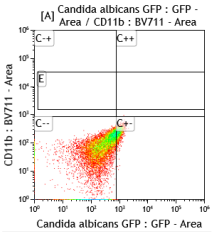

Gate	%Gated	X-Med
All	100.00	251.09
C--	86.27	204.17
C-+	0.01	-9,317.62
C+-	13.72	934.87
C++	0.01	1,418.25
E	0.00	N/A

6. CD11b With GFP No Treatment

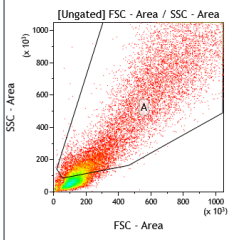

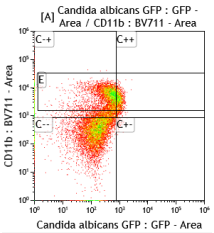

Gate	%Gated	X-Med
All	100.00	222.33
C--	51.26	139.98
C-+	38.00	371.82
C+-	0.69	921.55
C++	10.05	937.92
E	36.56	540.89

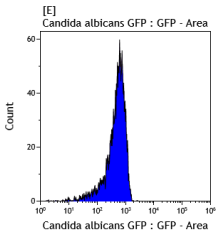

Gate	X-Med
All	540.89

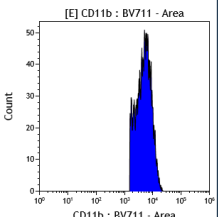

Gate	X-Med
All	4,966.60

7. Non-labelled With *C. albicans* (wild-type) treated with BRD5529

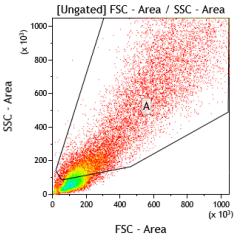

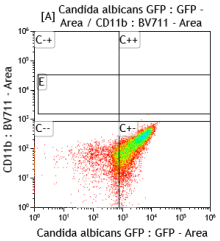

Gate	%Gated	X-Med
All	100.00	1,543.63
C--	25.26	503.03
C-+	0.00	N/A
C+-	74.72	2,422.14
C++	0.02	5,014.13
E	0.00	N/A

8. CD11b With *C. albicans* (wild-type) treated with BRD5529

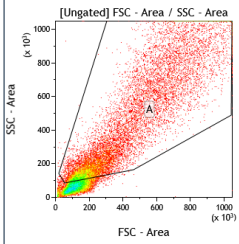

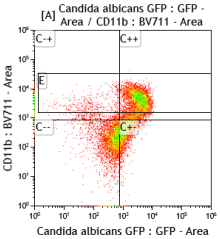

Gate	%Gated	X-Med
All	100.00	1,141.59
C--	30.06	472.09
C-+	6.67	55.66
C+-	23.11	1,154.78
C++	40.16	3,275.09
E	36.09	3,314.59

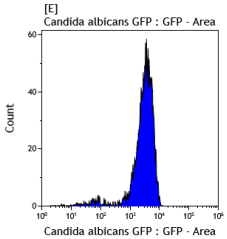

Gate	X-Med
All	3,314.59

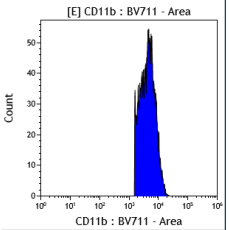

Gate	X-Med
All	4,354.09

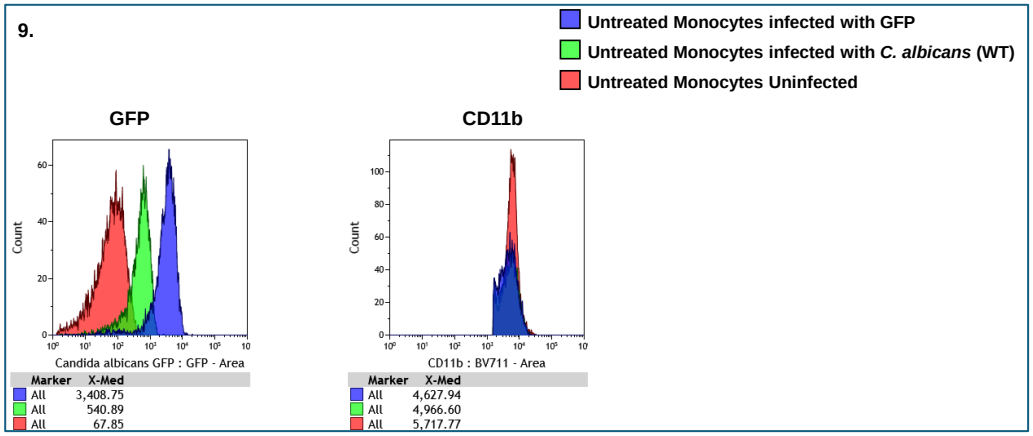
9.
Untreated Monocytes infected with GFP
Untreated Monocytes infected with C. albicans (WT)
Untreated Monocytes Uninfected
GFP
Count
Candida albicans GFP : GFP - Area
Marker X-Med
All 3,408.75
All 540.89
All 67.85
CD11b
Count
CD11b : BV711 - Area
Marker X-Med
All 4,627.94
All 4,966.60
All 5,717.77